ABSTRACT

This work deals with the deagglomeration process in viscous fluids. The process is that in which aggregates of particles suspended in a fluid are broken when the fluid is sheared.

A mathematical model is proposed to predict the size distribution of agglomerates (i.e. the degree of breakage) as a function of the shear stress in the fluid, the initial agglomerate size distribution and the agglomerate strength distribution. The most general form of the model allows the shear stress to be an arbitrary function of time. Two restricted forms of the model have also been derived. The simplest form gives the size distribution, at a given shear stress, that obtains at equilibrium when all the agglomerates, degradable at that stress level, have been broken. The third form of the model predicts the time-varying change of the size distribution in response to a step-change in the fluid shear stress.

Experimental work was performed to test the validity of the model. A concentric-cylinder apparatus was built to provide the shear stress field and an analysis technique was devised to obtain the agglomerate size distributions. Artificial agglomerates made by a novel method were used in this study.

Data were obtained for the equilibrium and the step-change in shear stress cases. Within the limitations imposed by experimental and sampling errors the theoretical calculations agree with the experimental results. In all instances the predictions of the model were qualitatively correct.

DEAGGLOMERATION IN SHEARED VISCOUS LIQUIDS

by

Ian Patterson

Department of Chemical Engineering
McGill University

A Thesis Submitted to the Faculty of Graduate Studies and Research in Partial Fulfilment of the Requirements for the Degree of Doctor of Philosophy

McGill University December 1972

ACKNOWLEDGEMENTS

The author wishes to express his gratitude to Dr. M.R. Kamal for the guidance and aid received during the course of this work, and for his comments and review of this thesis.

Acknowledgement is also due to:

The National Research Council of Canada for financial aid.

The personnel, particularly Mr. A. Krish and Mr. S. Jakab, of the Department of Chemical Engineering's machine shop for help received in the construction of the apparatus.

Dr. H.S. Goldsmith for helpful comments and criticisms.

Finally, the author is indebted to DuPont of Canada Limited and Union Carbide Canada Limited for materials provided by them.

TABLE OF CONTENTS

	Page
ABSTRACT	
ACKNOWLEDGEMENTS	i
TABLE OF CONTENTS	ii
LIST OF TABLES	vii
LIST OF ILLUSTRATIONS	viii
1. INTRODUCTION	1
1.1 GENERAL INTRODUCTION	1
1.2 DEFINITION OF TERMS	2
1.3 GENERAL OBJECTIVE OF THE PRESENT WORK	4
2. SURVEY OF PREVIOUS AND RELATED WORK	5
2.1 GENERAL CONSIDERATIONS	5
2.2 DISPERSION OF SOLIDS IN RUBBER AND PLASTICS	7
2.2.1 Rubber	7
2.2.2 Plastics	9
2.3 PARTICLE BEHAVIOUR IN SHEAR FIELDS	18
2.4 COMMINUTION	27
2.5 SHEAR DEGRADATION OF MACROMOLECULES	33
2.6 SUMMARY OF THE RELEVANT LITERATURE	39
2.7 OBJECTIVE OF THE PRESENT WORK	42

Page

				Page
3.	EXPERIMENTAL			45
	3.1	GENERAL CONSIDERATIONS		45
	3.2	DESIGN CRITERIA AND DIMENSIONS OF THE APPARATUS		47
	3.3	DESCRIPTION OF THE APPARATUS		49
		3.3.1	Mechanical Arrangement	49
		3.3.2	Temperature Control	53
		3.3.3	Cylinder Wall Temperature Movement	56
		3.3.4	Measurement of Cylinder Rotational Speed	56
	3.4	CHOICE OF POLYMER		58
	3.5	CHOICE OF AGGLOMERATES		60
	3.6	PREPARATION OF AGGLOMERATES		62
	3.7	SAMPLE PROBE		67
	3.8	METHOD OF ANALYSIS		69
	3.9	DESCRIPTION OF THE DEAGGLOMERATION EXPERIMENTS		73
	3.10	MEASUREMENT OF TEMPERATURE PROFILES		77
4.	THEORY			83
	4.1	GENERAL FEATURES OF THE MODEL		83
	4.2	EQUILIBRIUM SIZE DISTRIBUTIONS		86
		4.2.1	Gain and Loss Functions	86
		4.2.2	Balance on the Original Agglomerates	93
		4.2.3	Balance on the Original and Gained Agglomerates	95
		4.2.4	Differential Equations for Equilibrium Size Distributions	96
		4.2.5	Determination of c_{ij} and ρ_σ	98
		4.2.6	Solution of the Differential Equations	103

Page

4.3 SIZE DISTRIBUTIONS DURING NON-EQUILIBRIUM DEAGGLOMERATION - STEP CHANGE IN SHEAR STRESS 104

4.3.1 General Considerations 104
4.3.2 Mass Balances on the i^{th} Particle Agglomerates 106
4.3.3 Differential Equations for the Step-Change in Shear Stress Case 108
4.3.4 Determination of the Breakable Fraction of Gained Agglomerates 110
4.3.5 Mass Balance on a Differential Strength Range σ to $\sigma + d\sigma$ 113
4.3.6 Solution of the Equations 118

4.4 SIZE DISTRIBUTIONS FOR A TIME-DEPENDENT SHEAR STRESS 121

4.4.1 Mass Balances 121
4.4.2 Distribution Function of the Breakable Remaining Original Agglomerates 125
4.4.3 Mass Balances on the Differential Strength Range σ to $\sigma + d\sigma$ 127
4.4.4 Scheme for the Solution of the Equations 129

5. RESULTS 131

5.1 VARIATION OF SHEAR STRESS AND TEMPERATURE IN THE EXPERIMENTAL APPARATUS 131

5.2 ESTIMATION OF ERRORS 135

5.2.1 Temperature Profiles as a Verification of Computed Valües 135
5.2.2 Estimate of Error in the Shear Stress 143

5.3 DEAGGLOMERATION RESULTS 147

5.3.1 Experimental Data and Comparison with Theory 147
5.3.2 Errors in the Experimental Deagglomeration Data 158

		Page
6.	DISCUSSION	162
6.1	EFFECT OF NON-UNIFORM TEMPERATURE AND SHEAR STRESS IN THE GAP	162
6.2	EQUILIBRIUM DEAGGLOMERATION RUNS	163
6.3	NON-EQUILIBRIUM DEAGGLOMERATION SIZE DISTRIBUTIONS	165
6.4	EFFECT OF AGGLOMERATE CONCENTRATION	167
6.5	DETERMINATION OF AGGLOMERATE STRENGTH DISTRIBUTION	168
6.6	DETERMINATION OF THE DEAGGLOMERATION RATE CONSTANT, K	173
6.7	EFFECTS OF SOME OF THE ASSUMPTIONS IN THE MODEL	175
6.7.1	The Values of c_{ij}	175
6.7.2	Reagglomeration	176
6.7.3	Collisions	177
6.8	COMPARISON WITH RESULTS FROM SUSPENSIONS	178
6.9	COMPARISON WITH COMMINUTION THEORIES	182
6.10	COMPARISON WITH PREVIOUS WORK ON DEAGGLOMERATION	186
6.11	EXTENSION OF THE MODEL TO MORE COMPLEX SYSTEMS	189
7.	CONCLUSION	192
7.1	SUMMARY AND CONCLUSIONS	192
7.2	SUGGESTIONS FOR FURTHER WORK	196
7.3	CLAIMS FOR ORIGINAL WORK	198

		Page
LIST OF SYMBOLS		200
REFERENCES		208
APPENDICES		
APPENDIX I	NUMERICAL SOLUTION OF THE EQUATIONS OF ENERGY AND MOTION	213
APPENDIX II	EXPERIMENTS WITH POLYETHYLENE	245
APPENDIX III	DETERMINATION OF THE PROPERTIES OF POLYETHYLENE GLYCOL	255
APPENDIX IV	DERIVATION OF THE MASS BALANCE EQUATION	259
APPENDIX V	NUMERICAL SOLUTION OF THE SIZE DISTRIBUTION DIFFERENTIAL EQUATIONS	265
APPENDIX VI	RELATIONSHIP BETWEEN THE DISTRIBUTION OF BREAKING AGGLOMERATES AND THE DISTRIBUTION OF PRODUCTS DURING NON-EQUILIBRIUM DEAGGLOMERATION	275

LIST OF TABLES

TABLE		Page
4-1	Mass Balance Equations	89
4-2	Relationships Between Degraded Portions of Agglomerates	91
4-3	Summary of Errors in the Computed Shear Stress	144

LIST OF ILLUSTRATIONS

FIGURE		Page
3-1	Schematic Diagram of the Apparatus	50
3-2	Photograph of the Concentric Cylinder Portion of the Apparatus	51
3-3	Cross-sectional Diagram of the Concentric Cylinders	54
3-4	Thermocouple Installation in the Cylinder Wall	57
3-5	Photomicrograph of the Artificial Agglomerates	65
3-6	Scanning Electron Micrograph of the Agglomerates Showing Bonds Between the Beads	66
3-7	Photograph of the Sampling Probes	68
3-8	Photograph of the Sample Dissolving Cell	70
3-9	Device Used to Mount and Position the Thermistor Temperature Measurement Probe	78
3-10	Experimental Determination of the Thermistor Probe Voltage Coefficient	80
3-11	Calibration of the Thermistor Probe Position in the Gap	82
4-1	Response of the Agglomerate Size Distribution to a Step-Change in Fluid Shear Stress	105
4-2	Relationships Between Agglomerate Portions in Species i for the Step-Change Case	114
4-3	Relationships Between Agglomerate Portions in Species i for an Arbitrary Time-Varying Shear Stress	123

FIGURE		Page
4-4	Response of the Size Distribution of the Original Agglomerates to an Arbitrary Time-Varying Shear Stress	126
5-1	Computed Mean Shear Stress as a Function of Inner Cylinder Rotational Speed	133
5-2	Computed Shear Stress Versus Dimensionless Gap Position for Varying Cylinder Wall Temperatures	134
5-3	Dimensionless Temperature Versus Dimensionless Radial Gap Position. 20 RPM	137
5-4	Dimensionless Temperature Versus Dimensionless Radial Gap Position. 30 RPM	138
5-5	Dimensionless Temperature Versus Dimensionless Radial Gap Position. 40 RPM	139
5-6	Dimensionless Temperature Versus Dimensionless Radial Gap Position. 50 RPM	140
5-7	Dimensionless Temperature Versus Dimensionless Radial Gap Position. 60 RPM	141
5-8	Dimensionless Temperature Versus Dimensionless Radial Gap Position. 80 RPM	142
5-9	Computed Temperature Profiles at 50 RPM, Showing the Effect of Thermal Conductivity Changes	145
5-10	Computed Shear Stress Profiles at 50 RPM, Showing the Effect of Different Values of Thermal Conductivity	146
5-11	Weight Percent of Species 1 to 8 Inclusive Versus Fluid Shear Stress for the Equilibrium Case. Run 1	148

FIGURE		Page
5-12	Weight Percent of Species 1 to 8 Inclusive, Versus Fluid Shear Stress for the Equilibrium Case. Run 2	149
5-13	Weight Percent of Species 1 to 8 Inclusive, Versus Fluid Shear Stress for the Equilibrium Case. Run 3	150
5-14	Weight Percent of Species 1 to 8 Inclusive, Versus Fluid Shear Stress for the Equilibrium Case. Run 4	151
5-15	Weight Percent of Species 1 to 8 Inclusive, Versus Fluid Shear Stress for the Equilibrium Case. Run 5	152
5-16	Weight Percent of Species 1 to 8 Inclusive, Versus Fluid Shear Deformation, Step Change Case. Run 6	153
5-17	Weight Percent of Species 1 to 8 Inclusive, Versus Fluid Shear Deformation, Step Change Case. Run 7	154
5-18	Weight Percent of Species 1 to 8 Inclusive, Versus Fluid Shear Deformation, Step Change Case. Run 8	155
5-19	Scatter Diagram of the Average Percent Deviation of the Agglomerate Weight Percent Determination	160
6-1	The Rate of Change of the Number of Nth Species Agglomerate with Fluid Shear Stress Versus Fluid Shear Stress. Run 1	171
I-1	Flow Chart for Numerical Solution of Equations of Motion and Energy	227
II-1	Log Viscosity Versus log Shear Rate for Polyethylene Sclair 8107.	246
II-2	Loss of Shearing Encountered with Runs Using Polyethylene	247

FIGURE		Page
II-3	Cross-section of Solidified Polyethylene Removed from the Apparatus	253
III-1	Viscosity Versus the Reciprocal of Absolute Temperature for the Polyethylene Glycol Used	256
III-2	Thermal Conductivity as a Function of Temperature for the Polyethylene Glycol Used	258
V-1	Flow Chart for the Numerical Solution of the Step-Change Case	273
VI-1	The Strength Distribution of the Breakdown Products of Agglomerates of Strength σ_2	277
VI-2	Derivation of the Strength Distribution of Products with Strengths Less than σ_5	279
VI-3	Derivation of the Overall Strength Distribution of the Breakdown Products	281

CHAPTER 1

INTRODUCTION

1.1 GENERAL INTRODUCTION

Almost from the first use of polymers, additives have been incorporated in them to render the combinations more suitable for the designated end use. A list of the additives most frequently found in commercial formulations would include pigments, thermal stabilizers, fillers, lubricants, ultraviolet stabilizers, antioxidants, impact modifiers and flame-retarding agents. Often, a small quantity of a different type of polymer will be added to produce a "polyblend" that has the optimum combination of desired characteristics. In each case, it is essential that the additives are dispersed uniformly throughout the polymeric matrix. Furthermore, it is important to achieve an optimum particle size or size distribution of the minor components. In some instances, the additives may have an opposite effect to that desired if they are non-uniformly distributed or if they possess the improper size distributions (1). Thus, it is desirable to quantatively understand the variables, both material and operational, which govern the incorporation process. Such knowledge should ultimately lead to improved processes and products.

It was the discovery of the reinforcing effect of carbon black in rubber at the beginning of this century (2) that gave the incorporation process added importance. At first, the incorporation of the carbon black was accomplished on a two-roll mill as part of the milling step in rubber processing. Later, closed mixers of various designs, such as the Banbury (3,4), were employed. The effectiveness of these techniques led to the extension of their use by the plastics industry where they play a major role at this time.

So far, we have referred, in general terms, to the process of incorporating additives into plastics and rubber. This process is rather complex because it involves a number of operations occurring simultaneously. As a consequence, some contradictions and misnomers have appeared in the literature concerned with these operations. To avoid ambiguities and misunderstanding, a list of the relevant terms and their corresponding definitions, as used in this work, are given in the next section.

1.2 DEFINITION OF TERMS

1.2a Agglomerates are particles containing a finite number of smaller particles which are aggregated. The smaller particles, referred to as the ultimate particles, are distinct from one another and do not necessarily have the same size, composition or structure. The ultimate particles are bound together in the agglomerate by Van der Waals' forces or some binder substance or adhesive.

1.2b Aggregates: are identical with agglomerates.

1.2c Deagglomeration: is the process in which agglomerates are broken down into smaller aggregates or into ultimate particles. Deagglomeration does not involve the breakdown of the ultimate particles themselves as in the process of comminution.

1.2d Mixing: is the process whereby material, usually a minor component, is redistributed in a matrix, which is usually the major component, in order to increase the homogeneity of the resulting combination. For the purposes of this work the additive will be considered as the minor component since it is usually employed in a small proportion relative to the polymer which is considered to be the major component.

1.2e Blending: is synonymous with mixing.

1.2f Dispersion: is the process that combines both deagglomeration and mixing simultaneously.

1.3 GENERAL OBJECTIVE OF THE PRESENT WORK

The objective of this work is to examine the deagglomeration process as it relates to liquids of high viscosity. As far as is practical, an attempt will be made to determine the fundamental process and material variables which govern this process. Specifically, it is desired to formulate a model that will predict the behaviour of agglomerates during deagglomeration, given the process conditions and material properties. In addition, experiments and suitable apparatus will be designed and employed to obtain data that will be used to test the proposed model.

CHAPTER 2

SURVEY OF PREVIOUS AND RELATED WORK

2.1 GENERAL CONSIDERATIONS

Deagglomeration, during dispersion, is the result of three separate actions (5). These are: breakdown due to impact, breakdown caused by attrition and shear breakdown. Shear breakdown occurs when the hydrodynamic forces acting on the agglomerate overcome the mechanical strength of the agglomerate, i.e. the strength of the weakest bond or combination of bonds linking the components of the agglomerate. Both attrition and impact breakdown result from collisions of agglomerates travelling at high velocities. In the case of attrition, agglomerates collide with each other, while impact breakdown is due to collisions of the particles with the impeller and walls of the apparatus.

As the viscosity of the fluid is increased, shear breakdown becomes more dominant while impact and attrition become less important. When the fluid is very viscous, like a polymer melt, the flow is usually laminar, and small particles tend to travel in a Stokesian manner along streamlines (6). When, in this case, an agglomerate collides with another or with the equipment, the relative velocity is very low and, accordingly, the kinetic energy available to cause breakdown will be low. Thus, it is expected that deagglomeration will proceed by shear forces with the other two mechanisms playing a negligible role.

A search of the literature for work that is relevant to the objectives of this research shows findings that fall roughly into the following four categories:

2.1a Research related to the dispersion of solids in rubber and plastics. The rubber industry has been primarily concerned with the rubber-carbon black system which is of a complex and specialized nature. Most of the work conducted on plastics only relates to the understanding of the mixing of solid particles in very viscous liquids.

2.1b Research related to the study of forces exerted by a shear field on suspended particles. Most of this work has been devoted to the behaviour of single particles of well-defined shape. However, some recent work has been concerned with systems involving many particles of irregular geometry.

2.1c Research relating to the comminution of solids. Comminution and deagglomeration have many features in common, and a close examination of the work in this field will be made.

2.1d Research relating to the mechanical degradation of large molecules by shear fields. In some respects, the problem of describing the change of molecular weight distribution due to shear degradation is very similar to the problem of describing the change of particle size distribution caused by deagglomeration.

The relevant results from each of the above areas will be described in detail in the following sections.

2.2 DISPERSION OF SOLIDS IN RUBBER AND PLASTICS

2.2.1 Rubber

Work in the rubber industry has concentrated on rubber-carbon black interactions. Progress in this area has been limited by the extreme complexity of the system. Carbon black is a complicated substance that is not well understood and its interaction with elastomers is far from simple. In addition, it exists with a very wide range of particle sizes (approx. 0.1 to 100μ) (7,8).

Literature reports recognize the two-step nature of the dispersion process which has been treated only qualitatively (9,10). It is thought that when the rubber is sheared in the presence of carbon black, agglomerates are formed with the rubber acting as a binder. These rubber-carbon black agglomerates are then broken up and mixed throughout the material (9,10). In addition to this type of agglomerate breakdown, there is also experimental evidence of breakage of the carbon black particle structure itself (11,12,13). This evidence is quite recent and will probably result in a re-examination of the carbon black deagglomeration process in rubber.

A further problem is the lack of a reliable and meaningful measure of the extent of carbon black dispersion. No dependable test exists that will directly give the size distribution of the deagglomerated particles. The enormous range of agglomerate sizes precludes the easy development of such a measurement. A few attempts have been made to put the measurement of breakdown on a quantitative basis. A microscopic method has been proposed by Leigh-Dugmore (14) but sometimes gave values less than zero, which is physically impossible. A revised procedure has been developed by Medalia (15) but his method only considers agglomerates larger than 6.5 microns in diameter and, like all microscopic methods, is tedious and time consuming. The use of electrical resistivity measurements has been described (11,12) but only as a relative measure of the breakdown and mixing.

The most common test used to measure carbon black dispersion in rubber is the oil adsorption test. As mixing proceeds, it is found that less oil will be adsorbed into the rubber-carbon black system. It is thought that this is due to the break-up of the agglomerates which is accompanied by the loss of voids. Prior to breakdown, these voids are available to hold the oil. Obviously, this is a highly relative test, depending not only on the agglomerate size, but on structure and other variables.

It seems fitting to conclude this brief survey with a quotation from reference 10 - "The process of mixing [carbon black and rubber] is not only one of the most important but also one of the most variable and intangible in the rubber industry".

2.2.2 Plastics

From the concepts of Danckwerts (16) and Lacey (17), workers in the plastics industry developed equations describing the mixing portion of the dispersion process. The basic description, as developed by Spencer and Wiley (18) and Mohr (19), applied to the mixing of two very viscous fluids. Mohr considered deformable, randomly placed cubes of the minor component and showed that the scale of segregation is given by (19):

$$s = \frac{\ell}{\gamma v_f} \qquad 2\text{-}1$$

where: s = scale of segregation

ℓ = length of a side of the original cube

γ = total amount of shear deformation

v_f = volume fraction of the minor component

Physically, s is interpreted as the average distance from the point of maximum concentration of one component (usually the minor one) to the nearest point of maximum concentration of the same component, for a large number of measurements (20). If the scale of segregation is less than the scale of scrutiny, no variation in the mixture can be detected.

The intensity of segregation is a measure of the variation of the scale of segregation and is defined, for this process, as the standard deviation of the concentration (measured randomly at points throughout the system) of one component divided by its average concentration. The quality of the mixture can thus be described by specifying the scale and intensity of segregation in the mixture.

These concepts have been applied to the additive-polymer system by assuming that the additive particles are so small that the minor component appears to behave as a continuous medium. If this assumption is correct, then the ultimate particles must be very much smaller than the scale of segregation and the binding forces negligibly weak. Thus, the dispersion process, by this assumption, reduces to one of simple mixing.

Equations describing mixing have been derived for several geometries. Spencer and Wiley (18) have discussed a coaxial cylinder geometry, and experiments performed by Bergen et al (21) have confirmed the validity of this approach to mixing. The extruder geometry, a helical channel, has been the subject of a number of investigations (4,22,23,24,25,26), but only qualitative agreement has been obtained for non-Newtonian fluids such as polymer melts (22,26). Bergan (25), assuming Newtonian behaviour, has obtained good agreement between experiment and theory for a coaxial cylinder mixer having a helical flow.

Gaskell (27) analyzed the shearing action in a two-roll mill with equal roll speeds and his analysis was extended to unequal roll speeds by Bergen (4). There does not appear to be any experimental confirmation of the predicted mixing action in a two-roll mill.

The deagglomeration portion of the dispersion process has been recognized by many authors (19,21,22,25,26,28,29) but has received little more than recognition of the problem. Bolen and Colwell (30) examined the deagglomeration of pigment particles by high shear stresses. They assumed that adequate mixing would be obtained and related the particle creation rate to shear stress and time by the following equation:

$$\frac{dn}{dt} = \frac{N_\infty (\tau_a - \tau_p)}{\tau_a} [1 - \exp(-k_c t)] \qquad 2\text{-}2$$

where
- n = number of particles per unit volume
- t = time
- N_∞ = particle creation rate at long times, $N_\infty = \lim_{t\to\infty} \frac{dn}{dt}$
- τ_a = average shear stress
- τ_p = minimum shear stress required to cause particle rupture
- k_c = rate constant

The justification given for equation 2-2 is the observation that "mixing tends to approach an equilibrium state [thus] the rate of approach is apt to be an exponential function of time". The term $(\tau_a - \tau_p)$ arises because it is expected that there is a minimum stress required to cause rupture. A problem with the proposed equation is that it gives $\frac{dn}{dt} = 0$ when $t = 0$. This difficulty is explained by suggesting that the agglomerates undergo twisting and stretching before rupture, and thus there is no instantaneous breakage.

It is assumed that the average shear stress, τ_a, is constant in a steady-state process and equation 2-2 is integrated to obtain:

$$\frac{n}{n_o} = 1 + N_\infty \left[\frac{\tau_a - \tau_p}{n_o\, k_c\, t}\right]\left[k_c t - 1 + \exp\,(-k_c t)\right] \qquad 2\text{-}3$$

where n_o = number of particles per unit volume at time, $t = 0$.

A minor difficulty in the application of equation 2-3 is that the average shear stress, τ_a, is not further defined or explained. A more serious problem is the use of the parameter N_∞. According to the justification for the form of equation 2-3, $\frac{dn}{dt}$ must approach zero as $t \rightarrow \infty$. Therefore, either N_∞ or $(\tau_a - \tau_p)$ must be zero, but it does not make sense for $(\tau_a - \tau_p)$ to be zero. The alternative, that $N_\infty = 0$, makes the equations useless. A way out of the difficulty is to postulate that reagglomeration is occurring, but the authors make no mention of this possibility, which raises other problems. The validity of the analysis has not been tested experimentally, but it is stated that since there are three independently adjustable parameters (τ_p, N_∞, κ_c), the equations should correlate the dispersion process adequately.

More recently, Smith (31) investigated pigment dispersion in polymer melts using a Brabender Plastograph. (This is a mixer of complex geometry described in reference (4), p. 314). The procedure consisted of blending 1% by weight of various pigments with low density polyethylene for varying lengths of time. Samples were sectioned and examined microscopically, and the area under a portion of the integral size distribution curve was determined. The limits for the area determination were identical for each sample but were not specified. The areas, thus found, were plotted against dispersion time (range 10 seconds to 30 minutes). This plot was found to be linear according to:

$$A_d = \text{const.} + \kappa_d t \qquad \text{2-4}$$

where A_d = area under the integral distribution curve, between arbitrarily selected limits, corresponding to time t

κ_d = a rate constant

t = dispersion time

The constant corresponding to the intercept was found not to vary, although κ exhibited a range of 3:1 from the most quickly dispersed pigment to the slowest. A further, interesting result was that for the 1:4 range of rotational speeds examined some pigments gave a κ_d independent of speed (roughly equivalent to shear rate) while others showed as much as a 1:4 change. Smith did not attempt to explain his data in terms of any deagglomeration mechanisms, but devoted his discussion to the problems of sampling technique and determining the true integral size distribution.

Similar procedures and equipment were used by Hess and Garret (32) to evaluate the degree of pigment (carbon black) agglomeration in printing inks. Using microscopic examination of thin films, an agglomeration index, A.I., was defined:

$$A.I. = 100 \frac{A_a}{v_p} \qquad 2\text{-}5$$

where A_a = fraction of area in the microscopic field of view covered by agglomerates

v_p = volume fraction concentration of pigment

An agglomerate was defined as a particle having a maximum chord of three microns or more. Some eighteen different carbon blacks were examined and compared via their agglomeration index values, but no information about breakdown other than agglomerate index values was presented.

A more fundamental approach was taken by McKelvey (22) who attempted to develop a simple model for deagglomeration. He considered two spherical particles in a uniform simple shear field of magnitude $\dot{\gamma}$. The particles have radius, r, and a centre to centre distance of d. It is postulated that there is a critical separation, d_c, such that when $2r \leq d \leq d_c$, the force acting to hold the particles in proximity to each other is a constant, and acts along the direction joining the particle centres. When $d > d_c$ the force is zero and there is no interaction. It is assumed that the hydrodynamic force acting on each sphere is given by Stokes' law. Using a cartesian co-ordinate system with its origin coincident with one sphere centre, a force balance gives:

$$\frac{dx}{dy} - \frac{x}{y} = -\frac{6\pi r \dot{\gamma} \mu d}{F_a} \qquad 2\text{-}6$$

where F_a = the force acting to hold the particles in proximity

μ = fluid viscosity

x,y = the co-ordinates of the second particle, related by $d = (x^2 + y^2)^{\frac{1}{2}}$

Because equation 2-6 is nonlinear, the approximation $d = (x + y)$ is introduced, and the equation is integrated with the condition that the second sphere has its centre initially at (x_o, y_o):

$$\left(\frac{x+y}{x_o+y_o}\right)\left(\frac{y_o}{x_o}\right) = \exp\left[\frac{6\pi r\dot{\gamma}\mu}{F_a} y_o \left(1 - \frac{y}{y_o}\right)\right] \qquad 2\text{-}7$$

The approximation for the centre to centre distance introduced to solve the equation has the effect of making the attractive force between the particles a function of position varying from F_a to $F_a/\sqrt{2}$, but is justified by the rough nature of the analysis.

Examining particle paths for various values of $\left(\frac{6\pi r\dot{\gamma}\mu}{F_a}\right)$ and initial orientations of the agglomerate leads to the following conclusions:

1. There is a critical shear stress below which deagglomeration will not occur.
2. At shear stresses only slightly greater than the critical stress only those agglomerates initially perpendicular to the flow will deagglomerate, all others will rotate to align with the flow and remain in this orientation.
3. High shear stresses promote deagglomeration.
4. If the attractive force, F_a, is independent of particle size (r) larger particles will deagglomerate at lower shear stresses.

The analysis, described as a crude approximation, is open to some severe criticisms. It is suggested that the nature of the force F_a is intermolecular attraction. Thus the force operates only over very small distances (~ 100 Å or less), and the two spheres in the agglomerate must be close together. Given this situation, it is not correct to apply Stokes' law and the lubrication approximation should be used. Also, the motion predicted for the non-deagglomerating situation (conclusion 2) is incorrect as shown by Bartok and Mason (33); the particle will continue to rotate in the flow in a well-defined orbit determined by its initial orientation. Finally, the analysis is limited to agglomerates of two spherical particles, and it is not obvious how it could be easily extended to multi-sphere agglomerates. To this writer's knowledge there has been no experimental evidence to support this deagglomeration hypothesis.

Investigations into the behaviour of particles in shear fields have been made, particularly by Mason and coworkers, and the relevant results are described in the next section.

2.3 PARTICLE BEHAVIOUR IN SHEAR FIELDS

The breakdown of agglomerates by hydrodynamic forces is a small portion of the present knowledge of particle motion in sheared fluids. An excellent summary of this field has been written by Goldsmith and Mason (34), and much of what follows has been abstracted from this reference. Although most of the work has been done with particles of well defined geometry which exist rarely, if at all, in a practical system, many general conclusions are useful. An example is the result used in the previous section 2-2 where it has been found that axisymmetric particles do not align themselves with the flow, but rotate in orbits. The particles undergo varying, but periodic, forces depending on their initial orientation, which determines the orbit. Thus, even if the initial orientation is unfavourable to particle deagglomeration it may rotate to a favourable position at a later time.

The behaviour of linear agglomerates of spheres has been examined and the forces acting on long, rod-like particles has been derived (33, pp. 137-144). In simple shear flow, the particle alternately experiences tension and compression as it rotates. The forces are at a maximum when the particle is aligned with the principal axes of the stress field, and the maximum tensile force is given by:

$$F_x = \frac{\pi \mu \dot{\gamma} \left(\frac{\ell_r^2}{4} - x_r^2\right)}{2 \left(\ell n\ 2r_e - 1.5\right)} \qquad 2\text{-}8$$

where F_x = the force at point x from the midpoint of the rod

μ = viscosity

$\dot{\gamma}$ = shear rate

ℓ_r = length of rod

x_r = distance from the midpoint of the rod

d = diameter of rod

r_e = equivalent axis ratio = $0.78\ \ell/d$

Equation 2-8 applies only when the particle lies in the plane of shear and has $\ell/d \gg 1$. More general equations for particles of arbitrary orientation and low ℓ/d are given in reference (33), but the features of a parabolic force distribution with the maximum at the centre and a linear dependence on the product $\mu\dot{\gamma}$ are unchanged. Forgacs and Mason (35) have experimentally confirmed the applicability of equation 2-8.

In any flowing system containing a concentration of particles, there will be particle collisions. If the flow is reversible, i.e. the creeping flow equations apply (36), the collisions of two spheres form a transient doublet which exists for a finite time. Thus an equilibrium will be reached with a certain fraction of the particle existing as doublets. The concentration of these doublets may be calculated from (37):

$$c_d = \frac{20}{3} c_s^2 \qquad 2\text{-}9$$

where c_d = volume concentration of doublets

c_s = volume concentration of single spheres initially in the system

Equation 2-9 applies only for uniform spheres at low concentrations where the change in c_s due to the formation of doublets is negligible. The effect of a finite lifetime is appreciable. When c_s = 0.02 fifteen percent of the spheres exist as doublets. A minority of the collisions give doublets that are not transient but assume a captive orbit, each describing a spherically ellipsoidal path.

The frequency of collisions for two particle interactions in a system containing different sized spheres has been derived (37):

$$F_c = \frac{\dot{\gamma}}{12} \sum_{i=1}^{N_s} \sum_{j=1}^{N_s} (r_i + r_j)^3 \, n_i n_j \qquad 2\text{-}10$$

where F_c = total number of collisions per unit volume per unit time

$\dot{\gamma}$ = shear rate, constant over the volume in which collisions take place

r_i, r_j = radii of spheres of species i and j, respectively

n_i, n_j = number concentration of species i and j, respectively

N_s = total number of species present

For axisymmetric particles at an arbitrary orientation to the shear field, Manley and Mason (38) have shown how the mean effective volume may be calculated, if the distribution of orientations is known. This mean effective volume is the volume swept out as the particle orbits in a manner similar to a precessing top. The calculation of collision frequencies is not simple because the particle does not spend equal time in all portions of its orbit. Recently, Gauthier (39) has determined the distribution of orbits for rods in both Newtonian and non-Newtonian Couette flow.

Zia and coworkers (40,41) have examined the behaviour and breakdown of chains of rigid spheres. The polystyrene spheres used had a thin metal coating and were aligned along a common axis by the application of a high strength electric field. It was found that when the field was removed and the suspending fluid sheared, the chain rotated as a rigid rod as predicted by the creeping motion equations. As the shear rate was increased to a large enough value, breakage occurred. This could not be explained by the creeping motion equations which do not allow breakdown for any value of shear. Further, it was found that the breaking was not reversible whereas the creeping motion equations demand reversibility of the flow.

Very recently Vadas (42) examined the behaviour of aggregations of 2μ sized polyvinyltoluene spheres in Poiseuille flow. The aggregates were very "flexible", showing markedly different relative orientations of parts of the agglomerate as they rotated in the shear field. It was also found that Brownian effects were not negligible, but caused a shortening of the period of rotation of the agglomerate. Size distribution of agglomerates were also measured with NaOH introduced as a coagulant. Higher shear rates tended to form agglomerates of four or more spheres into a cluster configuration rather than a chain. The distribution also shifted towards larger agglomerates as sections further away from the capillary entrance were examined. This was ascribed to shear-induced collisions, which caused the larger aggregates to grow at the expense of the smaller ones.

In a related work, van den Tempel (43) derived an equation for agglomerate size distributions and used it to predict the viscosity of emulsions. This equation, given below, applied to the steady-state distributions of agglomerates composed of monodisperse, spherical particles. A mass balance on the i^{th} species yields:

$$\frac{dn_i}{dt} = 0 = \tfrac{1}{2} \sum_{j+k=i} 4\pi D_{jk}\, d_{jk}\, n_k n_j - n_i \sum_{j=1} 4\pi\, D_{ji}\, d_{ji}\, n_j$$

$$+ \tfrac{1}{2} \sum_{j+k=1} \frac{4}{3}\, d^3_{jk}\, \dot{\gamma}\, n_j n_k - n_i \sum_{j=1} \frac{4}{3}\, d^3_{ji}\, \dot{\gamma}\, n_j$$

$$+ \sum_{m=i+1} 2\, n_m\, \dot{\gamma}\, B - n_i\, \dot{\gamma}\, B\, (i - 1) \qquad \text{2-11}$$

where n_i = number of agglomerates of species i per unit volume

D_k, D_j = diffusion coefficients of k-particle and j-particle agglomerates, respectively

$D_{jk} = D_j + D_k$

d_{jk} = distance between j-particle and k-particle agglomerate centres after they have collided

$\dot{\gamma}$ = shear rate, assumed uniform everywhere

B = constant

t = time

The first and third terms give the rate of production of i^{th} species agglomerates due to collisions caused by Brownian motion and the shear field, respectively. The second and fourth terms give the corresponding rates of loss. The loss terms appear when small agglomerates collide to form larger agglomerates. It is assumed that the collisions are inelastic. The fifth term represents the gain in the i^{th} particle due to the breakdown of larger agglomerates by the shear field. The loss of i-particle agglomerates by the same process is given by the last term. With respect to the present work, where it is assumed that agglomeration does not occur, only the last two terms will be discussed, and equation 2-11 reduces to:

$$\frac{dn_i}{dt} = \sum_{m=i+1} 2n_m \dot{\gamma} B - n_i \dot{\gamma} B(i - 1) \qquad 2\text{-}12$$

The rate of breakdown, as given in equation 2-12, incorporates a number of inherent assumptions. First, it is assumed that the agglomerates are linear in form so that an i-particle agglomerate has (i-1) bonds. Further, it is assumed that the probability of breaking a bond is proportional to the shear rate. The proportionality is adjusted by the constant B, which depends on the strength of the bonds. Implicit, although not stated by the author, are the assumptions that all the bonds are of equal strength, and that the probability of disruption is the same for each bond.

If the restriction as to linearity of configuration is accepted, then the force distribution within the agglomerates would not give an equal probability of breaking for each bond. In addition, as shown by equation 2-8, the force is a function of the product of shear rate and viscosity (i.e. shear stress), and hence it would be more reasonable to expect the rate of breakage to be a function of the shear stress rather than the shear rate.

A further objection to this model (equation 2-12) is that it does not predict an equilibrium distribution, other than single particles, as $t \rightarrow \infty$. The model also predicts that this "distribution" will obtain for any finite value of shear rate or shear rate-viscosity combination.

Experimentally, the theory was tested by substituting:

$$D_{jk}\, d_{jk} = \frac{kT}{3\pi\mu} \qquad 2\text{-}13$$

where k = Boltzmann's constant

T = temperature

μ = viscosity

in equation 2-11 and calculating the viscosity as a function of the shear rate. The predictions were made to fit experimentally determined results on a system of natural rubber latex in water by allowing B to vary with the shear rate. The results showed that B exhibited a minimum at shear rates 1 sec^{-1}. The value of B varied about 20:1 over five decades of shear rate variation. These findings could not be used to either confirm or invalidate the shear rate breakdown terms since they were not tested independently of the collision terms. Although steady state distributions of agglomerates for $i \leq 3$ were calculated, there were no experimental results for comparison.

2.4 COMMINUTION

Comminution can be defined as the breaking of a solid, usually but not necessarily homogeneous, by mechanically applied stresses. Thus, operations such as crushing, grinding and milling are comminution processes.

Epstein (44) is generally credited with the first theoretical derivation of a breakage process that yields a logarithmico-normal size distribution of the products, although he cites an earlier Russian paper. Prior to Epstein's work, the logarithmico-normal size distribution had been found to hold experimentally for a wide range of substances but no satisfactory theoretical explanation had been advanced.

Briefly, Epstein's concepts are as follows. The comminution process may be viewed as one composed of a large number of discrete events or steps. It may then be described in terms of two functions, $p_N(y)$ and $F(x,y)$. The function $p_N(y)$ describes the probability of breakage of size y in the N^{th} step, and $F(x,y)$ gives the weight fraction distribution of particles of size x, $x \leq y$, resulting from the breakage of a unit mass of particles of size y. These two functions have become known as the selection function, $p_N(y)$, and the breakage function, $F(x,y)$. With the assumption that $p_N(y)$ is a constant, independent of y, and that $F(x,y)$ normalized over the interval, 0 to y, is also independent of y, it can be shown that the distribution of sizes at the n^{th} step tends to a logarithmico-normal distribution as $n \to \infty$. This occurs, regardless of the initial size distribution.

Bass (45) has derived the mass balance for a comminution process using Epstein's concepts of a breakage function and a selection function. His result,known as the fundamental equation of comminution, is:

$$\frac{\partial^2 f(x,t)}{\partial x \partial t} = -k(x)\,\frac{\partial f(x,t)}{\partial x} + \int_x^{x_m} \frac{\partial B(x,\alpha)}{\partial x}\,k(\alpha)\,\frac{\partial f(\alpha,t)}{\partial x}\,d\alpha \qquad \text{2-14}$$

where $f(x,t)$ = weight fraction of material smaller than size x, when a feed with distribution $f(x,o)$ is ground for a time, t

$k(x)$ = is the selection function defined as the fractional rate of breakage of material of size x

$B(x,\alpha)$ = is the breakage function giving the fraction of material smaller than size x resulting from breaking material of size α, and which does not breakdown further.

x_m = the largest size in the feed.

The first term on the right hand side of equation 2-14 gives the rate of loss of material of size x and the integral gives the rate of gain due to breakage of material greater than size x.

Reid (46) has pointed out that the definition of the function $\kappa(x)$ as given above leads to a rate of breakage that is independent of time and hence is equivalent to a first-order reaction description of the breakage process. In the same paper he discusses three degenerate cases of equation 2-14. Each case has an analytic solution.

The first case is where $\kappa(\alpha)$ is zero, giving the result that there is no breakage and the distribution remains at its initial (feed) value. The second case is when $\frac{\partial B}{\partial x} = 0$, hence B = constant. This corresponds to breakage from any size to an infinitisimally small product (a powder). The fractional rate of breakage of size x is a constant equal to $\kappa(x)$, giving an exponential decay. The third case is when the following equation is true:

$$\kappa(x) \frac{\partial B(x,\alpha)}{dx} = C \qquad 2\text{-}15$$

where C = constant

This gives:

$$\kappa(\alpha) = C\alpha \qquad 2\text{-}16$$

and

$$B(x,\alpha) = \frac{x}{\alpha} \qquad 2\text{-}17$$

The solution to equation 2-14 for this case is:

$$[1-f(x,t)] = [1-f(x,o)]e^{-Cxt} \qquad 2\text{-}18$$

This solution states that all the material above size x decays exponentially as if it were of size x. This can be seen by realizing that $[1-f(x,t)]$ is the fraction of material larger than size x.

In practice it has been found that none of the above degenerate cases are useful in describing real systems. Instead, the continuous size distribution is divided into small discrete intervals, and the mass balance is formulated for the i^{th} interval (46,47,48,49).

$$\frac{dw_i(t)}{dt} = \sum_{j=1}^{i-1} b_{i,j}\, k_j(t)w_j(t) - k_i(t)w_i(t) \qquad 2\text{-}19$$

where $w_i(t)$ = fractional weight of the i^{th} interval at time t

$b_{i,j}$ = the weight fraction of material in the j^{th} interval that breaks to the size in the i^{th} interval

$k_i(t)$ = the fractional weight of breakage of the amount in interval i at time t

By making the assumption that $\kappa_i(t)$ is independent of time, $\kappa_i = \frac{1}{w_i(t)} \frac{dw_i(t)}{dt}$, Reid (46) was able to obtain an analytical solution to equation 2-19:

$$w_i(t) = \sum_{n=1}^{i} a_{n,i}\, e^{-\kappa_n t} \qquad \text{2-20}$$

where

$$a_{n,i} = \sum_{j=n}^{i-1} \frac{\kappa_j b_{i,j} a_{n,j}}{\kappa_i - \kappa_n} \qquad n \neq i \qquad \text{2-20a}$$

$$a_{i,i} = w_i(o) - \sum_{n=1}^{i-1} a_{n,i} \qquad n = i \qquad \text{2-20b}$$

The assumption of $\kappa_i \neq \kappa_i(t)$ is justified if $\kappa_i = \kappa_{i+1} = \kappa$ for all i since then $\kappa_i = \frac{1}{w_i(t)} \frac{dw_i(t)}{dt}$, a constant for all intervals and all species degrade at the same rate. A second case where the assumption is justified is when one κ ($\kappa=\kappa_n$) is controlling, and all other κ's ($\kappa=\kappa_i, i\neq n$) satisfy the criterion $\kappa_i \ll \kappa_n$ ($i\neq n$).

Reid cites some work where it has been found experimentally that the time-independence of κ_i is justified but concludes that, in general, the assumption cannot be made a priori. Using experimental results to obtain the breakage function, b_{ij}, Reid calculated the selection function and obtained good agreement between the predicted and actual size distributions.

Herbst and Fuerstenau (49) were able to show that, using the same assumptions as Reid (46), it is not necessary to have the complete breakage function to estimate the selection function if a single-sized feed is used. The selection function for the largest interval must be known and it is assumed that the size distribution is of a particular type with some, but not all, of the distribution parameters specified. The size distributions produced by ball-milling dolomite were closely predicted by Herbst and Fuerstenau using the above treatment of the comminution equation.

Using the same practical equation (2-19) as Reid, and Herbst and Fuerstenau but without the assumption of time-independence of the selection function, Klimpel and Austin (48) obtained numerical solutions. Like Reid, they obtained the breakage function directly from experimental results. The selection functions were then determined by curve fitting. The curve fitting was complex because the selection function is now variable with both time and size interval, i.e. $\kappa = \kappa_i(t)$. The problem was simplified by assuming either a logarithmic or polynomial dependence of κ on size with only the appropriate coefficients to be determined. The two materials examined, anthracite coal and limestone, were found to have selection functions that were strongly dependent on time.

The work done on comminution has been, thus far, tested with results obtained in commercial equipment. In these circumstances it does not appear possible to theoretically derive relationships for the breakage functions. The one exception is Herbst and Fuerstenau, who have been able to do so because of the restrictive assumptions of single-sized feed and functional form of product distributions. Thus the solution of the comminution problem, with respect to obtaining a completely predictive model, does not seem close.

2.5 SHEAR DEGRADATION OF MACROMOLECULES

The mechanical degradation of polymer molecules has been studied by a number of workers (50-60). The shear stresses required to cause molecular breakage have been generated either by high speed stirring or by an ultrasonic source. In ultrasonic degradation, frequencies in the neighbourhood of one megahertz are usually employed. As shown by Gooberman (51), the length of the cavitation pressure wavefront is roughly of the same order of magnitude as the molecular dimensions. Further, the wavefront passes before appreciable flow of the solvent occurs (51). Thus there is little or no orientation of the molecule before it is presented to the stress gradient. This is in contrast to degradation caused by high shear rate stirring as studied by Minowa et al (50) and others (57-59).

In this case, the evidence is that the molecular configuration is altered by the flow that also generates the breakdown forces.

There has been no attempt to elucidate the mechanism of breakdown for high speed stirring (50) although Mostafa (61) and Gooberman (51) have tried to relate the shear stresses developed in ultrasonically induced degradation to molecular bond strengths. Forms of the rate equations which have been used include:

$$\frac{dM_t}{dt} = -k_1 M_t \qquad \text{2-21}$$

and

$$M_1 \frac{d(1/M_t)}{dt} = k_2 \qquad \text{2-22}$$

where t = time measured from initiation of shear

M_t = weight average molecular weight at time, t

M_1 = limiting molecular weight, below which degradation does not occur

k_1, k_2 = rate constants

Minowa et al (50) have concluded that neither of the above equations apply for breakdown induced by high speed stirring.

Ovenall and coworkers (53) postulated a breakdown of the following form:

$$\frac{dB_i}{dt} = k_3(P_i - P_e)n_i \qquad \text{for } P_i > P_e$$
$$= 0 \qquad \text{for } P_i \leq P_e \qquad 2\text{-}23$$

where $\frac{dB_i}{dt}$ = rate of breakage of molecules of degree of polymerization (DP), P_i, per unit volume

P_e = degree of polymerization below which molecules will not break

n_i = number of molecules of DP P_i

k_3 = a rate constant independent of DP of i and n_i but a function of the experimental conditions, e.g. polymer, solvent, intensity of shear etc.

Assuming that only fragments larger than $P_e/2$ are formed and that all bonds are equally likely to break, equation 2-23 yields upon integration:

$$\frac{B_b}{n_o} = \left[\frac{4P_o}{3P_e} - 1\right] - \left[\frac{4P_o}{3P_e} - \frac{1}{2}\right] \exp\left(-\frac{3}{2} k_3 t P_e\right) - \left[\frac{P_s}{P_e} - \frac{1}{2}\right] \exp\left(-\frac{1}{2} k_3 t P_o\right) \qquad 2\text{-}24$$

where B_b = number of bonds broken after shearing for a time, t

t = time of shearing

n_o = original number of molecules present

P_o = degree of polymerization of starting material

If the starting material is polydisperse, then equation 2-24 can be applied with P_o equal to the number average DP.,

$$(P_o)_{polydisperse} = \frac{\sum_{i=1}^{\infty} P_i n_i}{\sum_{i=1}^{\infty} n_i} \qquad 2\text{-}25$$

Jellinek and White (64) derived an equation of the form:

$$\frac{dB_i}{dt} = K_4(P_i - P_e)(P_i - 1)n_i, \quad P_i > P_e \qquad 2\text{-}26$$

where K_4 = rate constant

assuming that any bond could be broken at random. Because the integration of equation 2-26 gave mathematical difficulties, it was modified to the form:

$$\frac{dB_i}{dt} = K_4' (P_i - 1)n_i \qquad P_i > P_e$$
$$= 0 \qquad P_i \leq P_e \qquad 2\text{-}27$$

The integrated form, analogous to equation 2-24 is:

$$\frac{B}{n_o} = \left[\frac{2P_o}{P_e} - 1\right] - \left[(\frac{2P_o}{P_e} - 1) + K_4'(P_o - P_e)t\right] \exp(-K_4' P_e t) \qquad 2\text{-}28$$

Minowa et al (50) compared calculated results from both equations 2-24 and 2-27 with experimentally determined results for shear degradation, and found that a choice between them was impossible. Ovenall (62) made the same comparison for ultrasonically degraded materials and arrived at the same conclusion.

Jellinek and White (55) have also integrated equation 2-27 in a form that allowed them to calculate the molecular weight distribution if the starting material was monodisperse. They tested this experimentally with ultrasonically degraded polystyrene and found satisfactory agreement.

Two items are worthy of note in the work in shear degradation. First, no experimental or theoretical attempt has been made to relate the degradation due to fluid shear with the shear stress developed. The effect of shear stress is included in the rate constant which becomes a function of the stress. This is caused by the difficulties inherent in calculating the shear stress in the equipment used due to its complex geometry (e.g. see ref. 50). Minowa et al (50) report a rate constant that varies linearly over a 3:1 range of impeller speeds. The use of the rate constants found by these workers is limited to the particular equipment which they have used. This criticism also implies that such parameters are limited in value, when it is attempted to gain some insight into the degradation process.

The second finding of significance is that it appears that both equations 2-24 and 2-28 apply equally well to fluid shear or ultrasonically caused degradation. It has been found that both the solvent and temperature at which the degradation is performed affect the degree of degradation (59,50), indicating that the molecular configuration is important. Degradation levels do not necessarily increase when the solvency is increased. Most work has been carried out at weight or volume concentrations in the range of 1-2%, so that this variable which could give information regarding molecular configuration during breakdown has not been investigated. If there were appreciable straightening of the molecules under the influence of the solvent flow, the parabolic force distribution found by Mason and co-workers (34) could be applied, at least as an approximation. The degraded molecular weight distribution would be different from that based on the random break assumption. In fact, it seems that breakdown proceeds in the same manner for both shear and ultrasonically induced degradation, insofar as distribution of breaks is concerned. Thus it may be concluded that the degradation of long-chain flexible molecules is not comparable to the breakdown of rigid particles.

2.6 SUMMARY OF THE RELEVANT LITERATURE

The findings available in the literature and reported in detail in sections 2.2 to 2.5 are briefly given, in summary, below.

2.6a The dispersion of carbon black in rubber has received much attention but all results have been qualitative in nature. This stems from the extreme complexity of the rubber-carbon black system, and more knowledge is required about the nature of the carbon black structure and its interaction with the rubber. Progress in solving the dispersion problem has been retarded by the lack of a quantitative, unambiguous measure of the deagglomeration achieved in the dispersion process.

2.6b Work in conjunction with the dispersion of additives in plastics has been concentrated on the mixing process. The achievements in this area have been considerable, particularly where simple mixer geometries are concerned. In contrast, deagglomeration has received little attention and the reported work either lacks experimental confirmation of the proposed theory or is strictly empirical. McKelvey (22) has performed a simple analysis of deagglomeration in which an agglomerate composed of two, equal-sized spheres is examined. His model yields behaviour of the agglomerate that is at variance with the known behaviour of two-sphere interactions, probably due to some questionable assumptions. Bolen and Colwell (30) developed a semi-empirical model for the deagglomeration process. They did not provide any experimental evidence, and an examination of the proposed equation reveals some apparent inconsistencies. Smith (31) published some semi-quantitative results for the deagglomeration of different pigments. He found that breakdown proceeded linearly with time, but that the rate depended on the particular pigment. There was no theoretical justification for his data.

2.6c The work reported, primarily by Mason and co-workers, on the behaviour of simple, well-defined particles and agglomerates during shear has yielded many significant results. The determination of the distribution of hydrodynamic forces, as well as the descriptions of particle-particle interactions and orbits is of particular interest, although not directly applicable to agglomerates of arbitrary shape and structure. Nevertheless, insight is gained into particle behaviour and the results provide a starting point for the analysis of limiting cases, such as a linear agglomerate.

2.6d Work on the comminution process has resulted in some fundamental relationships based on the derivation of the mass-balance equation for the system. The impetus for this work was provided by Epstein (44) who proposed the concepts of a breakage function and a selection function to determine how and when a particle degrades. However, the models, thus far have been tested with results obtained in complex, industrial-type equipment. Under these circumstances it has not been possible to derive the breakage function theoretically. In every instance reported, the breakage function has been found experimentally using a portion of the data. The model is then tested on the remaining data for that particular system. This difficulty can be avoided by making some restrictive assumptions about the breakage function or the product distributions, but the general applicability of these assumptions has not been demonstrated.

2.6e The work done on the mechanical degradation of polymer molecules has not established a quantitative relationship between shear stresses and kinetic parameters. There is considerable doubt about the degradation mechanism, and models for the process are generally proposed on a semi-empirical basis. Progress has been hampered by conducting experiments in devices of complex geometry, thus precluding the determination of the shear field. Jellinek and White (55) have successfully predicted the change in size distribution of an initially monodisperse polymer as a result of shear degradation, but they have not related it quantitively to the shear conditions.

2.7 OBJECTIVE OF THE PRESENT WORK

The present work attempts to deal with the deagglomeration process as occurs during the dispersion of solids in plastic melts. An effort is made to avoid those difficulties and complications which other workers have encountered, and to achieve results that are of practical interest. Emphasis is put on the study of systems that can be treated theoretically, although this may result in analyzing systems that are simplistic compared with commercial practice. The main components of this work are outlined below.

2.7a Definition of the problem: As stated above it has been decided to work mainly on the problem of deagglomeration. As stated in previous sections, mixing has received much successful study and, so far as possible, it will not be treated here.

2.7b Selection of the System: It is desirable to choose a system that involves simple experimental techniques and analytical procedures. In addition it must be amenable to reasonable theoretical analysis. For reasons that will be given later, it has been found that a system of artificially-made agglomerates of glass beads in a matrix of polyethylene glycol satisfies the above criteria. The shear field produced in circular Couette flow has been found to be suitable for the purpose of this work. (Chapter 3).

2.7c Theoretical Analysis: A model for the process should be as simple as possible, consistent with providing an accurate description. The proposed model allows the calculation of agglomerate size distribution as a function of time and shear stress. (Chapter 4).

2.7d Analysis of the Results and Testing of the Proposed Model: The results are analyzed from the points of view of experimental error and techniques. Experimental data are compared with predictions obtained from the proposed model. A brief comparison is made between this work and previously cited work on deagglomeration. Finally, some comments are made regarding the model's utility and possible extension to commercial systems. (Chapters 5 and 6).

Each of the above components will be dealt with in detail in the following chapters.

CHAPTER 3

EXPERIMENTAL

3.1 GENERAL CONSIDERATIONS

It is apparent from the discussion in Chapter 2, that previous experimental work on the deagglomeration process is difficult to interpret except in a qualitative or semi-qualitative manner. This is due to the complex flows found in the commercial types of mixers employed and has resulted in the absence of any meaningful model for the process. To avoid this difficulty three flows for which the applied shear stresses could be determined were considered for this work. These flows are: Poiseuille flow in a tube, plane Couette flow, and circular Couette flow. Poiseulle flow was rejected because the shear stress is non-uniform across the tube cross-section. Plane Couette flow, although attractive because of its uniform shear stress field, is difficult to realize experimentally and was not used for this reason. Circular Couette flow was chosen as a compromise between the Poiseuille and plane Couette flows.

It has the disadvantage that the shear field is inherently non-uniform across the gap between the two cylinders, but this variation can be made small if the gap width is small in relation to the cylinder radii. Van Wazer (4) recommends a gap-to-radius ratio of about 0.05. The cup-and-bob implementation of circular Couette flow is unsatisfactory for this work. Preliminary calculations show that if a small clearance between the end of cup and the bob is used, then the power requirements would be unreasonably large for high viscosity fluids. A small clearance is desirable to minimize the amount of polymer and agglomerates used. The second disadvantage is a practical one - with hot viscous fluids, such as polymer melts, cleaning the apparatus would be difficult.

Thus, the alternative of sealing one end of the gap was considered. This, however, introduced an unknown end effect. To estimate the magnitude of this end effect, the equations of motion and energy were solved for the proposed apparatus using appropriate boundary conditions and material characteristics. It was necessary to solve the equations numerically, and the method is given in Appendix I. The calculations showed that, for the anticipated apparatus dimensions, the end effects were negligible for 80% of the gap height.

Based on the above arguments, a circular Couette flow apparatus was designed and constructed as detailed in the following two sections.

3.2 DESIGN CRITERIA AND DIMENSIONS OF THE APPARATUS

The following constraints were applied to the design of the concentric cylinder apparatus with one sealed end:

3.2a The gap should be as large as possible to give a large gap width/agglomerate size ratio and to minimize wall effects.

3.2b The gap height/gap width ratio, $\frac{h}{w}$, should be large so that a uniform flow field exists over a large proportion of the gap.

3.2c The cylinder diameter/gap width ratio should be large to achieve a good approximation to a linear velocity profile.

3.2d Consistent with meeting the above requirements, all dimensions should be as small as possible to minimize the power requirements and the cost.

Since it was anticipated that the largest agglomerate diameter would be of the order of 100μ, a gap width of 0.150 inches was chosen. This gave a minimum gap width to agglomerate diameter ratio of about 40. The choice was based on the following considerations of possible wall effects.

In the context of the present work, the walls can play two roles. The first is the "classical" wall effect where the flow is disturbed by the presence of the wall. The second effect is the modification of the deagglomeration process due to deagglomeration by collision with the walls. As pointed out in section 2.1, this latter effect is expected to be negligible in the polymer agglomerate systems to be studied. A comprehensive review of the classical wall effect for single particles and suspensions is found in reference (34). The behaviour of single particles at various distances from the wall is well characterized, but this is not true for suspensions of particles. For dilute suspensions, however, the work of Karnis et al (63) shows that under certain conditions the distortion of the velocity profile is negligible. These conditions are quite close to those contemplated for this work, viz. a gap width to agglomerate diameter ratio of 40 and a volume concentration of one percent or less.

On the basis of the numerical solutions to the motion and energy equations, it was decided to make the gap height to width ratio equal to twelve. This gave a depth of ten gap widths where the end effect was negligible. For the chosen gap width, the height would be 1.8 inches, a practical value.

Choosing $(\frac{R_o - R_i}{R_o}) = 0.05$, where R_o and R_i are the outer and inner cylinder radii, respectively, results in an outer cylinder diameter of six inches if $(R_o - R_i) = 0.15$

inches. The proposed value of $(\frac{R_o - R_i}{R_i}) = 0.05$ gives a calculated variation of shear rate across the gap of the order of 5% of the mean value, which was considered acceptable. For example, with an inner cylinder rotational speed of 100 RPM, the shear rate (for a Newtonian fluid) is 204 sec^{-1} at the inner wall, decreasing to 195 sec^{-1} at the outer wall.

Using the conditions given above, the Taylor Number, N_{Ta}, was calculated to be less than 10^{-2} for a fluid of 10^5 poises. Thus no problem was anticipated with Taylor instability since the transition from orderly flow occurs at $N_{Ta} \approx 41.3$ (64).

The final apparatus design was based on the preceding estimates, and the dimensions for the cylinders selected were:

R_i = 2.85 inches, radius of inner cylinder

R_o = 3.00 inches, radius of outer cylinder

w = 0.15 inches, gap width

H = 2.50 inches, gap height

3.3 DESCRIPTION OF THE APPARATUS

3.3.1 Mechanical Arrangement

A schematic diagram of the equipment is shown in Figure 3-1 and a photograph is given in Figure 3-2.

The outer cylinder was fabricated from mild steel in three identical pieces, each being a 120° arc of the circle.

FIGURE 3-1: Schematic Diagram of the Apparatus Showing the Heat Transfer Fluid Circuit

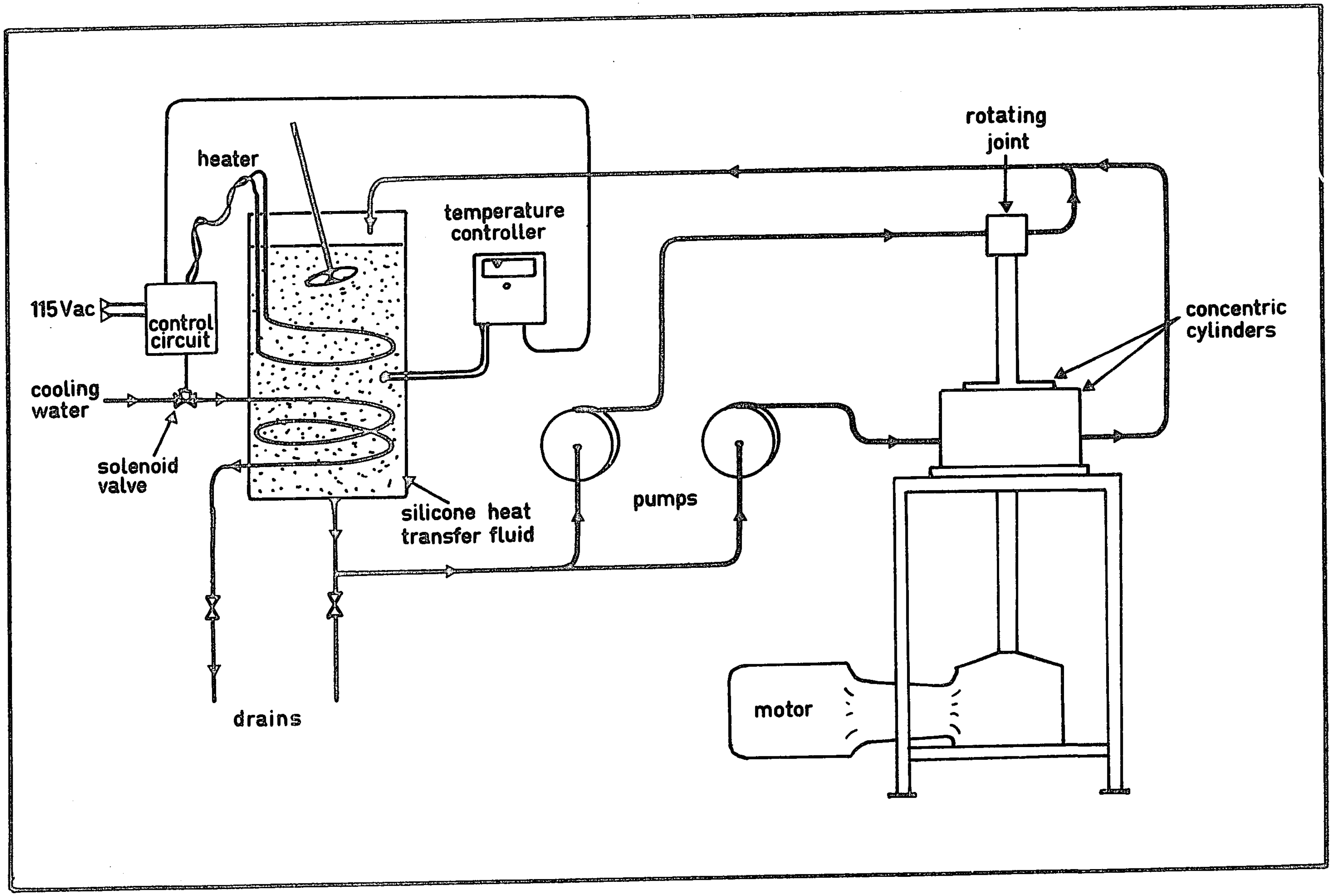

heater
temperature controller
rotating joint
115Vac
control circuit
concentric cylinders
cooling water
solenoid valve
pumps
silicone heat transfer fluid
motor
drains

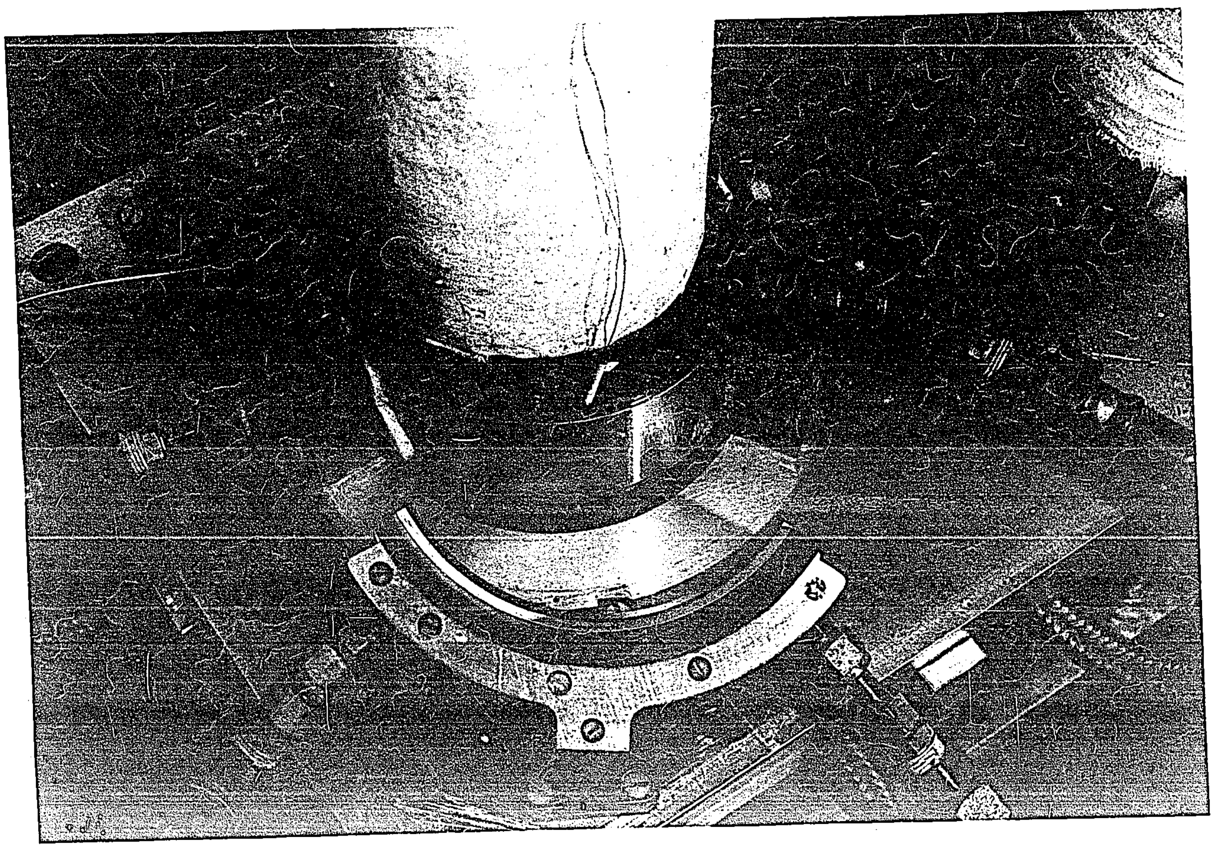

FIGURE 3-2: Photograph of the Concentric Cylinders with the Outer Cylinder Partially Disassembled. Some Solidified Polyethylene Glycol is Visible in the Gap

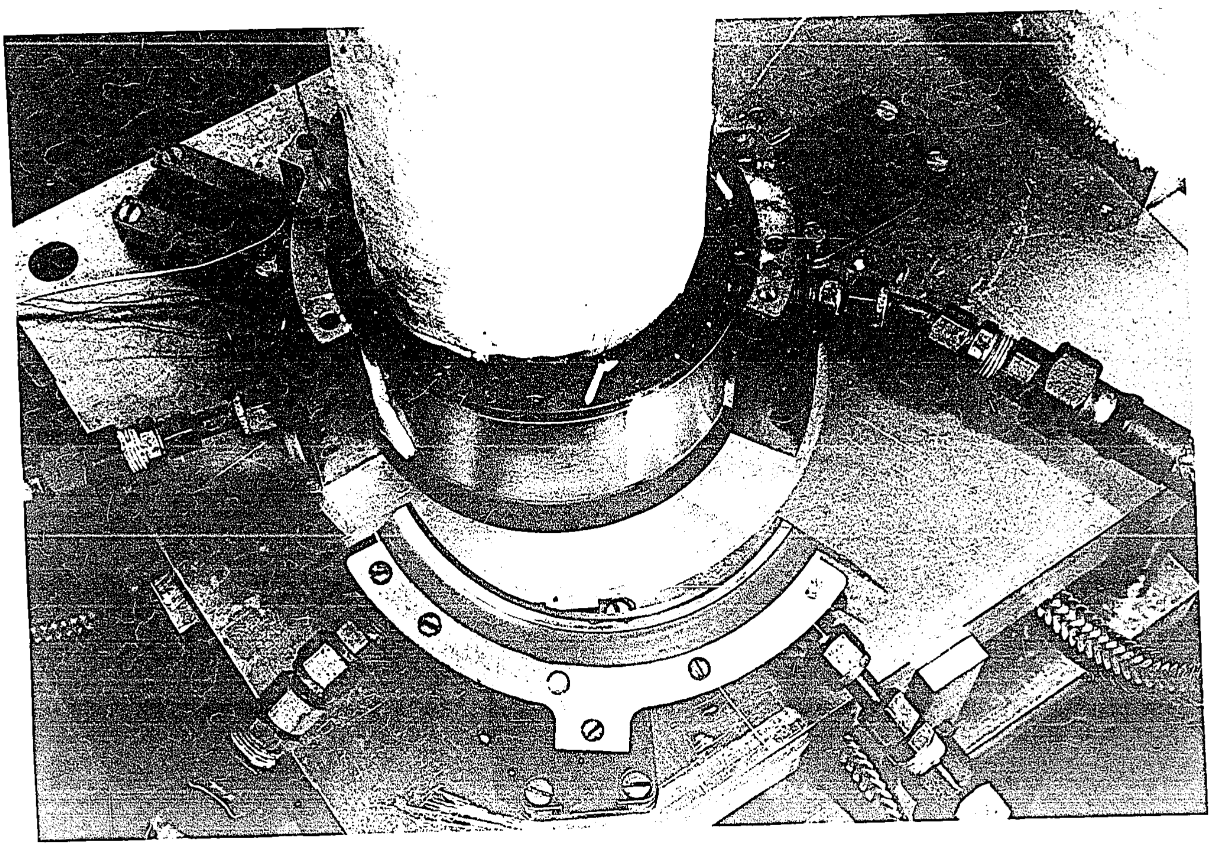

FIGURE 3-2: Photograph of the Concentric Cylinders with the Outer Cylinder Partially Disassembled. Some Solidified Polyethylene Glycol is Visible in the Gap

These pieces were bolted together to form the complete cylinder, but were easily disassembled to remove the solidified sample and clean the apparatus.

The complete cylinder was clamped to a thick base plate and accurately positioned relative to the inner cylinder by three bolts. The bolts were stationed at 120^{o} intervals around the cylinder and travelled in a radial direction. The bolts and their carriers had differential threads that allowed very small increments of travel. By this means the concentricity of the two cylinders could be adjusted to less than 0.0003 inches. The concentricity was verified by a dial gauge accurate to 0.0001 inch. It was found that the adjustments had to be carefully done after the apparatus was at the temperature selected for the experiment. If the adjustment was done at room temperature, the concentricity changed due to the differential thermal expansion of the base plate.

The inner cylinder was positioned by the drive shaft, which extended downwards through the base plate. The base plate was provided with both radial and axial bearings. There was no measurable play in these bearings.

The working surface of each cylinder was hard chrome plated to resist abrasion and to aid in removal of the sample. To ensure roundness, each cylinder was precision ground after all other machining was finished. The maximum deviation from roundness was measured as 0.0004 inches for the inner cylinder and 0.0005 inches for the outer cylinder.

The outer cylinder was fabricated with an integral step that formed the bottom of the gap. (See Figure 3-3). The resulting clearance of 0.010 inches between the step and the inner cylinder was sealed with a polytetrafluoroethylene (PTFE) packing material. The pressure in the packing could be adjusted by a wedge-shaped ring which was threaded onto the inner cylinder. A hole in the base plate allowed access to the ring.

3.3.2 Temperature Control

Temperature control was effected by a heat transfer fluid and reservoir system. The fluid used was a silicone type (Dow Corning 210H) that allowed operation to a maximum temperature of 600°F. Total system capacity was approximately five litres, with the reservoir (ten inch diameter by sixteen inches high) accounting for four litres. The fluid was pumped in two independent streams, one for each cylinder, at the rate of about three litres per minute for each stream. The reservoir contained three heaters of 1 kW each (Chromolox, rod type) and a 3/8 inch copper cooling coil. A four inch diameter, variable speed (0-60 RPM) turbine

FIGURE 3-3: Cross-sectional View of the Concentric Cylinders Showing the Heat Transfer Fluid Flow and Disposition of the Sheared Suspension

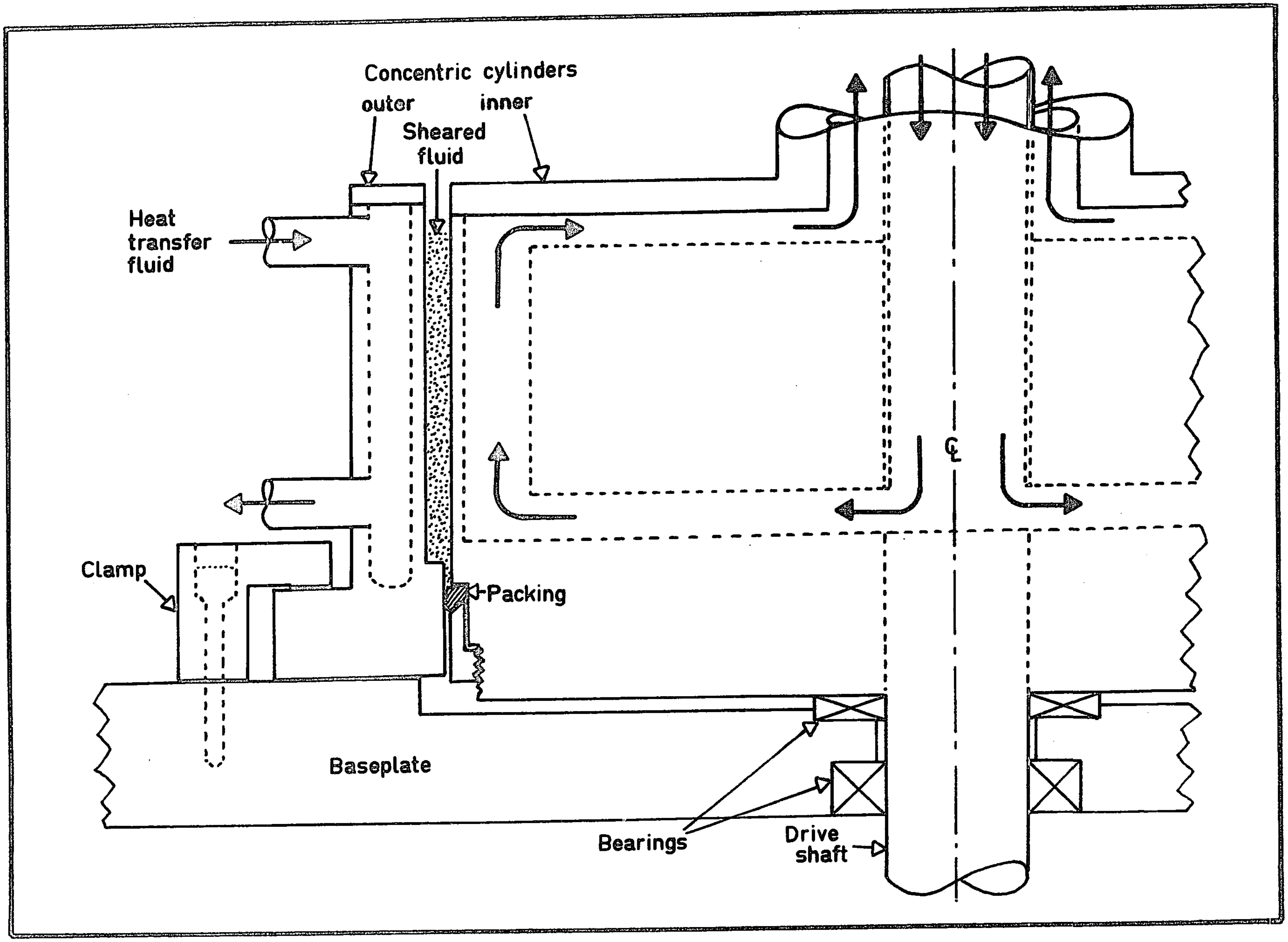
Concentric cylinders
outer
inner
Sheared fluid
Heat transfer fluid
Clamp
Packing
Baseplate
Bearings
Drive shaft
CL

stirrer was installed to aid heat transfer and minimize temperature non-uniformities.

The reservoir fluid temperature was measured by an iron-constantin thermocouple immersed in the fluid. This thermocouple was connected to a West model J controller (range 0-800°F). This unit applied simple on-off control and was connected to two of the 1 kW heaters and to a solenoid valve in the water line feeding the cooling coil. Control action was such that when the two controlled heaters were on, the valve shut off cooling water flow, and vice versa. The third heater was connected directly to the power line through a variable voltage transformer (Powerstat). Power to this heater was adjusted manually and was not switched by the controller.

The temperature stability achieved was $\pm$ 0.5°F short term (approximately 30 minutes) and $\pm$ 1°F for periods up to eight hours. To obtain cylinder temperatures greater than 300°F, it was necessary to insulate the apparatus as completely as possible. The reservoir and the piping were permanently insulated. The cylinder and base plate portion of the apparatus had removable insulation. The insulation was required because of the large heat transfer area which produced large heat losses.

3.3.3 Cylinder Wall Temperature Measurement

Four thermocouples were installed, in both the inner and outer cylinders, at dimensionless heights (referred to the gap width) of 3.3, 6.7, 10.0 and 13.3 above the bottom of the gap. The thermocouples were insulated from the cylinder by two-hole ceramic tubing, and they were held in place by copper oxide cement. After the cement was dry, the thermocouples were ground flush with the cylinder wall (see Figure 3-4).

3.3.4 Measurement of Cylinder Rotational Speed

The inner cylinder speed was measured by means of a magnetic pickup and tachometer.

The steel coupling that connected the inner cylinder driveshaft to the motor driveshaft had fifty equally spaced teeth milled into it. A magnetic pickup of the variable reluctance type produced a pulse as each tooth rotated past it. The pulses were fed to a tachometer that gave a direct reading in revolutions per minute (RPM). The number of teeth and the tachometer were such that a frequency of 60Hz was equal to 72 rpm. Since the power line frequency is accurately controlled at 60 Hz, the calibrations could be readily checked by coupling the tachometer input to the power line.

FIGURE 3-4: Thermocouple Installation in the Cylinder Walls

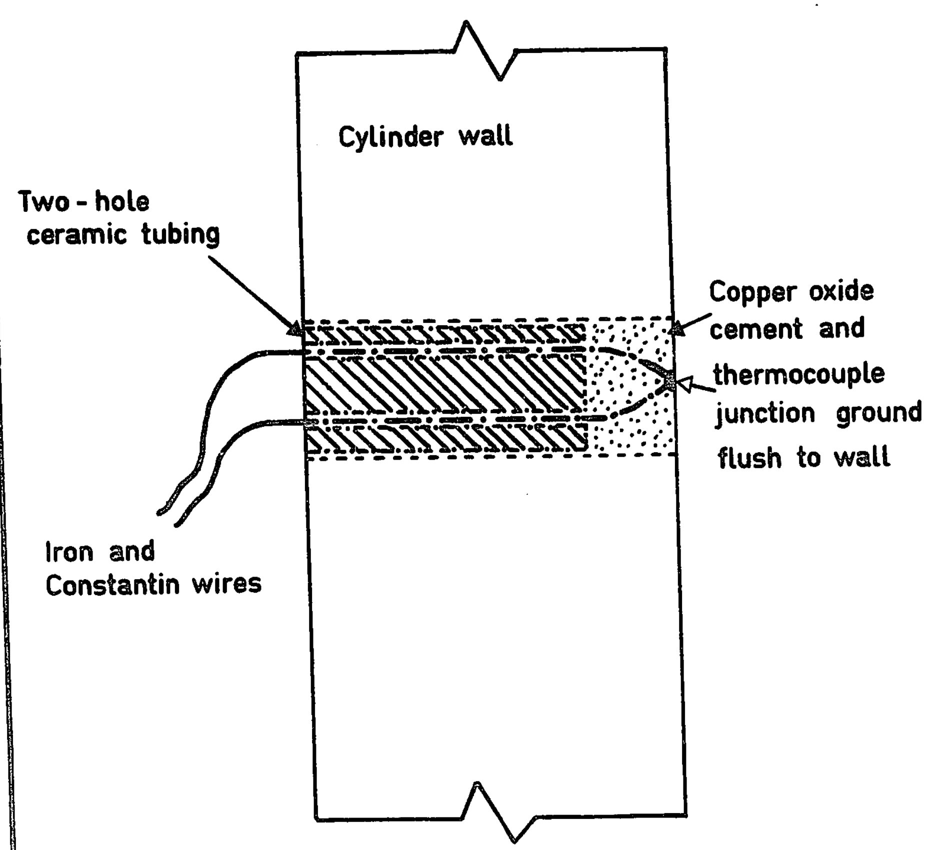
Cylinder wall
Two - hole
ceramic tubing
Copper oxide
cement and
thermocouple
junction ground
flush to wall
Iron and
Constantin wires

3.4 CHOICE OF POLYMER

The original intent of this work was to use commercially available thermoplastic resins such as polyethylene, polypropylene and polystyrene. However, flow instabilities were encountered with this type of polymer and the idea was abandoned. A description of the difficulties and results obtained with polyethylene is given in Appendix II.

Following the failure to achieve a satisfactory flow with high molecular weight polymer melts, other materials were examined. It was desired to have as high a viscosity as possible consistent with small viscoelastic effects (these two requirements are usually contradictory in nature). Further, the polymer had to be available in, or easily convertible to, a solid, powder form at room temperature. Additional desirable properties were;

1. a melting temperature less than 400°F, and
2. the material should have good thermal stability at the melt and experimental temperatures.

Possible candidates that were considered for this study were the polyvinyl alcohols, polyvinyl acetates, polyethylene waxes, crystalline petroleum-based waxes, and the polyethylene glycols. Of these it was found that only the high molecular weight polyethylene glycols were suitable.

The low molecular weight polyethylene glycols are low-viscosity liquids at room temperature. Commercially available solid polyethylene glycols (at room temperature) have nominal molecular weights of 4000, 6000 and 20,000. These substances which are supplied in flake form, are white and crystalline. They melt in the range 130-150°F and exhibit Newtonian behaviour in the shear rate range of interest (see Appendix III). The material selected for this study is a blended polyethylene glycol of approximately 14,000 weight average molecular weight supplied by Union Carbide Canada Ltd. under the trade name "CARBOWAX".

A preliminary trial run with the chosen material indicated that the flow was stable. The flow pattern was examined by placing small (approx. 1 mm^3) packets of carbon black particles at various points in the gap. Except for a small area in the corner where the seal was located, the flow was orderly and laminar, as determined by examination of different cross-sections after varying amounts of shear strain (RPM x time) had been applied. It was found that the tracer particles remained at the point where they had been placed, except for displacement in the circumferential direction. It should be noted that all of the foregoing runs were conducted with the top of the gap open to the atmosphere.

The results showed no evidence of Taylor instability for the largest Taylor number employed ($N_{Ta} \approx 0.24$; viscosity 3.5×10^3 cp, RPM = 120). This is well below the transition point ($N_{Ta} \approx 41.3$) at which viscous instability occurs.

A useful property of polyethylene glycol was its water solubility. This property not only made apparatus cleaning easy, but also allowed the development of a unique method of deagglomeration analysis, as described in section 3.8.

A disadvantage of polyethylene glycol (for this work) was the need to operate the apparatus with wall temperatures within 3-4^{o}F of the freezing temperature of the polymer. Operation in this manner was required to obtain a suitably high viscosity of the melt.

3.5 CHOICE OF AGGLOMERATES

Brief reference has been made in Chapter 2 to the complexity of carbon blacks. This complexity is due, in large measure, to the very small ultimate particle size and broad agglomerate size distribution. These characteristics require the use of an electron microscope, preferably of the scanning type to completely analyze a carbon black size distribution. Unfortunately, the electron microscope is not suited to the analysis of a large number of samples and is costly to use.

As previously mentioned (section 2.2), the oil absorption test for carbon blacks does not yield a satisfactory measure of deagglomeration. For a preliminary study of the deagglomeration process, it has been decided to avoid the complexities introduced by the use of carbon black.

Other commonly used pigments include the metal oxides, of which titanium dioxide and zinc oxide are the most important. Little work has been published on the particle and agglomerate structures of these materials. Published information is very meagre for other pigments such as ferric oxide, cadmium oxides, etc. (65). In the metallurgical field, some embryonic work has been reported on agglomerates formed by the sintering process (66,67).

In view of the above findings, it was determined to produce artificial agglomerates. Other workers have produced controlled agglomerates. Medalia (15) formed closely sized agglomerates of carbon black using a styrene-butadiene resin as a binder. After forming the agglomerates the binder was cured to produce non-degradable aggregates which had diameters in the range 30-50μ. These agglomerates were of very high complexity because the agglomerate size was at least two orders of magnitude larger than the ultimate particle size, and hence, each agglomerate contained very large numbers of the particles. The object of that work was not to disperse the agglomerates, but to introduce a controlled agglomerate to the system under study. Lewis and Nielsen (68) produced artificial agglomerates from soda-lime glass beads. These beads were fused together to give a permanent, strong agglomerate. Such agglomerates are unsuited to this work due to their high strength. Also, the highly ordered, deformable agglomerates produced by Zia et al (40,41) are not suitable for the purposes of the current deagglomeration study.

The method used in this work was an amalgamation of Medalia's (15) method and that of Lewis and Nielsen (68). Soda-lime glass beads of a nominal size range of 10-53u manufactured by Microbeads Division of Cataphote Corporation were selected as the starting material. Polystyrene molding compound, Dow Canada 683C, was chosen as the binder to join the glass beads together in the agglomerate. This compound has a glass transition temperature of 100^{o}C which is above the melting temperature of polyethylene glycol (approx. 60^{o}C). This ensures that the binder will remain rigid at the experimental temperatures.

3.6 PREPARATION OF AGGLOMERATES

The glass beads used in this study were obtained by fractionation of the starting material in an Infrasizer (69), a proprietry air elutriation device. The fraction collected for use contained more than 90% (by number) of beads in the size range 30-35μ diameter. Attempts to produce monodisperse beads by sieving (both normally and ultrasonically agitated) were unsuccessful. Ten runs of the Infrasizer, of three hours duration each, yielded a total of 300 grams in the required size range. This material was blended together and was used as the source of ultimate particles for the artificial agglomerates.

About 125 grams of the ultimate particles were placed in a tall 150 ml. beaker. A 3% (by weight) solution of polystyrene in methylene chloride was added slowly with stirring. In order to achieve even wetting of the beads, a small excess of the solution was used. When the beads had settled, the excess liquid was siphoned off so that just sufficient solution to fill the interstices remained. The methylene chloride was allowed to evaporate slowly at ambient conditions for three days. Then the beads were placed under vacuum, and the vacuum was slowly increased from 0 to 29" Hg over a 12 hour period. When the maximum vacuum level was reached, the sample was kept under these conditions for a further 36 hours.

The beaker was then split by a hot wire glass cutter leaving a monolithic cylinder of beads bound together by the polystyrene. A stack of sieves with the following standard meshes was assembled - 120/170/200/230/270. The monolithic cylinder was placed on the top sieve and the stack was gently tapped and moved circularly. The 120 mesh sieve had a rough surface that tended to knock off agglomerates. The subsequent screens not only sized the agglomerates, but also tended to degrade them. Thus, it was necessary to stop after approximately one minute of sieving to collect the agglomerates. Previous experience showed that the fraction that passed the 200 mesh and was retained on the 230 mesh sieve (-200,+230) gave agglomerates of one to ten beads. This was the fraction that was collected. Care was taken to keep the sieving operation as constant as possible with regard to sieve motion and time between collections. A total of 250 grams of the glass bead-polystyrene mixture yielded about fifteen grams of agglomerates.

Some idea of the nature of these agglomerates can be gained from the photomicrographs in Figures 3-5 and 3-6. Figure 3-6 was obtained by a scanning electron microscope, and clearly shows the solid polystyrene bridges holding the beads together. It was calculated that the amount of polystyrene added, if spread uniformly over the beads would increase the diameter by 0.14μ. Obviously most of the polystyrene was in the bridges and the diameter increase was negligible.

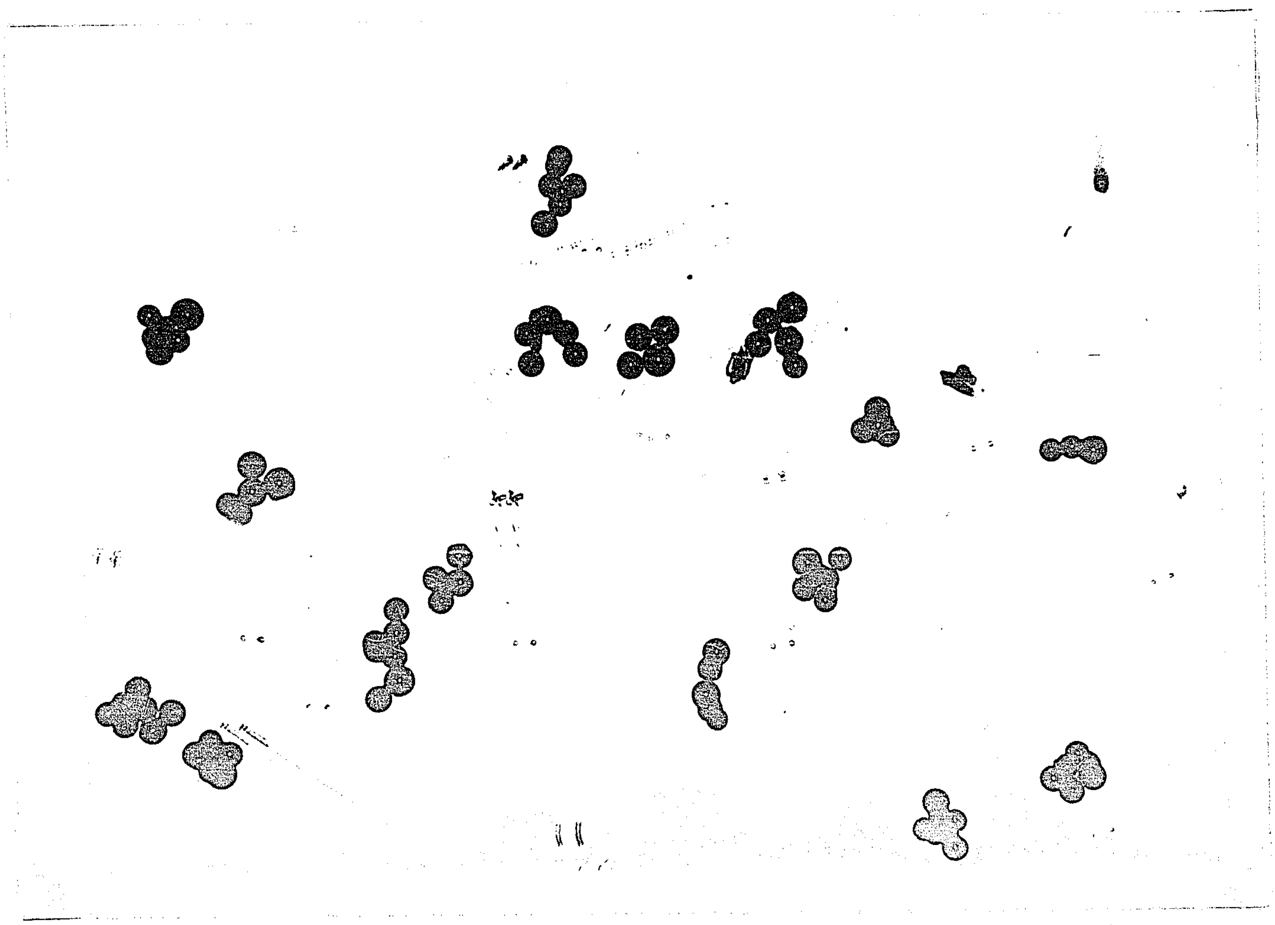

FIGURE 3-5: Photomicrograph of a Random Sample of the Artificial Agglomerates Depicting Various Configurations

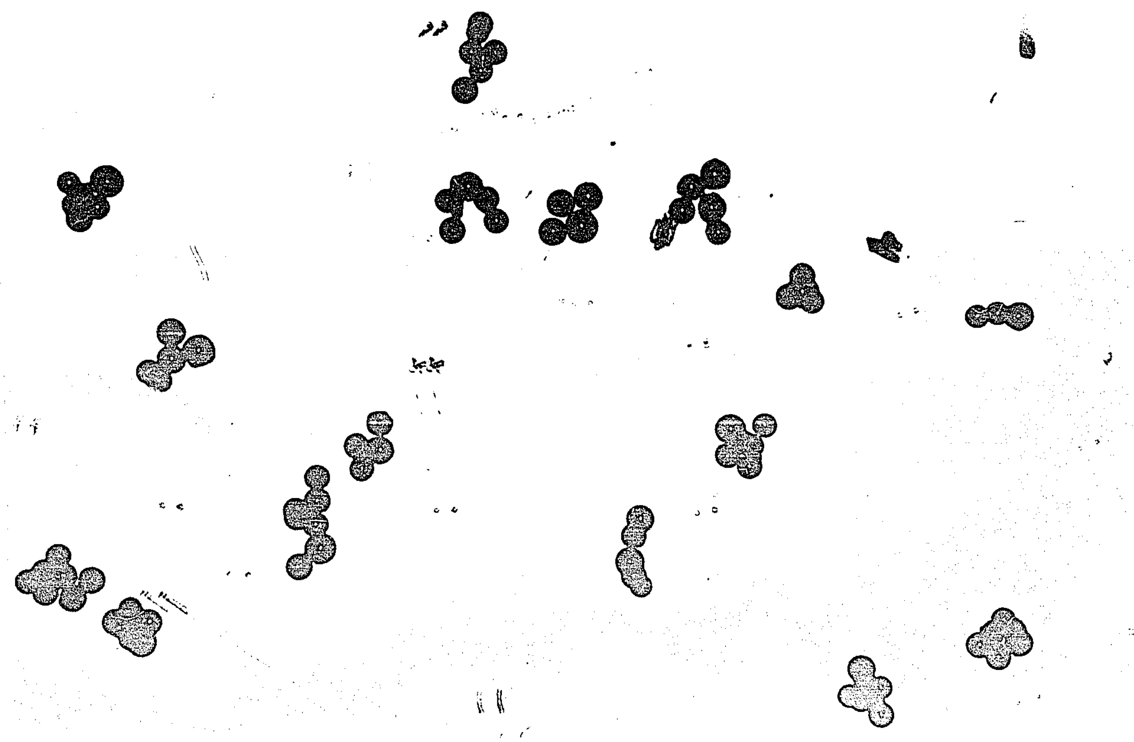

FIGURE 3-5: Photomicrograph of a Random Sample of the Artificial Agglomerates Depicting Various Configurations

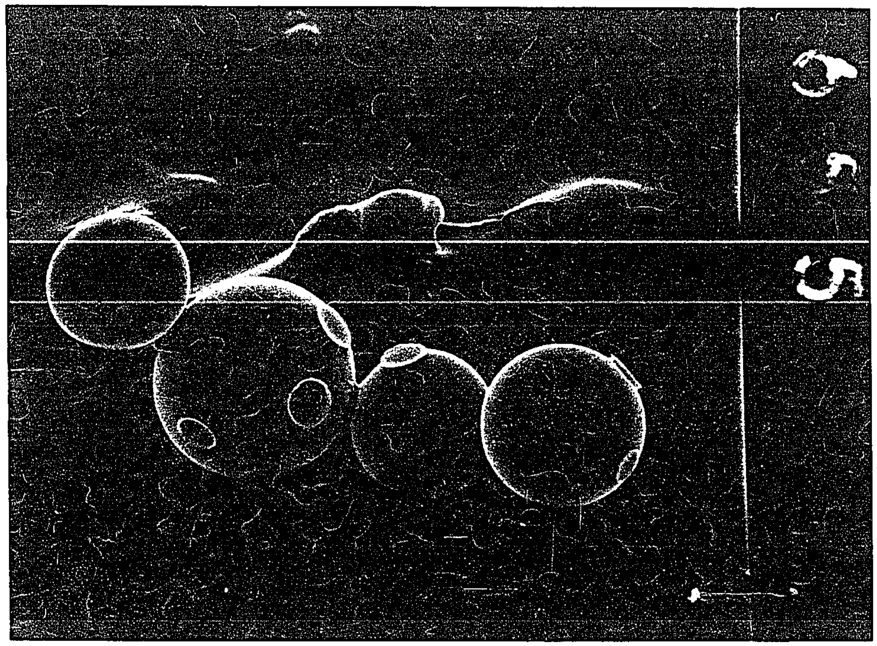

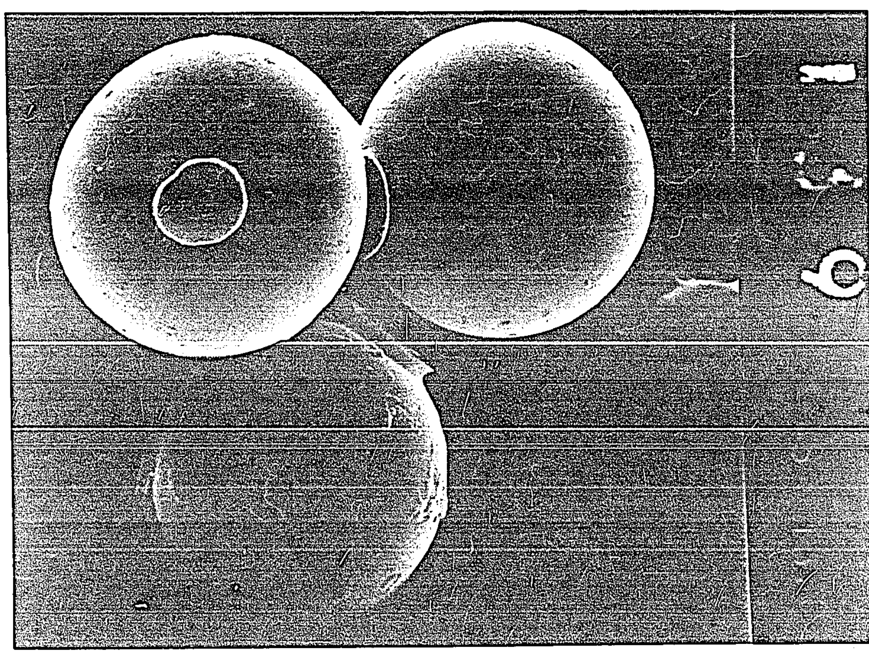

FIGURE 3-6: Scanning Electron Micrographs of the Artificially made Agglomerates. The Polystyrene Bridges Between the Glass Beads are Clearly Visible

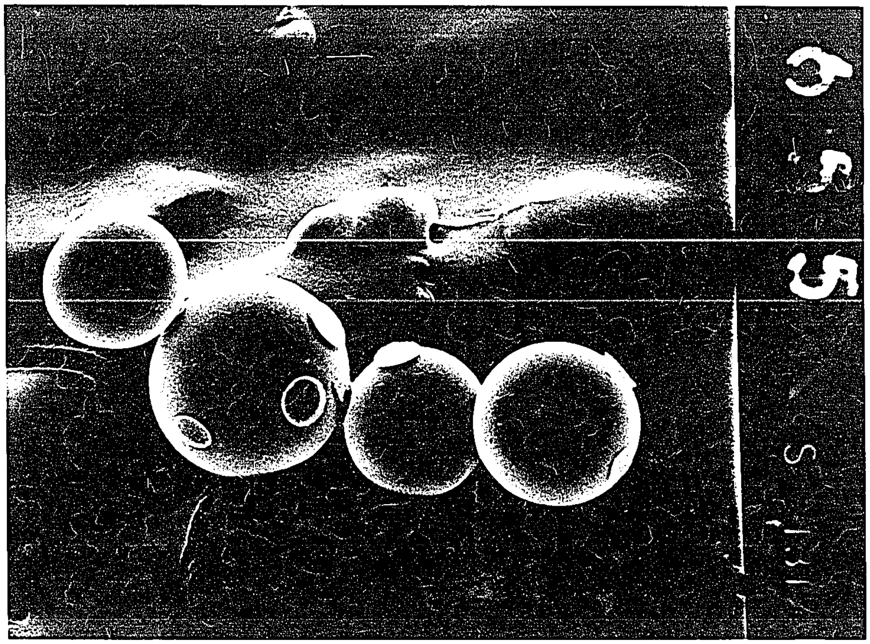

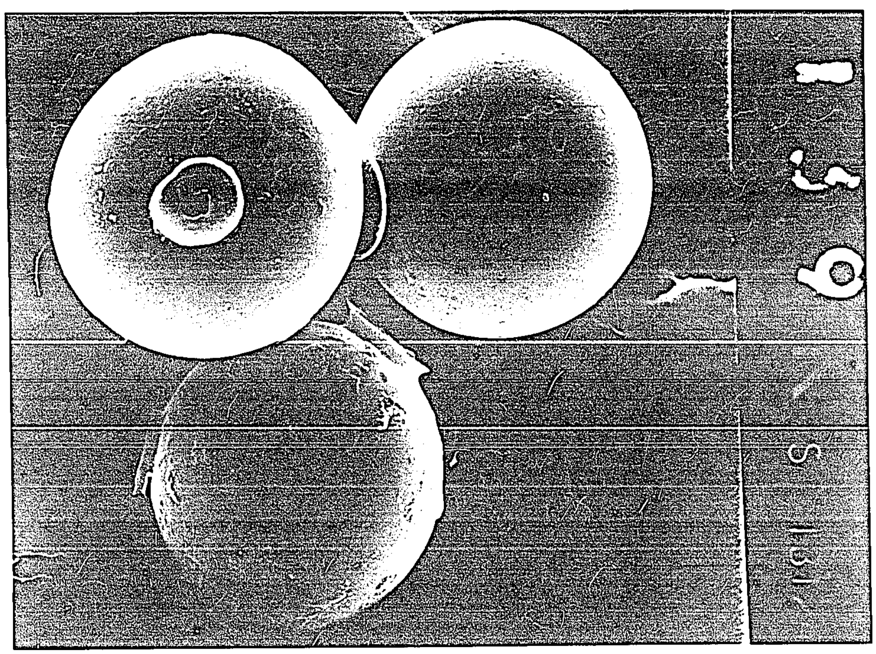

FIGURE 3-6: Scanning Electron Micrographs of the Artificially made Agglomerates. The Polystyrene Bridges Between the Glass Beads are Clearly Visible

3.7 SAMPLE PROBE

The sample probe shown in Figure 3-7, was developed to permit the withdrawal of representative samples of the solid-liquid dispersion.

The probe was constructed from two pieces of telescoping, square brass tubing. The two pieces of tubing were operated as a syringe to extract a sample from the polymer melt-agglomerate suspension. The smaller tube was blocked at both ends to form the plunger with the larger tube acting as the body of the syringe. Appropriate stops were fabricated and attached to the tubes to limit the travel of the plunger and to give samples of a reproducible size.

Operation of the probe was as follows; with the plunger in the fully forward position the probe was inserted into the melt to a chosen depth. The plunger was then slowly retracted to the limit of its travel. The probe was then withdrawn from the melt and put aside to cool. After one minute, the polyethylene glycol had crystallized and the sample was ejected by pushing the plunger to the other limit of its travel. The solid sample, approximately 3/32" x 3/32" x 5/32", was conveniently stored for analysis at a later time and the probe was ready for reuse.

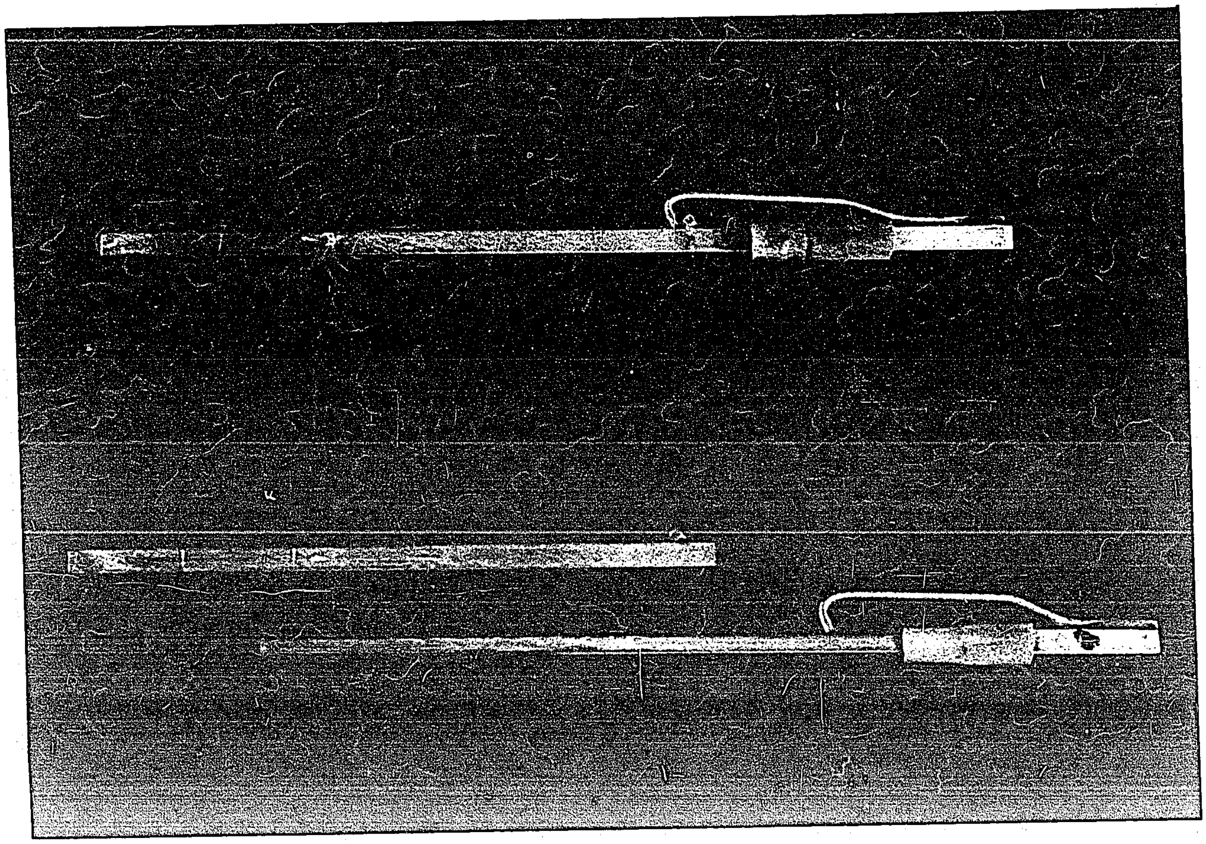

FIGURE 3-7: Photograph of the Sampling Probes Used. An Assembled Probe is Shown Above a Second, Disassembled, Probe

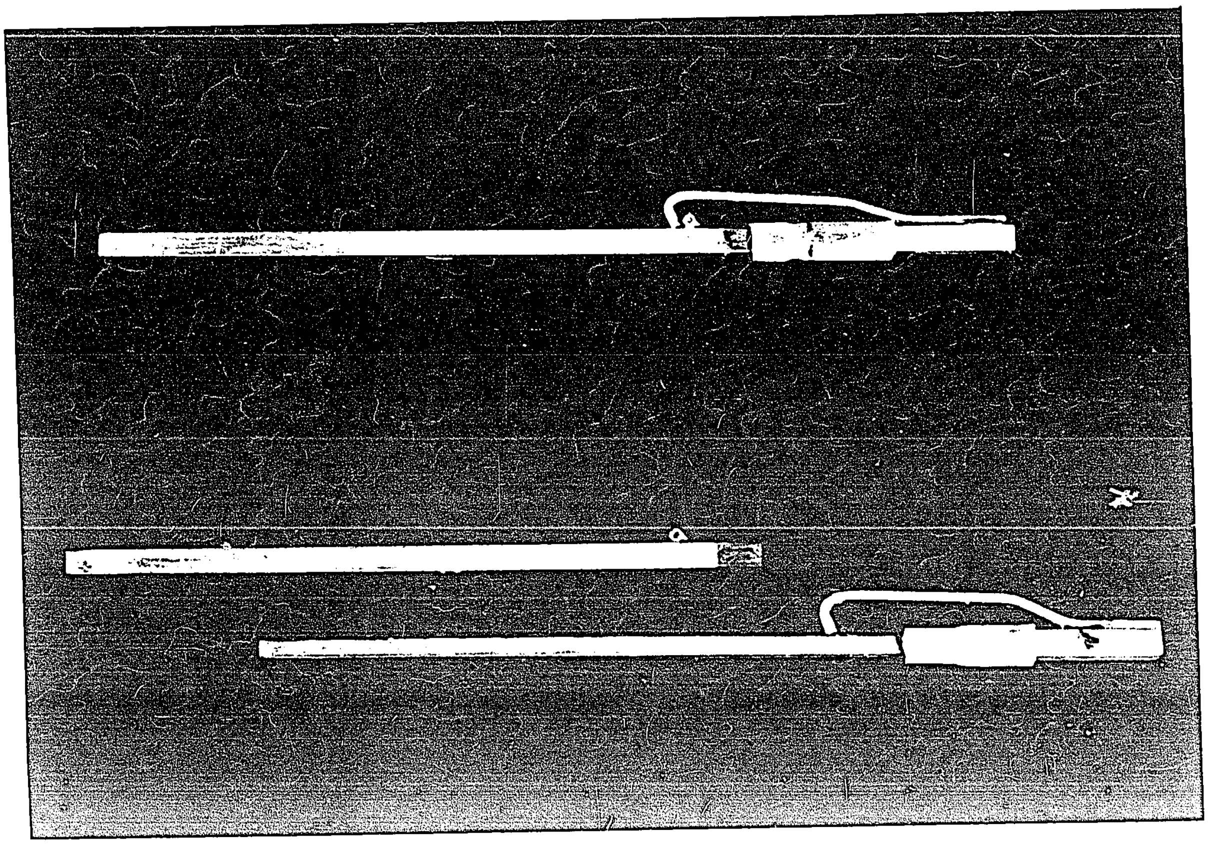

[illegible] Photograph of [illegible] Assembled Pr[illegible] Shown [illegible] [illegible] Disassembled [illegible] Prob[illegible]

3.8 METHOD OF ANALYSIS

A water-tight cell was constructed, as shown in Figure 3.8, from polymethylmethacrylate. Openings were machined into the top and bottom and with glass installed in them, functioned as windows for the cell. A small U-shaped, open-ended cage was fabricated from 60 mesh brass screen. This was attached to the inside of the bottom glass near the centre. A fill tube and a vent tube was installed as shown.

Sample analysis proceeded as follows; the sample to be analyzed was placed in the cage and silicone stopcock grease applied to the mating surfaces of the cell halves. The cell was then assembled and degassed water was transferred to the cell using a squeeze bottle. This was done as quickly as possible with care being taken to completely fill the cell. When filling was complete, both fill and vent tubes were sealed and the cell was inverted.

As the polyethylene glycol dissolved, the agglomerates were released and precipitated to the lower (top) glass surface. If the glass surface was slightly dirty, it was found that the agglomerates would stick and remain at the point of contact with the surface. While the sample was dissolving, it was necessary to manipulate the cell at

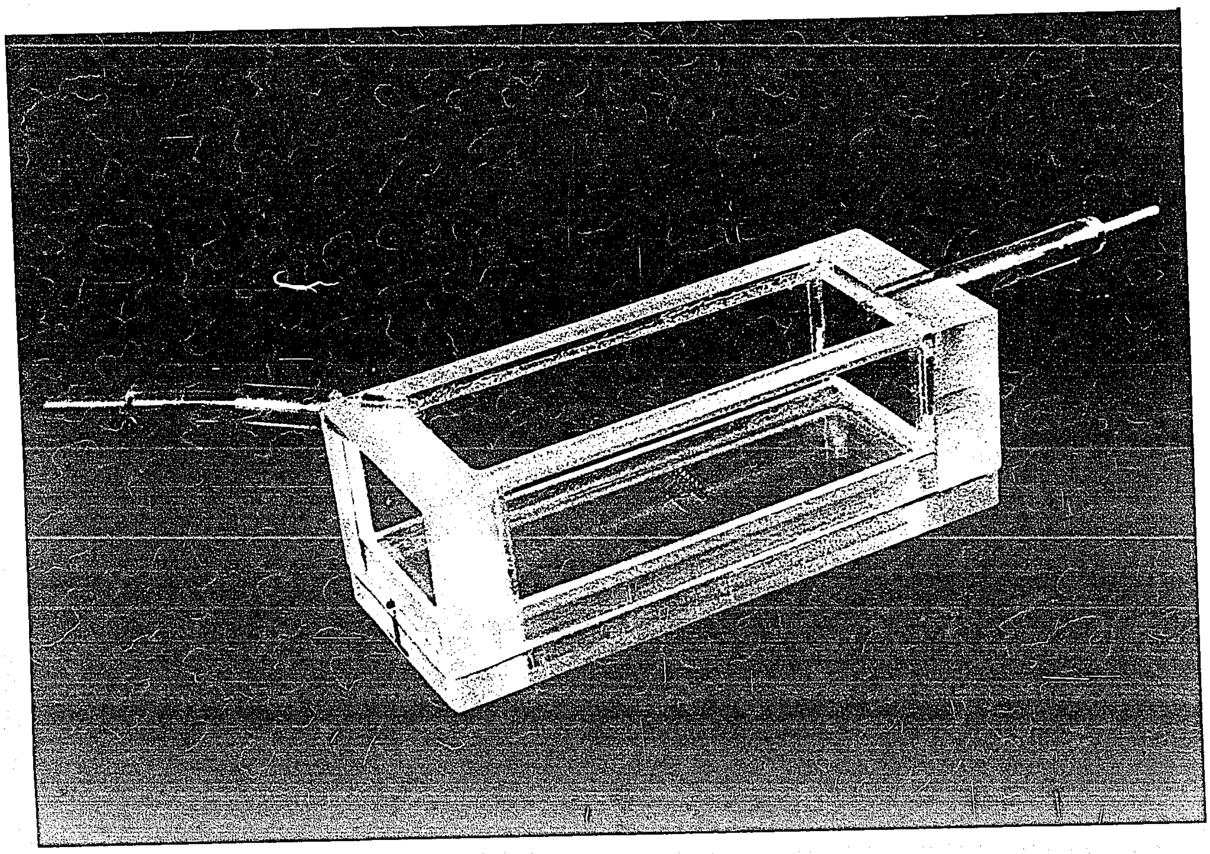

FIGURE 3-8: Photograph of the Cell Used for Dissolving the Sample. The Wire Mesh Cage Can be Seen Attached to the Lower Glass Surface. The Cell is Shown in the Filling or "Normal" Position

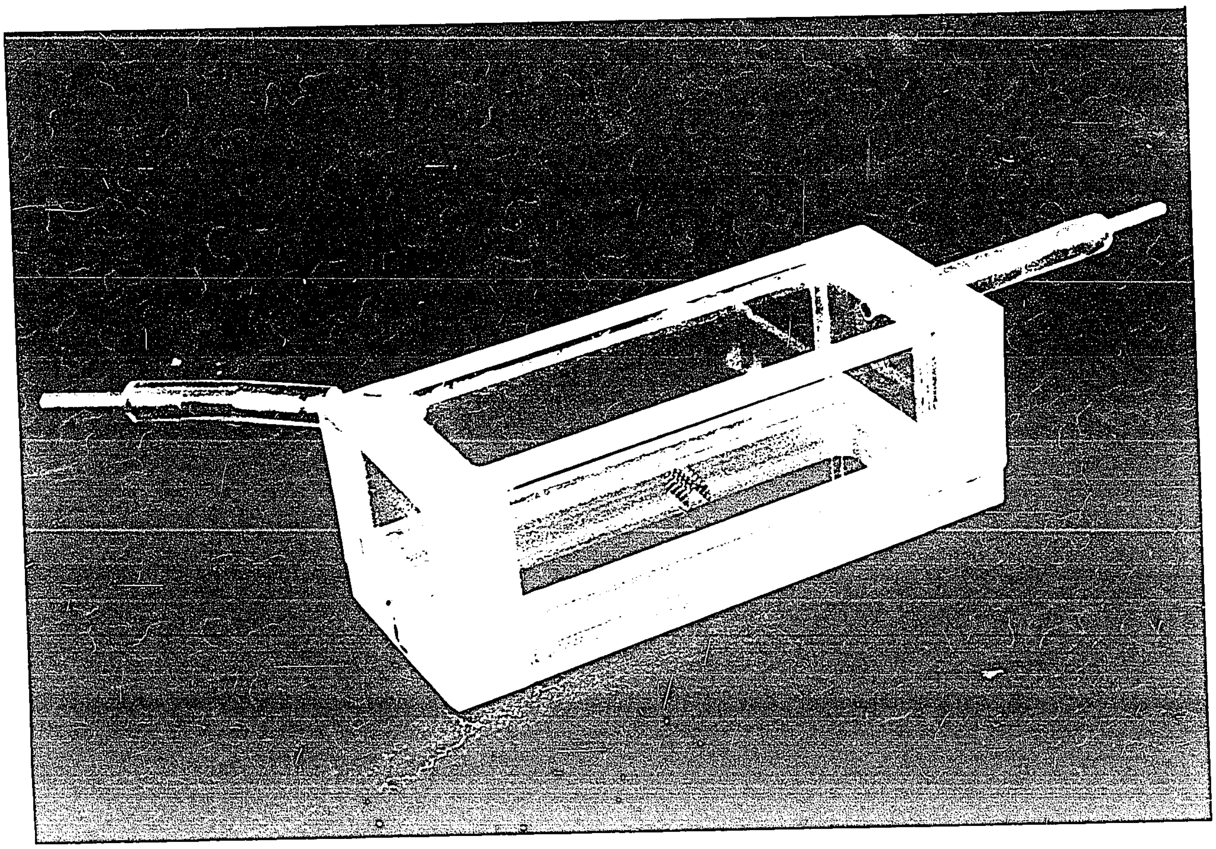

FIGURE 3-[illegible]: Photograph of the Cell Used for Dissolving the Sample. The Wire Mesh Cage Can be Seen Attached to the Lower Glass Surface. The Cell is Shown in the Filling or "Normal" Position

different angles up to thirty degrees from the horizontal to distribute the agglomerates evenly over the surface. If this was not done, the agglomerates tended to precipitate on top of each other and could not be distinguished as separate agglomerates on examination. Viewing the cell against a dark background with a light source directed obliquely towards the observer allowed the precipitating agglomerates to be seen with the naked eye. Depending on the size of the sample, the time required for complete dissolution was about twenty-five to thirty minutes. Ten minutes after dissolution had started, it was necessary to tap the cell gently to dislodge any agglomerates that were adhering to the mesh cage. This tapping was continued at one to two minute intervals until the polyethylene glycol was completely dissolved.

Sample size was important but not critical. If the sample was too large, it was difficult to prevent some agglomerates from precipitating on top of others. If the sample was too small, then more samples had to be analyzed to get a significant number of agglomerates. The optimum sample contained about 2000 to 2500 beads.

After precipitation was complete, the cell, still in the inverted position, was transferred to a microscope stage. The microscope used had a travelling stage with one inch of travel in both the lateral and longitudinal directions. A jig attached to the stage positioned the cell so that it was square with the axes of travel. With the stage at the extremes of its travel, the cell was lined up so that the edge of the field of view coincided with one corner of the cell. The cell was then scanned from one side to the other in the longitudinal direction. As each agglomerate crossed the centre of the field of view, the number of beads in it was counted and a tally made in the appropriate category. Thus, the number fraction versus beads per agglomerate distribution was found for this scan.

When the other side of the cell was reached the stage was stepped,in the lateral direction, a distance equal to the diameter of the field of view and the next scan commenced. At the end of the one inch travel in the lateral direction the cell was shifted one inch and the process repeated. Two cell shifts were required to scan the whole surface and obtain the number fraction vs. beads per agglomerate distribution for the whole sample. Since the precipitation process was not completely random, it was necessary to count all the agglomerates from a given sample.

A combination of transmitted and incident illumination was normally used. By manipulating the relative intensities of each illumination type, it was possible to detect beads that would normally be hidden underneath the agglomerate.

A magnification of seventy-five diameters was found to be convenient for the counting. The counting procedure took between two and one half to three hours depending somewhat on the nature and size of the sample.

3.9 DESCRIPTION OF THE DEAGGLOMERATION EXPERIMENTS

Initially, the polyethylene glycol was converted to a powder by ball milling in a one litre Abbé mill. One half inch steel balls were used, and the milling time was three hours. The powder was sieved, and the fraction that passed sixty mesh was used.

Sufficient powder to fill the gap to a depth of two inches was weighed into a container slightly larger than the volume of powder. A known weight of the agglomerates was added slowly to the powder in small portions. After the addition of each portion, it was mixed with the powder using a spatula. When the addition was complete the container was tightly capped. Further blending was carried out by manually manipulating the container in a tumbling motion about all three axes. These operations were performed gently to avoid, as much as possible, the mechanical breakdown of the agglomerates.

The mixture was then transferred to the heated apparatus via a funnel. When the gap was filled and all the polymer was melted, three samples were taken at each of three different, equally spaced circumferential positions. Generally, samples were only taken at one depth, although, in someruns, additional samples were taken at different depths. The purpose of these samples was twofold. Samples were taken at different positions to check how well the blending operations succeeded in evenly distributing the agglomerates. Secondly, it was necessary to establish the initial number fraction distribution after the blending and filling operations but prior to the application of any shear.

The inner and outer wall temperatures were measured and recorded. All runs were made in the range 140 to 147^{o}F, with the inner wall temperature being about 3.5^{o}F higher than the outer wall.

In the runs having shear stress as the independent variable, the available RPM range was divided into six steps of twenty RPM and the sample was sheared for two minutes at each speed. For the runs with time as the independent variable the speed was selected and the sample was sheared for varying periods of time.

At the end of each step the apparatus was stopped. Samples were then taken at a depth of one-half the depth of the polymer in the gap. Six samples, two each at three equally spaced circumferential positions, were taken. Prior to the next step, cylinder wall temperatures were again measured and recorded. The maximum shift occurred during the 120 RPM runs and was no more than 2^oF.

If the largest agglomerate is estimated to behave as a 100μ diameter sphere, then the settling velocity (Stokes region) is 1.3×10^{-2} in/min. This agglomerate will settle about 0.2 inch during a typical run which lasts twenty minutes. Because the velocity is proportional to the square of the radius, the smaller agglomerates will settle less in a given time. If the spatial distribution of agglomerates in the gap is random, there will be a shift in the distribution only in the top 0.2 inch and bottom 0.2 inch of the gap during the run.

The samples were analyzed as previously described. Usually only three samples at each condition were analyzed, the extra samples being taken as a safeguard against accidental loss of the sample during analysis. The exception to this was the zero shear (initial) samples of which a total of eight were normally counted. Each run gave between thirty to forty samples. Each sample took between three and one-half to four hours to analyze including cell preparation, sample dissolution and counting. Each run thus represents three to four weeks of work.

Since a substantial portion of the experimental work was consumed by the visual counting of the agglomerates, some effort was expended in investigating automated counting techniques. Attempts to use a Quantimet (70) "image analyzing computer" were unsuccessful because of reflections from the beads which gave false counts. A further difficulty resulted from the concepts involved in the operation of the instrument. The Quantimet operates on a two-dimensional projected image. Thus, for the machine, a tetrahedrally arranged four bead agglomerate is indistinguishable from a triangularly arranged three bead agglomerate. Both of these types were frequently found in the present work.

A type of particle analyzer that is almost ideally suited for the present application is the Coulter particle counter. This instrument measures particle volume. A description of its use in counting aggregates of latex particles is given by Kubitschek (71). Unfortunately, the particular configuration of the instrument required for this work was not available to the author.

Many particle sizing methods are based on sedimentation in the Stokes' law region. These, and other methods are reviewed by Herdan (72). In general, these methods require the production of a uniform dispersion in the suspending medium. Because the agglomerates under study are fragile, it is doubtful that a uniform dispersion could be obtained without altering the size distribution.

3.10 MEASUREMENT OF TEMPERATURE PROFILES

The temperature profile across the gap was measured with a probe so as to have a check on the numerical solutions of the equations of motion and energy. The probe, manufactured by Victory Engineering Corp., was in the form of a hypodermic needle with a thermistor embedded at the tip. The needle had a diameter of 0.018 inch (26 gauge) and a length of two inches.

The probe was inserted from the top of the gap. A simple fixture was devised to support the needle and to position it at various locations within the gap. It was necessary to support the needle as close as possible to the point where it entered the polymer melt because of the needle's flexibility. Even so, it was found that the profiles at higher speeds (> 60 RPM) were irregular, probably due to bending of the probe.

The supporting and positioning arrangement is shown in Figure 3-9. The supporting cylinder that also acts as a positioning device was made from polyacetal rather than metal. Polyacetal is preferred because of its lower thermal conductivity and self-lubricating qualities. This support/

FIGURE 3-9: A Diagram Showing the Fixture Used to Mount and Position the Thermistor Probe. The Drawing is Approximately to Scale

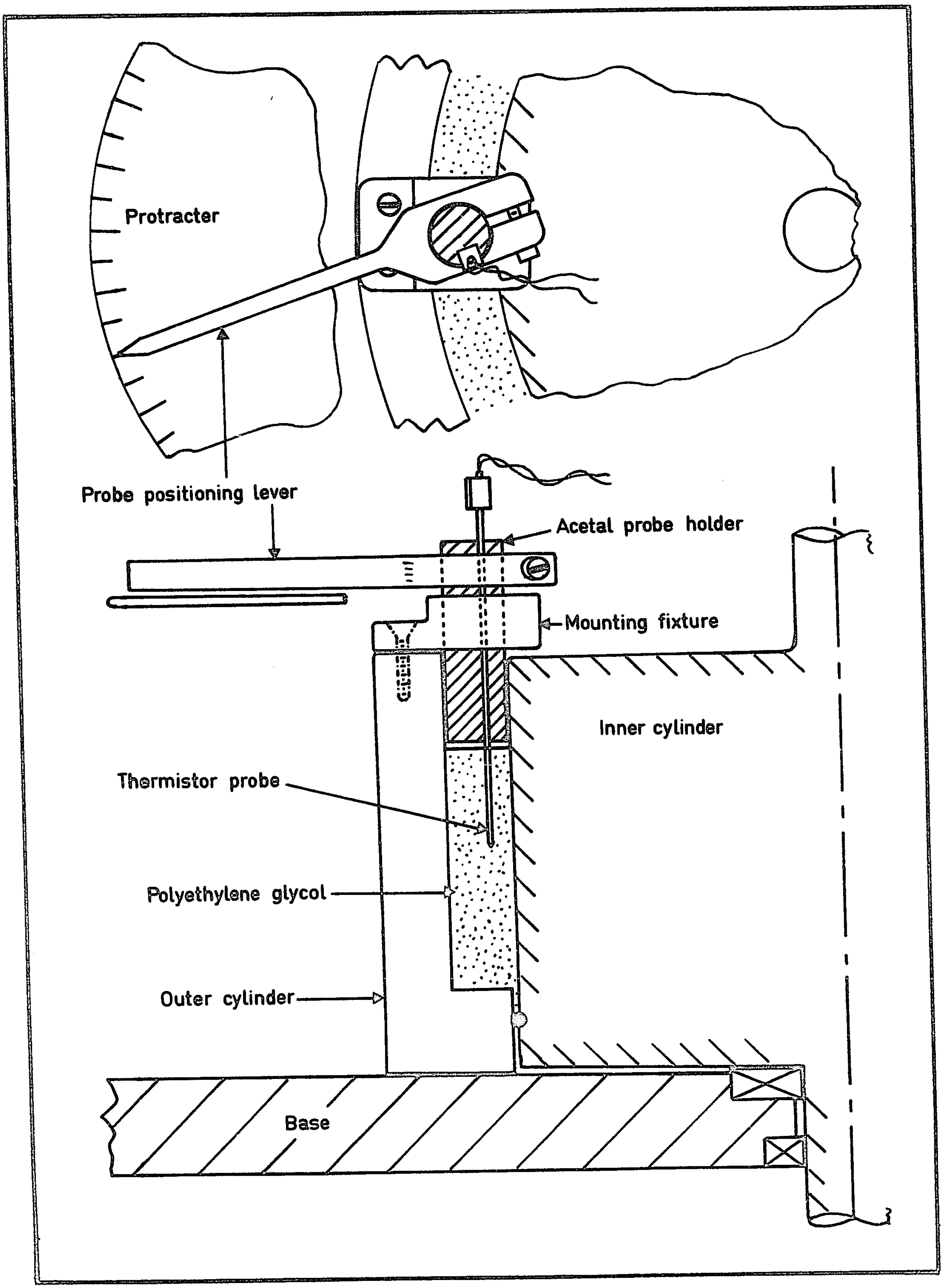
Protracter
Probe positioning lever
Acetal probe holder
Mounting fixture
Inner cylinder
Thermistor probe
Polyethylene glycol
Outer cylinder
Base

positioning cylinder extended down into the gap and stopped about 1/32 inch above the polymer melt surface. The probe position was read by means of a protractor.

The probe comprised one arm in a Wheatstone bridge and the unbalanced bridge voltage fed to a DC amplifier with a gain of, approximately, twelve. Provision was made for adjusting the output of the amplifier to zero volts for any probe temperature in the range 130-155^{o}F. The amplifier and Wheatstone bridge thus converted the change of the resistance of thermistor with temperature to a corresponding voltage change with temperature. Because the temperature coefficient of resistance is non-linear, the voltage change with temperature is also non-linear.

The thermistor-amplifier combination was calibrated with a precision laboratory mercury-in-glass thermometer with 0.1^{o}F divisions. Using a magnifier, temperature differences on the order of 0.02^{o}F could be estimated. The calibration, plotted as the amplifier output voltage coefficient of temperature, $\frac{dV}{dt}$, versus temperature,T, is shown in Figure 3-10.

The probe was used by establishing one cylinder wall as the reference temperature as measured by the thermocouples embedded in it. With the probe in position against this wall, the output voltage was adjusted to zero. The voltage

FIGURE 3-10: Determination of the Thermistor Probe Temperature Coefficient. The Open Circles Represent Experimental Points

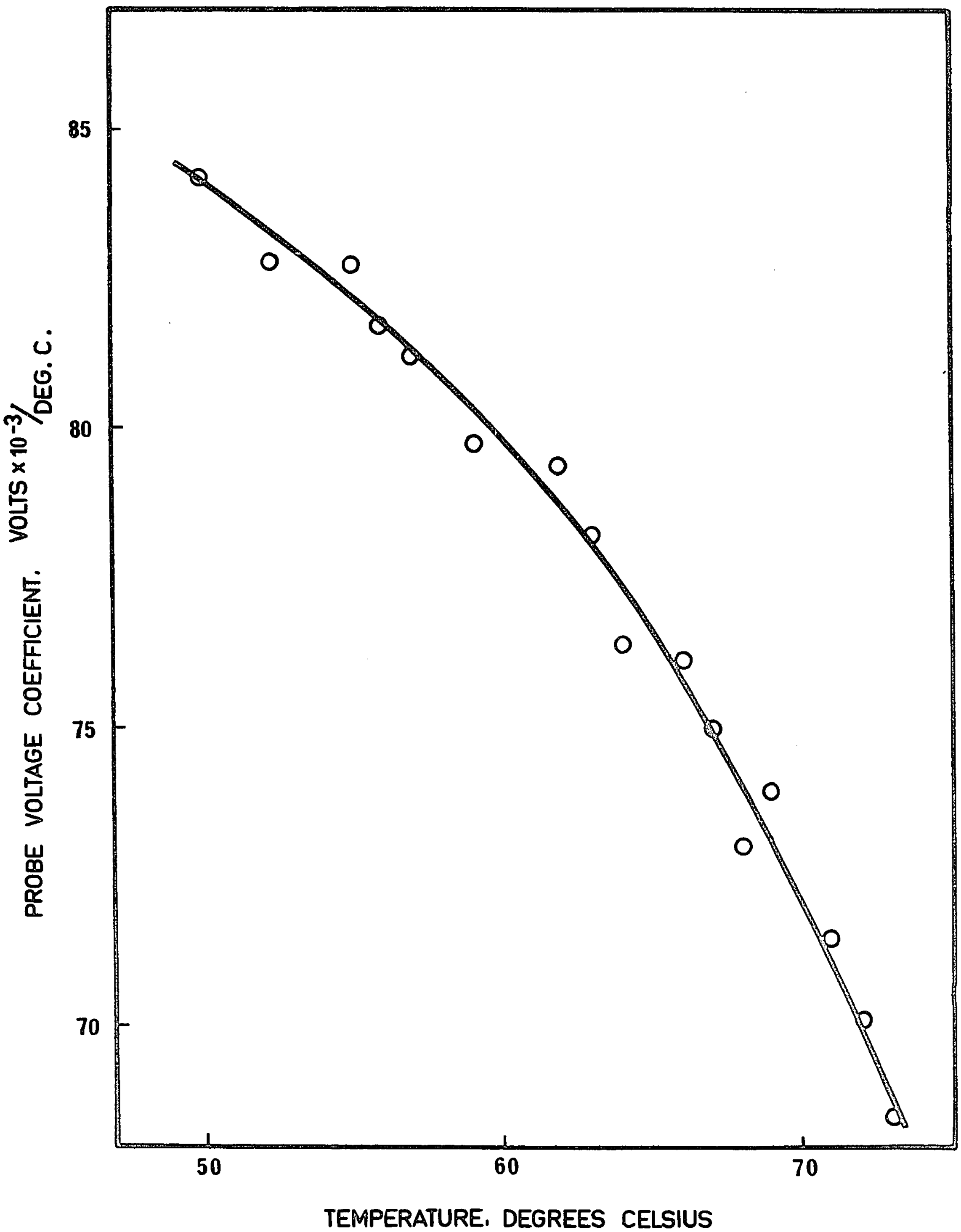
PROBE VOLTAGE COEFFICIENT. VOLTS x 10^-3/DEG. C.
85
80
75
70
50
60
70
TEMPERATURE, DEGREES CELSIUS

change for other positions of the probe was recorded as it traversed the gap. By using the appropriate value of the temperature coefficient, these readings were converted to accurate temperature differences, referenced to the wall temperature.

The operation of the probe and the positioning fixture was verified by establishing a temperature difference between the two cylinders, which were stationary with polyethylene glycol in the gap. A temperature profile was then taken with the cylinders remaining stationary. A profile obtained under these conditions should be linear. The experimentally obtained profile (Figure 3-11) shows only small deviations from linearity indicating the correct functioning of the probe and its positioning device.

FIGURE 3-11: Verification of Correct Probe Positioning in the Gap. A Temperature Difference, $T_i - T_o = 4.3^oF$, Existed Across the Gap. The Points Represent Measured Temperatures While the Curve is the Computed Temperature Profile. The Fluid was Stationary

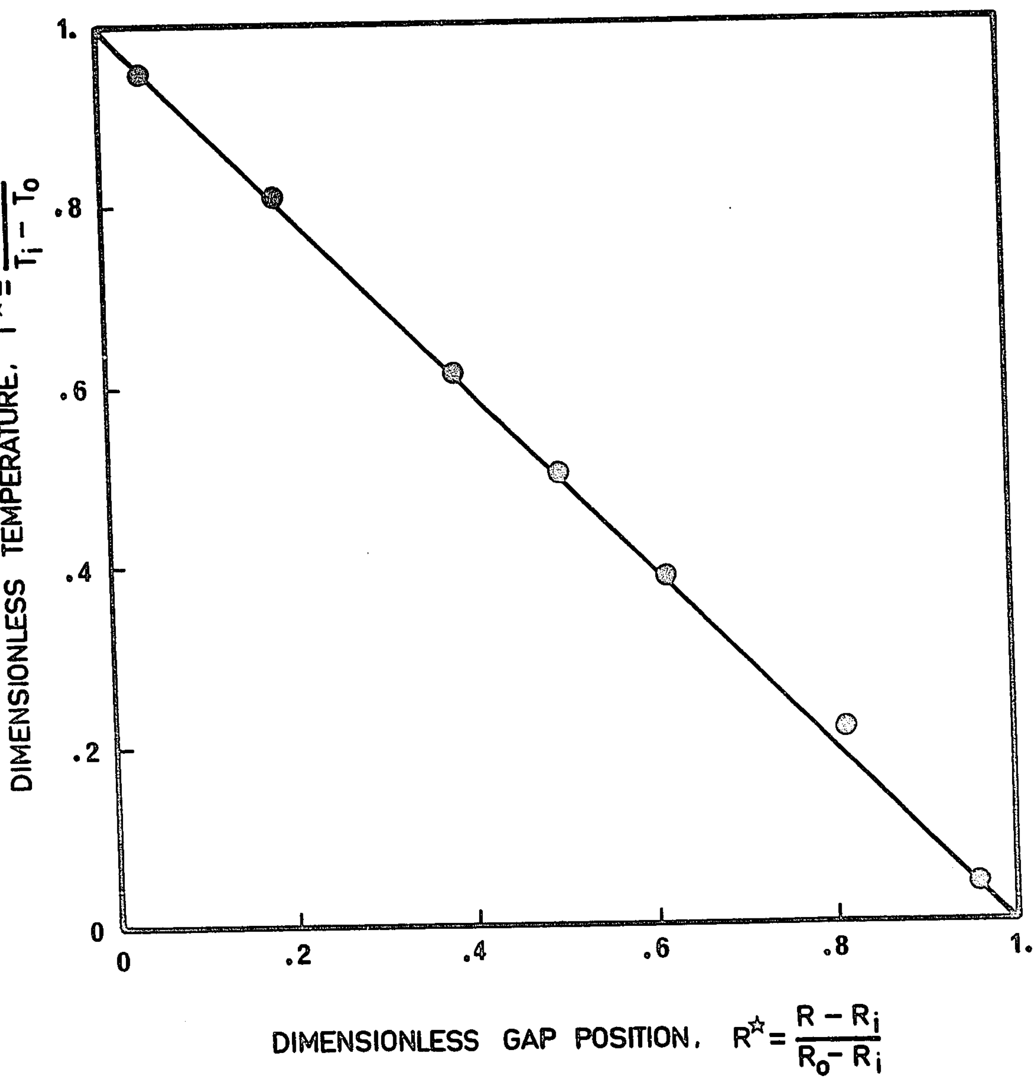
1.
.8
.6
.4
.2
0
0
.2
.4
.6
.8
1.
DIMENSIONLESS TEMPERATURE, $T^{\star} = \frac{T - T_o}{T_i - T_o}$
DIMENSIONLESS GAP POSITION, $R^{\star} = \frac{R - R_i}{R_o - R_i}$

CHAPTER 4

THEORY

4.1 GENERAL FEATURES OF THE MODEL

The identification of the important parameters in a process is often aided by a clear physical picture of the process. In this chapter, a model using equations developed from a proposed mechanism of the deagglomeration process will be presented.

We consider an agglomerate composed of a number of particles bonded together and having one of a large number of possible configurations. It is assumed that deagglomeration is caused by the hydrodynamic forces acting upon the agglomerate and that collisions between aggregates make only a minor contribution. This assumption is reasonable because of the small agglomerate sizes and large viscosities involved. It is also assumed that there will exist a certain orientation of the agglomerate (with respect to the shear stress field) such that the magnitude of the field required to cause breakdown is a minimum. This orientation will be called the "most favourable orientation".

In addition it is assumed that the breaking strengths are randomly distributed throughout all the bond positions in all agglomerates. Thus, for a large agglomerate population, different species of agglomerates possess equal fractions of bonds of a given strength, and these fractions are the same as the fraction of all bonds of that strength for the total population. This assumption relates to the appearance of a bond of given strength in a specified position in the agglomerate. It is distinct from the breaking strength distribution, which is discussed later.

The minimum breaking force, which is associated with the most favourable orientation, will depend on the structure of the agglomerate. Structure involves both configuration, which is the spatial arrangement of the particles in the agglomerate, and the distribution of bond strengths within the particle. The structure is expected to be dependent on the method of production of the agglomerates.

If the agglomerate is placed in a fluid undergoing simple shear flow, then the magnitude of the shear stress will be the variable determining whether the agglomerate will degrade. Given a certain value of shear stress, τ, and agglomerate population, there will be a fraction of the population that will degrade. This fraction is specified as having a minimum breaking strength of σ, or less, where σ is associated with the applied shear stress, τ.

Initially, when shearing is commenced, not all of this degradable fraction will be in an orientation that is favourable for breakage. It is assumed, however, that if shearing is continued for a sufficiently long time all the agglomerates will rotate to the orientation that causes breakdown. Thus, eventually, all of the fraction will be broken and an equilibrium related to the magnitude of the shear stress will be established. If the shear stress is increased, a new equilibrium will be achieved after an additional time.

In this manner, the equilibrium breakdown distribution is associated with the magnitude of the shear stress field and the approach to equilibrium is associated with the amount of shear strain that has occurred. The rate of approach to equilibrium is thus determined by the shear rate.

For the purposes of simplifying the analysis, the model will be presented in three parts. The first part, section 4.2, will develop equations to predict the distribution of sizes at equilibrium, and the second part, section 4.3, is concerned with the approach to equilibrium for a step change in shear stress. The third part, section 4.4, will present equations that permit the calculation of the size distributions for a shear stress that is an arbitrary function of time.

For the purposes of this study the size of an agglomerate is determined solely by the number of beads it contains.

4.2 EQUILIBRIUM SIZE DISTRIBUTION

4.2.1 Gain and Loss Functions

The objective of this section is to present a model that will predict the equilibrium agglomerate size distribution corresponding to a constant applied shear stress. It is necessary to know the initial distribution (before the application of shear) and the magnitude of the shear stress. As indicated earlier, it will be assumed that sufficient time has elapsed to ensure the deagglomeration of all breakable agglomerates by the prevailing shear stress.

Let n_i be the number of agglomerates containing i particles (hereafter referred to as an i-particle agglomerate). As a result of the applied shear stress, agglomerates containing more than one bead will be broken down to smaller agglomerates. This leads, generally, to a gain in the number of the smaller agglomerates and a loss of the agglomerates of larger size. Define a gain function, G_i, such that:

$$(dn_i)_g = G_i(\tau)d\tau \qquad 4\text{-}1$$

where $(dn_i)_g$ is the number of i-particle agglomerates gained in the incremental shear stress range between τ and $\tau + d\tau$, per unit volume. The remainder of this discussion applies to unit volume of the sample. Rewriting equation 4-1 in the form:

$$\frac{(dn_i)_g}{d\tau} = G_i(\tau) \qquad 4\text{-}2$$

it is apparent that $G_i(\tau)$ may be considered as the gain in i-particle agglomerates per unit shear stress in the range of shear stress between τ and $\tau + d\tau$. This gain is provided by the breakdown of j-particle agglomerates, where $j > i$.

Similarly, a loss function, L_i, may be defined:

$$L_i = \frac{(dn_i)_\ell}{d\tau} \qquad 4\text{-}3$$

where L_i is the loss in i-particle agglomerates per unit shear stress in the range of shear stress between τ and $\tau + d\tau$. This loss represents the breakdown of i-particle agglomerates to smaller, k-particle, agglomerates where $k < i$.

The quantity $G_i(\tau)$, hereafter called G_i for brevity, is the sum of the gain of the i-particle agglomerates from all the j-particle agglomerates ($j > i$) breaking down. A quantity, $g_{i,j}$, is defined to represent the gain by the i^{th} species due to breakdown of a particular j-species. Consistent with G_i and L_i, $g_{i,j}$ is defined per unit stress over shear stress range between τ and $\tau + d\tau$.

Thus, a mass balance for the gains and losses gives the following:

$$G_i = \sum_{j=i+1}^{N} g_{i,j} \qquad 4\text{-}4$$

and

$$L_i = \sum_{k=1}^{i-1} \frac{k}{i} g_{k,i} \qquad 4\text{-}5$$

where N is the number of particles in the largest agglomerate in the system. In this work the largest agglomerate is taken as that which contains the largest number of beads.

A mass balance for each species and for the whole system yields:

$$D_i = G_i - L_i \qquad 1 \le i \le N \qquad 4\text{-}6$$

and

$$\sum_{i=1}^{N} i\, D_i = 0 \qquad 4\text{-}7$$

where D_i is the net difference between gain and loss for each species.

If equations 4-4 and 4-5 are substituted into equation 4-6, the resulting system is as shown in Table 4-1. This system contains N equations and $\frac{N^2+1}{2}$ unknowns.

It is now assumed that when an agglomerate splits it will yield only two portions. For example, a five-particle agglomerate may break to simultaneously yield, two agglomerates with two and three particles each or two agglomerates of one and four particles each. However, it is forbidden for a five-

TABLE 4-1

MASS BALANCE EQUATIONS

$$D_1 = 0 + g_{1,2} + g_{1,3} + \cdots\cdots\cdots\cdots\; g_{1,N}$$

$$D_2 = -\frac{1}{2}\, g_{1,2} + 0 + g_{2,3} + \cdots\cdots\cdots\cdots\; g_{2,N}$$

$$D_3 = -\frac{1}{3}\, g_{1,3} + \frac{2}{3}\, g_{2,3} + 0 + \cdots\cdots\cdots\cdots\; g_{3,N}$$

$$\vdots$$

$$D_{N-1} = -\frac{1}{N-1}\, g_{1,N-1} - \frac{2}{N-1}\, g_{2,N-1} - \frac{3}{N-1}\, g_{3,N-1} - \cdots\cdots\cdots\cdots + 0 + g_{N-1,N}$$

$$D_N = -\frac{1}{N}\, g_{1,N} - \frac{2}{N}\, g_{2,N} - \frac{3}{N}\, g_{3,N} - \cdots\cdots\cdots\cdots - \frac{N-1}{N}\, g_{N-1,N} + 0$$

particle agglomerate to breakdown so as to give, simultaneously a single particle and two two-particle agglomerates. On the other hand, sequential breakdown is allowed - e.g. a five-particle agglomerate may degrade to give a two-particle and a three-particle agglomerate. Each of these "degradation products" may split at some value of the shear stress higher than that which caused the five-particle agglomerate to split. Further, it is assumed that the agglomerates acquired via breakdown and entering a particular species, i, are indistinguishable from the undegraded agglomerates remaining in the species i. This assumption follows from the assumption of random distribution of breaking strengths over all positions in all agglomerates.

These assumptions result in the following equation 4-8, which is demonstrated numerically in Table 4-2.

$$g_{i-j,i} = g_{j,i} \qquad 3 \le i \le N \qquad 4\text{-}8$$

The gains of different species may be related by using a parameter, c_{Ki}, defined as follows:

$$g_{K,i} = c_{Ki}\, g_{K+1,i} \qquad 4 \le i \le N \qquad 4\text{-}9$$

The factor c_{Ki} represents the relative frequency in which the breakdown of species i yields K-particle agglomerates in preference to (K + 1)-particle agglomerates. As an example,

TABLE 4-2

RELATIONSHIPS BETWEEN DEGRADED PORTIONS
OF AGGLOMERATES

No. of Beads	Possible Splits	Relationships	
1	None		
2	1:1		
3	1:2		
4	1:3 1:2	$g_{1,4} = g_{3,4}$	$c_{14} = \frac{g_{1,4}}{g_{2,4}}$
5	1:4	$g_{1,5} = g_{4,5}$	$c_{15} = \frac{g_{1,5}}{g_{2,5}}$
	2:3	$g_{2,5} = g_{3,5}$	
6	1:5	$g_{1,6} = g_{5,6}$	$c_{16} = \frac{g_{1,6}}{g_{2,6}}$
	2:4	$g_{2,6} = g_{4,6}$	$c_{26} = \frac{g_{2,6}}{g_{3,6}}$
	3:3		
7	1:6	$g_{1,7} = g_{6,7}$	$c_{17} = \frac{g_{1,7}}{g_{2,7}}$
	2:5	$g_{2,7} = g_{5,7}$	$c_{27} = \frac{g_{2,7}}{g_{3,7}}$
	3:4	$g_{3,7} = g_{4,7}$	
8	1:7	$g_{1,8} = g_{7,8}$	$c_{18} = \frac{g_{1,8}}{g_{2,8}}$
	2:6	$g_{2,8} = g_{6,8}$	$c_{28} = \frac{g_{2,8}}{g_{3,8}}$
	3:5	$g_{3,8} = g_{5,8}$	$c_{38} = \frac{g_{3,8}}{g_{4,8}}$
	4:4		

consider that the five-particle agglomerates split in the ratio 2:3 twice as often as they split in the ratio 1:4. Then $c_{15} = \frac{g_{1,5}}{g_{2,5}} = 0.5$.

When equations 4-8 and 4-9 are substituted into equation 4-6 along with equations 4-4 and 4-5 the following is obtained (see Appendix IV):

$$\sum_{j=i+1}^{N} C_{ij} g_{1,j} - C_{ii} g_{1,i} = D_i \qquad 1 \le i \le N \qquad \text{4-10}$$

where

$$C_{ij} = 1, \qquad 2 \le j \le N \qquad \text{4-10a}$$

$$C_{i(i+1)} = 1, \qquad 2 \le i \le (N-1) \qquad \text{4-10b}$$

$$C_{ij} = \prod_{k=1}^{j-(k+1)} \frac{1}{c_{kj}}, \qquad i+2 \le j \le 2i \qquad \text{4-10c}$$

$$C_{ij} = \prod_{k=1}^{j-1} \frac{1}{c_{kj}}, \qquad 2i+1 \le j \le N \qquad \text{4-10d}$$

$$C_{ii} = 0 \qquad \text{4-10e}$$

$$C_{ii} = \sum_{i=1}^{j-1} \frac{i}{j} C_{ij}, \qquad 2 \le i \le N \qquad \text{4-10f}$$

In equation 4-10 the first term on the left hand side represents the gains and the second term represents the losses. The relationship 4-10 contains N equations and (2N - 1) unknowns, which are $g_{i,j}$, $2 \leq i \leq N$, and D_i, $1 \leq i \leq N$. The N equations are not all independent since the overall mass balance, equation 4-7, must be satisfied.

In order to find the distributions, an additional (N - 1) relationships must be found. From a physical point of view, equation 4-9 specifies the relative frequency of the types of breakdown. What is needed, is a knowledge of the fraction of each species that will deagglomerate for a differential increase in the shear stress. The necessary relationships are developed in the next two subsections.

4.2.2 Balance on the Original Agglomerates

Prior to the application of any shear stress, it is assumed that there is an initial breaking distribution for the agglomerates in the i^{th} species given by the following form:

$$dQ_{io} = A_{io} \rho_{i\sigma} \, d\sigma \qquad 4\text{-}11$$

where dQ_{io} represents the incremental number of i-particle agglomerates that have a breaking strength in the range between σ and $\sigma + d\sigma$. The parameter A_{io} may be considered a scaling factor and $\rho_{i\sigma}$ is a strength distribution function depending on i and σ. The total number of i-particle aggregates initially present is given by:

$$Q_{io} = \int_0^\infty A_{io}\rho_{i\sigma}\, d\sigma \qquad 4\text{-}12$$

For the purposes of the present treatment, where equilibrium conditions prevail and the agglomerates break in their most favourable orientation, the breaking strength, σ, corresponds to some level of the applied shear stress, τ, and is equal to it. At any applied shear stress, τ, the number of the original (initial) agglomerates remaining is defined as Q_{ior}. Therefore, at this arbitrary shear stress value, the differential amount lost, $dQ_{ior} = (dn_{io})_\ell$, of the remaining original agglomerates is given by:

$$dQ_{ior} = (dn_{io})_\ell = A_{io}\rho_{i\tau} d\tau \qquad 4\text{-}13$$

and the amount of the original agglomerates remaining is:

$$Q_{ior} = \int_\tau^\infty A_{io}\rho_{i\tau} d\tau \qquad 4\text{-}14$$

Since all the agglomerates with a strength $\sigma \leq \tau$ will break at the applied shear stress, τ. The differential fraction lost of original remaining agglomerates is:

$$\frac{dQ_{ior}}{Q_{ior}} = \frac{\rho_{i_\tau} d\tau}{\int_{\tau}^{\infty} \rho_{i_\tau} d\tau} \qquad 4\text{-}15$$

4.2.3 Balance on Original and Gained Agglomerates

As the applied shear stress is increased from zero to the final value, τ_f, agglomerates will break down at intermediate values of shear stress corresponding to the breaking strengths of the weaker agglomerates. Thus, the number of original agglomerates is gradually depleted and new, smaller agglomerates are formed at these intermediate stress levels. These new, gained, agglomerates will undergo breakage at the stress levels corresponding to their breaking strengths.

According to the assumption stated earlier, agglomerates gained at a given stress level are indistinguishable from those already present. It follows that the normalized breaking strength distribution over the same range of breaking strengths must be the same for both the gained agglomerates and the original agglomerates. It is noted that the distribution of agglomerate strengths commences at the shear stress magnitude, τ, for which the portion of gained aggregates under consideration has been produced.

Thus, if the total number of i-particle agglomerates that are present when the shear stress has a value, τ, is Q_i, the fraction of these that will be broken at τ is identical with that given by equation 4-15 and is:

$$\frac{(dn_i)_\ell}{Q_i} = \frac{\rho_{i_\tau} d\tau}{\int_\tau^\infty \rho_{i_\tau} d\tau} \qquad 4\text{-}16$$

and

$$L_i = \frac{(dn_i)_\ell}{d\tau} = \frac{Q_i \rho_{i_\tau}}{\int_\tau^\infty \rho_{i_\tau} d\tau} \qquad 4\text{-}17$$

where Q_i is the total number of i-particle agglomerates and is equal to the sum of the gained and the original remaining i-particle agglomerates.

4.2.4 Differential Equations for Equilibrium Size Distribution

It follows from the assumption of a random distribution of breaking strengths over all positions in all the agglomerates that the strength distribution function cannot vary with the species, hence:

$$\rho_{i_\tau} = \rho_{(i+1)_\tau} \qquad 4\text{-}18$$

The subscript referring to the species, i, is thus omitted from the distribution function and equation 4-17 becomes:

$$L_i = \frac{(dn_i)_\ell}{d\tau} = \frac{Q_i \rho_\tau}{\int_\tau^\infty \rho_\tau d\tau} \qquad 4\text{-}19$$

Combining equations 4-10 and 4-19 gives:

$$L_i = C_{ii} g_{1,i} = \frac{Q_i \rho_\tau}{\int_\tau^\infty \rho_\tau d\tau} \qquad 4\text{-}20$$

For convenience and brevity, define:

$$I_\tau = \frac{\rho_\tau}{\int_\tau^\infty \rho_\tau d\tau} \qquad 4\text{-}21$$

Then from equations 4-20 and 4-21

$$g_{1,i} = \frac{Q_i}{C_{ii}} I_\tau \qquad 4\text{-}22$$

Substituting from equation 4-22 into equation 4-10 yields:

$$\sum_{j=i+1}^{N} \frac{C_{ij}}{C_{jj}} Q_j I_\tau - Q_i I_\tau = D_i \qquad 1 \le i \le N \qquad 4\text{-}23$$

Since

$$D_i = \frac{(dn_i)_g - (dn_i)_\ell}{d\tau} = \frac{dQ_i}{d\tau} \qquad 4\text{-}24$$

Substituting for D_i in equation 4-23 gives:

$$\sum_{j=i+1}^{N} \frac{c_{ij}}{c_{jj}} Q_j \Big|_\tau - Q_i \Big|_\tau = \frac{dQ_i}{d\tau} \qquad 1 \le i \le N \qquad 4\text{-}25$$

which is the required system of differential equations describing the equilibrium size distribution variation with shear stress.

4.2.5 Determination of c_{ij} and ρ_τ

It remains to determine the relative frequency parameters, c_{ij}, and the strength distribution function, ρ_τ. The factors affecting the breakdown of a given agglomerate can be considered in the two categories of bond strength and structure. In the present instance bond strength is primarily a function of the manufacturing technique. Some control was exerted over this variable, but it should be expected that a distribution of strengths was produced. The configuration of the agglomerate affects the breakdown in two ways. First, the configuration determines the internal stresses because the hydrodynamic forces depend directly on the shape of the agglomerates. Secondly, the structure determines the number of bonds to be broken. For example, a linear three-particle agglomerate needs only one bond to be broken, but a three particle agglomerate with the particles at the vertices of a triangle and each particle bonded to the other two requires two broken bonds to deagglomerate.

No attempt will be made to handle bond strength and configuration separately. To do so would require some quantitative data about the agglomerate structure. The minimum data would probably be a knowledge of "effective agglomerate diameter" and "shape factor" distributions. These data were not determined due to experimental difficulties. Instead, some assumptions will be made about the minimum breaking strength required for deagglomeration.

It has been assumed that breaking strengths are randomly distributed throughout all the agglomerates. This implies that the relative frequencies of the splits will not be a function of the shear stress. That is, in a four-particle agglomerate the ratio of 1:3 splits to 2:2 splits will be the same at a low shear stress as at a high magnitude of the stress. Thus

$$c_{ij} \neq c_{ij}(\tau) \qquad 4\text{-}26$$

and

$$C_{ij} \neq C_{ij}(\tau) \qquad 4\text{-}27$$

since C_{ij} values depend only on the values of c_{ij} (equations 4-10a-f).

It is assumed that, as a first approximation, the ease with which an i-particle agglomerate is split from a j-particle agglomerate will not depend on the size of the j-particle agglomerate. For example, the assumption states that a single bead splits from a five-bead agglomerate as readily as it splits from a six or eight-bead agglomerate. Similarly, the same assumption applies to a two-bead agglomerate splitting away, and thus $c_{ij} = \frac{g_{1,j}}{g_{2,j}} \neq c_{ij}(j)$. Extending the situation to any two adjacently sized agglomerates, i and i + 1, being split away leads to $c_{ij} \neq c_{ij}(j)$; i.e. the relative frequencies, c_{ij}, are independent of the size, j, of the parent agglomerate.

It is proposed that the c_{ij} is a function of i (i is the number of particles in the smaller of the two portions formed by the split). This is easy to visualize when the agglomerate is a linear string of particles. Then the force varies as the square of the distance from the end as discussed in section 2.3 (33,35). The result is that the agglomerate will always tend to break closer to the midpoint than towards the end. Since $c_{ij} = \frac{g_{i,j}}{g_{i+1,j}}$ and if the particles are of uniform diameter with i proportional to the distance from the end then, for a linear agglomerate:

$$c_{ij} = \left(\frac{i}{i+1}\right)^2 \qquad \begin{cases} 1 \le i \le \frac{j-2}{2}, & j \text{ even} \\ 1 \le i \le \frac{j-3}{2}, & j \text{ odd} \\ 4 \le j \le N \end{cases} \qquad 4\text{-}28$$

Estimating the variation of c_{ij} for other configurations is more difficult. As the agglomerate becomes larger closed forms dominate over the linear, open configurations. Comparing an open form agglomerate with a closed type, both with the same number of particles, the closed form agglomerate not only has less force acting upon it but, in general, has more bonds between the particles to be broken. In addition, it is likely that when a large portion is split from a closed type agglomerate the number of bonds to be broken, and hence the force required to break them will increase faster than the force acting to cause the split. The result is that as the configuration becomes more closed the tendancy will be for small portions of the agglomerate to break off. Thus c_{ij} is greater than one and tends to decrease as i is increased. This is in contrast to the linear agglomerate where c_{ij} is less than one and tends to increase as i is increased. At large i both types of agglomerate tend to $c_{ij} = 1$. Because no data are available on the distribution of configurations it is assumed that the effects of each type are roughly equal and tend to cancel so that $c_{ij} \approx 1$ for all i.

Due to the lack of configurational data and the qualitative nature of the agglomerate production it is not possible to deduce the strength distribution function theoretically. Two alternatives are possible. The first is to adapt some independent measurement of bond strength to the agglomerates used in the present work. A method, such as that used by Rumpf (66) for sintered agglomerates might be tried. The second alternative is to use part of the experimental data to find the strength distribution. One method is as follows. For the largest agglomerates, i = N, there is only loss and no gain. Thus, for any shear stress, τ, the aggregates present are all remaining original agglomerates, $Q_N = Q_{Nor}$. The fractional cumulative loss, L_{cum}, for any shear stress, τ, may be found directly from:

$$L_{cum} = \frac{Q_{No} - Q_N}{Q_{No}} \qquad 4\text{-}29$$

If the scaling factor A_{No} is chosen such that the distribution of strengths is normalized;

$$A_{No} = Q_{No} \qquad 4\text{-}30$$

Then, from equation 4-12, the fractional cumulative loss is given by:

$$L_{cum} = \int_0^{\tau} \rho_{\tau} d\tau = \frac{Q_{No} - Q_N}{Q_{No}} \qquad 4\text{-}31$$

at any shear stress, τ.

Differentiating equation 4-31 yields:

$$-dQ_N \quad = \quad \rho_\tau \, d\tau \qquad \text{4-32}$$

or, rearranging:

$$\rho_\tau \quad = \quad - \frac{dQ_N}{d\tau} \qquad \text{4-33}$$

The advantages and difficulties of each method of determining ρ_τ are discussed in detail in Chapter 6.

4.2.6 Solution of the Differential Equations

Equations 4-25 may or may not have an analytical solution depending on the functional forms of c_{ij} and ρ_τ. In either case, the simultaneous solution of the equations is avoided by solving the set in reverse, starting with i = N and proceeding through i = N-1, i = N-2 etc. to i = 1. In the present work, the solution has been obtained numerically, and the computer program for the condition c_{ij} = 1, and assuming an exponential distribution of breaking strengths, is given in Appendix V.

4.3 SIZE DISTRIBUTIONS DURING NON-EQUILIBRIUM DEAGGLOMERATION - STEP CHANGE IN SHEAR STRESS

4.3.1 General Considerations

The breakdown model proposed in the previous sections allows the determination of the distributions at equilibrium (i.e. at long times after the initiation of shearing) for a constant shear stress. Equivalently, the shear stress must change so slowly that the agglomerates will only degrade when the most favourable orientation is reached. In this case the amount of any species that breaks down is determined only by the magnitude of the shear stress. Thus it is possible to give the equilibrium distribution as a function of the shear stress.

When the stress is suddenly changed, not all of the portion that will be broken when equilibrium is reached degrades at the instant of stress change. There will be a gradual approach to the new equilibrium distributions which will be determined by the new shear stress magnitude. This gradual approach is a result of the random orientations of the agglomerates, most of which need to rotate towards their most favourable orientations before they degrade.

We consider a number distribution of the agglomerate strengths as shown in figure 4-1. The shear stress is stepped from a value τ_1 to a new value τ_5 at time, t = 0. Before

FIGURE 4-1: The Change of the Agglomerate Size Distribution for a Species i, in Response to a Step Change of the Fluid Shear Stress

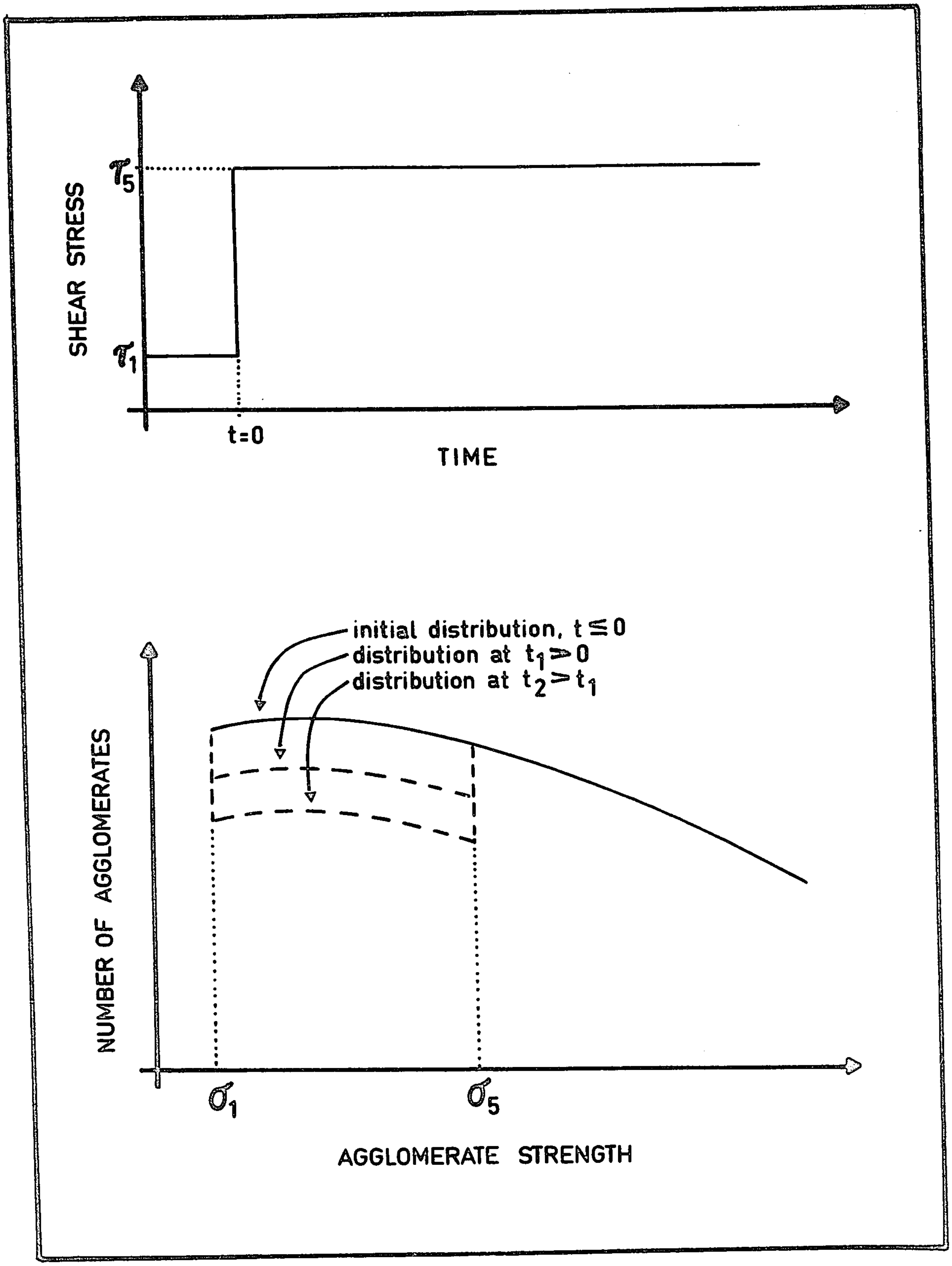
SHEAR STRESS
τ_5
τ_1
t=0
TIME
initial distribution, t ≤ 0
distribution at $t_1 > 0$
distribution at $t_2 > t_1$
NUMBER OF AGGLOMERATES
σ_1
σ_5
AGGLOMERATE STRENGTH

shearing, at $t < 0$, the agglomerates have a strength distribution that corresponds to the equilibrium distribution at shear stress τ_1. Referring to the strength distribution it is seen that the total number of agglomerates in the i^{th} species, Q_i, at any time, t, is given by the area under the curve. Further, these agglomerates, Q_i, may be divided into two portions. The first portion is Q_i', the agglomerates that are sufficiently weak that they will degrade at the applied stress. Q_i' is represented by the area under the curve between the limits of σ_1 and σ_5. The second portion comprises the agglomerates, Q_i'', that will not break down for any orientation of the applied shear stress. This portion corresponds to the area under the curve with limits of σ_5 and ∞.

4.3.2 Mass Balances on the i^{th}-Particle Agglomerates

For reasons that are given below, separate mass balances are made for the breakable agglomerates (those with strengths $\leq \sigma_5$) and the stable agglomerates (strengths $> \sigma_5$). The mass balances are performed in a manner similar to that for the equilibrium situation.

In the derivation of the equilibrium equations it was assumed that agglomerates which broke did not degrade further at the value of the shear stress at which they broke. With a non-equilibrium step-change in shear stress, there is the possibility of an "apparent sequential breakdown" at the same value of shear stress. This occurs because the aggregate does not have to be in its most favourable orientation to experience breakage. As an example, consider the step shear stress change as shown in figure 4-3 and an agglomerate of strength σ. Under equilibrium conditions this agglomerate would degrade at a shear stress τ where $\tau_1 < \tau < \tau_5$. This agglomerate will break before it attains its most favourable orientation producing two smaller agglomerates that have strengths greater than σ, the strength of the parent agglomerate. Either one or both of the new agglomerates must then have strengths between σ and σ_5 or between σ_5 and ∞. If the strength is between σ and σ_5, the product agglomerate will undergo further breakdown. The product(s) with strength(s) greater than σ_5 are stable and do not degrade further*. Thus the breakable agglomerates in the j^{th} species, Q'_j, produce agglomerates entering the i-species, $i < j$ that contribute to both Q'_i, which are breakable, and Q''_i, which are stable. Letting f_j be the instantaneous fraction of the degrading j^{th}-species agglomerates that produce breakable i-species agglomerates, and making the mass balances in the same manner as for the equilibrium case yields:

*Hereafter, if an agglomerate has a strength σ, $\sigma_1 \leq \sigma \leq \sigma_5$, it will be referred to as "breakable". If the strength σ, $\sigma > \sigma_5$ obtains, the agglomerate is called "stable".

$$\sum_{j=i+1}^{N} f_j C_{ij} g_{1,j} - C_{ii} g_{1,i} = D'_i \qquad 1 \le i \le N \qquad 4\text{-}34$$

$$\sum_{j=i+1}^{N} (1 - f_j) C_{ij} g_{1,j} = D''_i \qquad 1 \le i \le N \qquad 4\text{-}35$$

Where equations 4-34 and 4-35 are for the breakable and stable agglomerates respectively. D'_i and D''_i represent the net rates of change in the number of breakable and stable agglomerates respectively. The coefficients, C_{ij} and C_{ii}, are as in the equilibrium mass balance, and are given by equations 4-10a-b.

4.3.3 Differential Equations for the Step-Change in Shear-Stress Case

Analogously with the equilibrium case, the term $C_{ii}\, g_{1,i}$ is identified with the rate of loss of agglomerates in the i^{th} species. It is assumed that the random orientation assumption applies and that the agglomerate breaks as soon as it orbits to a position where the hydrodynamic forces exceed the breaking strength. That is, the agglomerate tends to orbit towards its most favourable orientation, but breaks before this orientation is achieved. Then, the rate at which it orbits towards the most favourable orientation depends on the shear rate and a reasonable approximation to the rate of loss, $L_{i\sigma}$, of i-agglomerate particles, $Q'_{i\sigma}$, of strength σ, is:

$$L_{i\sigma} = \frac{(dQ'_{i\sigma})_\ell}{dt} = K\,\dot{\gamma}\,Q'_{i\sigma} \qquad 4\text{-}36$$

where K is a rate constant, assumed to be independent of agglomerate structure. From equation 4-36 it is seen that the fractional loss per unit time, $\frac{1}{Q'_{i\sigma}} \frac{(dQ'_{i\sigma})_\ell}{dt}$, is constant for constant shear rate. Thus, the fractional rate of loss is the same for agglomerates of any strength and the subscript σ may be omitted and equation 4-36 rewritten as:

$$L_i = \frac{(dQ'_i)_\ell}{dt} = K\,\dot{\gamma}\,Q'_i \qquad 4\text{-}37$$

Equating the rate of loss given by equation 4-37 with the term $C_{ii}g_{1,i}$ and rearranging gives:

$$g_{1,i} = \frac{K\,\dot{\gamma}\,Q'_i}{C_{ii}} \qquad 4\text{-}38$$

Substituting for $g_{1,i}$ in equations 4-34 and 4-35 and noting that $D'_i = \frac{dQ'_i}{dt}$ and $D''_i = \frac{dQ''_i}{dt}$ gives:

$$\sum_{j=i+1}^{N} f_j \frac{C_{ij}}{C_{jj}} K\,\dot{\gamma}\,Q'_j - K\,\dot{\gamma}\,Q'_i = \frac{dQ'_i}{dt} \qquad 1 \le i \le N \qquad 4\text{-}39$$

$$\sum_{j=i+1}^{N} (1-f_j) \frac{C_{ij}}{C_{jj}} K\,\dot{\gamma}\,Q'_j = \frac{dQ''_i}{dt} \qquad 1 \le i \le N \qquad 4\text{-}40$$

To facilitate comparison of equations 4-39 and 4-40 with certain presumed aspects of the agglomerates' physical behaviour to be discussed in Chapter 6. it is useful to rewrite them in terms of the shear strain, γ, rather than shear rate and time. Substituting for $\dot{\gamma} = \frac{d\gamma}{dt}$ and rearranging yields;

$$\sum_{j=i+1}^{N} f_j \frac{C_{ij}}{C_{jj}} K Q'_j - K Q'_i = \frac{dQ'_i}{d\gamma} \qquad 1 \leq i \leq N \qquad \text{4-39a}$$

$$\sum_{j=i+1}^{N} (1-f_j) \frac{C_{ij}}{C_{jj}} K Q'_j = \frac{dQ''_i}{d\gamma} \qquad 1 \leq i \leq N \qquad \text{4-40a}$$

Equations 4-39 and 4-40, for the breakable and stable agglomerates respectively, correspond to equation 4-25 in the equilibrium situation.

The value of the rate constant, K, is determined from experimental data and is discussed more fully in Chapter 6. An expression for the fraction, f_j, of the gained agglomerates that are breakable is derived in the following subsection.

4.3.4 Determination of the Breakable Fraction of Gained Agglomerates

The breakdown products entering the i^{th}-species come from the j-species, $j > i$. The breakdown products will have a certain strength distribution. If this distribution is known then the fraction that is breakable is found by applying the limits of σ_1 and σ_5 to the integration of the product distribution function, and dividing by the total amount of product. In general, the strength distribution of the products will depend on the strength distribution of the breakable agglomerates producing the products. Accordingly, the following strength distributions are defined. In general the distributions are functions of time and are defined as the instantaneous distributions of the agglomerates present at time t. First, the stable and breakable i-particle agglomerates, Q''_i and Q'_i respectively, are subdivided such that:

$$Q'_i = Q'_{ior} + Q'_{ig} \qquad 4\text{-}41$$

$$Q''_i = Q''_{io} + Q''_{ig} \qquad 4\text{-}42$$

where

Q'_{ior} = the breakable i-particle agglomerates remaining, at time t, of those originally present before shearing.

Q'_{ig} = the breakable i-particle agglomerates gained by the breakdown of j-particle agglomerates, $j > i$, at time t.

Q''_{io} = the stable i-particle agglomerates originally present, Q''_{io} is independent of time.

Q''_{ig} = the stable i-particle agglomerates gained by the breakdown of j-particle agglomerates, $j > i$, present at time t.

Now define:

$\int_{\sigma_5}^{\infty} A_{io}\rho_\sigma d\sigma$ = Q''_{io}; the strength distribution of the agglomerates comprising Q''_{io}. This distribution is time-independent.

$\int_{\sigma_5}^{\infty} a_{i\sigma} d\sigma$ = Q''_{ig}; the instantaneous strength distribution, at time t, of the agglomerates in Q''_{ig}.

$\int_{\sigma_1}^{\sigma_5} e_{i\sigma} d\sigma$ = Q'_{ig}; the instantaneous strength distribution, at time t, of the agglomerates in Q'_{ig}.

$\int_{\sigma_1}^{\sigma_5} A_{it}\rho_\sigma d\sigma$ = Q'_{ior}; the instantaneous strength distribution, at time t, of the agglomerates in Q'_{ior}.

$\int_{\sigma_1}^{\infty} h_{i\sigma} d\sigma$ = the instantaneous strength distribution of the products being produced, at time t, by the breaking of agglomerates in Q'_{ig}.

$\int_{\sigma_1}^{\infty} b_{i\sigma} d\sigma$ = the instantaneous strength distribution of the products being produced, at time t, by the breaking of the agglomerates in Q'_{ior}.

$\int_{\sigma_1}^{\infty} s_{i\sigma} d\sigma$ = the instantaneous strength distribution, at time t, of the products being produced by the breaking of agglomerates in Q'_t.

$$\int_{\sigma_1}^{\infty} s_{i\sigma}\, d\sigma = \int_{\sigma_1}^{\infty} h_{i\sigma}\, d\sigma + \int_{\sigma_1}^{\infty} b_{i\sigma}\, d\sigma$$

The relationship between the various agglomerate subdivisions, their strength distributions and the agglomerate "flow" is illustrated in figure 4-4. From the definitions and figure 4-4 it is seen that the instantaneous strength distribution of the products produced by the i^{th} species is $\int_{\sigma_1}^{\infty} s_{i\sigma} d\sigma$. Thus, the fraction, f_i, can be found:

$$f_i = \frac{\int_{\sigma_1}^{\sigma_5} s_{i\sigma} \, d\sigma}{\int_{\sigma_1}^{\infty} s_{i\sigma} \, d\sigma} \qquad 4\text{-}43$$

when the distribution function, $s_{i\sigma}$, is known. The function can be found by writing a mass balance for a differential strength range. This is done in the next section.

4.3.5 Mass Balance on a Differential Strength Range

Let the amount in the gained, breakable i-particle agglomerates, Q'_{ig}, within the strength range from σ to $\sigma + d\sigma$ be $E_{i\sigma}$. Then:

$$E_{i\sigma} = e_{i\sigma} \, d\sigma \qquad 4\text{-}44$$

From equation 4-36, the rate of loss, $\frac{(dE_{i\sigma})_\ell}{dt}$, will be

$$\frac{(dE_{i\sigma})_\ell}{dt} = K \dot{\gamma} E_{i\sigma} = K \dot{\gamma} e_{i\sigma} \, d\sigma \qquad 4\text{-}45$$

FIGURE 4-2: Relationships Between the Various Portions of the Agglomerates Comprising Species i and their Response to a Step Change in the Fluid Shear Stress

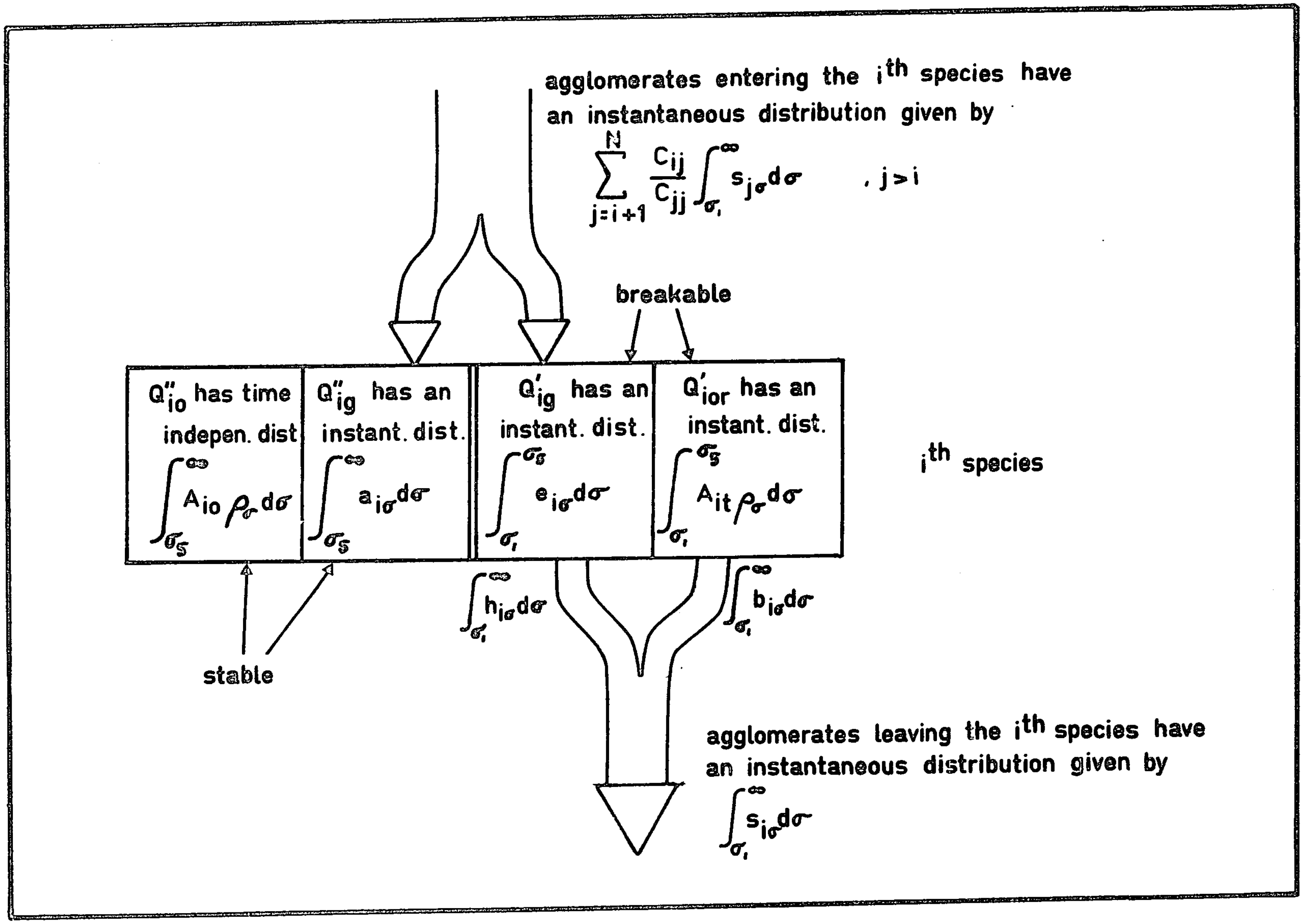

agglomerates entering the i^{th} species have an instantaneous distribution given by
$\sum_{j=i+1}^{N} \frac{C_{ij}}{C_{jj}} \int_{\sigma_1}^{\infty} s_{j\sigma} d\sigma$, $j > i$
breakable
Q''_{io} has time indepen. dist
$\int_{\sigma_5}^{\infty} A_{io} \rho_\sigma d\sigma$
Q''_{ig} has an instant. dist.
$\int_{\sigma_5}^{\infty} a_{i\sigma} d\sigma$
Q'_{ig} has an instant. dist.
$\int_{\sigma_1}^{\sigma_5} e_{i\sigma} d\sigma$
Q'_{ior} has an instant. dist.
$\int_{\sigma_1}^{\sigma_5} A_{it} \rho_\sigma d\sigma$
i^{th} species
$\int_{\sigma_1}^{\infty} h_{i\sigma} d\sigma$
$\int_{\sigma_1}^{\infty} b_{i\sigma} d\sigma$
stable
agglomerates leaving the i^{th} species have an instantaneous distribution given by
$\int_{\sigma_1}^{\infty} s_{i\sigma} d\sigma$

The gain into the strength range results from the breakage of all j-species, $j > i$. Each j-species produces agglomerates with the strength distribution function $s_{j\sigma}$ and the amount in the range σ to $\sigma + d\sigma$ is $s_{j\sigma}d\sigma$. From the mass balance (equation 4-39) the amount of $s_{j\sigma}d\sigma$ that enters the i^{th} species, $(Q'_{ij})_g$, is:

$$(Q'_{ij})_g = \frac{C_{ij}}{C_{jj}} s_{j\sigma}d\sigma \qquad 4\text{-}46$$

where the coefficients C_{ij} and C_{jj} are defined by equations 4-10a-f. The total amount gained in the i^{th} species due to breakdown in all the j-species, Q'_{ig}, is

$$Q'_{ig} = \sum_{j=i+1}^{N} \frac{C_{ij}}{C_{jj}} s_{j\sigma}\, d\sigma \qquad 4\text{-}47$$

The rate at which they are gained is:

$$\frac{dQ'_{ig}}{dt} = \sum_{j=i+1}^{N} \frac{C_{ij}}{C_{jj}} \frac{ds_{j\sigma}}{dt}\, d\sigma \qquad 4\text{-}48$$

The mass balance is now written:

$$\frac{de_{i\sigma}}{dt}\, d\sigma = \sum_{j=i+1}^{N} \frac{C_{ij}}{C_{jj}} \frac{ds_{j\sigma}}{dt}\, d\sigma - K \dot{\gamma}\, e_{i\sigma}d\sigma \qquad 4\text{-}49$$

$$\sigma_1 \leq \sigma \leq \sigma_5$$

Examination of equations 4-49 shows that distribution function for the i^{th} species, $e_{i\sigma}$, is in terms of the distribution function of the degradation products of the j-species, $s_{j\sigma}$, $j > i$. If the relationship between the breaking j-species distribution function, $e_{j\sigma}$, and its product's distribution function is known then equations 4-49 can be solved in reverse order. Referring to figure 4-4 and the definitions given earlier it is seen that:

$$s_{j\sigma} = h_{j\sigma} + b_{j\sigma} \tag{4-50}$$

The relationships between breaking species distribution functions, $e_{j\sigma}$ and $A_{jt}\rho_\sigma$, and product distribution functions, $h_{j\sigma}$ and $b_{j\sigma}$ respectively are derived in Appendix VI and are:

$$h_{j\sigma*} = \rho_{\sigma*} \int_{\sigma_1}^{\sigma*} \frac{e_{i\sigma}}{[\int_{\sigma_1}^{\infty} \rho_\sigma \, d\sigma]} \, d\sigma \qquad \sigma_1 \leq \sigma* \leq \sigma_5 \tag{4-51}$$

$$= \rho_{\sigma*} \int_{\sigma_1}^{\sigma_5} \frac{e_{i\sigma}}{[\int_{\sigma_1}^{\infty} \rho_\sigma \, d\sigma]} \, d\sigma \qquad \sigma_5 \leq \sigma* \leq \infty \tag{4-51a}$$

$$b_{i\sigma^*} = \rho_{\sigma^*} \int_{\sigma_1}^{\sigma^*} \frac{A_{it}\,\rho_\sigma}{[\int_{\sigma_1}^{\infty} \rho_\sigma \, d\sigma]} \, d\sigma \qquad \sigma_1 \le \sigma^* \le \sigma_5 \qquad 4\text{-}52$$

$$= \rho_{\sigma^*} \int_{\sigma_1}^{\sigma_5} \frac{A_{it}\,\rho_\sigma}{[\int_{\sigma_1}^{\infty} \rho_\sigma \, d_\sigma]} \, d\sigma \qquad \sigma_5 \le \sigma^* \le \infty \qquad 4\text{-}52a$$

Since the balance is being made only on the breakable agglomerates with $\sigma_1 \le \sigma \le \sigma_5$ equation 4-50 becomes after substitution from equation 4-51 and 4-52:

$$s_{j\sigma} = \rho_\sigma \int_{\sigma_1}^{\sigma} \frac{e_{j\sigma} + A_{jt}\rho_\sigma}{[\int_{\sigma_1}^{\infty} \rho_\sigma \, d\sigma]} \, d\sigma \qquad \sigma_1 \le \sigma \le \sigma_5 \qquad 4\text{-}53$$

Differentiating to obtain $\frac{ds_{j\sigma}}{dt}$ and substituting into the mass balance, equation 4-49 yields:

$$\frac{de_{i\sigma}}{dt} = \sum_{j=i+1}^{N} \frac{C_{ij}}{C_{jj}} \rho_\sigma \int_{\sigma_1}^{\sigma} \frac{\frac{de_{j\sigma}}{dt} + \rho_\sigma \frac{dA_{jt}}{dt}}{[\int_{\sigma_1}^{\infty} \rho_\sigma \, d\sigma]} \, d\sigma - K \dot{\gamma} e_{i\sigma} \qquad 4\text{-}54$$

Equations 4-54 are only valid for $\sigma_1 \le \sigma \le \sigma_5$. They may be solved in reverse order starting with i = N, i = N-1, i = N-2 ... etc. The term $\rho_\sigma \frac{dA_{jt}}{dt}$ is known since:

$$\frac{d(A_{jt}\rho_\sigma)}{dt} = \rho_\sigma \frac{dA_{jt}}{dt} = -K\dot{\gamma} A_{jt}\rho_\sigma \qquad 4\text{-}55$$

from the definitions and equation 4-36. Solving 4-55 with the initial condition, $A_{jt} = A_{jo}$ when $t = 0$, gives A_{jt}, which is also required:

$$A_{jt} = -K\dot{\gamma} A_{jo} e^{-K\dot{\gamma}t} \qquad 4\text{-}56$$

4.3.6 Solution of the Equations

The components necessary to find f_i are now known and the following scheme may be used to calculate it:

1. Solve equations 4-54 in reverse order to obtain $e_{i\sigma}$ for all i.
2. Using the relationship derived in Appendix VI the instantaneous distribution function of the degradation products, $s_{i\sigma}$, may be found from $e_{i\sigma}$ and $A_{it}\rho_\sigma$, the distribution functions of the agglomerates producing the products. The relationships are given in this chapter as equations 4-51, 4-51a, 4-52 and 4-52a.
3. The required fraction, f_i, is thus found by equation 4-43:

$$f_i = \frac{\int_{\sigma_1}^{\sigma_5} s_{i\sigma}\, d\sigma}{\int_{\sigma_1}^{\infty} s_{i\sigma}\, d\sigma} \qquad 4\text{-}43$$

The appropriate function for $f_i = f_i(t)$ is substituted in the mass balance, equations 4-39 and 4-40,

$$\sum_{j=i+1}^{N} f_j \frac{C_{ij}}{C_{jj}} K \dot{\gamma} Q'_j - K \dot{\gamma} Q'_i = \frac{dQ'_i}{dt} \qquad 4\text{-}39$$

$$\sum_{j=i+1}^{N} (1-f_j) \frac{C_{ij}}{C_{jj}} K \dot{\gamma} Q'_j = \frac{dQ''_i}{dt} \qquad 4\text{-}40$$

which are for the breakable and stable deagglomerates, respectively. When the equations are solved numerically, as in this work, the program used for the equilibrium case are easily modified to solve equations 4-39 and 4-40. The calculation of f_i was also performed numerically. The appropriate scheme is shown in Appendix V.

An alternative method to calculate the size distributions can be discerned. In the scheme described above it is necessary to find $e_{i\sigma}$. However, if $e_{i\sigma}$, the distribution function for the gained breakable agglomerates, Q'_{ig}, is known, then Q'_{ig} may be found from the definition:

$$Q'_{ig} = \int_{\sigma_1}^{\sigma_5} e_{ig}\, d\sigma \qquad 4\text{-}56$$

It is also necessary to find $a_{i\sigma}$, the distribution function for the stable gained agglomerates, Q''_{ig}, so that Q''_{ig} may be computed

$$Q''_{ig} = \int_{\sigma_5}^{\infty} a_{i\sigma} \, d\sigma \qquad 4\text{-}57$$

The distribution function, $a_{i\sigma}$, is found from a mass balance in the differential strength range from σ to $\sigma + d\sigma$ for the agglomerates in Q''_{ig}, the stable gained agglomerates. This is done in the same manner, as for the agglomerates Q'_{ig}, detailed in section 4.3.5. The mass balance yields:

$$\frac{da_{i\sigma}}{dt} = \sum_{j=i+1}^{N} \frac{C_{ij}}{C_{jj}} \frac{ds_{j\sigma}}{dt} \qquad 4\text{-}58$$

It remains to determine Q'_{ior}, Q''_{io} being known from the initial condition and is time-invariant. From the definitions in section 4.3.4:

$$Q'_{ior} = \int_{\sigma_1}^{\sigma_5} A_{it} \, \rho_\sigma \, d\sigma \qquad 4\text{-}59$$

and

$$A_{it} = - K \dot{\gamma} A_{io} e^{-K\dot{\gamma}t} \qquad 4\text{-}56$$

as previously shown. The amount of agglomerates in the i^{th} species, Q_i, is available from

$$Q'_i = Q''_{io} + Q''_{ig} + Q'_{ig} + Q'_{ior} \qquad 4\text{-}60$$

where all the right hand side terms of the equation can be computed as outlined above.

The choice between the two methods depends on the ease of solution. The amount of computation involved in each case is about the same when the equations are solved numerically. If a program exists for the solution of the equilibrium case, it is easily converted to do some of the computation for the step-change in stress case. This situation obtained in this work, and the first scheme presented was used to find the size distributions.

4.4 SIZE DISTRIBUTIONS FOR A TIME-DEPENDENT SHEAR STRESS

4.4.1 Mass Balances

In this section, the equations describing the size distributions obtained when the shear stress is an arbitrary function of time will be derived. The derivation follows that given in the previous section for the step-change of shear stress modified to account for the varying shear stress. When the modification is obvious, the equations are not derived in detail. The same nomenclature has been retained insofar as possible. The function relating shear stress to time is:

$$\tau_5 = g(t) \qquad \text{4-61}$$

where τ_5 is directly comparable to τ_5 for the step-change case and is now a function of time, instead of being constant for

$t > 0$. It is assumed that $\tau_5 = \tau_{5_o}$ at $t = t_o$ and that the equilibrium distribution for τ_{5_o} has been obtained when $t = t_o$.

The derivation begins with mass balances on the stable, Q''_i, and breakable, Q'_i, agglomerates. As in the previous section the stable and breakable agglomerates are further subdivided into "gained" and "remaining original" categories. The same symbols are used to denote the appropriate distribution functions except in the case of Q'_{ior}, the remaining original agglomerates that are breakable. The new distribution function for these aggregates is defined by:

$$\int_{\sigma_1}^{\sigma_5} \alpha_{i\sigma}\, d\sigma = Q'_{ior} \qquad 4\text{-}62$$

The relationship between the distributions and the agglomerate "flow" for this case is illustrated in figure 4-3. It will be seen that there are two additional "flows" due to the time-varying nature of the shear stress. These flows are explained as follows: consider the agglomerates in the strength range from σ_a to $\sigma_a + d\sigma$. At time $t = t_\alpha$ the shear stress τ_5 is such that $\tau_5 < \sigma_a$ and the agglomerates belong to the stable division. At time $t = t_\beta$, $t_\beta > t_\alpha$, the shear stress has increased to a new value such that $\tau_5 > \sigma_\alpha$ and the agglomerates now belong to the breakable division. In particular the agglomerates in the strength range from σ_5 to $\sigma_5 + d\sigma$ for Q''_{io} and Q''_{ig}

FIGURE 4-3: Relationships Between the Various Portions of the Agglomerates in Species i and their Response to a Time-Varying Fluid Shear Stress

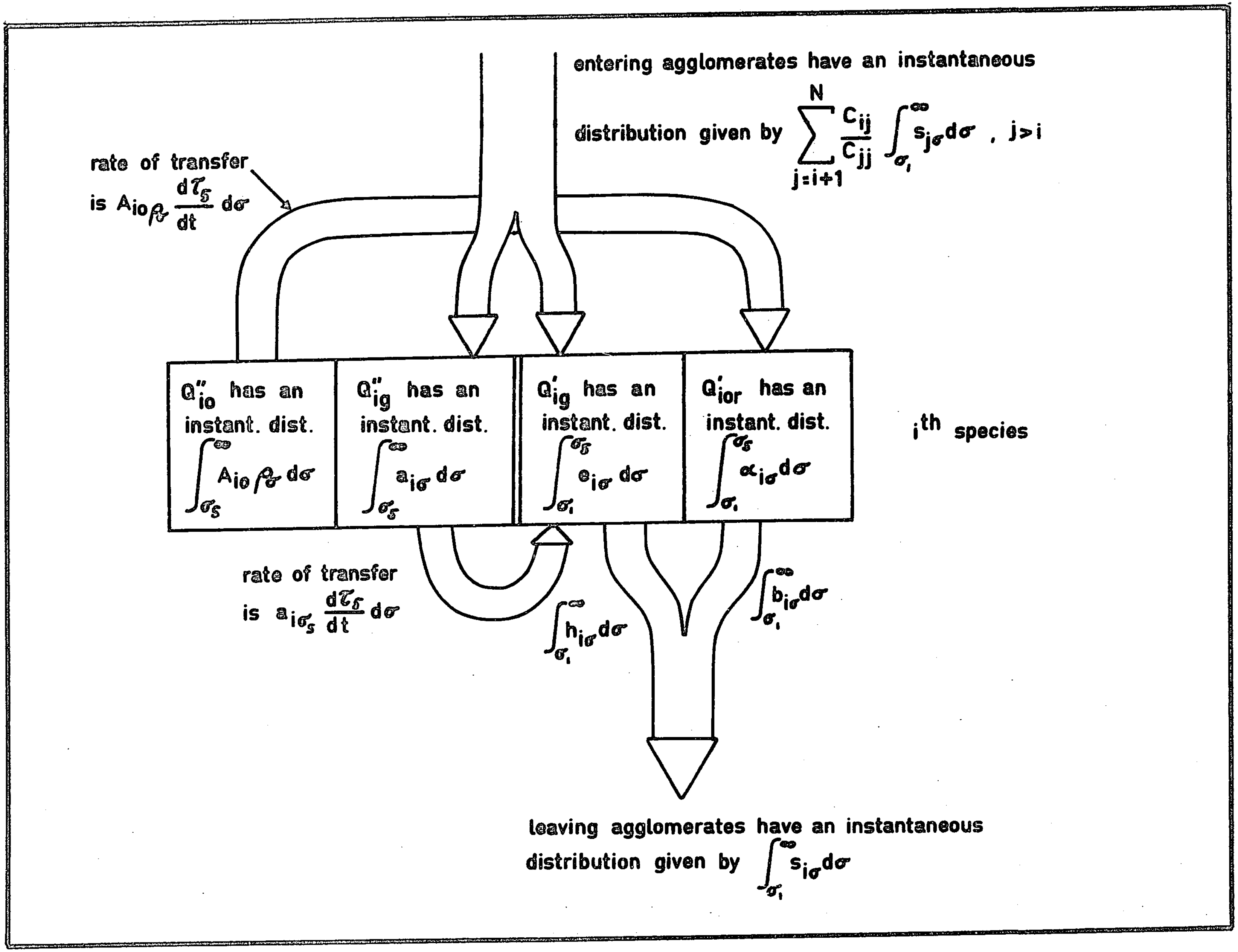

entering agglomerates have an instantaneous
distribution given by $\sum_{j=i+1}^{N} \frac{C_{ij}}{C_{jj}} \int_{\sigma_1}^{\infty} s_{j\sigma} d\sigma$, $j>i$
rate of transfer
is $A_{io}\rho_\sigma \frac{d\tau_\delta}{dt} d\sigma$
Q''_{io} has an instant. dist. $\int_{\sigma_\delta}^{\infty} A_{io}\rho_\sigma d\sigma$
Q''_{ig} has an instant. dist. $\int_{\sigma_\delta}^{\infty} a_{i\sigma} d\sigma$
Q'_{ig} has an instant. dist. $\int_{\sigma_1}^{\sigma_\delta} e_{i\sigma} d\sigma$
Q'_{ior} has an instant. dist. $\int_{\sigma_1}^{\sigma_\delta} \alpha_{i\sigma} d\sigma$
i^{th} species
rate of transfer
is $a_{i\sigma_\delta} \frac{d\tau_\delta}{dt} d\sigma$
$\int_{\sigma_1}^{\infty} h_{i\sigma} d\sigma$
$\int_{\sigma_1}^{\infty} b_{i\sigma} d\sigma$
leaving agglomerates have an instantaneous
distribution given by $\int_{\sigma_1}^{\infty} s_{i\sigma} d\sigma$

are given by $A_{io}\rho_{\sigma_5} d\sigma$ and $a_{i\sigma_5} d\sigma$, respectively, and these are the agglomerates being transferred. The rate at which they will disappear from Q_i'' and reappear in Q_i' is:

$$A_{io}\rho_{\sigma_5} \frac{d\tau_5}{dt} d\sigma = \text{rate of loss from } Q'_{io} = \text{rate of gain by } Q'_{ior} \quad 4\text{-}63$$

$$a_{i\sigma_5} \frac{d\tau_5}{dt} d\sigma = \text{rate of loss from } Q''_{ig} = \text{rate of gain by } Q'_{ior} \quad 4\text{-}64$$

The mass balances for the breakable and stable agglomerates may now be performed and they will be identical with the step-change case except for the two additional terms given by equations 4-63 and 4-64. The mass balance yields:

$$\sum_{j=i+1}^{N} f_j \frac{C_{ij}}{C_{jj}} K \dot{\gamma} Q_j' + A_{io}\rho_{\sigma_5} \frac{d\tau_5}{dt} + a_{i\sigma_5} \frac{d\tau_5}{dt} - K \dot{\gamma} Q_i' = \frac{dQ_i'}{dt} \quad 4\text{-}65$$

$$\sum_{j=i+1}^{N} (1-f_j) \frac{C_{ij}}{C_{jj}} K \dot{\gamma} Q_j' - [A_{io}\rho_{\sigma_5} + a_{i\sigma_5}] \frac{d\tau_5}{dt} = \frac{dQ_i''}{dt} \quad 4\text{-}66$$

for the breakable and stable agglomerates respectively. The shear rate, $\dot{\gamma}$, is not constant but is now a function of time. The function is obtained through the constitutive equation relating shear stress and shear rate and the known time dependency of shear stress, equation 4-61. If the fluid is Newtonian with a viscosity, μ, then:

$$\dot{\gamma} = \frac{g(t)}{\mu} \quad 4\text{-}67$$

is the required expression for shear rate. In the same manner as for the step-change case, f_j, is found from the agglomerate distribution function, $s_{j\sigma}$, which is, in turn obtained by solving the equations for differential mass balances for Q''_{ig}, Q'_{ig} and Q'_{ior}. In order to make a differential mass balance on Q'_{ior} the distribution function, $\alpha_{i\sigma}$ must be known. This distribution function is derived in the next subsection.

4.4.2 Distribution Function of the Breakable Remaining Original Agglomerates

For the general case of a time varying shear stress the length of time that the original agglomerates, in a strength range of σ to $\sigma + d\sigma$, have been breaking down depends on the relationship between time and shear stress, equation 4-61. Referring to figure 4-4, the agglomerates in the range from σ_{5_1} to $\sigma_{5_1} + d\sigma$ have only been degrading for a differential amount of time when

$$\tau = \tau_{5_1} = g(t_1) \qquad 4\text{-}68$$

However, at some later time, t_*, the length of time that they will have been subject to breakage shear stresses is $(t_* - t_1)$. For the general strength range, σ to $\sigma + d\sigma$, the amount of agglomerates is $\alpha_{i\sigma} d\sigma$ and from equation 4-36 the rate of breakage is:

FIGURE 4-4: The Change in the Size Distribution of the Original Agglomerates in Species i in Response to a Time-Varying Fluid Shear Stress

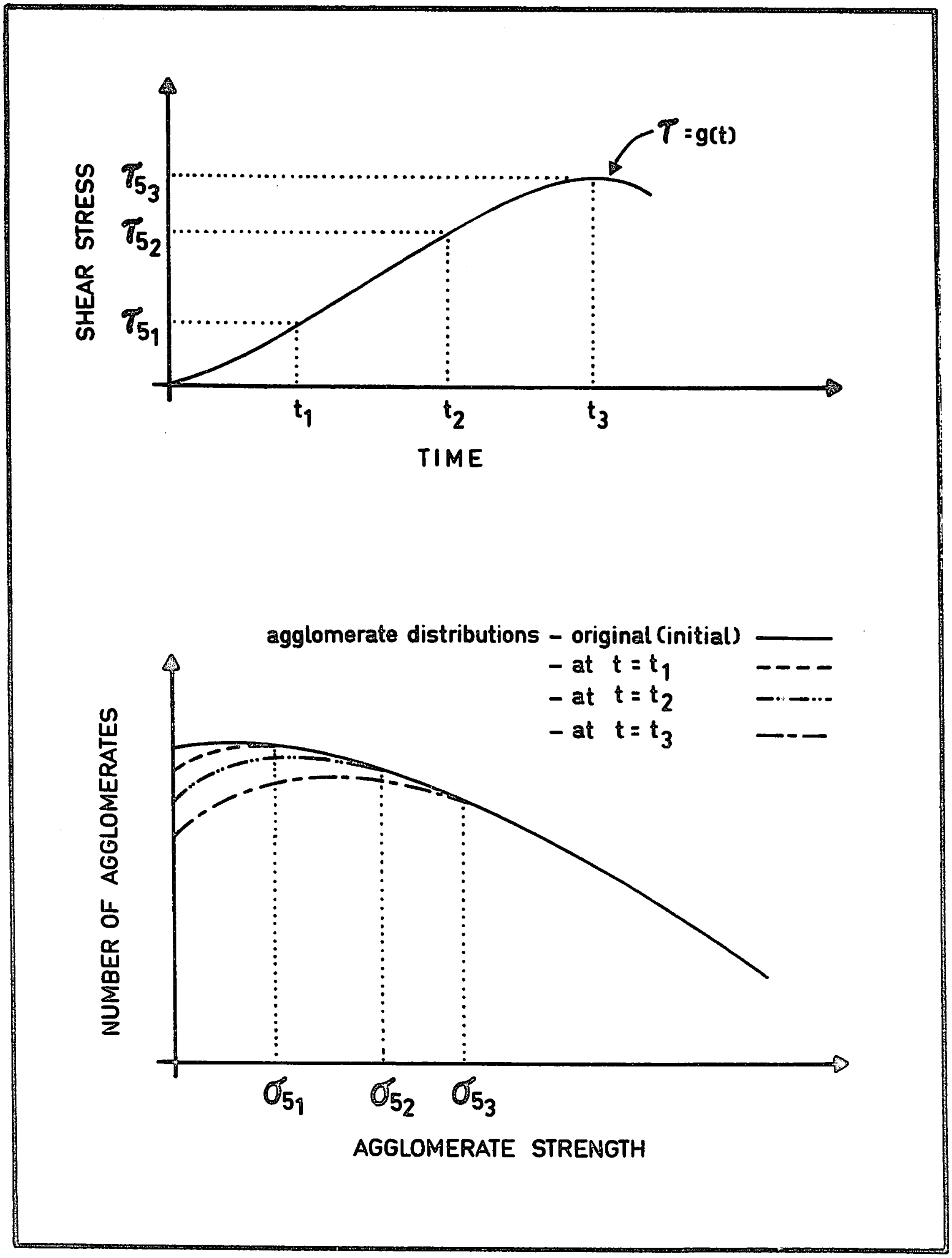

τ = g(t)
SHEAR STRESS
τ_{5_3}
τ_{5_2}
τ_{5_1}
t_1
t_2
t_3
TIME
agglomerate distributions - original (initial)
- at $t = t_1$
- at $t = t_2$
- at $t = t_3$
NUMBER OF AGGLOMERATES
σ_{5_1}
σ_{5_2}
σ_{5_3}
AGGLOMERATE STRENGTH

$$\frac{d\alpha_{i\sigma}}{dt} = K \dot{\gamma} \alpha_{i\sigma} \qquad 4\text{-}69$$

At the time when τ_5 becomes equal to σ, these agglomerates are transferred from Q''_{io} to Q'_{ior}. The amount is $A_{io}\rho_\sigma d\sigma$ and they begin breaking at the rate given by equation 4-69. The time at which the transfer occurs, t_σ

$$t_\sigma = g^{-1}(\tau_{5\sigma}) \qquad 4\text{-}70$$

and thus equation 4-69 does not apply for $t < t_\sigma = g^{-1}(\tau_{5\sigma})$. The initial condition for equation 4-69 is thus $\alpha_{i\sigma} = A_{io}\rho_\sigma$ when $t = t_\sigma = g^{-1}(\tau_{5\sigma})$.

For a Newtonian fluid, substituting for $\dot{\gamma}$ from equation 4-67 and integrating equation 4-69 gives the required expression for the distribution function:

$$\alpha_{i\sigma} = \exp\left[\frac{K}{\mu} \int g(t)dt\right] \times \text{constant} \qquad 4\text{-}71$$

where the constant is evaluated from the initial condition

$$\alpha_{i\sigma} = A_{io}\rho_\sigma \quad \text{when } t = g^{-1}(\tau_{5\sigma}) \qquad 4\text{-}72$$

4.4.3 Mass Balances on the Differential Strength Range σ to $\sigma + d\sigma$

The mass balances are identical with those for the step-change case except for the term added due to agglomerate transfer caused by the time change of shear stress. From equation

4-49, the balance for Q'_{ig} yields.

$$\frac{de_{i\sigma}}{dt} = \sum_{j=i+1}^{N} \frac{C_{ij}}{C_{jj}} \int_{\sigma_1}^{\sigma_5} \frac{ds_{i\sigma}}{dt} d\sigma - K \dot{\gamma} e_{i\sigma} + a_{i\sigma_5} \frac{d\tau_5}{dt} \qquad 4\text{-}73$$

The balance on the remaining original agglomerates, Q'_{ior}, gives:

$$\frac{d\alpha_{i\sigma}}{dt} = A_{io}\rho_{\sigma_5} \frac{d\tau_5}{dt} - K \dot{\gamma} \alpha_{i\sigma} \qquad 4\text{-}74$$

Finally, the instantaneous distribution of the gained unbreakable agglomerates, Q''_{ig}, is found from

$$\frac{da_{i\sigma}}{dt} = \sum_{j=i+1}^{N} \frac{C_{ij}}{C_{jj}} \int_{\sigma_5}^{\infty} \frac{ds_{i\sigma}}{dt} d\sigma - a_{i\sigma_5} \frac{d\tau_5}{dt} \qquad 4\text{-}75$$

The relationship between the distribution function of the degrading species and the distribution function of the agglomerates produced is as derived in Appendix VI and given below, except that it is noted that the limit, σ_5 is now a function of time, given by equation 4-61.

$$h_{j\sigma^*} = \rho_{\sigma^*} \int_{\sigma_1}^{\sigma^*} \frac{e_{i\sigma}}{[\int_{\sigma_1}^{\infty} \rho_\sigma \, d\sigma]} d\sigma \qquad \sigma_1 \le \sigma^* \le \sigma_5 \qquad 4\text{-}51$$

$$h_{j\sigma^*} = \rho_{\sigma^*} \int_{\sigma_1}^{\sigma_5} \frac{e_{i\sigma}}{[\int_{\sigma_1}^{\infty} \rho_\sigma \, d\sigma]} \, d\sigma \qquad \sigma_5 \leq \sigma^* \leq \infty \qquad \text{4-51a}$$

$$b_{i\sigma^*} = \rho_{\sigma^*} \int_{\sigma_1}^{\sigma^*} \frac{\alpha_{i\sigma}}{[\int_{\sigma_1}^{\infty} \rho_\sigma \, d\sigma]} \, d\sigma \qquad \sigma_1 \leq \sigma^* \leq \sigma_5 \qquad \text{4-76}$$

$$b_{i\sigma^*} = \rho_{\sigma^*} \int_{\sigma_1}^{\sigma_5} \frac{\alpha_{i\sigma}}{[\int_{\sigma_1} \rho_\sigma \, d\sigma]} \, d\sigma \qquad \sigma_5 \leq \sigma^* \leq \infty \qquad \text{4-76a}$$

4.4.4 Scheme for the Solution of the Equations

The scheme for solution of the equations is very similar to the one detailed for the step change in shear stress case. As previously, all equations are solved in reverse order, starting with i = N and proceeding to i = 1.

1. Solve equation 4-74 to obtain the distribution function, $a_{i\sigma}$, which is required for the next step.
2. Solve equation 4-73 to obtain the distribution function, $e_{i\sigma}$, for Q'_{ig}.
3. Solve equation 4-75 to get the distribution function, $\alpha_{i\sigma}$.
4. Apply equations 4-51a and 4-76a to find the distribution functions of the degradation products, $s_{i\sigma}$.

5. Use the relationship, equation 4-43

$$f_i = \frac{\int_{\sigma_1}^{\sigma_5} s_{i\sigma} \, d\sigma}{\int_{\sigma_1}^{\infty} s_{i\sigma} \, d\sigma} \qquad 4\text{-}43$$

6. Finally the overall mass balances, equations 4-65 and 4-66 may now be solved, resulting in the desired size distributions of the agglomerates.

CHAPTER 5

RESULTS

5.1 VARIATION OF SHEAR STRESS AND TEMPERATURE IN THE EXPERIMENTAL APPARATUS

It was explained in section 3.1 that the direct measurement of the shear stress (or shear rate) in the experimental apparatus would be very difficult. Instead, these parameters were computed by numerically solving the equations of motion and energy with the appropriate boundary conditions (the equations and the computer program are given in Appendix I). The computed results are presented in this section. The numerical solution was verified indirectly by comparing computed and measured temperature profiles. These results are given in the next subsection.

Wall curvature and temperature differences caused the shear stress to vary slightly across the gap, hence the stress applied to an agglomerate depended on its position in the gap. The sample analysis procedure did not determine the agglomerates' positions in the gap and thus introduced a small error (which is discussed in section 5.3.2). For the above reason the deagglomeration results are presented in terms of the mean shear stress in the gap, τ_m, defined by:

$$\tau_m = \frac{1}{R^*} \int_0^1 \tau_{R^*} \, dR^* \qquad 5\text{-}1$$

where

R^* = dimensionless radial gap position = $\dfrac{R - R_i}{R_o - R_i}$

R = radial position in the gap

R_i = inner cylinder radius

R_o = outer cylinder radius

τ_{R^*} = shear stress at position R^*

The calculated mean shear stress as a function of inner cylinder speed is given in figure 5-1 for the condition of the inner cylinder wall 4.3°F hotter than the outer cylinder. This condition obtained during the experimental runs. The case of identical inner and outer cylinder wall temperatures is shown for comparison. It is seen that both conditions lead to small deviations from linearity at the higher speeds. These deviations are caused by shear heating of the fluid.

It was observed experimentally that the temperature difference between the two cylinders remained almost constant (within 0.1°F) although the wall temperatures varied by as much as $\pm$ 0.5°F from the set point temperature. The effect of this temperature variation on the shear stress was investigated, and the computed profiles are plotted in figure 5-2 for an inner cylinder speed of 50 RPM. Figure 5-2 shows that a change

FIGURE 5-1: Computed Mean Shear Stress as a Function of Inner Cylinder Rotational Speed. Curves are Shown for Equal Inner and Outer Cylinder Wall Temperatures and for the Case with the Inner Cylinder Wall Temperature 4.3°F Higher than the Outer Cylinder Wall Temperature

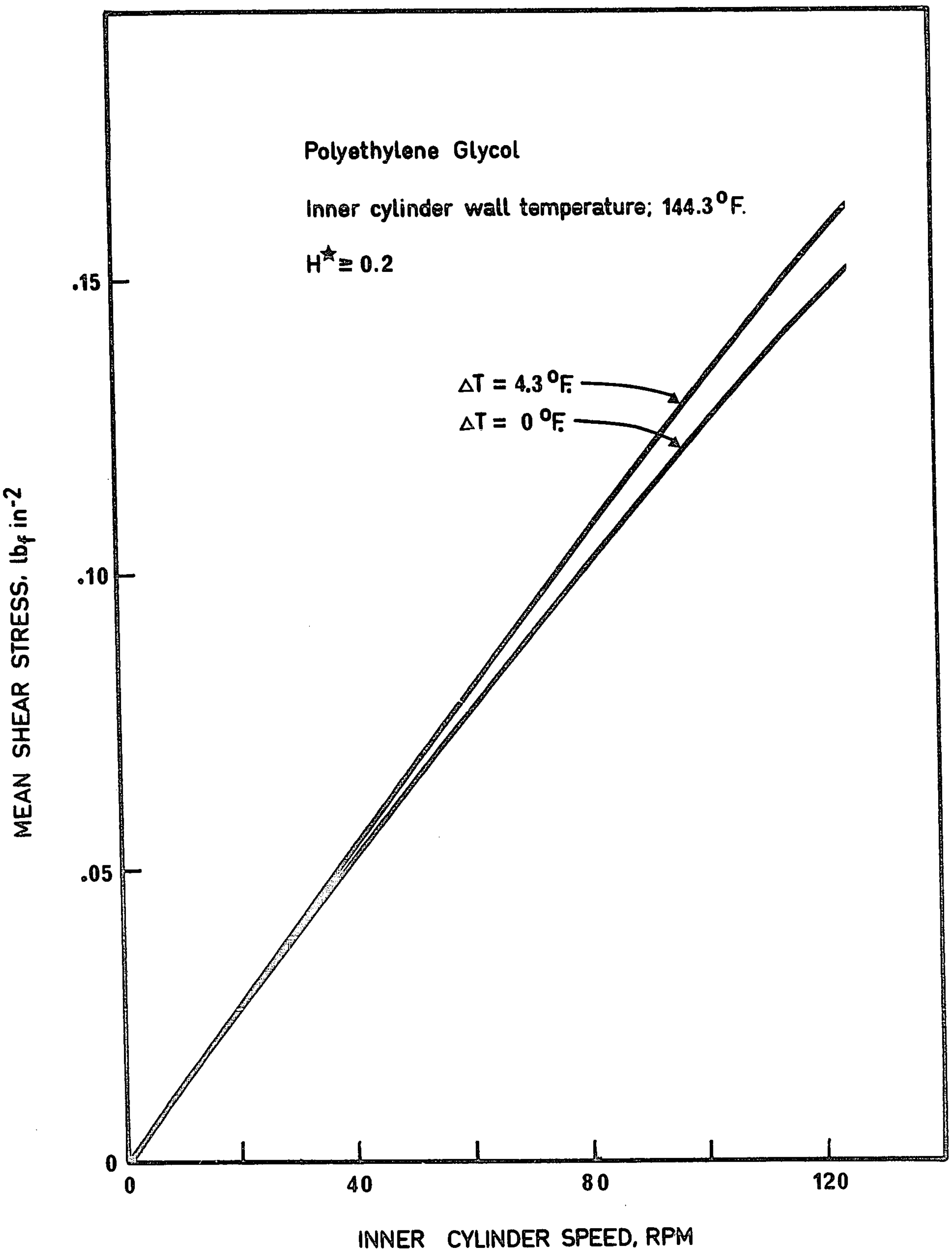

Polyethylene Glycol
Inner cylinder wall temperature; 144.3 °F.
H* ≥ 0.2
ΔT = 4.3 °F.
ΔT = 0 °F.
MEAN SHEAR STRESS, lbf in-2
.15
.10
.05
0
0
40
80
120
INNER CYLINDER SPEED, RPM

FIGURE 5-2: Computed Shear Stresses as a Function of Dimensionless Position in the Gap are Shown for Four Different Conditions of Inner and Outer Cylinder Wall Temperatures

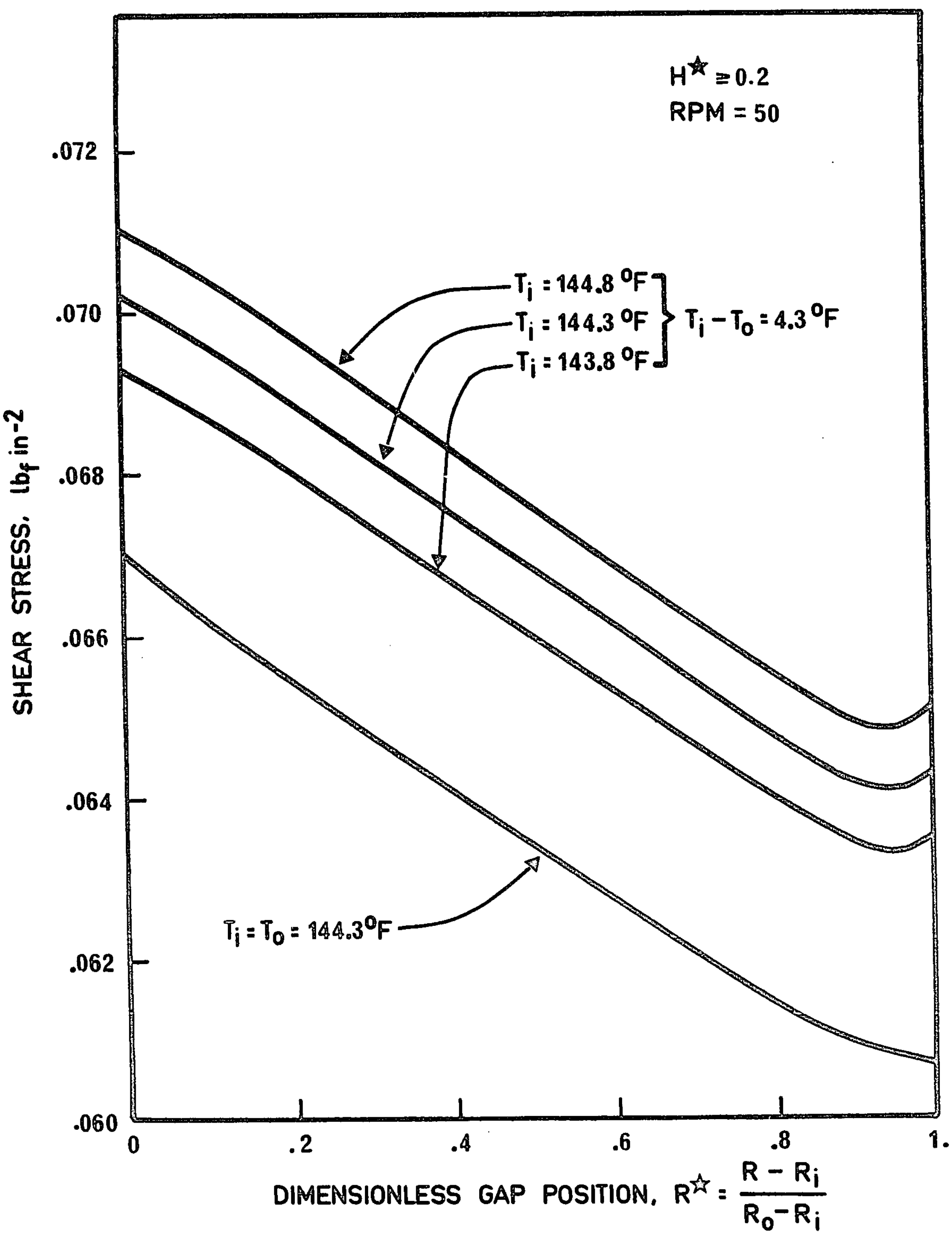

H* ≥ 0.2
RPM = 50
.072
.070
.068
.066
.064
.062
.060
SHEAR STRESS, lbf in-2
Ti = 144.8 °F
Ti = 144.3 °F
Ti = 143.8 °F
Ti − To = 4.3 °F
Ti = To = 144.3°F
0
.2
.4
.6
.8
1.
DIMENSIONLESS GAP POSITION, R* = (R − Ri)/(Ro − Ri)

of $0.5^{\circ}F$ in the wall temperatures causes the shear stress profile (and hence the mean shear stress) to shift by about 1%. Also included in figure 5-2 is the profile calculated for equal wall temperatures. Examining the profiles it is seen that the case of unequal wall temperatures has an inflection point at $R^* \approx 0.8$ and a minimum at $R^* \approx 0.96$ while the isothermal case has neither of these features. The minimum is due to the competing effects of the temperature gradient and the shear rate variation across the gap. The falling temperature, as R^* increases, tends to raise the fluid viscosity, and thus increase the shear stress. However, due to wall curvature, the shear rate, and hence the shear stress, decreases with increasing R^*. The two effects together cause the minimum and the inflection points.

5.2 ESTIMATION OF ERRORS

5.2.1 Temperature Profiles as a Verification of Computed Values

It was decided that measured temperature profiles could be used to check the numerical solution of the motion and energy equations. This avoids the very difficult problem of determining the shear stress or shear rate in the experimental apparatus. The check is possible because of the coupling of the equations through the viscosity and its temperature dependence.

The experimental measurements and computed profiles are shown in figures 5-3 to 5-8. The range of measured temperatures at each position is indicated by the I-shaped vertical lines. Computed profiles are shown as a continuous curve. The agreement is good up to an inner cylinder speed of 50 RPM. Above this speed the deviation of the experimental values becomes more pronounced and irregular. The disagreement worsens as the speed increases.

The disagreement could be caused by both frictional heating of the probe and probe bending and movement. The effect of frictional heating is difficult to estimate quantitively and the irregular nature of the deviations suggests that they are primarily caused by the probe bending and moving away from its nominal position. The bending would be caused by the drag force acting on the probe. No probe movement could be observed, but the maximum deviation required to explain the discrepancy at 80 RPM would be 0.015 inches at the probe tip. Since the probe was submerged to about two-thirds of its length, the visible movement would be somewhat smaller than 0.005 inches, hence the difficulty of visually detecting the presumed movement.

The agreement between computed and experimental values for temperature gives confidence that the numerical solution of the equations is correct. This suggests that the calculated

FIGURE 5-3: Dimensionless Temperature, $T^* = \frac{T - T_o}{T_i - T_o}$, as a Function of Dimensionless Position, $R^* = \frac{R - R_i}{R_o - R_i}$, at an Inner Cylinder Rotational Speed of 20 RPM. The Solid Curve is a Computed Result. The Vertical Bars Indicate the Range of Temperatures Measured in Three Trials

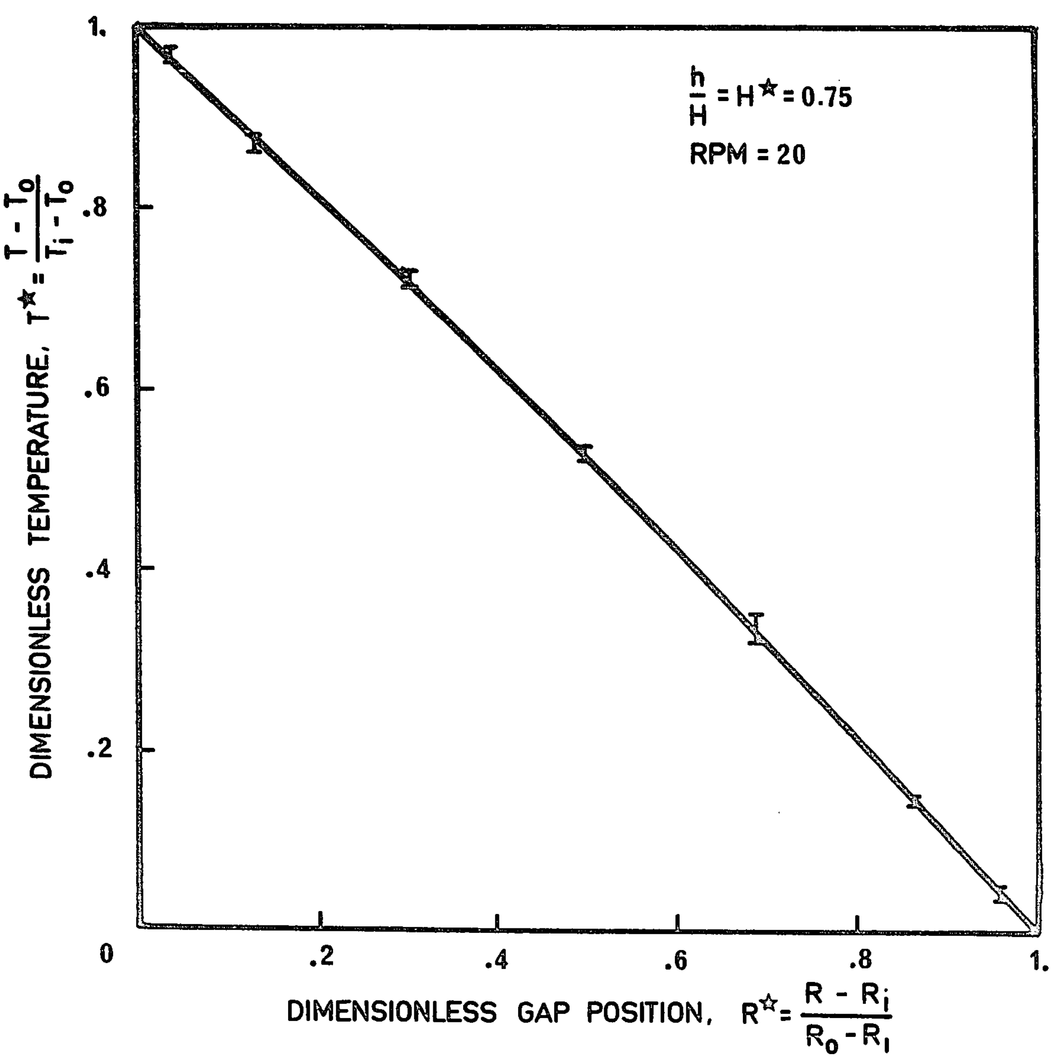

$\frac{h}{H} = H^{\star} = 0.75$
RPM = 20
DIMENSIONLESS TEMPERATURE, $T^{\star} = \frac{T - T_o}{T_i - T_o}$
DIMENSIONLESS GAP POSITION, $R^{\star} = \frac{R - R_i}{R_o - R_i}$
0
.2
.4
.6
.8
1.

FIGURE 5-4: Dimensionless Temperature, $T^* = \frac{T - T_o}{T_i - T_o}$, as a Function of Dimensionless Position, $R^* = \frac{R - R_i}{R_o - R_i}$, at an Inner Cylinder Rotational Speed of 30 RPM. The Solid Curve is a Computed Result. The Vertical Bars Indicate the Range of Temperatures Measured in Three Trials

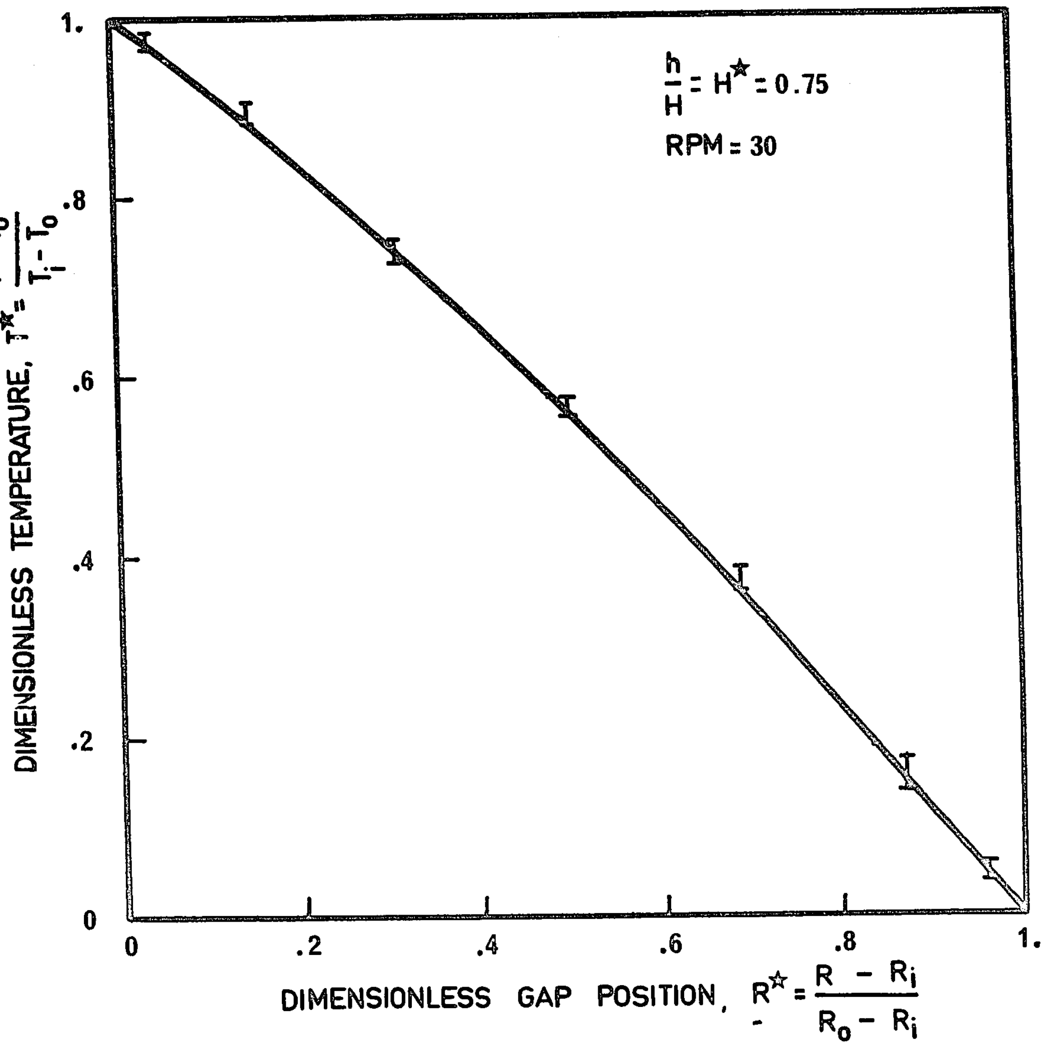

h/H = H* = 0.75
RPM = 30
DIMENSIONLESS TEMPERATURE, $T^{*} = \frac{T - T_o}{T_i - T_o}$
DIMENSIONLESS GAP POSITION, $R^{*} = \frac{R - R_i}{R_o - R_i}$
0
.2
.4
.6
.8
1.

FIGURE 5-5: Dimensionless Temperature, $T^* = \frac{T - T_o}{T_i - T_o}$, as a Function of Dimensionless Position, $R^* = \frac{R - R_i}{R_o - R_i}$, at an Inner Cylinder Rotational Speed of 40 RPM. The Solid Curve is a Computed Result. The Vertical Bars Indicate the Range of Temperatures Measured in Three Trials

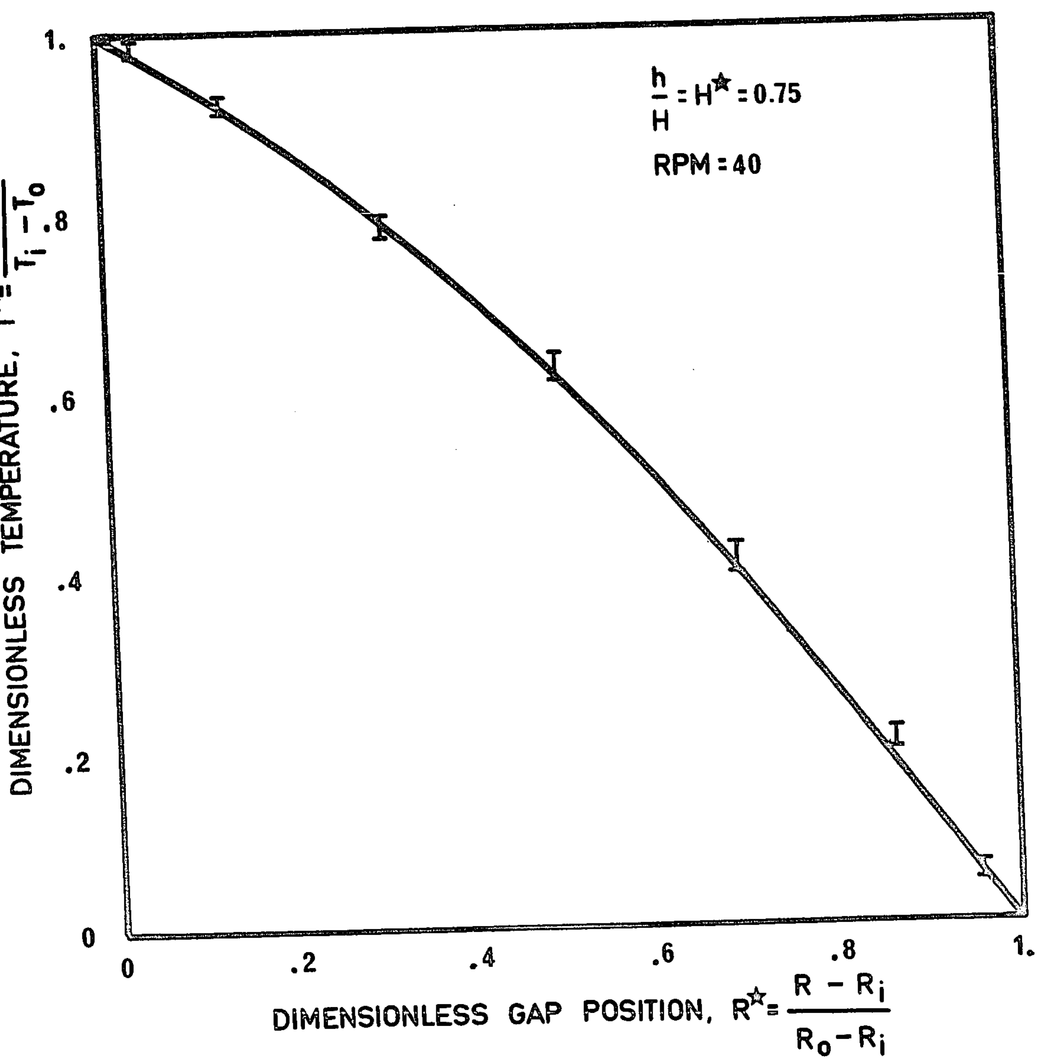

h/H = H* = 0.75
RPM = 40
DIMENSIONLESS TEMPERATURE, T* = (T - To)/(Ti - To)
1.
.8
.6
.4
.2
0
0
.2
.4
.6
.8
1.
DIMENSIONLESS GAP POSITION, R* = (R - Ri)/(Ro - Ri)

FIGURE 5-6: Dimensionless Temperature, $T^* = \frac{T - T_o}{T_i - T_o}$, as a Function of Dimensionless Position, $R^* = \frac{R - R_i}{R_o - R_i}$, at an Inner Cylinder Rotational Speed of 50 RPM. The Solid Curve is a Computed Result. The Vertical Bars Indicate the Range of Temperatures Measured in Three Trials

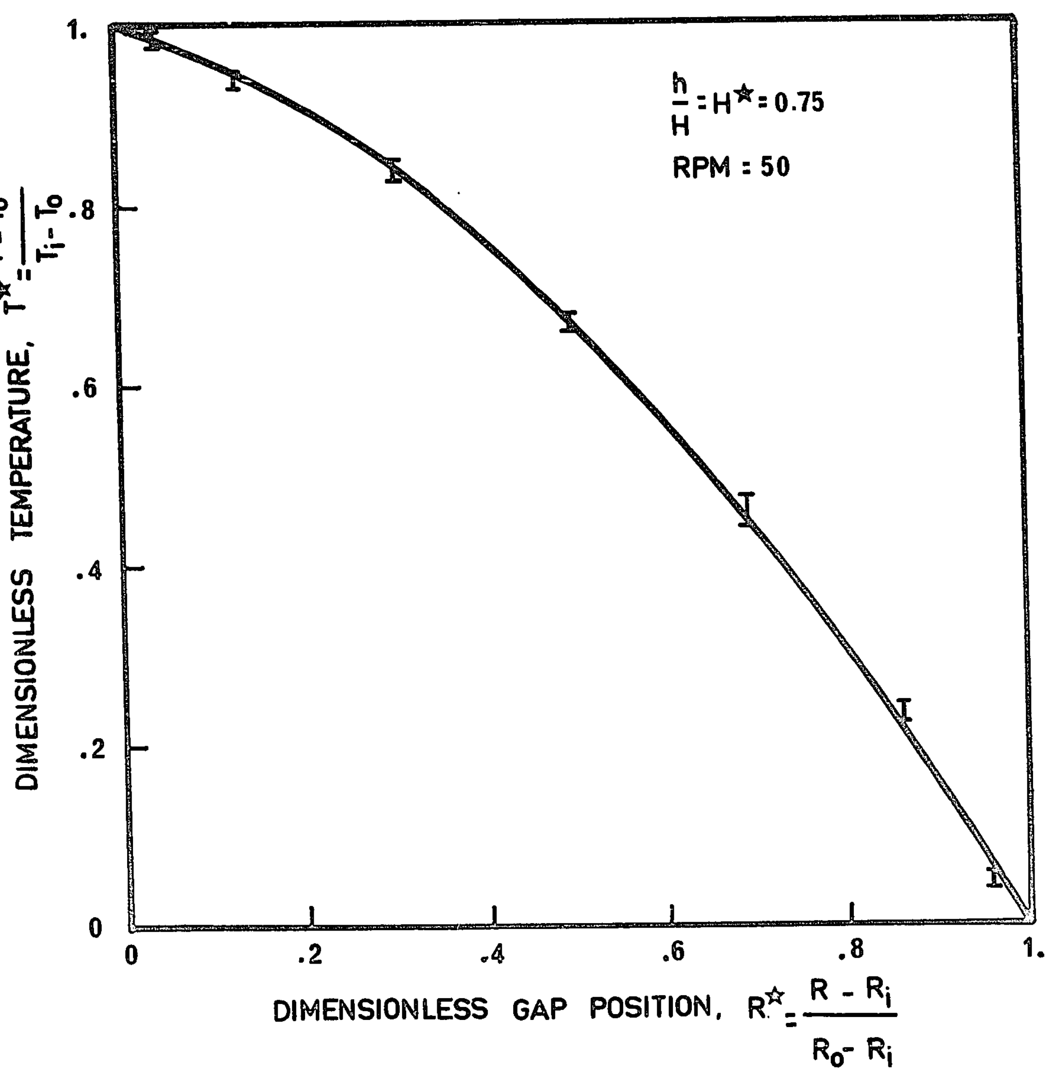

$\frac{h}{H} = H^{☆} = 0.75$
RPM : 50
DIMENSIONLESS TEMPERATURE, $T^{☆} = \frac{T - T_o}{T_i - T_o}$
1.
.8
.6
.4
.2
0
0
.2
.4
.6
.8
1.
DIMENSIONLESS GAP POSITION, $R^{☆} = \frac{R - R_i}{R_o - R_i}$

FIGURE 5-7: Dimensionless Temperature, $T^* = \frac{T - T_o}{T_i - T_o}$, as a Function of Dimensionless Position, $R^* = \frac{R - R_i}{R_o - R_i}$, at an Inner Cylinder Rotational Speed of 60 RPM. The Solid Curve is a Computed Result. The Vertical Bars Indicate the Range of Temperatures Measured in Three Trials

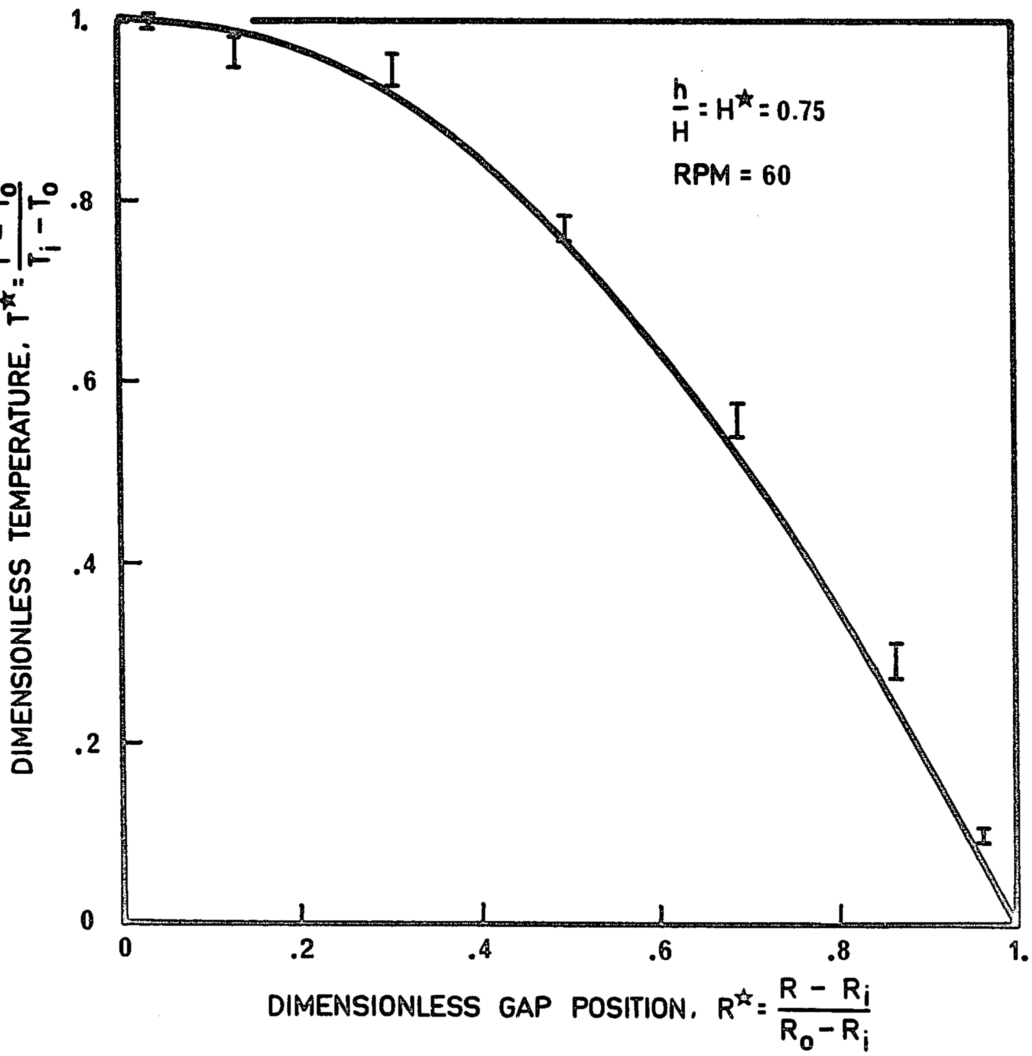

h/H = H* = 0.75
RPM = 60
DIMENSIONLESS TEMPERATURE, T* = (T - To)/(Ti - To)
1.
.8
.6
.4
.2
0
0
.2
.4
.6
.8
1.
DIMENSIONLESS GAP POSITION, R* = (R - Ri)/(Ro - Ri)

FIGURE 5-8: Dimensionless Temperature, $T^* = \frac{T - T_o}{T_i - T_o}$, as a Function of Dimensionless Position, $R^* = \frac{R - R_i}{R_o - R_i}$, at an Inner Cylinder Rotational Speed of 80 RPM. The Solid Curve is a Computed Result. The Vertical Bars Indicate the Range of Temperatures Measured in Three Trials

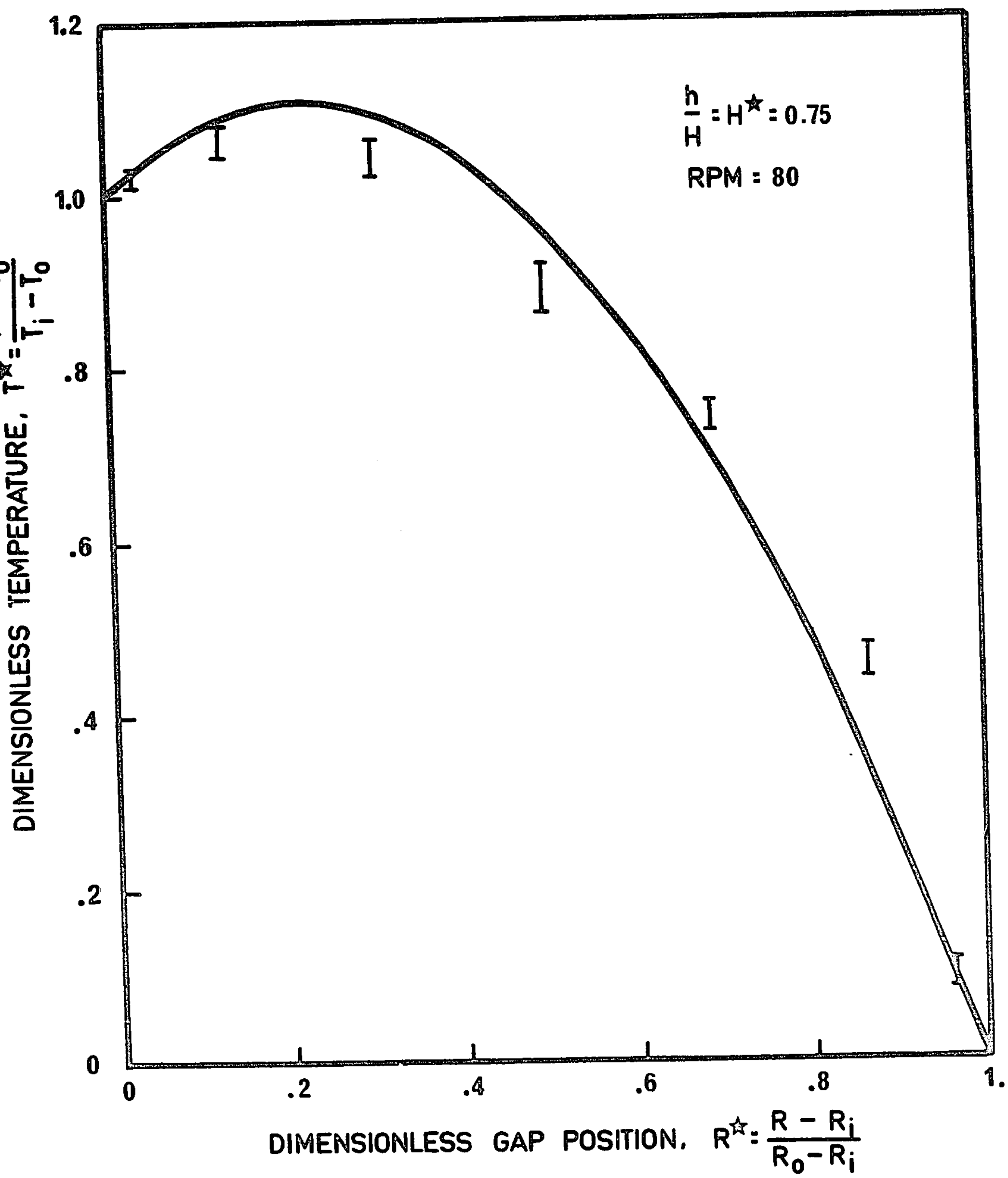

1.2
1.0
.8
.6
.4
.2
0
0
.2
.4
.6
.8
1.
$\frac{h}{H} = H^{\star} = 0.75$
RPM = 80
DIMENSIONLESS TEMPERATURE, $T^{\star} = \frac{T - T_o}{T_i - T_o}$
DIMENSIONLESS GAP POSITION, $R^{\star} = \frac{R - R_i}{R_o - R_i}$

shear stress should be close to the actual experimental shear stress. An estimate of the error due to this indirect verification of the shear stress values is given in the next subsection.

5.2.2 Estimate of Error in the Shear Stress

Errors may be caused by uncertainties in the values of thermal conductivity, fluid viscosity and cylinder wall temperatures. These errors and their contribution to the error in the computed shear stress values are summarized in Table 5-1. The errors in viscosity and thermal conductivity were estimated to be $\pm 2\%$ and $\pm 6\%$ respectively. These estimates were obtained by considering the scatter of the measured values (see Appendix III). The error in the thermal conductivity measurements is similar to that reported by Shoulberg (74). He estimated the accuracy of the experimental technique employed in this work to measure thermal conductivity to be 7%. The computed effects of a 6% change in thermal conductivity and a 1% change in viscosity are shown in figures 5-9 and 5-10, respectively. The change in shear stress due to the estimated errors in viscosity and thermal conductivity are, respectively, $\pm 2\%$ and $\pm 1\%$.

The effect of errors in wall temperature measurement can be found by reference to figure 5-2. An indeterminancy of $0.5^{\circ}F$ in both wall temperatures produces a shift in the shear stress profile of about 1.1%.

TABLE 5-1

SUMMARY OF ERROR CONTRIBUTIONS TO THE ERROR IN THE COMPUTED SHEAR STRESS

PARAMETER	ESTIMATED PARAMETER ERROR	ERROR IN SHEAR STRESS
viscosity	$\pm$ 2%	$\pm$ 2%
thermal conductivity	$\pm$ 6%	$\pm$ 1%
wall temperatures	$\pm 0.5^{\circ}F$ ($\pm$.35%)	$\pm$ 1.1%
	TOTAL	$\pm$ 4.1%

FIGURE 5-9: Dimensionless Temperature, $T^* = \frac{T - T_o}{T_i - T_o}$, Versus Dimensionless Gap Position $R^* = \frac{R - R_i}{R_o - R_i}$, for an Inner Cylinder Rotational Speed of 50 RPM. Two Computed Results for a Fluid Thermal Conductivity of Six Percent Larger and Six Percent Smaller than the Nominal Value are Shown as Continuous Curves. The Measured Temperature Ranges are Shown as Vertical Bars and are the Result of Three Trials

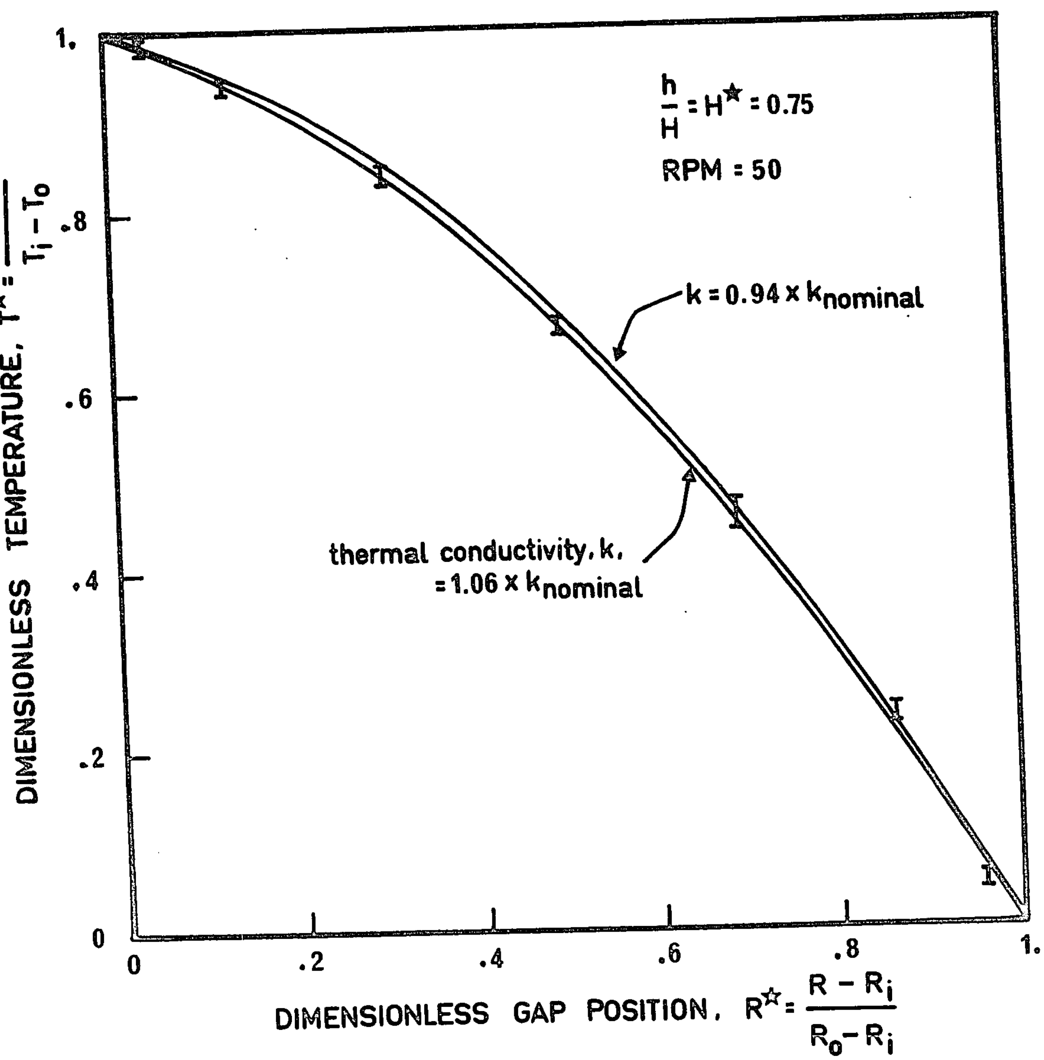

$\frac{h}{H} = H^{\star} = 0.75$
RPM = 50
$k = 0.94 \times k_{nominal}$
thermal conductivity, k, $= 1.06 \times k_{nominal}$
DIMENSIONLESS TEMPERATURE, $T^{\star} = \frac{T - T_o}{T_i - T_o}$
DIMENSIONLESS GAP POSITION, $R^{\star} = \frac{R - R_i}{R_o - R_i}$
0
.2
.4
.6
.8
1.

FIGURE 5-10: Computed Shear Stress Profiles Showing the Change Due to a Fluid Thermal Conductivity that is Six Percent Larger, or Smaller, than the Nominal Value

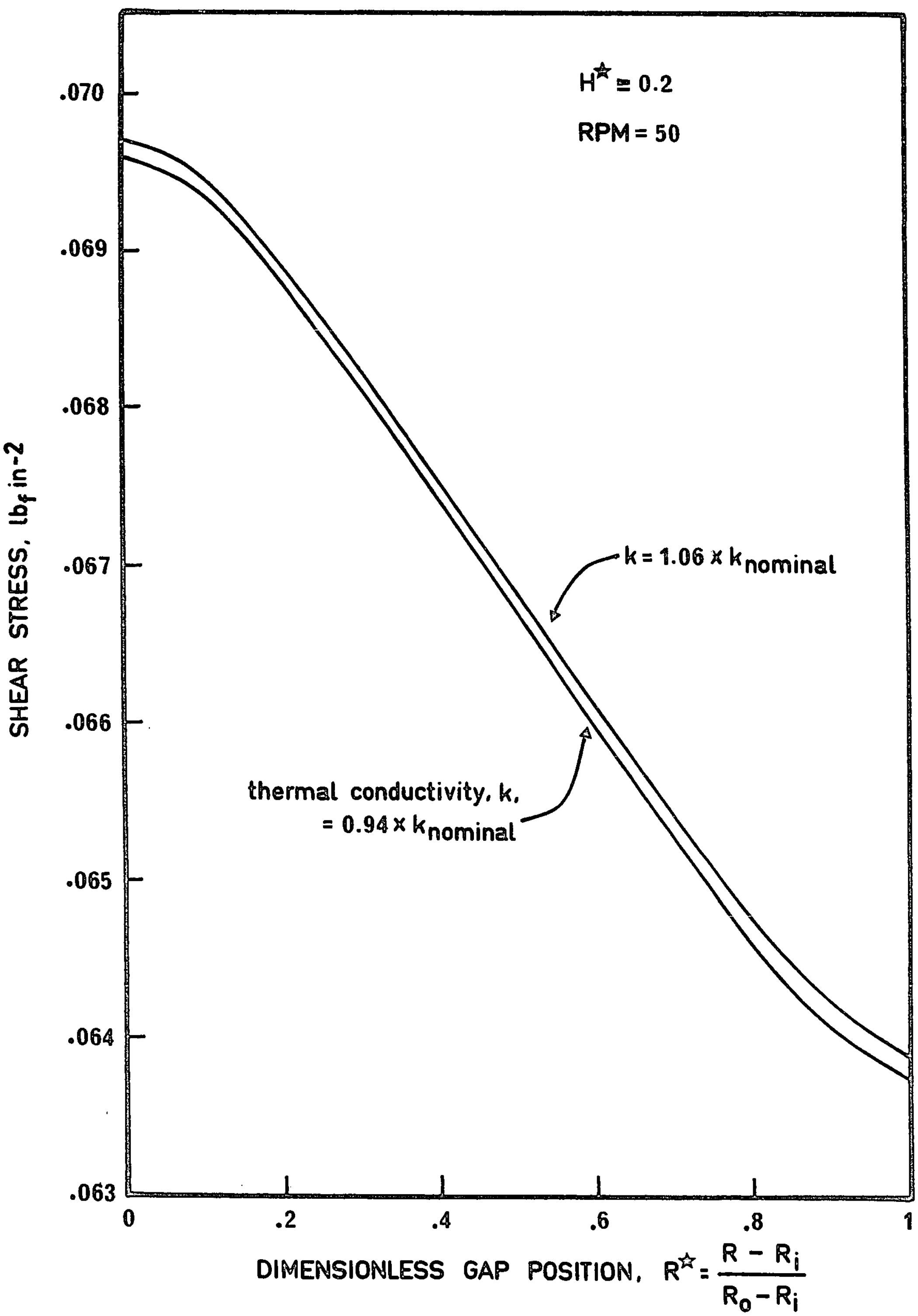

H☆ ≅ 0.2
RPM = 50
k = 1.06 x knominal
thermal conductivity, k, = 0.94 x knominal
.070
.069
.068
.067
.066
.065
.064
.063
SHEAR STRESS, lbf in-2
0
.2
.4
.6
.8
1.
DIMENSIONLESS GAP POSITION, R☆ = (R − Ri)/(Ro − Ri)

A reasonable estimate for the overall maximum possible error for the computed shear stress is thus about 4%. The error introduced by the use of the mean shear stress to correlate the deagglomeration results is discussed in section 5.3.2.

5.3 DEAGGLOMERATION RESULTS

5.3.1 Experimental Data and Comparison with Theory

A total of eight runs were conducted using the synthetic agglomerates. The results of the five equilibrium runs are presented in figures 5-11 to 5-15 and the step change in shear stress runs are plotted in figures 5-16 to 5-18. Experimental data are indicated by the points corresponding to the appropriate agglomerate size. Theoretically calculated results are represented by the continuous curves. In each case the shear stress used has been the mean shear stress as defined by equation 5-1. To avoid crowding of the larger agglomerates' data the results are plotted in terms of weight percent instead of the number percent derived in the theory. Number and weight percent are defined as:

$$\text{number percent of the } i^{th} \text{ species} \equiv \frac{n_i}{\sum_i n_i} \times 100\% \qquad 5\text{-}2$$

$$\text{weight percent of the } i^{th} \text{ species} \equiv \frac{i n_i}{\sum_i i n_i} \times 100\% \qquad 5\text{-}3$$

FIGURE 5-11: The Change in Weight Percent, for Species $i = 1$ to $i = 8$, Versus Fluid Shear Stress for the Equilibrium Case. Values Computed from the Model are Shown as Continuous Curves; Experimental Results are Indicated by the Appropriate Symbol. The Agglomerate Concentration was One Percent by Weight

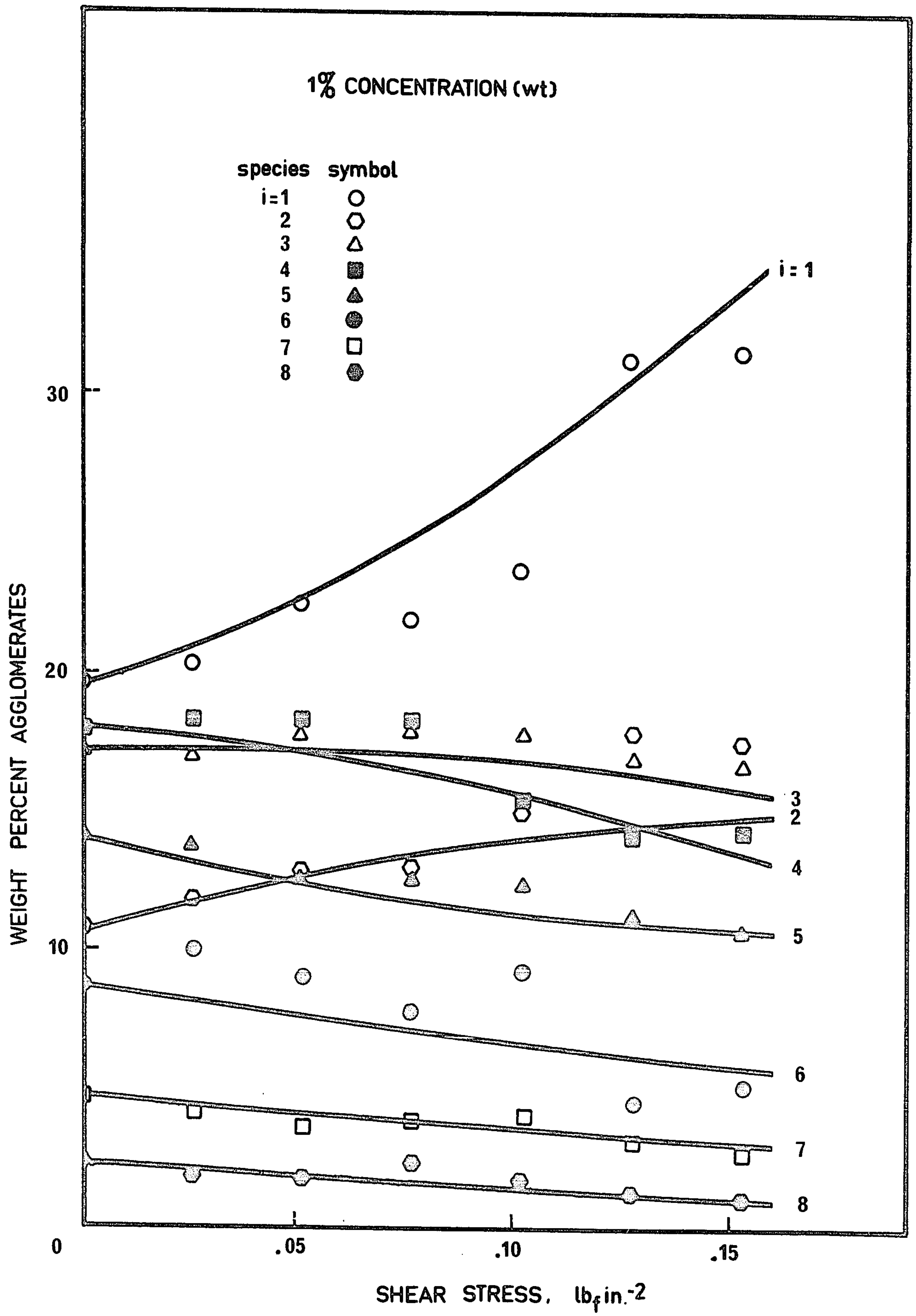
1% CONCENTRATION (wt)
species symbol
i=1
2
3
4
5
6
7
8
i : 1
3
2
4
5
6
7
8
30
20
10
0
.05
.10
.15
WEIGHT PERCENT AGGLOMERATES
SHEAR STRESS, $lb_f in.^{-2}$

FIGURE 5-12: Similar to Figure 5-11 Except for a Different Initial Size Distribution. The Change in Weight Percent, for Species $i = 1$ to $i = 8$, Versus Fluid Shear Stress for the Equilibrium Case. Values Computed from the Model are Shown as Continuous Curves; Experimental Results are Indicated by the Appropriate Symbol. The Agglomerate Concentration was One Percent by Weight

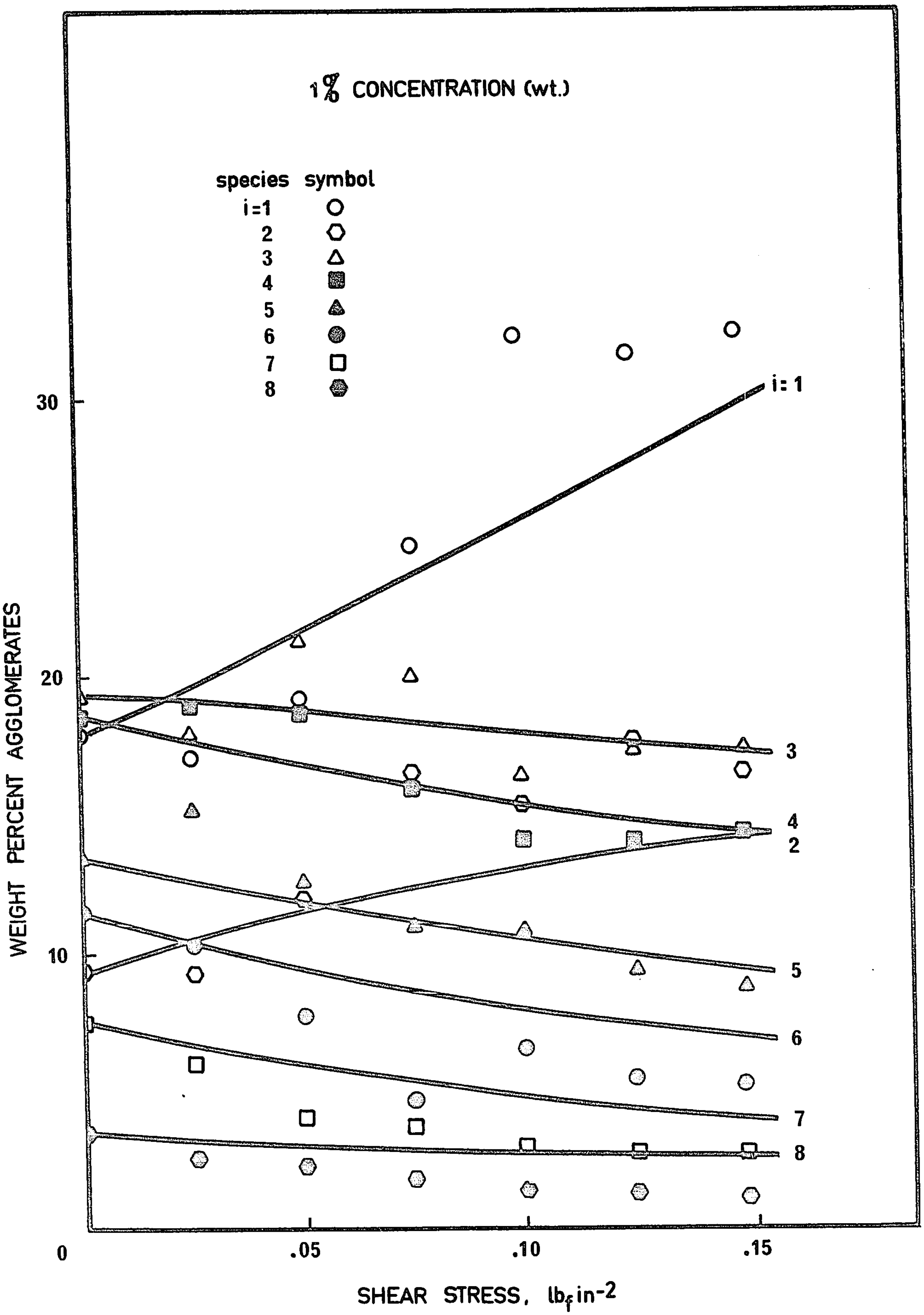
1% CONCENTRATION (wt.)
species symbol
i=1
2
3
4
5
6
7
8
i: 1
3
4
2
5
6
7
8
30
20
10
0
.05
.10
.15
WEIGHT PERCENT AGGLOMERATES
SHEAR STRESS, lbf in-2

FIGURE 5-13: Similar to Figures 5-11 and 5-12 Except for a Different Initial Size Distribution. The Change in Weight Percent, for Species $i = 1$ to $i = 8$, Versus Fluid Shear Stress for the Equilibrium Case. Values Computed from the Model are Shown as Continuous Curves; Experimental Results are Indicated by the Appropriate Symbol. The Agglomerate Concentration was One Percent by Weight

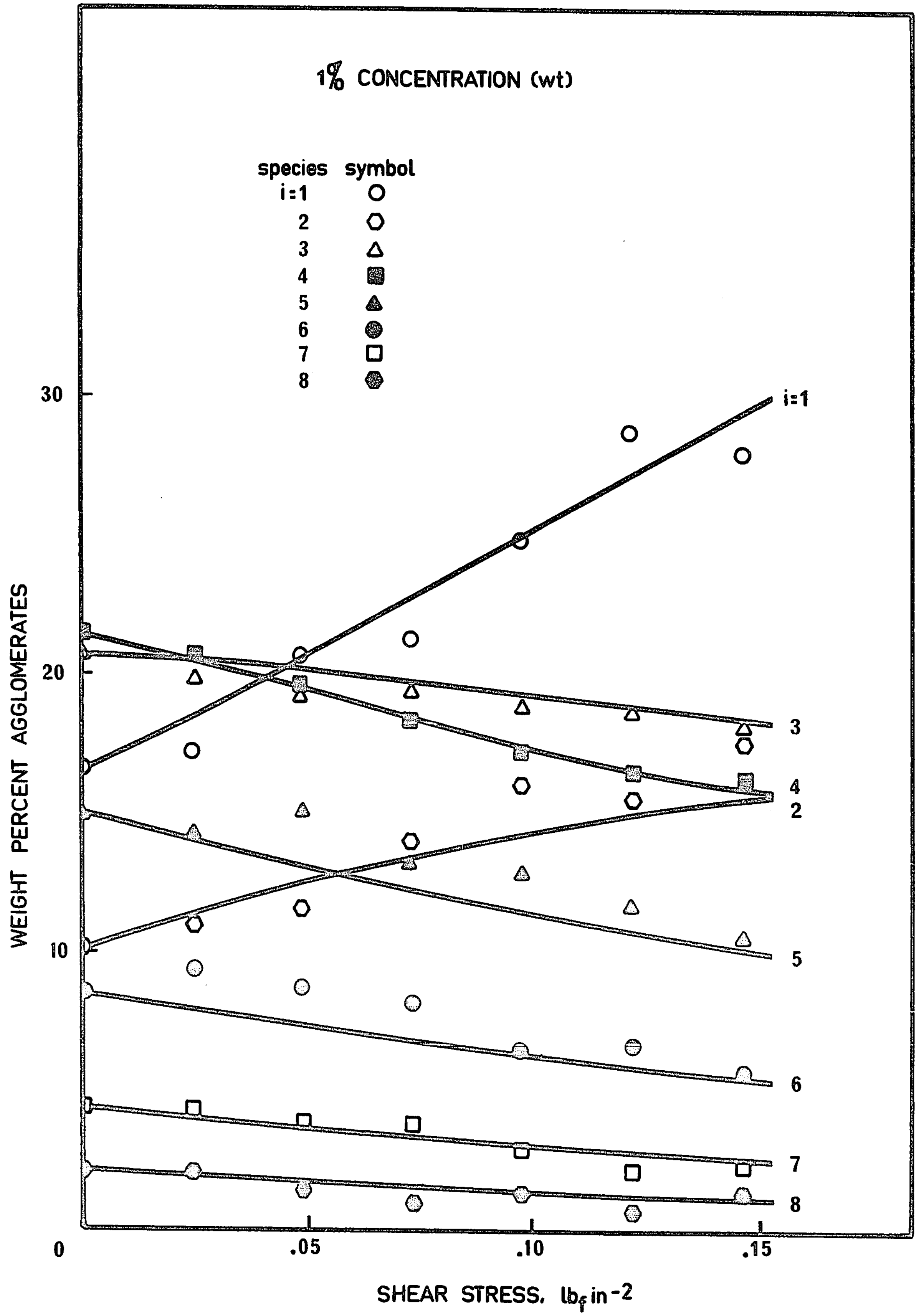

1% CONCENTRATION (wt)
species symbol
i=1
2
3
4
5
6
7
8
WEIGHT PERCENT AGGLOMERATES
30
20
10
0
.05
.10
.15
SHEAR STRESS, lbf in-2
i=1
3
4
2
5
6
7
8

FIGURE 5-14: The Change in Weight Percent, For Species $i = 1$ to $i = 8$, Versus Fluid Shear Stress for the Equilibrium Case. Values Computed from the Model are Shown as Continuous Curves; Experimental Results are Indicated by the Appropriate Symbol. The Agglomerate Concentration was Two Percent by Weight

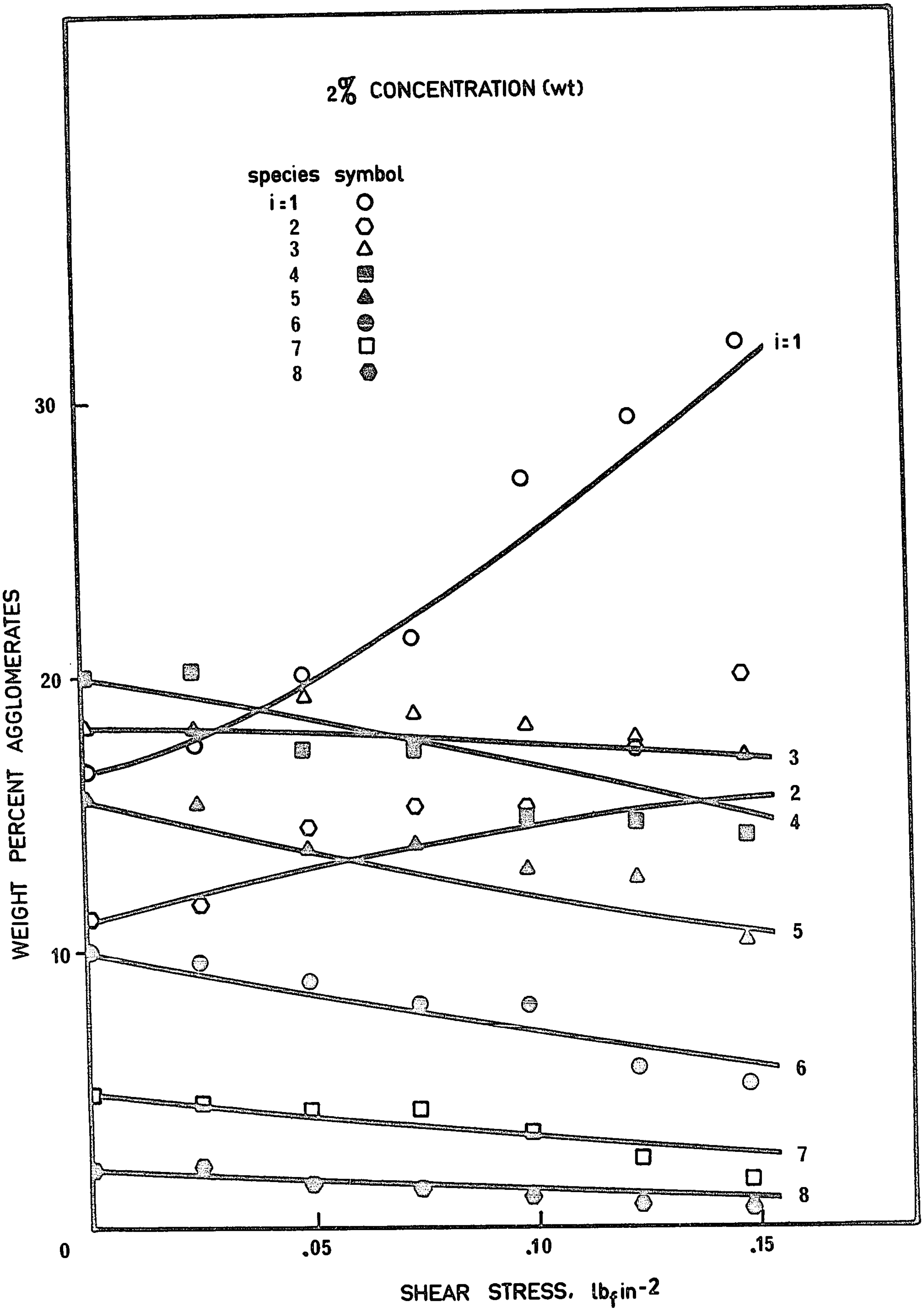

2% CONCENTRATION (wt)
species symbol
i=1
2
3
4
5
6
7
8
30
20
10
0
.05
.10
.15
WEIGHT PERCENT AGGLOMERATES
SHEAR STRESS, $lb_f in^{-2}$
i=1
3
2
4
5
6
7
8

FIGURE 5-15: The Change in Weight Percent, for Species $i = 1$ to $i = 8$, Versus Fluid Shear Stress for the Equilibrium Case. Values Computed from the Model are Shown as Continuous Curves; Experimental Results are Indicated by the Appropriate Symbol. The Agglomerate Concentration was One-Half Percent by Weight

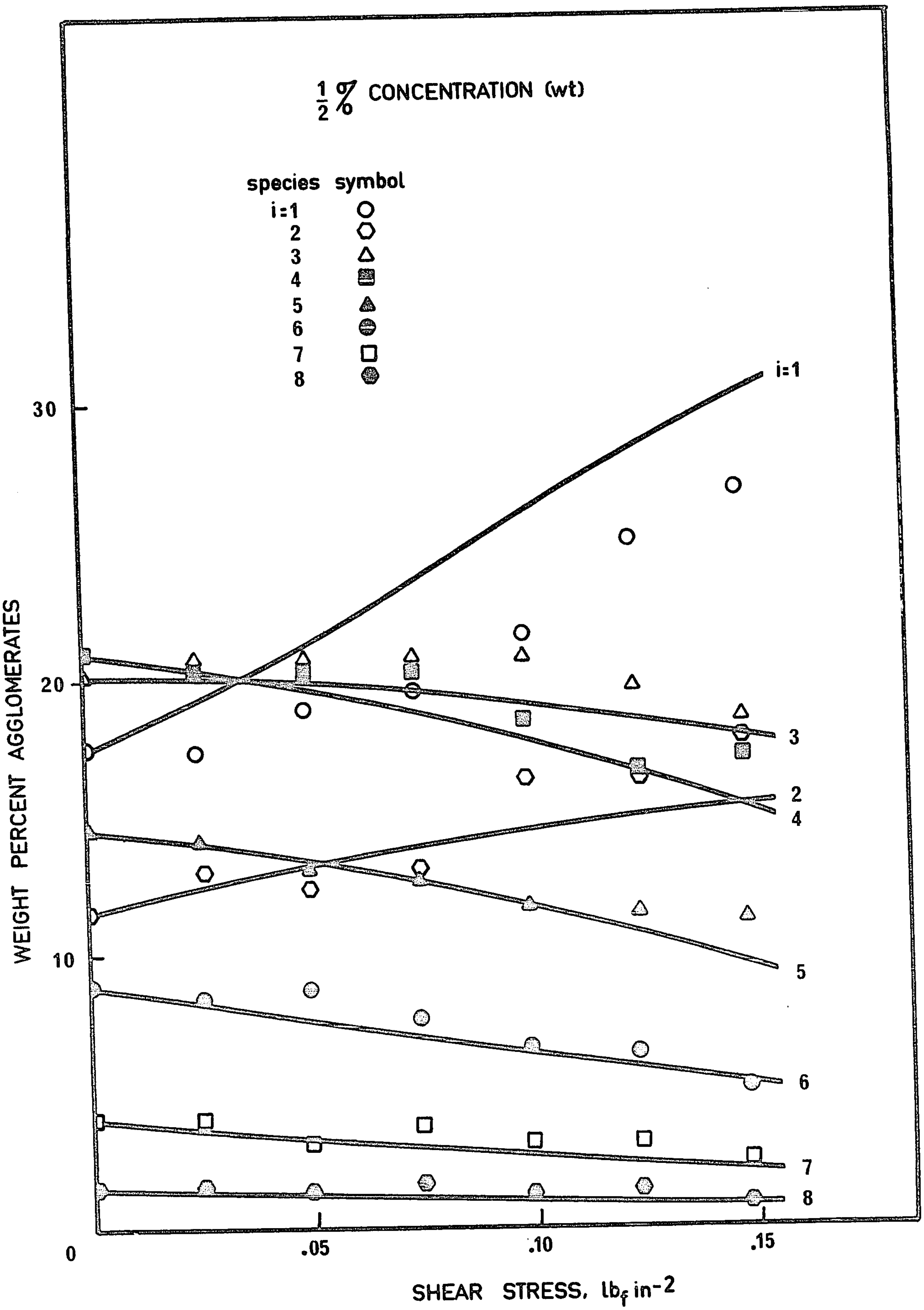

$\frac{1}{2}$ % CONCENTRATION (wt)
species symbol
i=1
2
3
4
5
6
7
8
30
20
10
0
.05
.10
.15
WEIGHT PERCENT AGGLOMERATES
SHEAR STRESS, $lb_f\ in^{-2}$
i=1
3
2
4
5
6
7
8

FIGURE 5-16: The Change in Weight Percent for Species $i = 1$ to $i = 8$ Versus the Shear Strain Imported to the Fluid. The Shear Stress of .074 lb_f/in^2 was applied in a Step-Like Manner. Results Predicted from the Model are Shown as Continuous Curves. Experimental Data for each Species are Indicated by the Appropriate Symbols

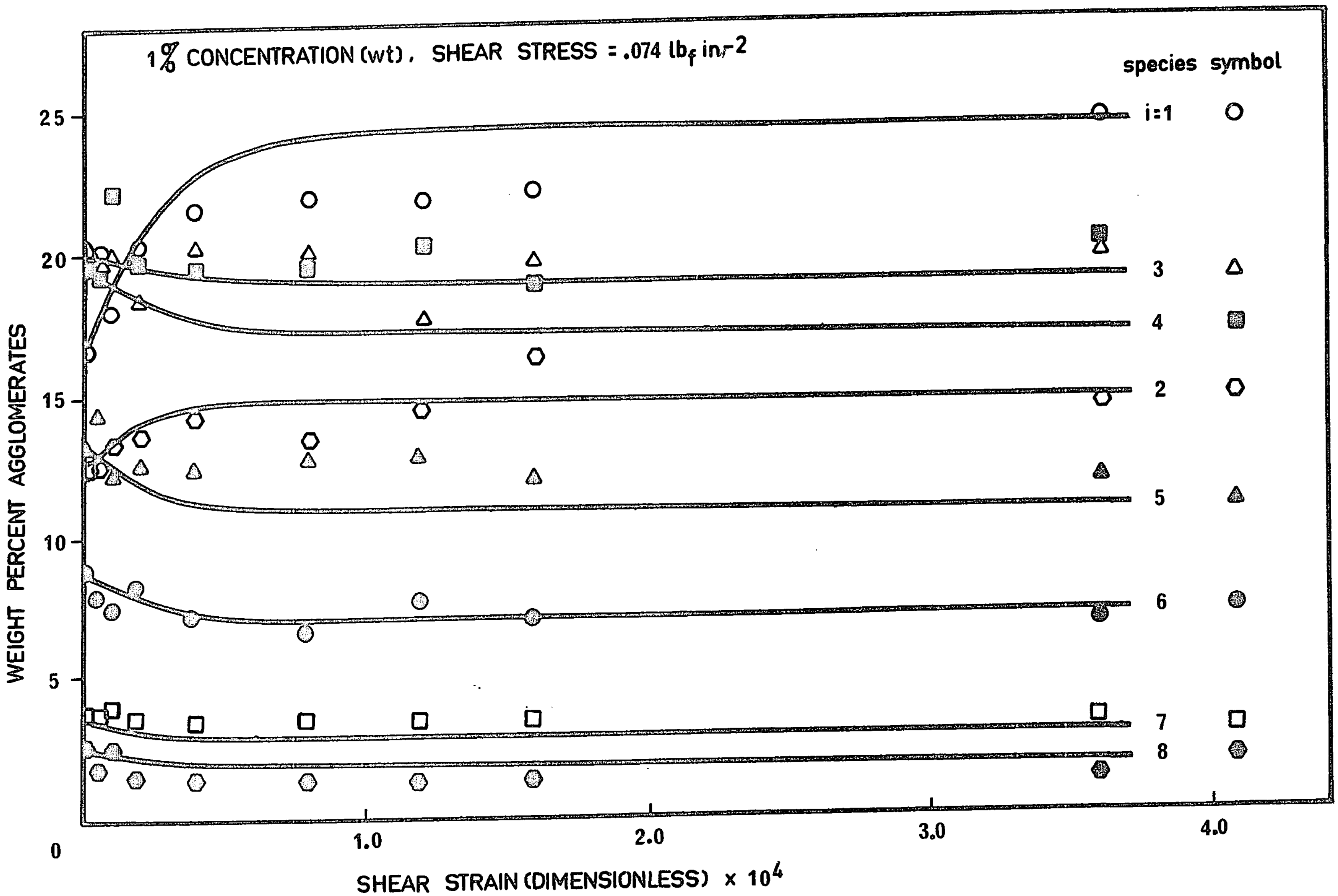

1% CONCENTRATION (wt), SHEAR STRESS = .074 lbf in.-2
species symbol
i=1
3
4
2
5
6
7
8
WEIGHT PERCENT AGGLOMERATES
25
20
15
10
5
0
1.0
2.0
3.0
4.0
SHEAR STRAIN (DIMENSIONLESS) x 10^4

FIGURE 5-17: The Change in Weight Percent for Species $i = 1$ to $i = 8$ Versus the Shear Strain Imported to the Fluid. The Shear Stress of 0.11 lb_f/in^2 was Applied in a Step-Like Manner. Results Predicted from the Model are Shown as Continuous Curves. Experimental Data for Each Species are Indicated by the Appropriate Symbols

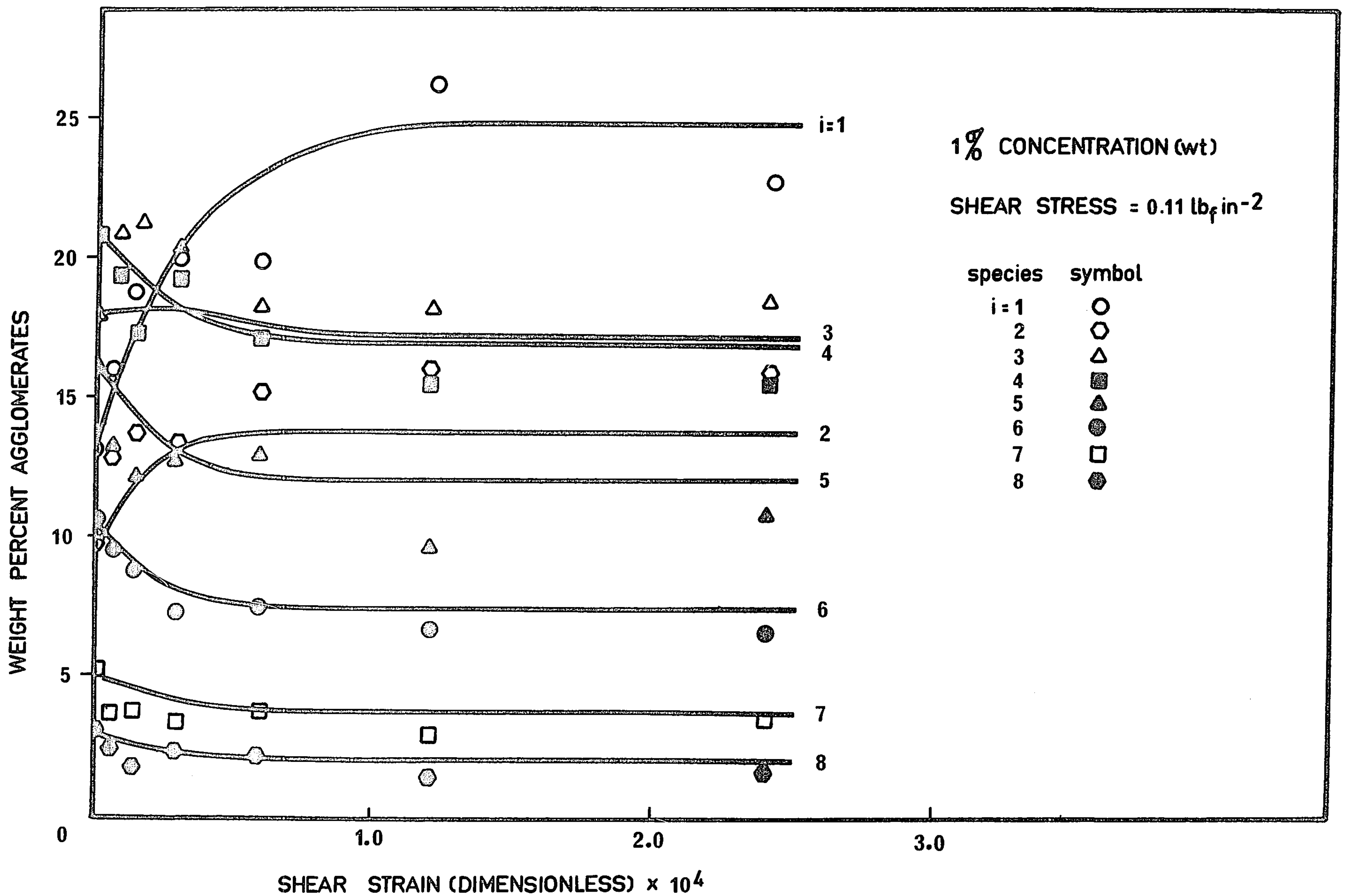

1% CONCENTRATION (wt)
SHEAR STRESS = 0.11 lbf in-2
species symbol
i = 1
2
3
4
5
6
7
8
i=1
3
4
2
5
6
7
8
WEIGHT PERCENT AGGLOMERATES
25
20
15
10
5
0
1.0
2.0
3.0
SHEAR STRAIN (DIMENSIONLESS) × 10^4

FIGURE 5-18: The Change in Weight Percent for Species $i = 1$ to $i = 8$ Versus the Shear Strain Imparted to the Fluid. The Shear Stresses of 0.074 and 0.15 lb_f/in^2 Were Applied in a Step-Like Manner. Results Predicted from the Model are Shown as Continuous Curves. Experimental Data for Each Species are Indicated by the Appropriate Symbols

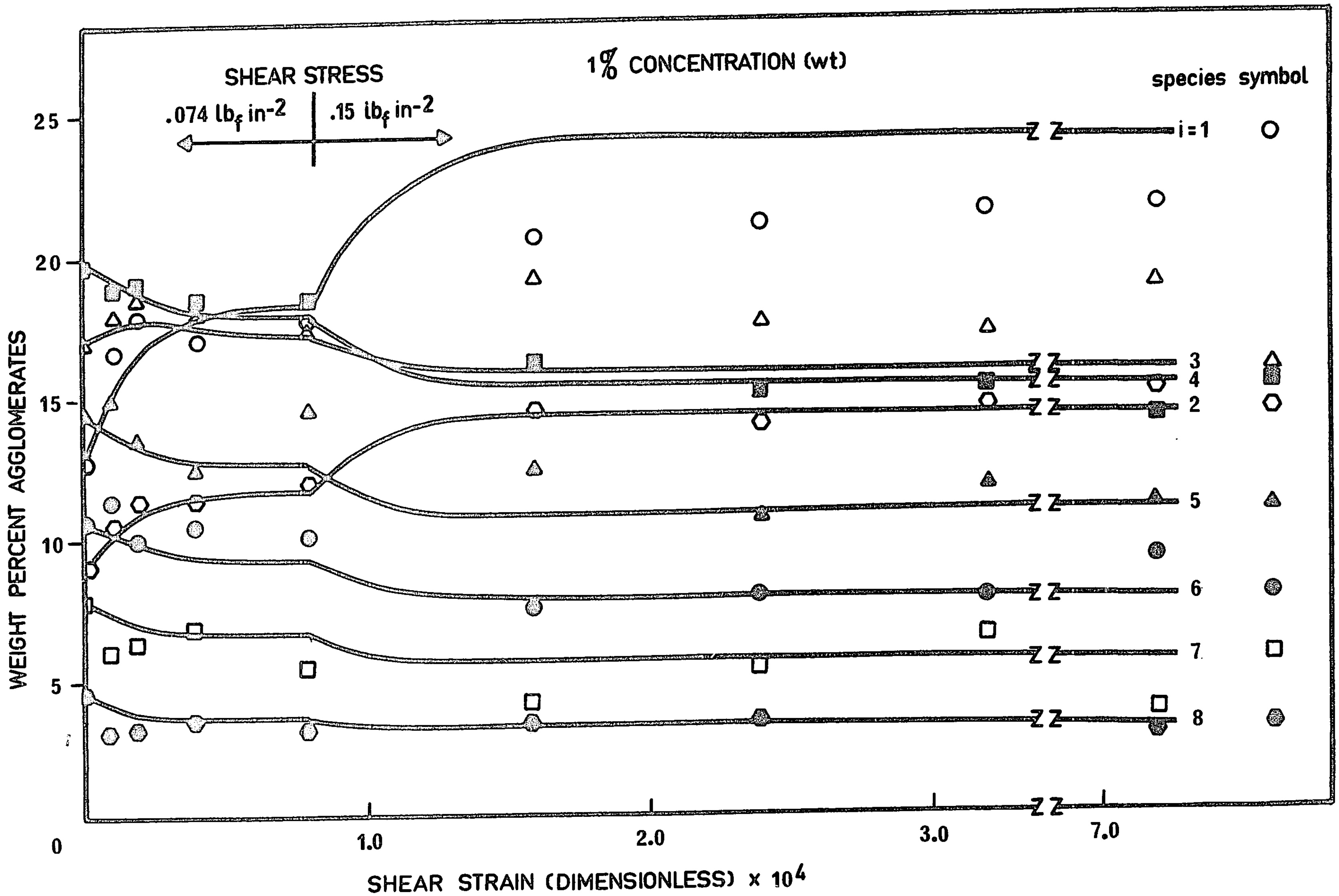

1% CONCENTRATION (wt)
SHEAR STRESS
.074 lbf in-2
.15 lbf in-2
species symbol
i = 1
3
4
2
5
6
7
8
WEIGHT PERCENT AGGLOMERATES
25
20
15
10
5
0
1.0
2.0
3.0
7.0
SHEAR STRAIN (DIMENSIONLESS) x 10^4

where

i = number of beads in the agglomerate

n_i = number of agglomerates containing i beads in the sample

In three of the five equilibrium runs the concentration of agglomerates was one percent by weight. The other two equilibrium runs had weight concentrations of one-half percent and two percent. The three step-change runs had a concentration of one percent by weight. The initial distribution was different for each run, although all runs employed aggregates from the same batch. Some breakdown occurred when the polymer-agglomerate mixture was prepared for each run, and unavoidable small differences in preparation caused the initial distributions to vary slightly.

The three step-change runs were conducted at different levels of mean shear stress: 0.074 lb_f/in^2, 0.11 lb_f/in^2 and 0.15 lb_f/in^2. The distributions are plotted versus γ_m which is the total mean shear strain imparted to the fluid, where γ_m is given by:

$$\gamma_m = \int_0^t \dot{\gamma}_m \, dt \qquad 5\text{-}4$$

where

$\dot{\gamma}_m$ = mean shear rate, defined in equation 5-5

t = time of shearing

The mean shear rate is defined in the same manner as mean shear stress:

$$\dot{\gamma}_m = \frac{1}{R^*} \int_0^1 \dot{\gamma}_{R^*} \, dR^* \qquad 5\text{-}5$$

where

$\dot{\gamma}_{R^*}$ = shear rate at radial position R*.

A note of explanation is in order concerning the run conducted at 0.15 lb_f/in^2 (figure 5-18). At the beginning of this run the motor speed control was inadvertantly set at a speed that was one-half the desired value. This was not corrected until after the fourth set of samples was collected, thus giving the unusual curves shown in figure 5-18. This was the last run of the program and insufficient agglomerates remained to allow a repetition.

It is seen from figures 5-11 to 5-18 that there is considerable scatter in the experimental results but that there is general agreement between theory and experiment. The scatter tends to be random, indicating that more samples should be taken, rather than showing a basic disagreement between the proposed model and the experimental system. An exception to the above statement is noticeable for the two-bead agglomerates at high stress levels in the equilibrium runs. The model seems to consistently underestimate the amount of these agglomerates compared with the experimental results. In the development of the model it has been assumed that agglomerate concentration does not influence deagglomeration. The results in figures 5-11 to 5-16 seem to indicate that this assumption is valid for the range of concentrations employed in this study.

Finally, it should be noted that this system is particularly sensitive to statistical variations if a small number of samples are taken. This is due to the interdependence of the weight fractions, via the overall mass balance. If the value obtained for a given species has a large error due to a sampling fluctuation, it will affect all the values for the other species at that stress level. The amount of scatter that may result from such errors is examined in the next section.

5.3.2 Errors in the Experimental Deagglomeration Data

The scatter in the deagglomeration data may be attributed to three types of error. The first of these is uncertainty in the value of the applied shear stress as previously discussed and amounts to $\pm 4\%$ maximum of the stress value. The second type is caused by employing a mean value of the shear stress to characterize the data. In fact, each sample contained material obtained from almost the whole gap, hence, at least some agglomerates were subjected to shear stresses that differed as much as 4% from the average value. The third type of error is related to statistical factors. As fewer agglomerates of a given species appear in the sample, the scatter becomes worse. This is particularly true as the agglomerates become larger because a small error in counting could lead to a large error in weight percent.

In the experimental work, an attempt has been made to reduce this scatter by taking three samples at each condition. It is the average of the three analyses that is plotted in figures 5-11 to 5-18. Unfortunately no significant statistical tests can be applied to only three results, but a crude estimate of the deviation can be obtained from a scatter diagram such as figure 5-19. The ordinate is the average percent deviation defined as:

$$\text{AVERAGE PERCENT DEVIATION} = \frac{|\varepsilon_i - \varepsilon_{avg}|}{\frac{1}{n}\sum_{1}^{n} |\varepsilon_1 - \varepsilon_{avg}|} \qquad 5\text{-}6$$

where

n = number of results

ε_i = value of replication i

FIGURE 5-19: Scatter Diagram of Average Percent Deviation Plotted Against the Weight Percent of the Determination. The Fitted Curve Shows the Trend of the Average Deviation

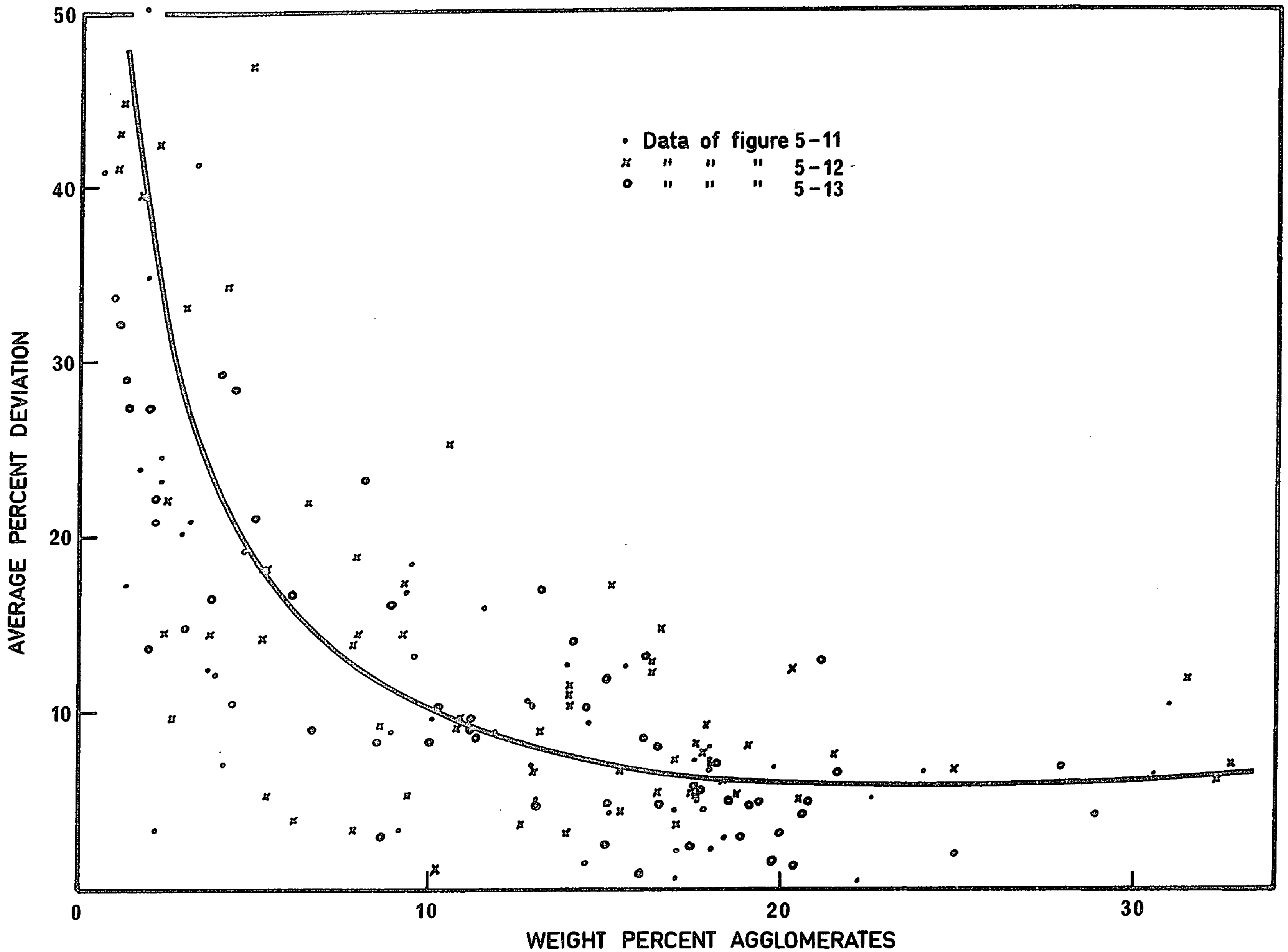

50
40
30
20
10
0
AVERAGE PERCENT DEVIATION
• Data of figure 5-11
x " " " 5-12
o " " " 5-13
10
20
30
WEIGHT PERCENT AGGLOMERATES

The standard deviation of three results is almost meaningless and has been avoided for this reason.

Figure 5-19 shows very high average deviations of twenty to forty percent for agglomerates accounting for 1% to 4% by weight of the agglomerate population. This corresponds to species with seven and eight beads per agglomerate of which there are generally less than ten per sample. As the number fraction of the agglomerates increases, the mean average deviation, as estimated by the solid curve, decreases until it becomes approximately constant at 6% for agglomerates accounting for weight fractions of 0.16 and higher. The overall error is, on the average, about ten percent for agglomerates representing more than fifteen weight percent. Agglomerates representing less than fifteen weight percent show errors gradually increasing until they reach about forty percent for weight fractions of two percent.

The average percent deviation reflects the statistical error in the sampling process in as much as systematic errors (e.g. a viscosity error) will shift the average and do not appear in the deviations from the average.

CHAPTER 6

DISCUSSION

6.1 EFFECT OF NON-UNIFORM TEMPERATURE AND SHEAR STRESS IN THE GAP

The two effects of variable fluid temperature and shear stress in the gap are not independent and, therefore, not easily separated from each other. One possible effect of a very large temperature gradient might be to vary the binding material's strength by softening the binder exposed to the high temperature region. In the present instance the temperature range in the gap is quite small, of the order of 4 to 5°F, and about 70°F below the glass transition temperature of the binder (T_g of polystyrene ≈ 210°F) (65). It is thus expected that the main effect of the temperature gradient in the gap will be its influence on the shear stress. In the previous chapter (section 5.1), it was shown that the effect of decreasing temperature from the inner to the outer cylinder on shear rate is partly offset by the effect of gap curvature. Thus the temperature gradient might be considered beneficial as it tends to produce a more uniform shear stress across the gap.

The effect of the non-uniform shear stress in the gap is to increase the scatter in the data. The uncertainty in the mean shear stress, as shown in the previous chapter, is about

± 4%. The variation about the mean amounts to, approximately, an additional ± 4% as can be seen from figure 5-2. Thus, the real shear stress which a given agglomerate experiences can deviate ± 8% from the nominal mean value used in the theoretical calculations. Referring to the equilibrium data in figures 5-11 to 5-18, it is seen that the discrepancy between the theoretical and the experimental results is not explained by the estimated error in the mean shear stress. The shear stress error causes a horizontal shift in the experimental data points, but due to the flatness of the weight percent versus shear stress curve, this shift reduces the discrepancy by a very small amount. The curves for the single and two-bead agglomerates have steeper slopes and the possible ± 8% error in shear stress can provide a partial explanation for the deviation of these species. It is thus concluded that the possible error in the shear stress values is not, in general, the prime explanation for the discrepancy between calculated and measured results. It seems likely that errors of a statistical nature are important and these errors are discussed later.

6.2 EQUILIBRIUM DEAGGLOMERATION RUNS

It was noted in the previous chapter that the agreement between theoretical and experimental values of the size distribution is good in a qualitative sense. That is, examining the results (figures 5-11 to 5-15) shows that the model predicts the general trend of the distribution shift without error. The degree of quantitative agreement is less satisfactory. In figures 5-11 to 5-15 it is seen that in some cases the experimental points are more or less evenly distributed about the theoretical prediction. Examples of this behaviour are the four-bead agglomerates in figure 5-12 and the single and seven-bead agglomerates in figure 5-13. In other instances, the experimental data tend to be displaced by an approximately constant amount above or below the theoretical values. The three bead agglomerates in figure 5-12 and the single bead agglomerates of figure 5-15 are examples. It is believed that this type of disagreement is caused by variable error in the determination of the initial distribution. The model requires that the initial distribution be known since this provides the initial conditions necessary to solve the differential equations 4-25 relating to the distributions to the shear stress. The system and procedures used in this work have resulted in measuring the different initial distributions for each run, although the agglomerates came from the same batch. The reasons for this variation are outlined in Chapter 3, and the magnitudes of the statistical errors involved are discussed in section 5.3 The fact that the different types of error (random or systematic) occur at random and are not confined to a particular species of agglomerates tends to confirm that there is no basic error in the model.

It has been mentioned in the previous chapter that, at high shear stresses, the theory generally gives values which are lower than the experimental results for the two-bead agglomerates. Below shear stresses of about 0.07 lb_f/in^2 experimental results are scattered both above and below the theoretical values. At shear stresses above 0.07 lb_f/in^2 the experimental values are consistently greater than the theoretical predictions, and the deviation increases with increasing shear stress. It may be that the coefficients, c_{ij}, which determine the distribution of the breakage products have not been chosen correctly or that the strength distribution function, ρ_σ, is not the same for all species, as has been assumed. The effects of varying the coefficients c_{ij}, and the strength distribution function are discussed in later sections of this chapter.

6.3 NON-EQUILIBRIUM DEAGGLOMERATION SIZE DISTRIBUTIONS

Figures 5-16 to 5-18 show the results obtained by following the shift in the distributions with time for deagglomeration occurring when a constant shear stress is applied in a step from zero stress at zero time. The change is plotted as a function of total mean shear strain, γ_m, rather than time on the abscissa. The mean shear strain (at constant shear stress, hence constant shear rate) is obtained from the relationship:

$$\gamma_{mean} = \dot{\gamma}_{mean} \ t \qquad 6\text{-}1$$

where t is the time elapsed since commencement of shearing. In the proposed model, it is assumed that the rate of breakdown is proportional to the shear rate. Thus, if the strength distribution is random, equal fractional breakages will occur at equal shear strains regardless of the rate of strain, as shown in equation 4-36. Of course, from a time point of view equal breakages will occur in a shorter time for the system with a higher shear rate. Figures 5-16 to 5-18 show that, within the accuracy of the scatter of the data, equal fractional breakages occur at the same shear strain. Unfortunately, due to the large amount of scatter, the data is not a severe test of this assumption.

A comparison between the experimental and calculated results for the step change case suggest that these results are subject to the same errors encountered in the equilibrium case. Also, the actual application of the shear stress is not a true step function. This departure from a true step change is important at short times (small shear strains), and amounts to an additional shear strain of about 400. Therefore, the data have been adjusted by adding this amount to the calculated shear strain.

As with the equilibrium case, the scatter of the experimental data is generally distributed evenly about the theoretical predictions. In some instances, the data for a particular species tends to lie wholly above or below the theoretical values (e.g. the six-bead agglomerates in figure 5-17 or the five-bead agglomerates in figure 5-18) but the occurrence is random, indicating that the probable cause is a relatively large error in the determination of the initial values.

6.4 EFFECT OF AGGLOMERATE CONCENTRATION

Three different concentrations of agglomerates were employed in the equilibrium runs to ascertain if the effect of concentration is not negligible. The proposed model assumes that concentration effects may be neglected. There are two possible mechanisms whereby the agglomerate concentration could affect the deagglomeration process. The first of these is due to the increased frequency of collisions. This possibility is discussed in detail in a later section devoted to collision effects. The second mechanism becomes important at very high agglomerate concentrations (50% and more) where the large volume fraction of agglomerates leads to physical contact between many particles and the formation of particle "bridges". These contacts may serve to transmit forces directly from one particle to another. It is not expected that the proposed model would be applicable in this case since it postulates that the only forces on the agglomerates are hydrodynamic in origin.

When the 2% and 1/2% concentration results (figures 5-14 and 5-15 respectively) are compared with the 1% results (figures 5-11 to 5-13), it is seen that the discrepancies between experimental and predicted values do not form any pattern. It is thus concluded that, within the accuracy allowed by the data, the assumption of the non-existence of a concentration effect is justified for concentrations less than 2% by weight.

6.5 DETERMINATION OF AGGLOMERATE STRENGTH DISTRIBUTION

Ideally, the agglomerate strength distribution should be ascertained independently of the deagglomeration results. In the present instance this was not practical and the following procedure was used. The results for the largest species, N, which underwent only breakdown and no gain (N = 8, for this work) were manipulated to give the fractional cumulative loss, $Loss_{cum}$, with respect to shear stress:

$$Loss_{cum} = \frac{Q_{No} - Q_{N\tau}}{Q_{No}} \qquad 6\text{-}2$$

where

Q_{No} = the original number of N-particle agglomerates before shearing has begun.

$Q_{N\tau}$ = the number of N-particle agglomerates at shear stress τ.

From the definition of fractional cumulative loss and equation 4-12:

$$\text{Loss}_{cum} = \int_0^{\tau} \frac{A_{No}}{Q_{No}} \rho_\sigma \, d\sigma \qquad 6\text{-}3$$

where

A_{No} = scaling factor

ρ_σ = strength distribution functions; $\rho_\sigma = \rho(\sigma)$ only.

and the strength distribution is found directly by differentiation of equation 6-3:

$$\frac{d(\text{Loss}_{cum})}{d\tau} = \frac{A_{No}}{Q_{No}} \rho_\sigma \qquad 6\text{-}4$$

Substituting from equation 6-2:

$$-\frac{dQ_{N\tau}}{d\tau} = A_{No} \, \rho_\sigma \qquad 6\text{-}5$$

where the shear stress, τ, has been substituted for agglomerate strength, σ, as suggested by earlier discussion. Thus a plot of $-\frac{dQ_{N\tau}}{d\tau}$ against τ ($= \sigma$) yields the strength distribution.

The difficulty with this method is that, for practical size distributions, the largest species has the fewest number of agglomerates. Thus, unless a large number of samples have been analyzed, statistical scattering of the data is quite large. The method requires that such data be differentiated which accentuates the scatter unless the data are smoothed before differentiation.

A possible approach for reducing the effect of scatter associated with the least abundant agglomerates would be to base the calculations on the population of agglomerates with fewer than N-beads per agglomerate. The criterion for choosing the expanded population is that the species gain due to breakdown of larger agglomerates is small and can be neglected. The reduction in variability of the data must be great enough to yield a worthwhile decrease in the uncertainty of the distribution function.

In this work the data were smoothed, but the alternative presented in the previous paragraph gave no improvement and was not used. A plot of $-\frac{dQ_{N\tau}}{d\tau}$ against strength, τ, is shown in figure 6-1 for the data of figure 5-11. Also shown are two possible distributions; a linear and an exponential function. It is seen that both distributions could be considered to fit the data equally well. The results of the other runs follow a similar pattern.

FIGURE 6-1: The Differential, $\frac{dQ_{N_\tau}}{d\tau}$, Versus Fluid Shear Stress for the Data from Figure 5-11. The Assumed Exponential Distribution Function is Fitted to the Data. A Linear Distribution Function is Shown for Comparison

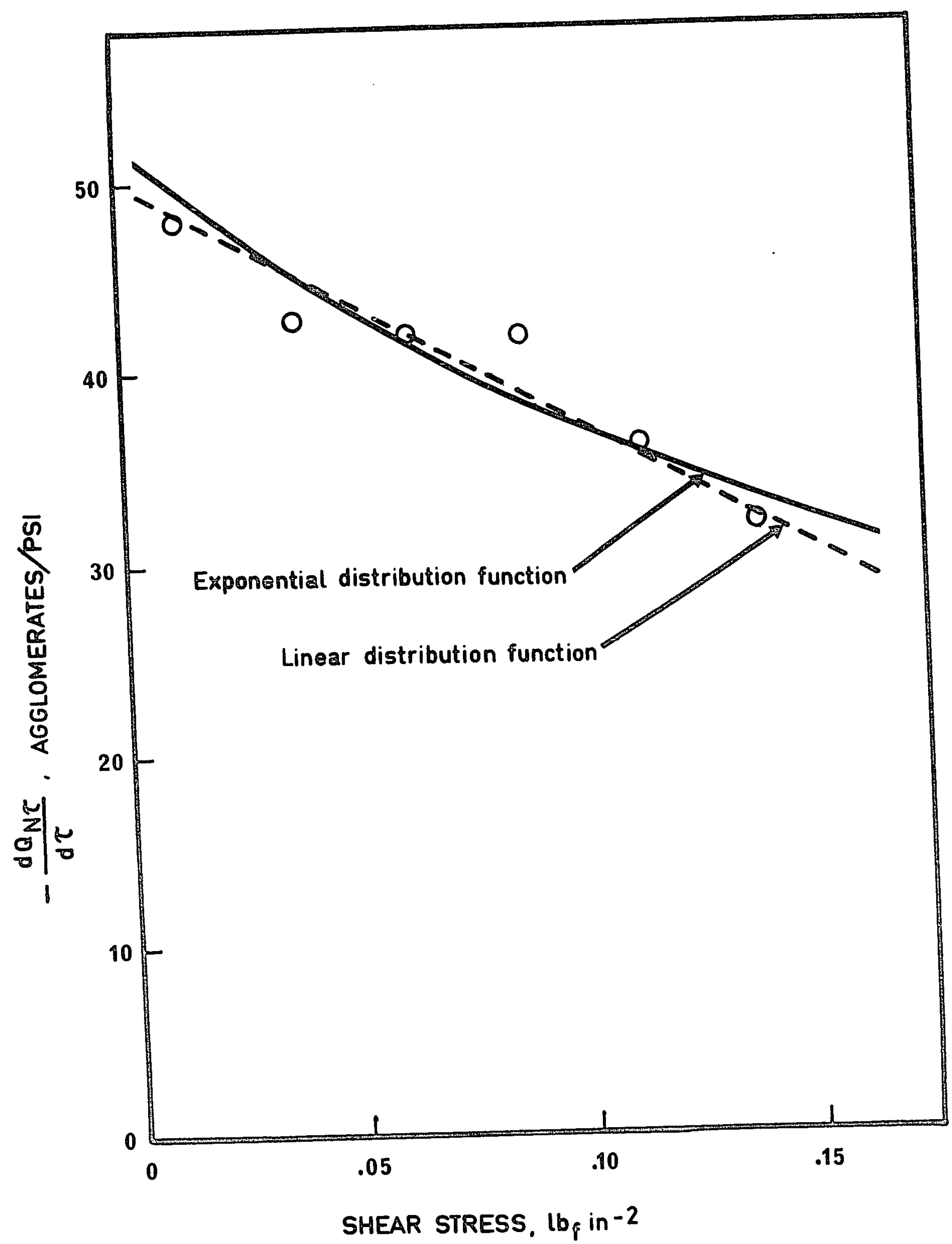

50
40
30
20
10
0
0
.05
.10
.15
Exponential distribution function
Linear distribution function
$-\frac{dQ_{N\tau}}{d\tau}$, AGGLOMERATES/PSI
SHEAR STRESS, lb_f in^{-2}

Intuitively, the linear distribution is not satisfactory because it implies the existence of a maximum agglomerate strength beyond which all agglomerates will be broken. The exponential distribution does not have this deficiency, and it exhibits a monotonically decreasing "tail" that is close to most experimentally determined distributions. The explanation for the apparently good fit of the linear distribution may be related to the fact that only a small portion of the whole distribution is examined in figure 6-1 and this small portion can be approximated with a straight line. The exponential function;

$$\rho_\sigma = e^{-\beta\sigma} \qquad 6\text{-}6$$

was chosen to represent the strength distribution function, where $\beta = 3.5\ \text{psi}^{-1}$ gave the best overall fit to the data. The complete distribution for any species, i, is given by equation 4-12:

$$Q_{io} = \int_0^\infty A_{io}\rho_\sigma \, d\sigma \qquad 4\text{-}12$$

thus, when ρ_σ is known, the scaling factor, A_{io}, which is not a function of σ is found from:

$$A_{io} = \frac{Q_{io}}{\int_0^\infty e^{-\beta\sigma} \, d\sigma} = \beta Q_{io} \qquad 6\text{-}7$$

where Q_{io} is the original amount in each species, i, before shearing, and is known from the initial distribution.

6.6 DETERMINATION OF THE DEAGGLOMERATION RATE CONSTANT, K

In the course of the derivation of the equations for the non-equilibrium conditions, it was assumed that the rate of breakdown, L_i, was specified by the rate constant, K:

$$L_i = K \dot{\gamma} Q_i' \qquad 4\text{-}37$$

where

$\dot{\gamma}$ = the shear rate

Q_i' = number of breakable agglomerates in species i.

As discussed in section 4.3 it was not possible to determine K theoretically. Instead the value of K was determined, for each step change run , by a trial and error procedure in which the value of K was adjusted to yield the best agreement between the experimental and calculated results. It was found that the value of K was almost constant, varying from 5.3×10^{-4} to 5.7×10^{-4}.

In terms of the physical model, K corresponds to the rate at which the particle orbit shifts towards the orbit that provides the orientation having maximum stress on the particle. It has been demonstrated by Gauthier et al (76) that the effect of inertial forces is to slow down the rate at which the equilibrium distribution of orbits is attained, the rate slowing as the Reynolds' number, Re_s, is increased. At a constant shear rate, Re_s varies as the square of the particle characteristic dimension, and for the agglomerates studied it is estimated that the size distribution gives a variation somewhat less than one decade in Re_s. From the results of Gauthier et al, a change in Re_s from 10^{-1} to 10^{-3} causes the number of orbits required to reach equilibrium to decrease by about 60%. Interpolating for a single decade of shear is risky since there are no data relating the dependence of the number of orbits on Re_s other than the two points mentioned above.

On the basis of the preceding discussion it is expected that K will vary with Re_s, which is a function of agglomerate size. Re_s is proportional to i^2 for a linear (straight chain) agglomerate and proportional to $i^{2/3}$ for a spherical agglomerate. The average Re_s for the agglomerates employed in this work will lie somewhere between these extremes.

Calculations were made, as described earlier, but with K varying linearly with i. Allowing K to vary in this manner did not yield a significantly better fit, between computed and experimental results, than the constant K. This may be attributable to the scatter in the data and it must be concluded that the data neither confirms nor rejects the assumption for the rate of breakdown as proposed in equation 4-37.

6.7 EFFECTS OF SOME OF THE ASSUMPTIONS IN THE MODEL

6.7.1 The Values of c_{ij}

In Chapter 4 arguments were presented to evaluate c_{ij}, the coefficients determining the distribution of the breakdown products. It was shown that $c_{ij} = 1$ for all i and j would be a reasonable first approximation for the agglomerate-polymer system studied.

An attempt was made to determine how a variation in c_{ij} would alter the calculated distributions. Towards this end, the equations were solved using $c_{ij} = i$ and, also, with $c_{ij} = \frac{1}{i}$. In both cases, the results differ by less than 2% from those obtained by assuming $c_{ij} = 1$. The system is thus quite insensitive to c_{ij}. The reason is found by more careful examination of the interaction between c_{ij} and the initial particle size distribution. For this, it is important to note that c_{ij} affects only products from species having four or more beads since the two-bead and three-bead species can only give one type of product . But, initially, the agglomerates containing four or more beads represent less than 25% of the total on a number basis. Further, the four-bead species can only degrade in two possible ways, both of which are estimated to be about equal in probability. Thus, excluding the four-bead agglomerates which account for about 10% of the total, c_{ij} will affect the breakdown distribution of only 15% of the total initial agglomerates.

To test the arguments resulting in $c_{ij} = 1$, an initial "inverted" agglomerate population is needed. In such a distribution the largest agglomerates would account for the largest number fraction, or a relatively large number fraction, of the initial undegraded sample.

6.7.2 Reagglomeration

It is not anticipated that significant reagglomeration took place. At any instant there would be a population of transient agglomerates resulting from the close approach of two distinct aggregates undergoing collision. However, it seems unlikely that these would form a permanent, larger agglomerate. For reagglomeration to occur, the binding forces acting on the two previously distinct agglomerates would have to be greater than the hydrodynamic forces tending to break them apart. The two most likely binding forces are electrostatic attraction and van der Waals' forces. In rare instances, it can be imagined that two irregularly shaped agglomerates might collide in such a fashion as to become mechanically locked together.

Electrostatic forces are an improbable agent for causing permanent reagglomeration since the resistivity of polyethylene glycol is not high enough to prevent the migration of electrical charges. This fact is exploited industrially where polyethylene glycol is used as an anti-static agent.

The effect of van der Waals' forces is more difficult to dismiss. For parallel, plane surfaces these forces are only effective at very small distances of the order of a few hundred angstroms or less. For the curved agglomerate surfaces involved a much closer approach of the colliding particles is implied, perhaps on the order of tens of angstroms. Further, there is some doubt that colliding particles in irreversible flows actually make contact (34,42).

The proposed model makes no provision for reagglomeration. Since, in this work, the strength distribution is derived from the deagglomeration results,the effect of reagglomeration is not visible. Rather, the true strength distribution is distorted so as to produce the experimentally determined distribution. A possible test for reagglomeration would be to determine the strength distribution independently of the deagglomeration experiments and to compare it with the distribution found from deagglomeration runs.

6.7.3 Effect of Collisions

It was noted briefly in Chapter 4 that deagglomeration could possibly take place by forces resulting from agglomerate collisions. On the basis of estimates of relative particle velocities and sizes, it was decided that collisions should not contribute significantly to agglomerate breakdown. If collisions were important, then the distributions at different concentrations should show considerable variation because, for unequally sized agglomerates, the frequency of collisions increases as the square of the volume concentrations (37). Unless a very small fraction of the collisions result in deagglomeration, it would be expected that the 16:1 range in frequency (4:1 range in concentration) would result in a proportionate range of collisions causing deagglomeration. In fact, the data show virtually no dependence on concentration, but only random scattering. The effect of collisions would produce a systematic shift in the data as concentration is varied. It is tentatively concluded that, for weight concentrations less than 2%, collisions have a negligible role in causing breakdown. The conclusion is tentative since the effect of collisions may be small, and hence masked by the scatter of the data.

6.8 COMPARISON WITH RESULTS FROM SUSPENSIONS

It is known that particles in a sheared fluid describe definite orbits in response to the flow (34). It is assumed in the proposed model that these orbits would shift (with respect to the flow) so as to maximize the forces on the particle. Karnis et al (77) have shown that single rods and discs in Newtonian fluids drift to orbits of maximum stress, if the particle shear Reynolds number is greater than 10^{-2}. The particle shear Reynolds number is given by:

$$Re_s = \frac{4\ell^2 \rho_f \dot{\gamma}}{\mu_f}$$

where

ℓ = characteristic particle dimension; diameter for discs, length for rods

$\dot{\gamma}$ = shear rate

ρ_f = density of the fluid

μ_f = viscosity of the fluid

Conversely values of $Re_s < 10^{-3}$ cause the orbits to drift so as to minimize the forces acting on the particle.

For the experimental system examined in this work, the characteristic length of the agglomerates varies from approximately 70μ for a doublet to about 200μ for the eight and nine-bead aggregates. The average shear rate in the gap varies from 40 sec^{-1} to 250 sec^{-1} depending on operating conditions. These extreme values give a range $10^{-3} \le Re_s \le 10^{-1}$. Thus, the direction of orbit drift is uncertain for doublets at low shear rates but all other species tend to assume the orbits of maximum stress.

More recently, Gauthier et al (76) have determined that the tendency of single, isolated particles to drift towards orbits of maximum or minimum stress is altered when the particles comprise a suspension. Instead of all the orbits shifting towards the extremes of maximum or minimum stress, there is a definite number fraction distribution of orbit types. The distribution is such that the greater fraction of the orbits are displaced in the direction of maximum stress when $Re_s \rangle\approx 10^{-2}$. As expected from the results with single particles, suspensions with $Re_s \langle\approx 10^{-3}$ give distributions with the larger fraction of the orbits displaced towards minimum stress. The same workers have found that the distribution of the orbit types is essentially independent of the suspension concentration up to a particle content of about 10% by volume.

The distribution is thought to result from particle interactions. In the absence of interactions, the particles would all drift to orbits of maximum stress at a uniform rate ($Re_s \rangle\approx 10^{-2}$). The collisions, however, alter the orbits of the colliding particles. After collision, some of the altered orbits will be closer to the maximum stress orbit than they were previously while others will be further away. Thus the distribution of orbit types is dynamic but, given sufficient time, all agglomerates will pass through orbits of maximum stress, which is the condition required for deagglomeration.

It was found by Gauthier et al (76) that for rod-like particles a variable number of orbits was required before the stable distribution of orbit types was attained. The number of orbits ranged from 600 at $Re_s \approx 10^{-3}$ to 1500 at $Re_s \approx 0.1$. In this work it is possible to estimate the number of orbits traversed by the agglomerates before reaching equilibrium.

The time for an orbit is given by (34):

$$t_{orbit} = \frac{2\pi}{\dot{\gamma}} (r_e + \frac{1}{r_e}) \qquad 6\text{-}8$$

where

r_e = equivalent ellipsoidal axis ratio.

The equivalent ellipsoidal axis ratio, r_e, may be obtained from the actual particle axis ratio, r_p, from figure 7 in reference 34. The relationship between r_e and r_p is, strictly, only valid for cylindrical particles.

In this work, particles with $.5 < r_p < 5$ were observed, giving $.75 < r_e < 4.5$. Rearranging the above equation to give the amount of fluid shear strain per orbit, γ_{orbit}:

$$\gamma_{orbit} = \dot{\gamma}_{orbit} = 2\pi(r_e + \frac{1}{r_e}) \qquad 6\text{-}9$$

The number of orbits the particle has undergone is then:

$$N_{orbit} = \frac{\gamma_{equil}}{\gamma_{orbit}} \qquad 6\text{-}10$$

where

γ_{equil} = the mean shear strain in the fluid when equilibrium is reached

From figures 5-16 to 5-18 the fluid shear strain at which equilibrium is reached is, approximately, $\gamma_{equil} \approx 5 \times 10^3$ for each run. This gives $150 < \approx N_{orbit} < \approx 600$ depending on the value of r_p. The number of orbits required to reach breakdown is not necessarily the same as the number of orbits needed to establish the final distribution of orbit types. Further, the use of the $r_e - r_p$ relationship cited above for the unsymmetrical agglomerates employed in this work is only a first-order approximation. Thus, agreement to within only an order of magnitude, for equilibrium in the two different systems, is not wholly unreasonable and indicates that the agglomerate behaviour is not far removed from that found for regularly shaped particles.

6.9 COMPARISON WITH COMMINUTION THEORIES

The most direct method of comparison is to compare the equations for each situation.

$$\frac{dw_i}{dt} = \sum_{j=1}^{i-1} b_{i,j} \, K_j \, w_j - K_i w_i \qquad \text{COMMINUTION GRINDING EQUATION} \qquad (2\text{-}19)$$

$$\frac{dQ_i}{d\tau} = \sum_{j=i+1}^{N} \frac{C_{ij}}{C_{jj}} \, I_\tau Q_j - I_\tau Q_i \qquad \text{EQUILIBRIUM DEAGGLOMERATION} \qquad (4\text{-}25)$$

The similarity between the equations is not surprising. They are both derived from mass balances over a small increment - in time for comminution and shear stress for deagglomeration.

The breakage function $b_{i,j}$ is directly comparable to $\frac{C_{ij}}{C_{jj}}$ in that they both determine the distribution of the breakdown products. Similarly κ_j has a role identical with that of ρ_T. In this work I_T is defined by equation 4-21 in terms of ρ_T, the agglomerate strength distribution with respect to shear stress, while κ_i is known as the selection function in comminution theory. Both specify the value of the independent variable at which a given particle (or group of particles) will break.

Reid (46), Herbst and Fuerstanau (49) and Kelsall and Reid (47) all solve the grinding equation by assuming that κ_i is not a function of time. Using experimentally determined $b_{i,j}$, they predict the size distribution as a function of time for varying systems with good results. As reported in Chapter 2, Reid (46) has demonstrated the three possible conditions under which the assumption that $\kappa_i \neq \kappa_i(t)$ holds. These conditions are i) all $\kappa_i = \kappa$, independent of i; ii) κ_i = constant x d_i and $b_{i,j} = d_i/d_j$ (d = particle diameter); iii) a particular κ, κ_n is such that $\kappa_n \gg \kappa_i$, $i \neq n$. Reid states that the assumption of $\kappa_i \neq \kappa_i(t)$ holds reasonably well for some situations such as ball milling, but is probably exact only for a few systems. In fact, it can never be exact since then the comminution equation will not predict a stable size distribution for long times. A possible solution is to allow $b_{i,j}$, which is a function of time, to become zero at long times. This is not logical, however, because $b_{i,j}$ indicates the manner in which the degradation products are distributed while κ_i gives the rate of breakdown. At equilibrium, it is the rate, κ_i, that should tend to zero.

Klimpel and Austin (48) used experimental results to first calculate the breakage function and then, using an optimization technique, found κ_i as a function of particle size, i. Since κ_i decreased with particle size, and particle size decreases with time, an equilibrium could be reached. In this context, the relationships $\kappa = \kappa(i)$ and $\kappa = \kappa(t)$ are equivalent. Referring to Reid's criteria for $\kappa \neq \kappa(t)$, it is observed that this is satisfied when $\kappa \neq \kappa_i(i)$.

The deagglomeration equations do not suffer from the above problem since the time variation of the rate of breakdown is incorporated in such a manner as to ensure that the rate approaches zero at long times.

The deagglomeration equation for the step change in shear stress is more directly comparable to the batch grinding equation:

$$\frac{dw_i}{dt} = \sum_{j=1}^{i-1} b_{i,j}\, \kappa_j\, w_j - \kappa_i w_i \qquad \text{COMMINUTION GRINDING EQUATION} \qquad (2\text{-}19)$$

$$\frac{dQ_i'}{dt} = \sum_{j=i+1}^{N} f_j \frac{C_{ij}}{C_{jj}} K \dot{\gamma} Q_j - K \dot{\gamma} Q_i \qquad \text{DEAGGLOMERATION STEP CHANGE} \qquad (4\text{-}39)$$

Like the batch grinding equation, the step change in shear stress equations for deagglomeration predict that Q_i' will approach zero at long times. This is consistent with the concept of an equilibrium distribution since Q_i' refers to agglomerates that will break down at the specified shear stress level. The use of the companion equation for Q_i'' allows the number fraction of agglomerates to be calculated at any time since $Q_i = Q_i' + Q_i''$. This method of splitting any species into degradable and non-degradable portions is only possible because the strength distribution with respect to the shear stress is assumed to be known. It does, however, allow an equilibrium distribution to be reached while retaining the description of breakdown as a first order process. This seems desirable since, as reported by Reid (80), most systems exhibit this behaviour.

The general case where the breakdown stress is a function of time does not appear to have been treated in the literature. In grinding or ball milling, this would amount to varying the drive speed continuously with time - a practice that is evidently not followed in the industry. This type of analysis might be useful in a grinding cycle where the particles are alternately subjected to high and low comminution forces.

6.10 COMPARISON WITH PREVIOUS WORK ON DEAGGLOMERATION

It was mentioned in Chapter 2 that previous work on the deagglomeration process is very sparse. McKelvey (22) modelled the deagglomeration process for the simplistic case of a two particle agglomerate. His model, which is discussed in detail in section 2.3, led to the following conclusions:

1. there is a critical shear stress, below which deagglomeration will not occur.
2. at shear stresses only slightly greater than the critical only those agglomerates initially perpendicular to the flow will deagglomerate.
3. high shear stresses promote deagglomeration.
4. if the attractive force between particles is independent of particle size larger particles will deagglomerate at lower shear stresses.

Each conclusion is examined in comparison with the present work. The first conclusion is true for the proposed model if, the strength distribution is such that it has a sharply defined lower limit. For most real systems, experience counsels that this is not true unless the agglomerates have been specially fabricated or selected. Most commercial agglomerates possess a distribution that has both a low-strength and a high-strength "tail" in the manner of a normal distribution. If the critical shear stress does not exist, then the second conclusion is meaningless. If the critical shear stress does exist the second conclusion is at variance with known particle behaviour in a shear field. On the other hand, the proposed model takes such behaviour into consideration.

Both models predict, correctly, that high shear stresses promote deagglomeration, which is McKelvey's third conclusion.

The fourth conclusion is true in both instances if the present model is reduced to the state where the strength distribution is unimodal. This is, as in the first conclusion, a highly idealized state which is even further removed from reality than the critical shear stress condition. In summary, the two models agree qualitatively for the very restrictive assumptions made by **the** McKelvey model. The predictive capacity of McKelvey's model has not been tested by experiment, whereas the proposed model has been shown to give results in agreement with experimental data within the limits of experimental error.

Bolen and Colwell (30) have proposed an equation to predict the rate of increase in the number of particles due to the breakage of agglomerates. The form of the equation has been chosen a priori to be an exponential function. The model has been shown in section 2.3, to suffer from some serious deficiencies. The choice of an exponential function is probably correct since there is accumulating evidence (including this work) that breakage of agglomerates is a first-order process.

However, the authors who proposed the equation on purely empirical grounds have not compared calculated predictions with experimental data. Furthermore, Bolen and Colwell's approach is only useful for the prediction of the variation of the total number of agglomerates with time. It does not offer any information about the particle size distribution during the deagglomeration process

Finally, Smith (31) investigated the breakdown of various pigments in polyethylene. He found that the rate of breakdown was constant over the range of times (up to 30 minutes) examined. This is in contrast with the results of the present work where equilibrium had been reached in about three minutes for the slowest run. The findings are also not in harmony with industrial practice where dispersion is achieved in similar but larger-scale equipment in three to ten minutes. In addition, the rate of breakdown cannot be independent of time, but must eventually tend to zero. Smith gives no theoretical basis for his findings, but merely fits a straight line, representing a constant decrease in average particle size, through his data. This type of relationship does not yield information about the size distribution unless the distribution type is invariant as the deagglomeration proceeds, and only one parameter of the distribution (e.g. mean particle size) is variable. Part of the difficulty in judging the model is the lack of theory and the fact that deagglomeration parameters (particularly shear stress) have not been characterized due to the complex shear field in the apparatus.

6.11 EXTENSION OF THE MODEL TO MORE COMPLEX SYSTEMS

The proposed model has been applied to a simple system involving a Newtonian fluid and artificially produced glass bead agglomerates with a size range of 30 to 120μ.

Real polymer-pigment systems exhibit two major departures from the idealized arrangement that has been studied in this work. Firstly, the suspending fluid is usually non-Newtonian (pseudoplastic) and viscoelastic in nature. The fluid, usually a polymer melt, has a viscosity two to three orders of magnitude larger than that of polyethylene glycol. In addition the agglomerates found in commercial pigments have a very large range of sizes, typically 0.1 to 200μ. It is expected that the effect of the viscoelastic nature of many commercial polymer melts on the deagglomeration process will be small. Chen (73) has measured the recoverable shear strain, S_R, for some commercial polyethylene melts. The recoverable shear strain is the ratio of the first normal stress difference to the shear stress; i.e. for viscometric flows:

$$S_R = \frac{-(\tau_{11} - \tau_{22})}{-\tau_{12}} \qquad 6\text{-}11$$

He found that S_R varied from about 0.2 to 2.0 depending on the polymer and the shear rate. From the viewpoint of the forces exerted on the particle the nature of the deagglomeration process is not altered even when the normal stress difference is of the same order of magnitude as the shear stress. The orientation, relative to fixed axes, at which the agglomerate will degrade will be different for the viscoelastic fluid than for the Newtonian one. This is due to the rotation of the principal axes by the normal stress difference, but is unimportant if the assumption of random particle orientations is valid. Also, the particle will breakdown at a lower value of τ_{12} in the viscoelastic fluid. This occurs only because τ_{12} is not the sole contribution to the degrading force and does not signify a different deagglomeration process.

The effect of the pseudoplasticity of the suspending fluid on the particle orientation, as found by Gauthier et al (76) is more important. They report that, unlike Newtonian liquids, the particles tend to assume orbits of minimum stress when the sheared fluid has a pseudoplastic nature. This behaviour is observed for flow regimes of $10^{-1} \lessapprox Re_s \lessapprox 10^{-3}$. Furthermore, the particles drift to the orbits of minimum stress at a rate that is one order of magnitude faster than they drift in the Newtonian fluid. Thus, it appears that an independent test of the proposed model will be necessary for the case of pseudoplastic melts.

Considering typical processing conditions for polyethylene in a Bolling type mixer gives

Shear rate, $\dot{\gamma}$, about 350 sec^{-1} (60 RPM, 12" diameter blade, 0.1" clearance blade to wall).

Melt viscosity, μ, about 10^5 cps.

Shear Reynolds' number, Re_s, $\approx 10^{-6}$ for a 10μ diameter agglomerate, $\approx 10^{-4}$ for a 100μ diameter.

The flow is in a range where inertia effects are negligible and the creeping flow equations apply. Zia et al (40,41) have shown that in this regime aggregates of spheres in contact behave as rigid bodies and will not break. Nevertheless, the Bolling mixer is widely used to produce deagglomeration (15,17,20). The explanation may lie in the fact that the processing conditions are such that the shear stress is very high (about 100 psi) and close to the region where melt fracture or instabilities occur (17). The behaviour of molten polymers in this region is poorly characterized and the results obtained by Zia and coworkers may not be applicable.

The proposed model is based on a known shear stress field that is orderly in the sense of laminar flow. If commercial processing is accomplished under turbulent conditions, it may, or may not, be possible to extend the model to cover such a case. In either event more basic knowledge about polymer melt behaviour at high shear stresses close to the flow instability region is required.

CHAPTER 7

CONCLUSIONS

7.1 SUMMARY AND CONCLUSIONS

In the preceding chapters, an effort was made to study a simplified deagglomeration process and to develop a mathematical model for such a process. Agglomerates were artificially produced from spherical glass beads and suspended in a polyethylene glycol melt, which was subsequently sheared in a concentric cylinder Couette apparatus to effect the deagglomeration. The analyses of the agglomerate size distributions were performed microscopically using a technique developed during this study. The experimental data thus obtained were used to test the proposed model of the deagglomeration process.

The testing of the model is limited by the errors and scatter of the experimental data. The uncertainty in the data ranges from about $\pm$ 10%, in the region where statistically caused scatter is small, to about $\pm$ 50% when only a few agglomerates of the species are present in the sample. The uncertainty not due to statistical causes comes primarily from the variation in shear stress across the gap and from errors in measuring the wall temperatures of the apparatus. Each variable contributes about equally to the error.

The model was tested with data representing equilibrium conditions as was the time variation of the size distributions due to a step-change in the shear stress. The equilibrium results were also tested at different agglomerate concentrations. In most cases the model correctly predicted the size distribution to within the estimated experimental error. When the predictions fell outside the estimated error, they did so in a random fashion except for the two-bead agglomerates at high shear stress. In all cases the qualitative prediction of the direction of change of size distribution was correct. No effect of concentration was predicted by the model and within the error limits and 4:1 range of concentrations tested no concentration effect was found experimentally.

It has been found that the strength distribution function of the artificial agglomerates employed could be represented equally well by either a linear or exponential function of strength. The linear representation was rejected on the physical grounds that it implied that no agglomerates would have a strength greater than a well defined, arbitrary value. The following exponential form was used

$$\rho_\sigma = e^{-\beta\sigma} \qquad 6\text{-}6$$

where

$\beta = 3.5\ lb_f/in^2$

It has been found that the experimental data do not provide a satisfactory test to determine the validity of the assumed values of c_{ij}. This is attributed to the fact that the initial size distributions of the experimental agglomerates contained only a small fraction (< 25%) of the degradable agglomerates for which the values of c_{ij} are fixed a priori. For these initial distributions the model predicts less than a ± 2% change in the distributions for the range $\frac{1}{i} \leq c_{ij} \leq i$.

The invariance of the results with different concentrations led to the tentative conclusion that collisions played only a minor role in deagglomeration, if at all. The effect of reagglomeration was also consigned to a minor role for the same reason. The direct detection of reagglomeration was not possible due to the method of analysis used.

The known behaviour of well-defined, regularly shaped particles in shear fields and in suspensions was extended to obtain a crude estimate of the expected behaviour of the agglomerates in this system. It was concluded that the behaviour of the agglomerates in the shear field was in qualitative agreement with the behaviour expected from such extrapolation. This gives a more sound basis for the model since it incorporates some features of the behaviour of single particles provided by this independent work.

The proposed model was compared with models derived to explain the comminution process. Although the equations are similar in many respects there are important differences. The most important of these differences is that the proposed model naturally leads to an equilibrium distribution at a given shear stress, while the comminution model achieves this only by forcing the breaking rate constant to be a function of time. There is no equivalent comminution model that corresponds to the equations giving the distributions for a time-varying shear stress.

The model was also compared with two models specifically proposed to describe deagglomeration. One of these models (McKelvey's) employed extreme simplifying assumptions, and under these restrictive conditions, agreement between it and the proposed model is qualitative. McKelvey's model had not been tested experimentally. The second model (Bolen and Colwell's) was purely empirical, with three adjustable constants to enable it to fit almost any data. In both cases a rigorous comparison was not possible since the earlier models did not predict size distributions.

Finally, a brief attempt was made to evaluate the applicability of this work to the conditions prevailing in commercial, complex mixers. Rough considerations suggest that the severe conditions employed in commercial dispersion processes might lead to melt flow instabilities, which in turn may significantly affect the dispersion process. At the present time, lacking knowledge of the polymer melt behaviour under these extreme conditions, it is not possible to determine if the model might be extended to such situations.

7.2 SUGGESTIONS FOR FURTHER WORK

The work reported here is one of the first studies to inquire into the nature of the breaking of randomly shaped agglomerates in a shear field. As a result, there are numerous questions which remain to be answered, and the author sugests the following areas for future investigation:

1. In the interests of more reliable data, an automatic counting technique should be developed or adapted from existing techniques. If such a technique were available it would allow more extensive sampling, thus reducing that portion of the uncertainty which is due to statistical fluctuations.
2. The agglomerate production technique should be refined or modified to allow agglomerates of controlled size distribution to be made. It would then be possible to produce agglomerates where the larger species contribute a major fraction of the total. This would allow a more severe test of the assumptions regarding c_{ij}, the breakdown product distribution coefficients.

3. The degree of deagglomeration should be extended so that almost complete degradation is obtained. This would confirm or negate the validity of the proposed model for the complete deagglomeration process.
4. There is a need for an experimental technique to measure the strength distribution of the agglomerates independently of the deagglomeration data. The direct, independent determination of the strength distribution would allow testing of the assumption that the distribution is invariant with agglomerate size.
5. In view of the results reported for the behaviour of single particles and suspensions, using particles of well-defined geometry, in pseudoplastic and viscoelastic fluids it is not certain that the proposed model may be directly applied to these systems. An incentive for examining these systems is that they are similar to those found in commercial dispersion processes.
6. Time-dependent (constant shear stress) experiments with varying agglomerate concentrations are required. These results would confirm, or reject, the model's assumption that the time-dependent size distribution is independent of agglomerate concentration.

7. The independence of concentration for the size distributions at equilibrium is not expected to hold for concentrated suspensions. There is a need to determine the critical concentration at which the mechanism changes and to develop equations for the new situation.
8. The equations that have been derived to predict the size distributions when the shear stress is an arbitrary function of time need to be tested since no data have been obtained for this condition.
9. The possible effect of bead size needs to be investigated since all results reported in this work have dealt with a single, relatively large, bead size.
10. Finally, the effect of using agglomerates made from irregularly shaped particles should be investigated.

7.3 CLAIMS FOR ORIGINAL WORK

1. Derivation of a model for the deagglomeration process, due to hydrodynamic forces in a sheared fluid, that predicts the size distribution of the agglomerates.

2. The presentation of equations giving the time-dependent size distributions due to a time-varying shear stress field.
3. Experimental measurements of agglomerate size distributions;
   a) at equilibrium, when all degradable agglomerates corresponding to a given shear stress have broken , and,
   b) the variation with time of size distributions resulting from a step change in the shear stress.
4. The results obtained indicate that, at low concentrations between 1/2% and 2% by weight, the distributions at equilibrium are independent of the concentration.
5. A new method for the preparation of artificial agglomerates has been developed.
6. The numerical solution of the equations for the non-isothermal, Newtonian flow contained between rotating coaxial cylinders with end effects and temperature-dependent fluid properties.
7. Experimental confirmation of the temperature profiles predicted for the flow described in 6) above.

LIST OF SYMBOLS

A	a square matrix
A_a	fractional area covered by agglomerates
A_d	area under the integral size distribution curve, equation 2-4
$A_{r,s}$	coefficient in finite difference form of equations of change
A.I.	agglomeration index (equation 2-5)
A_i;A_{it};A_{io}	scaling factors for strength distribution functions
$a_{i\sigma}$	strength distribution function of gained, stable agglomerates
$a_{n,i}$	coefficient defined by equations 2-20a and 2-20b
B	empirical constant, equation 2-11
B_b	number of bonds broken at time, t
$b_{i,j}$;$B(x,t)$	breakage function
B_i	amount of breakage of species i
$B_{r,s}$	coefficient in finite difference form of equations of change
$b_{i\sigma}$	strength distribution function of original agglomerate, Q'_{ior}, breakage products
C	empirical constant
C_1	variable coefficient defined by equation 1-24
$C_{r,s}$	coefficient in finite difference form of equations of change
C_v	specific heat at constant volume
C_p	specific heat at constant pressure
C_{ij}	coefficients in agglomerate mass balance

c_{ij}	relative frequency of types of agglomerate breakage
c_d	volume concentration of doublets
c_s	volume concentration of single spheres
D	diagonal of a matrix
$D_{jk};D_j$	diffusion coefficients
D_i	net difference in the number of agglomerates in the i^{th} species
$D_{r,s}$	coefficient in the finite difference form of the equations of change
d_{jk}	distance between a j-particle agglomerate and a k-particle agglomerate after collision
d_s	distance between two agglomerates
d	particle diameter
$E_{i\sigma}$	amount of gained, breakable agglomerates of strength σ in the i^{th} species
$E_{r,s}$	coefficient in the finite difference form of the equations of change
$e;\hat{e}$	iteration error; maximum iteration error
F_a	attractive force between agglomerates
F_c	number of collisions per unit time per unit volume
F_x	force at point x in a rod-like particle
f_i	instantaneous fraction of i^{th} species that is breakable
f_p	temperature dependent form of powerlaw model for viscosity
$f(x,t)$	weight fraction of material smaller than size x after grinding for a time, t

G_i	gain function for the i^{th} species
$G_{r,s}$	coefficient in the finite difference form of the equations of change
$g(t)$	time dependent function of shear stress
$g_{i,j}$	gain of agglomerates by the i^{th} species due to breakage in the j^{th} species
H	height of gap
h	distance between mesh points
$h_{i\sigma}$	strength distribution function, at any instant, of the i^{th} species agglomerates' breakage products
$I_{T,\infty}$	integral defined by equation 4-21
K	rate constant
K_r	ratio of inner to outer cylinder diameters
k	Boltzmann's constant
$k_c; k_d; k_1; k_2; k_3; k_4; k_4'$	Rate constants
$k(x)$	selection function given by fractional rate of breakage of material smaller than size x
$k_i(t)$	selection function for i^{th} species
k_t	thermal conductivity
L	lower triangular matrix
L_i	loss function for the i^{th} species
ℓ	length
ℓ_r	length of rod-like particle
M_t	weight average molecular weight at time, t

M_l	limiting molecular weight
N	largest agglomerate species initially present in the system
N_s	total number of spheres
N_∞	particle creation rate at long time
n	number of agglomerates per unit volume
n_o	number of particles per unit volume at time, t = 0
P	pressure; degree of polymerization
P_e	limiting degree of polymerization, below which degradation does not occur
Q_i	number of agglomerates, per unit volume, in the i^{th} species
q	heat flux
R_i	radius of inner cylinder
R_o	radius of outer cylinder
R	radial position in the gap
R*	dimensionless radial position in the gap
Re_s	shear Reynolds' number
r	radius of particle
r_e	equivalent axis ratio for a particle, equation 2-8
r_p	axis ratio of an ellipsoidal particle
S	scale of segregation
$S_{i\sigma}$	strength distribution function of the gained agglomerate, Q'_{ig}, breakage products

S_R	recoverable shear strain
T	temperature of fluid, at a point in the gap
T*	dimensionless temperature of fluid in the gap
T_w	temperature of inner cylinder wall
Ta	Taylor number
t	time
U	upper triangular matrix
V	velocity
v	vector of the unknown variable in a system of simultaneous equations
$V_{\theta K}$	tangential velocity at the inner cylinder wall
V*	dimensionless velocity
v_f	volume fraction of dispersed component
v_p	volume fraction of pigment
w	width of gap between the concentric cylinders
w_i	weight fraction of the i^{th} species
X	arbitrary dependent variable
x	cartesian co-ordinate
x_m	largest of particles or agglomerates
Y	arbitrary independent variable
y	cartesian co-ordinate
z	axial position
z*	dimensionless axial position

Greek Letters

α	thermal diffusivity
α_g	over-relaxation factor
α_{opt}	optimum over-relaxation factor
$\alpha_{i\sigma}$	distribution function of original remaining breakable agglomerates, Q'_{ior}, in the i^{th} species
β	empirical constant, equation 6-6
γ	shear strain (deformation)
$\dot{\gamma}$	shear rate
γ_m	mean shear strain, equation 5-5
$\dot{\gamma}_m$	mean shear rate
$\underline{\underline{\Delta}}$	rate of deformation tensor
δ_K	K^{th} element of the displacement vector between two iteration matrices
ϵ_i	value of a replicated result, i
η	non-Newtonian viscosity
η_o	reference, non-Newtonian, viscosity
λ_e	estimated largest eigenvalue of the iteration matrix
λ_m	largest eigenvalue of the iteration matrix
μ	Newtonian viscosity
ρ	density
ρ_σ	strength distribution function of initial (unsheared) agglomerates
$\underline{\underline{\tau}}$	shear stress tensor
τ_a	average shear stress

τ_p	minimum shear stress to cause particle rupture
τ_m	mean shear stress
σ	agglomerate strength, defined as the minimum shear stress in the fluid required to cause breakage when the agglomerate is in its most favourable orientation
ϕ	Rayleigh quotient
ω	angular velocity of the inner cylinder

Subscripts and Superscripts

The usage indicated here for subscripts and superscripts is generally followed; exceptions are defined in the text.

g	subscript, indicates the gain portion of the subscripted variable
i	subscript, refers to the i^{th} species
j	subscript, refers to the j^{th} species
k	subscript, refers to the k^{th} species
ℓ	subscript, indicates the loss portion of the subscripted variable
m	subscript, summation index
m	superscript, refers to the m^{th} iteration
N	subscript, indicates the N-particle species
o	subscript, original (initial) value of the variable at time, t = 0
r	subscript, value of the remaining portion of the original variable value

t	subscript, the subscripted variable is a function of time
σ	subscript, the subscripted variable is a function of σ
'	superscript, indicates breakable agglomerates
"	superscript, indicates stable agglomerates

REFERENCES

1. Stoy, William S., in Modern Plastics Encyclopedia, pp. 218-222, McGraw-Hill, New York (1971).

2. Schidrowitz, P. and Dawson, T.R., eds; History of the Rubber Industry, W. Hefner and Sons, Cambridge (1952).

3. Bergan, J.T., in Processing of Thermoplastic Materials, E.C. Bernhardt, ed., Reinhold Publishing, New York, pp. 424-435 (1959).

4. Van Wazer, J.R., Lyons, J.W., Kim, K.Y. and Colwell, R.E., Viscosity and Flow Measurement, Wiley, New York (1963).

5. Daniel, F.K., J. Oil Colour Chemists' Assoc., 54, 84 (1971).

6. Levich, V.E., Physicochemical Hydrodynamics, Chp. V, Prentice Hall, New Jersey (1962).

7. Heckman, F.A., Rubber Chem. Tech., 38, 1245 (1964).

8. Hess, W.M., Ban, L.L., Eckert, F.J. and Chirico, U., Rubber Chem. Tech., 41, 356 (1968).

9. Boonstra, B.B., J. Appl. Poly. Sci., 11, 389 (1967).

10. Boonstra, B.B. and Medalia, A.I., Rubber Chem. Tech., 36, 115 (1963).

11. Gessler, A.M., Rubber Chem. Tech., 43, 943 (1970).

12. Voet, A. and Aboytes, P., Rubber Chem. Tech., 43, 1359 (1970).

13. Heckman, F.A. and Medalia, A.I., J. Inst. Rubber Ind., 3, 66 (1969).

14. Leigh-Dugmore, C.H., Rubber Chem. Tech., 29, 1303 (1956).

15. Medalia, A.I., Rubber Chem. Tech., 34, 1134 (1961).

16. Danckwerts, P.V., Chem. Eng. Sci., 2, 1 (1953).

17. Lacey, P.M.C., J. Appl. Chem. (London), 4, 257 (1954).

18. Spencer, R.S. and Wiley, R.M., J. Colloid Sci., 6, 133 (1951).

19. Mohr, W.D., in Processing of Thermoplastic Materials, ed. E.C. Bernhardt, p. 117, Reinhold, New York (1959).

20. Mohr, W.D., Saxton, R.L. and Jepson, C.H., Ind. Eng. Chem., 49, 1855 (1957).

21. Bergen, J.T., Carrier, E.W., Krumhansl, J.A., SPE ANTEC IV, 97 (1958).

22. McKelvey, J.M., Polymer Processing, Wiley, New York (1962).

23. Maddock, B.H., SPE Journal, 16, 383 (1959).

24. Tadmor, Z. and Klein, I., Engineering Principles of Plasticating Extrusion, Van Nostrand Reinhold Co., New York (1970).

25. Bergen, J.T., in Rheology Vol. IV, R. Eirich, ed., p. 285, Academic Press, New York (1967).

26. Irving, H.F. and Saxton, R.L., in Mixing - Theory and Practice Vol. II, Vincent W. Uhl and J.B. Gray, eds., p. 169, Academic Press, New York (1969).

27. Gaskell, R.E., J. Appl. Mech., 17, 334 (1950).

28. Moore, W.R., Trans. J. Plastics Inst., 32, 247 (1964).

29. Langton, N.H., Rubber and Plastics Weekly, 143, 149 (1962).

30. Bolen, W.R. and Colwell, R.E., SPE Tech. Papers IV, 98 (1958).

31. Smith, M.J., A New Method for Measuring the Rate at which Pigments Disperse During Mixing, Powder Technology Symp., Leeds, May 1971.

32. Hess, W.M. and Garret, M.D., J. Oil Colour Chemists Assoc., 54, 24 (1971).

33. Bartok, W. and Mason S.G., J. Colloid Sci., 7, 354 (1952).

34. Goldsmith, H.L., and Mason, S.G., in Rheology, Vol. IV, F.R. Eirich, ed., Acadmic Press, New York (1967).

35. Forgacs, O.L. and Mason S.G., J. Colloid Sci., 14, 457 (1959).

36. Slatterly, J.C., J. Fluid Mech., 19, 625 (1964).

37. Manley, R.St.J. and Mason, S.G., Can. J. Chem., 33, 765 (1955).

38. Manley, R.St.J. and Mason, S.G., Proc. Roy. Soc., A238, 117 (1956).

39. Gauthier, F.J., Ph.D. Thesis, McGill University (1970).

40. Zia, I.Y., Ph.D. Thesis, McGill University (1966).

41. Zia, I.Y., Cox, R. . and Mason, S.G., Proc. Roy. Soc., A300, 421 (1967).

42. Vadas, E.B., M.Sc. Thesis, McGill University (1971).

43. van den Tempel, M., in Rheology of Emulsions, P. Sherman, ed., p. 1, Pergamon Press, Oxford (1963).

44. Epstein, B., Ind. Eng. Chem., 40, 2289 (1948).

45. Bass, L., Z. Angew Math. Phys., 5, 283 (1954).

46. Reid, K.J., Chem. Eng. Sci., 20, 953 (1965).

47. Kelsall, D.F. and Reid, K.J., Joint AIChE - I. Chem. Eng. Symp., Series 4, 4:14, London (1965).

48. Klimpel, R.R. and Austin, L.G., Ind. Eng. Chem. Fund., 9, 230 (1970).

49. Herbst, J.A. and Fuerstenau, D.W., Trans AIME, 241, 538 (1968).

50. Minoura, Y., Kasuya, T., Kawamura, S. and Nakano, A., J. Poly. Sci., A-2 5, 125 (1967).

51. Gooberman, G., J. Poly. Sci., 42, 25 (1960).

52. Gooberman, G. and Lamb, J. Poly. Sci., 42, 35 (1960).

53. Ovenall, D.W., Hastings, G.W. and Allen, P.E.M., J. Poly. Sci., 33, 207 (1958).

54. Allen, P.E.M., Burnett, G.M., Hastings, G.W., Melville, H.W. and Ovenall, D.W., J. Poly. Sci., 33, 207 (1958).

55. Jellinek, H.H.G. and White, G., J. Poly. Sci., 6, 745 and 757 (1951).

56. Mostafa, M.A.K., J. Poly. Sci., 22, 535 (1956); ibid 27, 473 (1956); ibid 28, 499 (1958); ibid 28, 519 (1958); ibid 33, 295, 311 (1958).

57. Mostafa, M.A.K., J. Poly. Sci., 12, 533 (1954).

58. Harrington, R.E. and Zimm, B.H., J. Phys. Chem., 69, 161 (1965).

59. Johnson, W.R. and Price, C.C., J. Poly. Sci., 45, 217 (1960).

60. Jellinek, H.H.G., Degradation of Vinyl Polymers, chps 1 and 4, Academic Press, New York (1955).

61. Mostafa, M.A.K., J. Poly. Sci., 33, 323 (1958).

62. Ovenall, D.W., J. Poly. Sci., 42, 455 (1960).

63. Karnis, A., Goldsmith, H.L. and Mason, S.G., J. Colloid Interface Sci., 22, 531 (1966).

64. Schlicting, H., Boundary Layer Theory, p. 500, sixth ed., McGraw-Hill, New York (1965).

65. Modern Plastics Encyclopedia, McGraw-Hill, New York (1971).

66. Rumpf, H., Chapter 15 in Agglomeration, W.A. Knepper, ed., Interscience, New York (1962).

67. Kuhn, W.E., Ultrafine Particles, Wiley, New York (1963).

68. Lewis, T.B. and Nielson, L.E., Trans. Soc. Rheol., 12, 421 (1968).

70. Fisher, C. and Cole, M., The Microscope, 16, 81 (1968).

71. Kubitschek, H.E., Research, 13, 128 (1960).

72. Herdan, G., Small Particle Statistics, 2nd ed., chps. 18, 19, 20, Butterworths, London (1960).

73. Chen, Ching-Li, Masters Thesis, Ecole Polytechnique, 1972.

74. Shoulberg, R.H., J. Appl. Poly. Sci., 7, 1597 (1963).

75. Ferry, John D., Viscoelastic Properties of Polymers, 2nd ed., p. 318, John Wiley, New York (1970).

76. Gauthier, F., Goldsmith, H.L. and Mason, S.G., Kolloid Z. Z. Polymere, 248, 1000 (1971).

77. Karnis, A., Goldsmith, H.L. and Mason, S.G., Can. J. Chem. Eng., 44, 181 (1960).

78. Lapidus, L., Digital Computation for Chemical Engineers, McGraw-Hill, New York (1962).

79. Carnahan, H., Luther, H.A. and Wilkes, J.O., Applied Numerical Methods, John Wiley, New York (1969).

80. Martin, D.W. and Tee, G.J., Computer J., 4, 242 (1962).

81. Carre, B.A., Computer J., 4, 73 (1962).

82. Reid, J.K., Computer J., 6, 200 (1964).

83. Ginn, R.F. and Denn, M.M., A.I.Ch.E.J., 15, 450 (1969).

84. Ginn, R.F. and Denn, M.M., A.I.Ch.E.J., 15, 454 (1969).

85. Lohe, P., Kolloid-Z u Z. Polymere, 204, 7 (1965).

86. ______________________, System/360 Scientific Subroutine Package, Version III, Programmers Manual International Business Machines, White Plains, N.J. (1968).

APPENDIX I

NUMERICAL SOLUTION OF THE EQUATIONS OF ENERGY AND MOTION

To have a rational basis for design of the equipment and, also, to know the shear field throughout the sample the numerical solution of the equations of energy and motion for the apparatus shown in figures 3-2 and 3-3 was undertaken.

I-1 EQUATION OF MOTION

The assumptions made in setting up the equation of motion are:

1. steady state flow;

$$\frac{\partial}{\partial t} = 0 \qquad \text{I-1}$$

2. uniform flow around the annulus;

$$\frac{\partial}{\partial \theta} = 0 \qquad \text{I-2}$$

3. the normal stress differences are neglibible;

$$(\tau_{rr} - \tau_{\theta\theta}) = (\tau_{rr} - \tau_{zz}) = 0 \qquad \text{I-3}$$

for vertical cylinders the r-component is zero and the z-component contains only hydrostatic pressure, thus the equation, in component form, reduces to:

$$-\frac{\partial \tau_{\theta z}}{\partial z} = \frac{1}{R^2}\frac{\partial}{\partial R}\left(R^2 \tau_{R\theta}\right) \qquad 1\text{-}4$$

now, despite its shortcomings, the power law representation for viscosity is used:

$$\eta = \eta_o \left|\frac{\underline{\underline{\Delta}}:\underline{\underline{\Delta}}}{2}\right|^{\frac{n-1}{2}} \qquad 1\text{-}5$$

and for the system of interest:

$$\left|\frac{\underline{\underline{\Delta}}:\underline{\underline{\Delta}}}{2}\right| = \dot{\gamma} = R\left[\frac{\partial}{\partial R}\left(\frac{V_\theta}{R}\right)\right]^2 + \left[\frac{\partial V_\theta}{\partial z}\right]^2 \qquad 1\text{-}6$$

The temperature effects for viscosity will be included as:

$$\eta_o = \eta_o(T) \qquad 1\text{-}7$$

and $\quad n = n(T) \qquad$ 1-8

it is convenient to compute the viscosity separately

$$\eta = f_p\left(\left|\underline{\underline{\Delta}}:\underline{\underline{\Delta}}\right|, T\right) \qquad 1\text{-}9$$

For the z-component of τ, using equation 1-9,

$$\frac{\partial \tau_{\theta z}}{\partial z} = -f_p \frac{\partial^2 V_\theta}{\partial z^2} - \frac{\partial f_p}{\partial z}\frac{\partial V_\theta}{\partial z} \qquad 1\text{-}10$$

similarly

$$-\frac{\partial}{\partial R}(R^2\tau_{R\theta}) = (2rf_p(\frac{\partial V_\theta}{\partial R}) - \frac{V_\theta}{R})$$

$$+ R^2 f_p (\frac{\partial^2 V_\theta}{\partial R^2} - \frac{1}{R}\frac{\partial V_\theta}{\partial R} + \frac{V_\theta}{R^2})$$

$$+ R^2 \frac{\partial f_p}{\partial R}(\frac{\partial V_\theta}{\partial R} - \frac{V_\theta}{R}) \qquad \text{I-11}$$

Substituting equations I-10 and I-11 into equation I-4 and collecting terms:

$$f_p \frac{\partial^2 V_\theta}{\partial R^2} + \frac{\partial f_p}{\partial R}\frac{\partial V_\theta}{\partial R} - \frac{\partial f_p}{\partial R}\frac{V_\theta}{R} + \frac{f_p}{R}\frac{\partial V_\theta}{\partial R} -$$

$$- \frac{f_p V_\theta}{R^2} + f_p \frac{\partial^2 V_\theta}{\partial z^2} + \frac{\partial f_p}{\partial z}\frac{\partial V_\theta}{\partial z} = 0 \qquad \text{I-12}$$

Equation I-12 is the governing differential equation of motion for the system. The equation is changed to dimensionless form as follows:

1. for gap width (radial direction)

$$R^* = \frac{R - K_r R_o}{R_o - K_r R_o} \qquad \text{I-13}$$

where R_o = radius of outside cylinder

$K_r = R_i/R_o$, R_i = radius of inside cylinder

R = radius at any point in the gap

2. for non-dimensionalized height

$$z^* = \frac{z}{H} \qquad \text{I-14}$$

where H = total height of the gap

z = perpendicular distance from any point in the gap to the bottom of the gap

3. for velocity, V_θ

$$V_\theta^* = \frac{V_\theta}{K_r R_o \omega} \qquad \text{I-15}$$

where ω = inner cylinder speed in radians/sec

V_θ = tangential velocity at any point in the gap

In terms of the non-dimensional variables, the boundary conditions for equation I-12 are:

$$V_\theta^*(0,z^*) = 1 \qquad \text{I-16}$$

$$V_\theta^*(R^*,0) = 0 \qquad \text{I-17}$$

$$V_\theta^*(1,z^*) = 0 \qquad \text{I-18}$$

$$\frac{\partial}{\partial z}[V_\theta(R^*,1)] = 0 \qquad \text{I-19}$$

In order to solve equation I-12 numerically it was converted to a finite difference approximation, with the gap divided into a square mesh by the usual technique (78,79). The following representations were chosen for the first and second derivatives, respectively, of a function $U = U(X,Y)$:

$$\left.\frac{\partial U}{\partial Y}\right|_{r,s} = \frac{X_{r+1,s} - X_{r-1,s}}{2h} \qquad \text{1-20}$$

$$\left.\frac{\partial^2 U}{\partial Y}\right|_{r,s} = \frac{X_{r+1,s} - 2X_{r,s} + X_{r-1,s}}{h^2} \qquad \text{1-21}$$

where

U = dependent variable, e.g. V_θ in equation 1-12

Y = independent variable, e.g. R in equation 1-12

h = the distance between two mesh lines, a constant

r,s = indices, locating the point on the mesh at which the derivatives are being represented.

Equation 1-12 is first converted to dimensionless form,using equations 1-13 to 1-15:

$$\frac{f_p V_\theta}{H^2}\frac{\partial^2 V_\theta{}^*}{\partial z^{*2}} + \frac{V_{\theta K}}{H^2}\frac{\partial f_p}{\partial z^*}\frac{\partial V_\theta{}^*}{\partial z^*} + \frac{f_p\, V_{\theta K}}{R_o^2(1 - K_r)^2}\frac{\partial^2 V_\theta{}^*}{\partial R^{*2}}$$

$$+ \left(\frac{1}{R_o(1-K_r)}\frac{\partial f_p}{\partial R^*} + \frac{f_p}{R^*\, R_o(1-K_r)+KR_o}\right)\frac{V_{\theta K}}{R_o^2(1-K_r)^2}\frac{\partial V_\theta{}^*}{\partial R^*}$$

$$- \left(\frac{1}{R_o(1-K_r)}\frac{\partial f_p}{\partial R^*} + \frac{f_p}{R^*\, R_o(1-K_r)+K_rR_o}\right)\frac{V_{\theta K}\, V_\theta{}^*}{R^*R_o(1-K_r)+K_rR_o}$$

$$= 0 \qquad \text{1-22}$$

Now, transforming I-22 to finite difference form:

$$\left[\frac{2f_{r,s}}{H^2h^2} + \frac{2f_{r,s}}{R_o^2(1-K_r)^2h^2} + \frac{C_1}{R^*R_o(1-K_r)+K_rR_o}\right] V_{r,s}$$

$$= \left[\frac{f_{r,s}}{H^2h^2} + \frac{f_{r,s+1} - f_{r,s-1}}{4H^2h^2}\right] V_{r,s+1}$$

$$+ \left[\frac{f_{r,s}}{H^2h^2} - \frac{f_{r,s+1} - f_{r,s-1}}{4H^2h^2}\right] V_{r,s-1}$$

$$+ \left[\frac{f_{r,s}}{R_o^2(1-K_r)^2h^2} + \frac{C_1}{2hR_o(1-K_r)}\right] V_{r+1,s}$$

$$+ \left[\frac{f_{r,s}}{R_o^2(1-K_r)^2h^2} - \frac{C_1}{2hR_o(1-K_r)}\right] V_{r-1,s}$$

I-23

where $$C_1 = (\frac{1}{R(1-K_r)} \frac{f_{r+1,s} - f_{r-1,s}}{2h} + \frac{f_{r,s}}{C_*R(1-K_r)+K_rR}$$

I-24

r = refers o position in the radial direction of the mesh

s = refers to position in the axial direction of the mesh

The subscript θ in V_θ has been dropped and the subscript p has been dropped from f_p to avoid confusion.

Equation I-23 may be rewritten as

$$A_{r,s}V_{r,s} = B_{r,s}V_{r,s+1} + C_{r,s}V_{r,s-1} + D_{r,s}V_{r+1,s} + E_{r,s}V_{r-1,s} \qquad \text{I-25}$$

where A, B, C, D and E are the appropriate coefficients from equation I-25 and are functions of position (r,s), device geometry and viscosity. $V_{r,s}$ is thus known in terms of the coefficients, $V_{r+1,s}$, $V_{r-1,s}$, $V_{r,s+1}$ and $V_{r,s-1}$. However, since the equation holds for each point, (r,s) on the grid it may be written for each point yielding n^2 equations with n^2 unknowns for an n by n mesh.

In the simple relaxation scheme for solving this problem an initial estimate of V is made for each point. Then equation I-25 is applied to calculate a new value of V working systematically around the grid. This process is continued until, on the $(m+1)^{th}$ iteration, $V^{m+1}_{r,s}$ calculated agrees with the previous value $V^{m}_{r,s}$ to within some predetermined criterion for each point.

Faster convergence of this scheme is obtainable if the Gauss-Seidel modification is used. In this modification, as soon as a new value of V is computed it is used in the next equation. Thus for increasing r and s.

$$A_{r,s}V^{m+1}_{r,s} = B_{r,s}V^{m}_{r,s+1} + C_{r,s}V^{m+1}_{r,s-1} + D_{r,s}V^{m}_{r+1,s} + E_{r,s}V^{m+1}_{r-1,s} \qquad \text{I-26}$$

where m refers to the n^{th} iteration and m+1 refers to the $n+1^{th}$ iteration.

An additional modification is to use the over-relaxation scheme, or accelerated Gauss-Seidel method:

$$V^{m+1}_{r,s} = V^{m}_{r,s}(1-\alpha_g) + \frac{\alpha_g}{A_{r,s}} (B_{r,s}V^{m}_{r,s+1} + C_{r,s}V^{m+1}_{r,s-1} + D_{r,s}V^{m}_{r+1,s} + E_{r,s}V^{m+1}_{r-1,s}) \qquad 1\text{-}27$$

where α_g is called the over-relaxation factor. A correct choice of α_g gives faster convergence than the use of the simple Gauss Seidel method. Different methods of choosing α_g are outlined later in this appendix.

It can be noted that finding a solution to equation 1-26 is the same as solving n simultaneous algebraic equations and the system may be written in the matrix form

$$AV = b \qquad 1\text{-}28$$

for n points in the grid there are n^2 equations and A is an $n^2 \times n^2$ matrix. For the second order finite difference scheme used, the matrix is of the block tridiagonal form:

A =

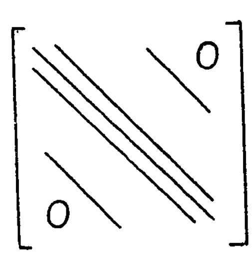

1-29

The solution of equation I-27 is:

$$V = A^{-1}b \qquad \text{I-30}$$

and the problem is now finding the inverse of A. The over-relaxation (or accelerated Gauss-Seidel) method has a strong recommendation when A is of the above form. This advantage is that convergence is guaranteed regardless of the value of det $|A|$ (80).

There is a problem occurring with the use of all relaxation schemes. The problem is the estimation of the error at any time during the iterations. Consider the usual criterion used, where the iterations are continued until the difference between successive values of the dependent variable, is less than some arbitrary value, δ_e. This does not guarantee that the error is less than δ_e but only that the rate of convergence is less than δ_e. Until recently the problem was solved by continuing the iterations until δ_e was two or three orders of magnitude smaller than the accuracy required.

A more reliable test has been suggested by Carré (81). He suggests that the largest error in the m^{th} iteration, $\hat{e}^m$, is bounded by

$$|\hat{e}^m| \leq \frac{\lambda_e |\hat{\delta}^m|}{1 - \lambda_e} \qquad \text{I-31}$$

where $|\hat{\delta}^m|$ is the arithmetically largest element of the displacement vector (the displacement vector is the difference between all elements, $X^k_{i,j} - X^{k-1}_{i,j}$). λ_e is the estimated largest eigenvalue of the matrix A. It may be estimated from the relation

$$\lambda_e = \alpha_{opt} - 1 \qquad \text{1-32}$$

where α_{opt} is the optimum relaxation factor. The optimum relaxation factor is the one that gives the fastest, stable convergence.

1-2 EQUATION OF ENERGY

Starting with the form:

$$\frac{\partial}{\partial t}(\rho C_v T) = -(\nabla\cdot\rho C_v T\underline{V}) - \underline{\nabla}\cdot\underline{q} - T\left(\frac{\partial P}{\partial T}\right)_\rho(\nabla\cdot\underline{V})$$

$$- (\underline{\underline{\tau}}:\underline{\nabla V}) + \rho T\,\frac{DC_v}{Dt} \qquad \text{1-33}$$

since $\underline{\nabla}\cdot S\underline{V} = S\underline{\nabla}\cdot\underline{V}$ 1-34

the energy equation reduces to

$$0 = \underline{\nabla}\cdot\underline{q} - \underline{\underline{\tau}}:\underline{\nabla V} \qquad \text{1-35}$$

and only the viscous dissipation and heat conduction terms are left. Working in terms of components

$$\underline{\underline{\tau}}:\underline{\nabla V} = \tau_{r\theta}\left[R\frac{\partial}{\partial R}\left(\frac{V_\theta}{R}\right) + \frac{1}{R}\left(\frac{\partial V_R}{\partial\theta}\right)\right] + \tau_{z\theta}\left[\frac{1}{R}\frac{\partial V_z}{\partial\theta} + \frac{\partial V_\theta}{\partial z}\right] \quad 1\text{-}36$$

since $\tau_{r\theta}$ and $\tau_{z\theta}$ are the only non-zero shear stresses. Substituting for $\tau_{r\theta}$ and $\tau_{z\theta}$:

$$\underline{\underline{\tau}}:\underline{\nabla V} = -f_p R^2\left[\frac{\partial}{\partial R}\left(\frac{V_\theta}{R}\right)\right]^2 - f_p\left[\frac{\partial V_\theta}{\partial z}\right]^2 \quad 1\text{-}37$$

also, since $\frac{\partial}{\partial\theta} = 0$;

$$\underline{\nabla}\cdot\underline{q} = \frac{1}{R}\frac{\partial}{\partial R}(rq_R) + \frac{\partial q_z}{\partial z} \quad 1\text{-}38$$

$$q_R = -k_T\frac{\partial T}{\partial R} \quad 1\text{-}39$$

$$q_z = -k_T\frac{\partial T}{\partial z} \quad 1\text{-}40$$

If k_T is allowed to be a function of temperature, $k_T = k_T(T)$ then making the substitutions

$$\underline{\nabla}\cdot\underline{q} = -\left[k_T\frac{\partial^2 T}{\partial R^2} + \frac{\partial T}{\partial R}\frac{\partial k_T}{\partial R} + \frac{k_T}{R}\frac{\partial T}{\partial R}\right] - \left[k_T\frac{\partial^2 T}{\partial z^2} + \frac{\partial T}{\partial z}\frac{\partial k_T}{\partial z}\right] \quad 1\text{-}41$$

The energy equation becomes:

$$0 = k_T \frac{\partial^2 T}{\partial R^2} + \frac{\partial T}{\partial R}\frac{\partial k_T}{\partial R} + \frac{k_T}{R}\frac{\partial T}{\partial R} + k_T \frac{\partial^2 T}{\partial z^2} + \frac{\partial T}{\partial z}\frac{\partial k_T}{\partial z}$$

$$+ f_p R^2 \left[\frac{1}{R}\frac{\partial V_\theta}{\partial R} - \frac{V_\theta}{R^2} \right]^2 + f_p \left[\frac{\partial V_\theta}{\partial z} \right]^2 \qquad \text{1-42}$$

with boundary conditions:

$$T(R_i,z) = T_w \qquad \text{1-43}$$

$$T(R^*,0) = T_w \qquad \text{1-44}$$

$$T(R_o,z) = T_w \qquad \text{1-45}$$

$$\frac{\partial}{\partial z}[T(R^*,H)] = 0 \qquad \text{1-46}$$

Using the previously described methods of obtaining the finite-difference equation and dimensionless variables the following equation is obtained:

$$0 = \frac{k_T T_w}{R_o^2(1-K_r)^2}\frac{\partial^2 T^*}{\partial R^{*2}} + \frac{T_w}{R_o^2(1-K_r)^2}\frac{\partial k_T}{\partial R^*}\frac{\partial T^*}{\partial R^*} + \frac{k_T T_w}{R_o(1-K_r)(R^* R_o(1-K_r)+K_r R_o}\frac{\partial T^*}{\partial R^*}$$

$$+ \frac{k_T T_w}{H^2}\frac{\partial^2 T}{\partial z^{*2}} + \frac{T_w}{H^2}\frac{\partial k_T}{\partial z^*}\frac{\partial T^*}{\partial z^*} + f_p \left[\frac{V_{\theta_K}}{H} \frac{\partial V_\theta{}^*}{\partial z^*} \right]^2$$

$$+ f_p (R^* R_o)(1-K_r R_o)+K_r R_o)^2 \left[\frac{1}{R^* R_o(1-K_r+K_r R_o} \left(\frac{V_{\theta_K}}{R_o(1-K_r)} \frac{\partial V_\theta{}^*}{\partial R^*} \right) - \frac{V_{\theta_K} V_\theta{}^*}{R^* R_o(1-K_r)+K_r R_o} \right]^2$$

1-47

where $T^* = \frac{T}{T_w}$ 1-48

and $V_{\theta_K} = \omega K_r R_o$ 1-49

and the finite difference form is

$$\frac{k_{r,s}T_w}{R_o^2(1-K_r)^2}\left[\left(\frac{T_{r+1,s} - 2T_{r,s} + T_{r-1,s}}{h^2}\right)\right]$$
$$+ \frac{T_w}{R_o^2(1-K)^2}\left[\left(\frac{k_{r+1,s} - k_{r-1,s}}{2h}\right)\left(\frac{T_{r+1,s} - T_{r-1,s}}{2h}\right)\right]$$
$$+ \frac{k_{r,s}T_w}{R_o(1-K_r)(R^*R_o(1-K_r)+K_rR_o)}\left[\left(\frac{T_{r+1,s} - T_{r-1,s}}{h^2}\right)\right]$$
$$+ \frac{k_{r,s}\ T_w}{H^2}\left[\left(\frac{T_{r,s+1} - 2T_{r,s} + T_{r,s-1}}{2h}\right)\right]$$
$$+ \frac{T_w}{H^2}\left[\left(\frac{k_{r,s+1} - k_{r,s-1}}{2h}\right)\left(\frac{T_{r,s+1} - T_{r,s-1}}{2h}\right)\right]$$
$$+ f_{r,s}\left[\left(\frac{V_{\theta_K}}{H}\ \frac{V_{r,s+1} - V_{r,s-1}}{2h}\right)\right]$$
$$+ f_{r,s}\left[(R^*R_o(1-K_r) + K_rR_o)^2\right]$$
$$\left[\frac{1}{R^*R_o(1-K_r)+K_rR_o}\ \frac{V_{\theta_K}}{R_o(1-K_r)}\ \frac{V_{r+1,s}-V_{r-1,s}}{2h} - \frac{V_{\theta_K}\ V_{r,s}}{(R^*R_o(1-K_r)+K_rR_o)}\right]^2$$
$$= 0$$ 1-50

Equation I-50 may be expanded and the terms collected to give a form such as

$$A_{r,s}T_{r,s} = B_{r,s}T_{r,s+1} + C_{r,s}T_{r,s-1} + D_{r,s}T_{r+1,s} + E_{r,s}T_{r-1,s} + G_{r,s} \qquad \text{I-51}$$

where the coefficients A, B, C etc. are functions of position, T_w and V.

Equation I-51 can be rewritten for the Gauss-Seidel method of accelerated relaxation and gives

$$T^{m+1}_{r,s} = T^{m}_{r,s}(1-\alpha_g) + \frac{\alpha_g}{A_{r,s}} [B_{r,s}T^{m}_{r,s+1} + C_{r,s}T^{m+1}_{r,s-1} + D_{r,s}T^{m}_{r+1,s} + E_{r,s}T^{m+1}_{r-1,s} + G_{r,s}] \qquad \text{I-52}$$

where α_g is the over-relaxation factor, and the superscript m refers to the m^{th} iteration.

As before, it is necessary to make initial guesses for all $T_{r,s}$ to start the iteration process; the values of $V_{r,s}$ are estimated from the previous solution of the equation of motion.

The flow chart depicting the computation scheme for the simultaneous solution of the two equations is shown in figure I-1. The program, written in Fortran IV, is given at the end of this appendix.

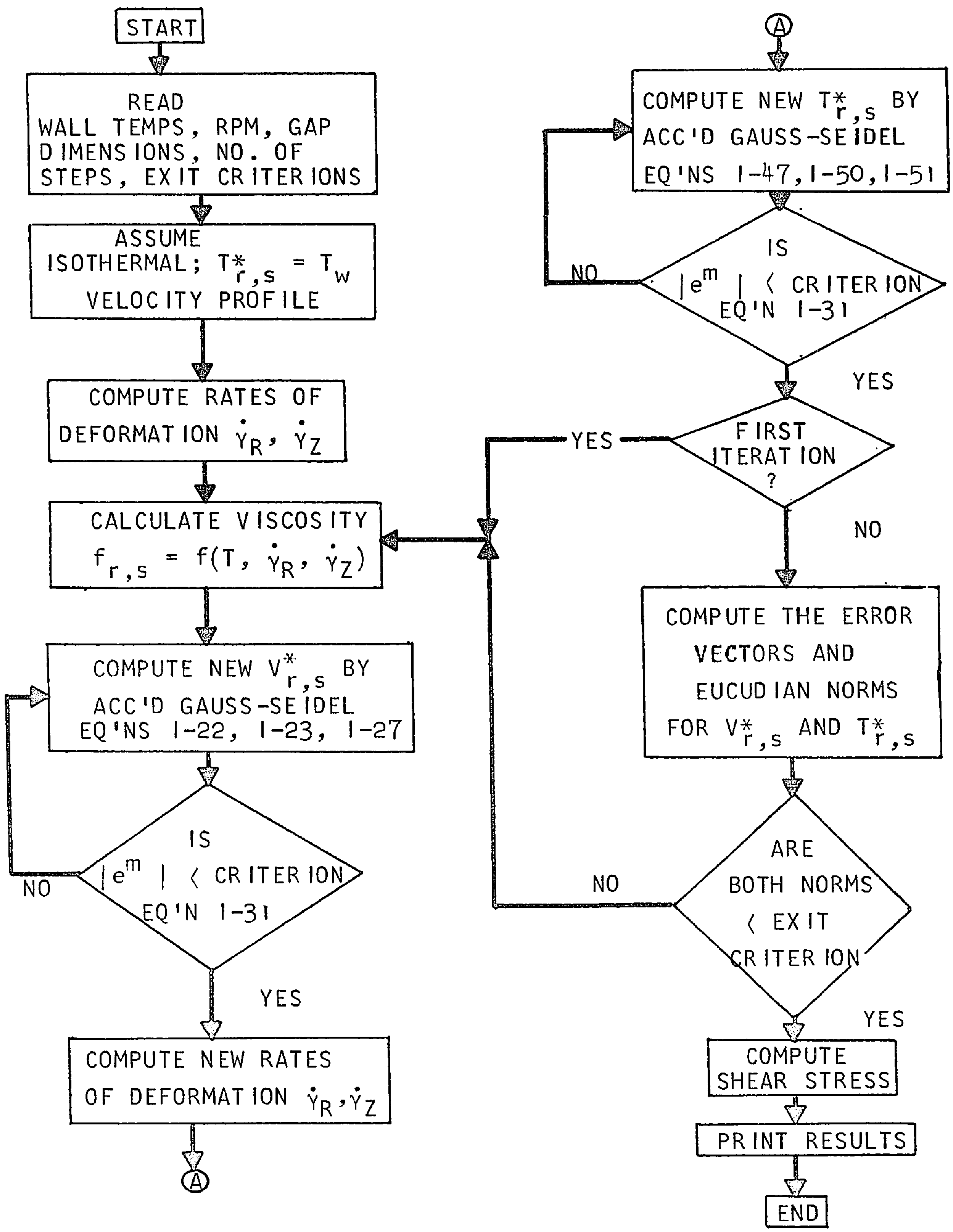

FIGURE 1-1: Flow Chart of Program for Numerical Solution of Equations of Motion and Energy

I-3 ESTIMATION OF THE OVER-RELAXATION PARAMETER FOR THE GAUSS-SEIDEL METHOD

As shown earlier, the finite difference equations give a set of algebraic equations that can be written in matrix form:

$$AV = b \qquad \text{I-28}$$

with solution

$$V = A^{-1} b \qquad \text{I-30}$$

and the problem is one of inverting matrix A. For the two equations (motion and energy) with the second order finite difference, A is of the block tridiagonal form, (equation I-29) and can be decomposed to

$$A = D - L - U \qquad \text{I-53}$$

where D is the diagonal and L and U are the upper and lower triangular matrices. If L + U can be rearranged to give the form $\begin{bmatrix} 0 & R \\ Q & 0 \end{bmatrix}$ where 0 is a null square submatrix, then the Gauss-Seidel method for inverting A will always converge (80). The problem is that the convergence is sometimes slow. This occurs when A is ill-conditioned. (i.e. det $|A|$ is not large and positive, or, equivalently, the largest real eigenvalue of A is close to unity). It is therefore desirable to use the over-relaxation or accelerated Gauss-Seidel methods.

The difficulty arises in choosing the optimum over-relaxation factor, α_{opt}. Carré (81) has given one method for estimating α_{opt}. He makes one iteration with $\alpha_g = 1$ and then 12 iterations with $\alpha_g = 1.375$. The displacement vector, $\delta^{(m)} = X^{(m)} - X^{(m-1)}$ is calculated and its norm, $n^{(m)}$, is found. It is then possible to estimate the largest eigenvalue since

$$\lim_{m\to\infty} \frac{n^{(m)}}{n^{(m-1)}} = \lambda_{max} \qquad \text{1-54}$$

and α_{opt} may be computed from λ_{max}. However, this gives a poor estimate for λ_{max} when m is small. Carré overcomes this by forming the ratios:

$$P^{(m-2)} = \frac{n^{(m-2)}}{n^{(m-3)}} \qquad \text{1-55}$$

$$P^{(m-1)} = \frac{n^{(m-1)}}{n^{(m-2)}} \qquad \text{1-56}$$

$$P^{(n)} = \frac{n^{(m)}}{n^{(m-1)}} \qquad \text{1-57}$$

and then using Aitken extrapolation

$$\lambda_{max} = P^{(m-2)} - \frac{(P^{(m-1)} - P^{(m-2)})^2}{P^{(m-2)} + P^{(m)} - 2P^{(m-1)}} \qquad \text{1-58}$$

The optimum value of α_g may then be found from

$$\alpha_{opt} = 2\left[1 + \left[1 - (\lambda_{max} + \alpha_g - 1)^2/\lambda_{max}\alpha_g^2\right]\right]^{-1} \quad \text{I-59}$$

provided $\alpha_g < \alpha_o$.

To make optimum use of this method a new value of α_g should be estimated after each iteration, and then there is a danger that α_g may become larger than the true optimum. When this occurs the numerical solution still converges but in an oscillatory manner. It is desirable to be near optimum value since the rate of convergence increases rapidly as α_g approaches α_{opt}. The advantages of the method are that it is easy to apply and takes a moderate amount of storage space.

A better method is due to Reid (82). The maximum eigenvalue, λ_{max}, is estimated from the ratio of the norms of the displacement vectors as in Carré's method. From this, a matrix of the form:

$$G_\lambda = \text{diag}(\lambda_{max}^{q_1/2}, \lambda_{max}^{q_2/2}, \ldots\ldots\ldots \lambda_{max}^{q_n/2}) \quad \text{I-60}$$

is constructed where $q_1, q_2 \ldots q_n$ are chosen from a set dictated by the matrix A. The eigenvectors are then estimated from

$$Z_i \cong G_\lambda^{-1}\,\delta^i \quad \text{I-61}$$

and they are used to form a Rayleigh quotient:

$$\phi = \frac{Z_i^T (L + L^T) Z_i}{Z_i^T D Z_i} \qquad \text{I-62}$$

The optimum relaxation factor is then calculated from:

$$\alpha_{opt} = \frac{2}{1 + (1 - \phi^2)^{1/2}} \qquad \text{I-63}$$

This method assures that α_{opt} will never become greater than the true optimum but suffers from the disadvantage that much more computation is required.

The choice of either Reid's or Carré's method depends on whether the matrix A is ill-conditioned or not, and its size. If the matrix is ill-conditioned Reid's method is better because it will not over-estimate the value of α_{opt}. When the matrix is large, Carré's method is better since it requires much less computation and storage space. The choice of Carré's method for large matrices is not automatic since, if the matrix is both large and ill-conditioned, Reid's method is recommended. Unfortunately, a large amount of computation is required to ascertain whether a large matrix is ill-conditioned.

In the present work Reid's method was used for a number of different sets of parameter values and the smallest α_{opt} found, $\alpha_{opt} = 1.4$, used in all subsequent computations.

I-4 COMPUTER PROGRAM

The following variables appear in the program.

A	array of coefficients for the finite difference equations
ALPHA	over-relaxation factor
B	array of coefficients for the finite difference equations
BRINK	a subroutine to compute the Brinkman number
C	array of coefficients for the finite difference equations
CRIT	criterion for exiting from the iteration loop
D	array of coefficients for the finite difference equations
DHT	mesh point
E	array of coefficients for the finite difference equations
ENT1, ENT2	euclidian norms of the temperature matrix
ENZ1, ENZ2	euclidian norms of the velocity matrix
F	array containing the viscosities at the mesh points
G	array of coefficients for the finite difference equations

GDOT	array of rates of deformation
H	distance between mesh points
HT	dimensionless height of fluid in the gap
IPRNTC	printing control variable
IPRNTR	printing control variable
ITNP	iteration counter
K	ratio of inner to outer cylinder radii
LINE	printing control variable
ND	number of mesh points
NS	number of mesh steps = ND-1
NPRNTC	printing control variable
NPRNTR	printing control variable
PI	3.141592
PRNT	subroutine to print results
R	outer cylinder radius
RGAM	tangential component of the rate of deformation
RI	inner cylinder radius
RPS	rotational speed of the inner cylinder
SHATE	subprogram to compute the rate of deformation
T	array containing the dimensionless temperatures at the mesh points
TAU	array containing the shear stresses at the mesh points
TC	array containing the thermal conductivities at the mesh points

TEMPRO	subprogram that solves the energy equation by the accelerated Gauss-Seidel method
TOW	wall temperature of the outer cylinder
TW	wall temperature of the inner cylinder
VELPRO	subprogram that solves the equation of motion by the accelerated Gauss-Seidel method
VISK	subprogram that computes the viscosity and thermal conductivity at each point
VTKR	tangential velocity at the inner cylinder wall
Z	array containing the dimensionless velocities of the mesh points
SGAM	array containing the z-component of the rate of deformation at the mesh points

```
                                                                                    29
0001              REAL K                                                            29
0002              COMMON Z(51,51), GDOT(51,51), T(51,51),  TC(51,51), F(51,51),     29
                 1 PHI(51), TAU(51,2), H, HT, R, RI, K, VTKR, RPS, TW, PI, CRIT,    29
                 2 ND, NS, LINE, NPRNTC, NPRNTR, IPRNTC, IPRNTR,TOW                 29
0003              DIMENSION DFL(51,51)
0004              DIMENSION STRES(51,51)
0005        321   FORMAT (1X,12(2X,E9.3))                                           29
0006        1000  FORMAT (7F10.4)                                                   29
0007        1001  FORMAT (5I5)                                                      29
0008        1002  FORMAT (1H1)                                                      29
0009        1003  FORMAT (1H )                                                      29
0010        1004  FORMAT (1H0)                                                      29
0011        1005  FORMAT (1H-)                                                      29
0012        1012  FORMAT (3X,'DIMENSIONLESS',6X,'DIMENSIONLESS VELOCITY V-THETA/V-TH 29
                 1ETA-RK AT DIMENSIONLESS RADIUS')                                  29
0013        1013  FORMAT (5X,'HEIGHT',8X,'R = ','0.0',6X,'0.1',6X,'0.2',6X,'0.3',6X, 29
                 1'0.4',6X,'0.5',6X,'0.6',6X,'0.7',6X,'0.8',6X,'0.9',6X,'1.0')      29
0014        1014  FORMAT (5X,F6.4,8X,11(2X,F7.4))
0015        1015  FORMAT (5X,F6.4,8X,11(2X,F7.3))                                   29
0016        1016  FORMAT (10X,'TO OBTAIN THE SHEAR RATE IN RECIPROCAL SECONDS MULTIP 29
                 1LY BY THE THE REVS/SEC')                                          29
0017        1017  FORMAT (3X,'DIMENSIONLESS',6X,'DIMENSIONLESS TEMPERATURE, T/TW AT 29
                 1DIMENSIONLESS RADIUS')                                            29
0018        1018  FORMAT (3X,'EUCLIDIAN NORMS FOR THE ERROR VECTORS ARE VEL1',E10.4, 29
                 1' VEL2',E10.4,' TEMP1',E10.4,' TEMP2',E10.4,' ITERATION NO. IS',I6 29
                 2)                                                                 29
0019        1020  FORMAT (3X,'DIMENSIONLESS',6X,'SHEAR RATE AT DIMENSIONLESS RADIUS'
                 1)
0020        1021  FORMAT (3X,'DIMENSIONLESS',6X,'SHEAR STRESS AT DIMENSIONLESS RADIU
                 1S')
0021        1022  FORMAT (10X,'TO OBTAIN THE SHEAR STRESS IN LBF/IN**2 MULTIPLY BY T
                 1HE REVS/SEC')                                                     29
0022        5     READ (5,1000) R,RI,HT,RPM,TW,TOW,CRIT                             29
0023              IF(R) 500,500,10                                                  29
0024        10    READ (5,1001) NS,NPRNTC,NPRNTR,IPRNTC,IPRNTR                      29
0025              ND = NS + 1                                                       29
0026              PI = 3.141592                                                     29
0027              RPS = RPM/60.                                                     29
0028              K = RI/R                                                          29
0029              VTKR = RI*2.*PI*RPS                                               29
0030              H = 1./NS
0031              ND1 = ND + 1
0032              DO 20 J=1,ND1
0033        20    PHT(J) = (J-1)*H                                                  29
0034              ITN = 0                                                           29
0035              WRITE (6,1002)
0036              ITNP = 0
0037              CALL PRNT
0038              CALL BRINK (TW,RPM,RI)
0039              WRITE (6,1002)                                                    29
            C                                                                       29
            C  BOUNDARY CONDITIONS FOR VELOCITY                                     29
            C                                                                       29
0040              Z(1,1) = 0.5
```

```
0041              DO 30 N =2,ND                                       29
0042              Z(N,1) = 0.0                                        29
0043              Z(1,N) = 1.0                                        29
0044        30    Z(ND,N) = 0.0                                       29
            C                                                         29
            C  INITIAL GUESSES FOR VELOCITY                           29
            C                                                         29
0045              NG = NS/5                                           29
0046              NG1 = NG + 1                                        29
0047              DO 40 N = 2,NG1                                     29
0048              DO 40 I = 2,ND
0049        40    Z(N,I) = 0.8                                        29
0050              NG2 = NG1 + NG                                      29
0051              N2 = NG1 + 1                                        29
0052              DO 46 N =N2,NG2
0053              DO 46 I = 2,ND
0054              N3 = NG2 + 1                                        29
0055        46    Z(N,I) = 0.6                                        29
0056              NG3 = NG2 + NG                                      29
0057              DO 51 N = N3,NG3                                    29
0058              DO 51 I = 2,ND
0059        51    Z(N,I) = 0.4                                        29
0060              NG4 = NG3 + NG                                      29
0061              N4 = NG3 + 1                                        29
0062              DO 56 N = N4,NG4                                    29
0063              DO 56 I = 2,ND
0064        56    Z(N,I) = 0.2                                        29
0065              N5 = NG4 + 1                                        29
0066              DO 61 N = N5,NS                                     29
0067              DO 61 I = 2,ND
0068        61    Z(N,I) = 0.0                                        29
            C                                                         29
            C BOUNDARY CONDITIONS AND INITIAL GUESSES FOR TEMPERATURE + SHEAR RATE   29
            C                                                         29
0069              DO 70 I=1,ND                                        29
0070              DO 70 J=1,ND                                        29
0071              T(I,J) = 1.0                                        29
0072        70    CDOT(I,J) = 100.                                    29
0073              DO 71 J=2,ND
0074              T(ND,J) = TOW/TW                                    29
0075              T(J,1) = T(ND,J)
0076        71    CONTINUE
0077              ENZ2 = 0.0                                          29
0078              ENZ1 = 0.0                                          29
0079              ENT1 = 0.0                                          29
0080              ENT2 = 0.0                                          29
0081              ITNP = 1
0082        74    ITN = ITN + 1                                       29
0083        75    DO 80 I=1,ND                                        29
0084              DO 80 J=1,ND                                        29
0085        80    DEL(I,J) = Z(I,J)                                   29
0086              CALL VISK                                           29
0087              CALL VELPRO                                         29
0088              CALL SHATL                                          29
```

```
                                                                   29
         SUMZ = 0.0                                                29
         DO 90 I=1,ND                                              29
         DO 90 J=1,ND                                              29
         TERMZ = (Z(I,J) - DEL(I,J))*(Z(I,J) - DEL(I,J))           29
   90    SUMZ = SUMZ + TERMZ                                       29
         ENZ1 = ENZ2                                               29
         ENZ2 = SQRT(SUMZ)                                         29
         DO 100 I=1,ND                                             29
         DO 100 J=1,ND                                             29
  100    DEL(I,J) = T(I,J)                                         29
         CALL TEMPRO                                               29
         SUMT = 0.0                                                29
         DO 110 I=1,ND                                             29
         DO 110 J=1,ND                                             29
         TERMT = (T(I,J) - DEL(I,J))*(T(I,J) - DEL(I,J))           29
  110    SUMT = SUMT + TERMT                                       29
         ENT1 = ENT2                                               29
         ENT2 = SQRT (SUMT)                                        29
         IF (ITN - 50) 120,120,115                                 29
  115    WRITE(6,1002)                                             29
         ITN = 0                                                   29
  120    WRITE(6,1018) ENZ1, ENZ2,ENT1,ENT2,ITNP
         ITNP = ITNP + 1                                           29
         IF(ENZ2/2. - CRIT) 125,125,74                             29
  125    IF(ENT2/2. - CRIT) 150,150,74                             29
  150    CALL PRNT                                                 29
         WRITE(6,1012)                                             29
         WRITE(6,1013)                                             29
         WRITE(6,1003)                                             29
         DO 155 J=1,ND,NPRNTR                                      29
         WRITE(6,1014) DHT(J), (Z(I,J),I=1,ND,NPRNTC)              29
         LINE = LINE + 1                                           29
         IF (LINE - 55) 155,155,154                                29
  154    CALL PRNT                                                 29
         WRITE (6,1012)                                            29
         WRITE(6,1013)                                             29
         WRITE(6,1003)                                             29
  155    CONTINUE                                                  29
  160    CALL PRNT                                                 29
         WRITE (6,1017)                                            29
         WRITE(6,1013)                                             29
         WRITE(6,1003)                                             29
         DO 165 J=1,ND,NPRNTR
         WRITE (6,1014) DHT(J), (T(I,J),I=1,ND,NPRNTC)             29
         LINE = LINE + 1                                           29
         IF (LINE - 55) 165,165,164                                29
  164    CALL PRNT                                                 29
         WRITE(6,1017)                                             29
         WRITE(6,1013)                                             29
         WRITE(6,1003)                                             29
  165    CONTINUE                                                  29
  170    CALL PRNT                                                 29
         WRITE (6,1016)                                            29
         WRITE(6,1004)
```

```
                                                                      29
0143           WRITE(6,1020)                                          29
0144           WRITE(6,1013)                                          29
0145           DO 175 J=1,ND,NPRNTR                                   29
0146           WRITE(6,1015) DHT(J), (GDOT(I,J),I=1,ND,NPRNTC)        29
0147           LINE = LINE + 1                                        29
0148           IF (LINE - 55) 175,175,174                             29
0149      174  CALL PRNT                                              29
0150           WRITE(6,1016)                                          29
0151           WRITE(6,1004)                                          29
0152           WRITE(6,1020)                                          29
0153           WRITE(6,1013)                                          29
0154      175  CONTINUE
          C
          C   SHEAR STRESS CALCULATION
          C
0155           DO 180 I=1,ND
0156           DO 180 J=1,ND
0157      180  STRES(I,J) = F(I,J)*GDOT(I,J)
          C
          C    SHEAR STRESS PRINTOUT
          C
0158      190  CALL PRNT
0159           WRITE (6,1022)
0160           WRITE (6,1004)
0161           WRITE (6,1021)
0162           WRITE (6,1013)
0163           DO 195 J=1,ND,NPRNTR
0164           WRITE (6,1014) DHT(J), (STRES(I,J),I=1,ND,NPRNTC)
0165           LINE = LINE + 1
0166           IF (LINE - 55) 195,195,194
0167      194  CALL PRNT
0168           WRITE (6,1022)
0169           WRITE (6,1004)
0170           WRITE (6,1021)
0171           WRITE (6,1013)
0172      195  CONTINUE                                               29
0173           GO TO 5                                                29
0174      500  STOP                                                   29
0175           END

  *OPTIONS IN EFFECT*  ID,EBCDIC,SOURCE,NOLIST,NODECK,LOAD,NOMAP
  *OPTIONS IN EFFECT*  NAME = MAIN    , LINECNT =       56
  *STATISTICS*    SOURCE STATEMENTS =      175,PROGRAM SIZE =    26184
  *STATISTICS*  NO DIAGNOSTICS GENERATED
```

```
                                                                                  29
0001              SUBROUTINE PRNT                                                 29
0002              REAL K                                                          29
0003              COMMON Z(51,51), GOOT(51,51), T(51,51),  TC(51,51), F(51,51),   29
                 1 PHT(51), TAU(51,2), H, HT, R, RI, K, VTKR, RPS, TW, PI, CRIT,  29
                 2 ND, NS, LINE, NFRNTC, NPRNTR, IPRNTC, IPRNTR,TOW               29
0004              RPM = RPS*60.0                                                  29
0005      1002    FORMAT (1H1)                                                    29
0006      1003    FORMAT (1H )                                                    29
0007      1004    FORMAT (1H0)                                                    29
0008      1005    FORMAT (1H-)                                                    29
0009      1006    FORMAT (10X,'THE NUMBER OF DISTANCE STEPS IS ',I5)              29
0010      1007    FORMAT (10X,'THE INNER CYLINDER RADIUS IS  ',F6.3,' INCHES')    29
0011      1008    FORMAT (1H+,T70,'THE OUTER CYLINDER RADIUS IS  ',F6.3,' INCHES')  29
0012      1009    FORMAT (10X,'THE GAP HEIGHT IS  ',F6.3,' INCHES')               29
0013      1010    FORMAT (1H+,T70,'CYLINDER RPM IS  ',F5.1)
0014      1011    FORMAT (10X,'THE INNER WALL TEMPERATURE, TW, IS  ',F6.1,' DEGREES
                 1F.')
0015      1012    FORMAT (1H+,T70,'THE OUTER WALL TEMPERATURE, TOW, IS  ',F6.1,' DEG
                 1REES F.')                                                       29
0016      1019    FORMAT (1H+,T70,'CONVERGENCE CRITERION SET AT CRIT = ',F8.6)    29
0017              WRITE (6,1002)                                                  29
0018              WRITE(6,1004)                                                   29
0019              WRITE(6,1005)                                                   29
0020              WRITE(6,1006) NS                                                29
0021              WRITE(6,1019) CRIT                                              29
0022              WRITE(6,1004)                                                   29
0023              WRITE(6,1007) RI                                                29
0024              WRITE(6,1008) R                                                 29
0025              WRITE(6,1004)                                                   29
0026              WRITE(6,1009) HT                                                29
0027              WRITE(6,1010) RPM                                               29
0028              WRITE(6,1004)                                                   29
0029              WRITE(6,1011) TW
0030              WRITE (6,1012) TOW                                              29
0031              WRITE(6,1005)                                                   29
0032              WRITE(6,1003)                                                   29
0033              LINE = 17                                                       29
0034              RETURN                                                          29
0035              END

*OPTIONS IN EFFECT*  ID,EBCDIC,SOURCE,NOLIST,NODECK,LOAD,NOMAP
*OPTIONS IN EFFECT*  NAME = PRNT     , LINECNT =        56
*STATISTICS*    SOURCE STATEMENTS =         35,PROGRAM SIZE =      1096
*STATISTICS*  NO DIAGNOSTICS GENERATED
```

FORTRAN IV G LEVEL 20 VELPRO DATE = 71335 12/38/15 PAGE 0001

```
      SUBROUTINE VELPRO
      REAL K
      COMMON Z(51,51), GDOT(51,51), T(51,51),  TC(51,51), F(51,51),
     1 DHT(51), TAU(51,2), H, HT, R, RI, K, VTKR, RPS, TW, PI, CRIT,
     2 ND, NS, LINE, NPRNTC, NPRNTR, IPRNTC, IPRNTR,TOW
      DIMENSION A(51,51),B(51,51),C(51,51),D(51,51),E(51,51)
  321 FORMAT (1X,12(2X,F9.3))
      ALPHA = 1.4
   40 DO 50 I=2,NS
      DO 50 J=2,ND
      E(I,J) = (F(I+1,J)-F(I-1,J))/(2.*H*R*(1.-K))+F(I,J)/(H*(I-1)*R*(1.
     1 - K) + K*R)
   50 A(I,J) = 2.*F(I,J)*(1./(H*H*HT*HT) + 1./(R*R*(1.-K)*(1.-K)*H*H))
     1 + E(I,J)/(H*(I-1)*R*(1.-K) + K*R)
      DO 60 I=2,NS
      DO 60 J= 2,NS
      B(I,J) = (F(I,J+1)+4.*F(I,J)-F(I,J-1))/(4.*H*H*HT*HT)
   60 C(I,J) = (F(I,J-1)+4.*F(I,J)-F(I,J+1))/(4.*H*H*HT*HT)
      DO 70 I = 2,NS
      DO 70 J = 2,ND
      D(I,J) = F(I,J)/(R*R*(1.-K)*(1.-K)*H*H) + E(I,J)/(R*(1.-K)*2.*H)
   70 E(I,J) = F(I,J)/(R*R*(1.-K)*(1.-K)*H*H) - E(I,J)/(R*(1.-K)*2.*H)
   75 DELK = 0.0
      DO 80 I = 2,NS
      DO 80 J = 2,NS
      TZ = Z(I,J)
      Z(I,J) = Z(I,J)*(1.-ALPHA)+ALPHA*(B(I,J)*Z(I,J+1)+C(I,J)*Z(I,J-1)+
     1D(I,J)*Z(I+1,J)+E(I,J)*Z(I-1,J))/A(I,J)
      DZ = Z(I,J)-TZ
      IF (ABS(DELK)-ABS(DZ)) 79,80,80
   79 DELK = DZ
   80 CONTINUE
      DO 90 I = 2,NS
      TZ = Z(I,ND)
      B(I,ND) = 2.*F(I,ND)/(H*H*HT*HT)
      Z(I,ND) = Z(I,ND)*(1.-ALPHA) + ALPHA*(D(I,ND)*Z(I+1,ND) + B(I,ND)*
     1 Z(I,NS) + E(I,ND)*Z(I-1,ND))/A(I,ND)
      DZ = ABS(Z(I,ND) - TZ)
      IF(ABS(DELK) - DZ) 89,90,90
   89 DELK = DZ
   90 CONTINUE
      ERRZ = DELK*(ALPHA - 1.)/(2. - ALPHA)
      IF(CRIT - ERRZ) 40,100,100
  100 IF (IPRNTC) 101,110,101
  101 CONTINUE
      WRITE (6,321) (DHT(J),( A(I,J),I=1,ND),J=1,ND)
      WRITE (6,321) (DHT(J),( B(I,J),I=1,ND),J=1,ND)
      WRITE (6,321) (DHT(J),( C(I,J),I=1,ND),J=1,ND)
      WRITE (6,321) (DHT(J),( D(I,J),I=1,ND),J=1,ND)
      WRITE (6,321) (DHT(J),( E(I,J),I=1,ND),J=1,ND)
      WRITE (6,321) (DHT(J),( F(I,J),I=1,ND),J=1,ND)
      WRITE (6,321) (DHT(J),( Z(I,J),I=1,ND),J=1,ND)
  110 RETURN
      END
```

```
0001            SUBROUTINE VISK
          C     THIS SUBROUTINE FOR VISCOSITY AND THERMAL CONDUCTIVITY OF
          C     POLYETHYLENE GLYCOL  PEG 6000
0002            REAL K, LGN                                                   2
0003            COMMON Z(51,51), GOPT(51,51), T(51,51),  TC(51,51), F(51,51),
               1 DHT(51), TAU(51,2), H, HT, R, RI, K, VTKR, RPS, TW, PI, CRIT,
               2 ND, NS, LINE, NPRNTC, NPRNTR, IPRNTC, IPRNTR,TOW
0004      321   FORMAT (1X,12(2X,E9.3))
0005            DO 40 I=1,NS
0006            J=1
0007            F(I,J) = 1./(T(I,J)*TW + 459.0)
0008            IF (F(I,J) - 1.635E-3) 35,36,37
0009      35    SLP = 2.52E+3
0010            GO TO 38
0011      36    F(I,J) = 0.0742
0012            GO TO 40
0013      37    SLP = 3.90E+3
0014      38    LGN =-SLP*(1.635E-3 - F(I,J)) - 1.130
0015            F(I,J) = EXP(2.303*LGN)/144.0
0016      40    CONTINUE
0017            DO 50 I=1,ND
0018            DO 50 J=2,ND
0019            F(I,J) = 1./(T(I,J)*TW + 459.0)
0020            IF (F(I,J) - 1.635E-3) 45,46,47
0021      45    SLP = 2.52E+3
0022            GO TO 48
0023      46    F(I,J) = 0.0742/144.0
0024            GO TO 50
0025      47    SLP = 3.90E+3
0026      48    LGN =-SLP*(1.635E-3 - F(I,J)) - 1.130
0027            F(I,J) = EXP(2.303*LGN)/144.0
0028      50    TC(I,J) = 0.024
0029            DO 60 I=1,ND
0030            J = 1
0031      60    TC(I,J) = 0.024
0032            RETURN
0033            END

*OPTIONS IN EFFECT*  ID,EBCDIC,SOURCE,NOLIST,NODECK,LOAD,NOMAP
*OPTIONS IN EFFECT*  NAME = VISK    , LINECNT =       56
*STATISTICS*    SOURCE STATEMENTS =         33,PROGRAM SIZE =       1094
*STATISTICS*  NO DIAGNOSTICS GENERATED
```

```
                                                                                        29
0001              SUBROUTINE TEMPRO                                                     29
0002              REAL K                                                                29
0003              COMMON Z(51,51), GDOT(51,51), T(51,51),  TC(51,51), F(51,51),         29
                 1 DHT(51), TAU(51,2), H, HT, R, RI, K, VTKR, RPS, TW, PI, CRIT,        29
                 2 ND, NS, LINE, NPRNTC, NPRNTR, IPRNTC, IPRNTR,TDW                     29
0004              DIMENSION A(51,51), B(51,51), C(51,51),  D(51,51), E(51,51), G(51,    29
                 151)
0005       321    FORMAT (1X,12(2X,F9.3))                                               29
0006              TWR = TW/(4.*R*R*(1.-K)*(1.-K)*H*H)
0007              ALPHA = 1.4                                                           29
0008              DO 40 I=2,NS                                                          29
0009              DO 40 J=2,ND                                                          29
0010              D(I,J) = TW*TC(I,J)/(HT*HT*H*H)                                       29
0011              E(I,J) = TW*TC(I,J)/(R*R*(1.-K)*(1.-K)*H*H)                           29
0012       40     A(I,J) = 2.*(D(I,J) + E(I,J))                                         29
0013              DO 50 I=2,NS                                                          29
0014              DO 50 J=2,NS                                                          29
0015              C(I,J) = TW*(TC(I,J+1) - TC(I,J-1))/(4.*HT*HT*H*H)                    29
0016              B(I,J) = D(I,J) + C(I,J)                                              29
0017       50     C(I,J) = D(I,J) - C(I,J) .                                            29
0018              DO 60 I=2,NS                                                          29
0019              DO 60 J=2,ND                                                          29
0020              G(I,J) = TC(I,J)*TW/(R*(1.-K)*(H*(I-1)*R*(1.-K) +K*R)*2.*H)           29
0021              D(I,J) = E(I,J) + TWR*(TC(I+1,J) - TC(I-1,J)) + G(I,J)                29
0022       60     E(I,J) = E(I,J) - TWR*(TC(I+1,J) - TC(I-1,J)) - G(I,J)                29
0023              DO 70 I=2,NS                                                          29
0024              DO 70 J=2,NS                                                          29
0025       70     G(I,J) = F(I,J)*((H*(I-1)*R*(1.-K) + K*R)*(VTKR*(Z(I+1,J) -           29
                 1 Z(I-1,J))/((H*(I-1)*R*(1.-K) + K*R)*R*(1.-K)*2.*H) - VTKR*Z(I,J)     29
                 2 /((H*(I-1)*R*(1.-K) + K*R)**2)))**2 + F(I,J)*(VTKR*(Z(I+1,J) -       29
                 3 Z(I-1,J))/(2.*HT*H))**2
0026              DO 74 I=2,NS                                                          29
0027              B(I,ND) = 2.*TW*TC(I,ND)/(H*H*HT*HT)                                  29
0028       74     G(I,ND) = F(I,ND)*((H*(I-1)*R*(1.-K) + K*R)*(VTKR*(Z(I+1,ND) -        29
                 1 Z(I-1,ND))/((H*(I-1)*R*(1.-K) + K*R)*R*(1.-K)*2.*H) - VTKR*          29
                 2 Z(I,ND)/((H*(I-1)*R*(1.-K) + K*R)**2)))**2                           29
0029       75     DELT = 0.0                                                            29
0030              DO 80 I=2,NS                                                          29
0031              DO 80 J=2,NS                                                          29
0032              TT = T(I,J)                                                           29
0033              T(I,J) = T(I,J)*(1.-ALPHA) + ALPHA*(B(I,J)*T(I,J+1) + C(I,J)*         29
                 1T(I,J-1) + D(I,J)*T(I+1,J) + E(I,J)*T(I-1,J) + G(I,J))/A(I,J)         29
0034              DT = ABS(T(I,J) - TT)                                                 29
0035              IF(ABS(DELT) - DT) 79,80,80                                           29
0036       79     DELT = DT                                                             29
0037       80     CONTINUE                                                              29
0038              DO 90 I=2,NS                                                          29
0039              TT = T(I,ND)                                                          29
0040              T(I,ND) = T(I,ND)*(1.-ALPHA) + ALPHA*(B(I,ND)*T(I,NS) + D(I,ND)*      29
                 1 T(I+1,ND) + E(I,ND)*T(I-1,ND) + G(I,ND))/(A(I,ND))                   29
0041              DT = ABS(Z(I,ND) - TT)                                                29
0042              IF(ABS(DELT - DT)) 89,90,90                                           29
0043       89     DELT = DT                                                             29
0044       90     CONTINUE
```

```
FORTRAN IV G LEVEL  20                  TEMPRO              DATE = 71335          12/38/15            PAGE 0002
                                                                                              29
 0045                ERRT = DELT*(ALPHA - 1.)/(2. - ALPHA)                                     29
 0046                IF(CRIT - ERRT) 75,100,100                                                29
 0047         100    IF (IPRNTC) 101,110,101                                                   29
 0048         101    CONTINUE                                                                  29
 0049                WRITE (6,321) (DHT(J), ( A(I,J),I=1,ND),J=1,ND)                          29
 0050                WRITE (6,321) (DHT(J), ( B(I,J),I=1,ND),J=1,ND)                          29
 0051                WRITE (6,321) (DHT(J), ( C(I,J),I=1,ND),J=1,ND)                          29
 0052                WRITE (6,321) (DHT(J), ( D(I,J),I=1,ND),J=1,ND)                          29
 0053                WRITE (6,321) (DHT(J), ( E(I,J),I=1,ND),J=1,ND)                          29
 0054                WRITE (6,321) (DHT(J), ( F(I,J),I=1,ND),J=1,ND)                          29
 0055                WRITE (6,321) (DHT(J), ( G(I,J),I=1,ND),J=1,ND)                          29
 0056                WRITE (6,321) (DHT(J), (TC(I,J),I=1,ND),J=1,ND)                          29
 0057                WRITE (6,321) (DHT(J), ( T(I,J),I=1,ND),J=1,ND)                          29
 0058         110    RETURN                                                                    29
 0059                END
```

```
FORTRAN IV G LEVEL  20                  VISKR               DATE = 71335          12/38/15            PAGE 0001

 0001                SUBROUTINE VISKR(GDOTR,TW,V,TC)
 0002                DIMENSION GDOT(1,1)
 0003                DIMENSION F(1,1)
 0004                J = 1
 0005                I = 1
 0006                GDOT(I,J) = GDOTR
 0007                 F(I,J) = (TW - 32.0)*5./9.
 0008                F(I,J) = 10.**((-3.5613 + 2.8193E-2*F(I,J) -8.7673E-5*F(I,J)**2)
                    1  + (8.250E-1 +1.1670E-2*F(I,J) -1.5085E-4*F(I,J)**2 +3.9453E-7
                    2   *F(I,J)**3)*(ALOG10(GDOT(I,J))) + (-9.9160E-1 +8.1741E-3*F(I,J)
                    3  -1.9181E-5*F(I,J)**2)*(ALOG10(GDOT(I,J)))**2)
 0009                V = F(I,J)
 0010                TC = 0.0516 - 2.7E-5*TW
 0011                RETURN
 0012                END

 *OPTIONS IN EFFECT*  ID,EBCDIC,SOURCE,NOLIST,NODECK,LOAD,NOMAP
 *OPTIONS IN EFFECT*  NAME = VISKR    , LINECNT =       56
 *STATISTICS*    SOURCE STATEMENTS =          12,PROGRAM SIZE =        932
 *STATISTICS*  NO DIAGNOSTICS GENERATED

 *STATISTICS*  NO DIAGNOSTICS THIS STEP 0
```

```
FORTRAN IV G LEVEL  20                    SHATE                 DATE = 71335          12/38/15              PAGE 0001

 0001                 SUBROUTINE SHATE                                                                      29
 0002                 REAL K                                                                                29
 0003                 COMMON Z(51,51), GDOT(51,51), T(51,51),  TC(51,51), F(51,51),                         29
                     1 DHT(51), TAU(51,2), H, HT, R, RI, K, VTKR, RPS, TW, PI, CRIT,                        29
                     2 ND, NS, LINE, NPRNTC, NPRNTR, IPRNTC, IPRNTR,TOW                                     29
 0004                 DIMENSION RGAM(51,51), ZGAM(51,51)                                                    29
 0005         321     FORMAT (1X,12(2X,E9.3))                                                               29
 0006                 DO 10 I=2,NS                                                                          29
 0007                 DO 10 J=2,NS                                                                          29
 0008                 RGAM(I,J) = 2.*PI*((K*(Z(I+1,J) - Z(I-1,J))/(2.*H*(1.-K))) -                         29
                     1 (K*Z(I,J)/(H*(I-1)*(1.-K) + K)))*RPS                                                 29
 0009                 ZGAM(I,J) = 2.*PI*RI*(Z(I,J+1) - Z(I,J-1))/(2.*HT*H)                                 29
 0010          10     GDOT(I,J) =  SQRT(RGAM(I,J)*RGAM(I,J) + ZGAM(I,J)*ZGAM(I,J))                         29
 0011                 DO 20 J=1,ND
 0012                 RGAM(1,J) = 2.*PI*((K*(Z(2,J) - Z(1,J))/(H*(1.-K)))
                     1 -  (K*Z(1,J)/(0.*(1.-K) + K)))*RPS
 0013                 GDOT(1,J) = ABS(RGAM(1,J))                                                            29
 0014          20     ZGAM(1,J) = 0.0                                                                       29
 0015                 DO 30 I=2,NS                                                                          29
 0016                 RGAM(I,ND) = 2.*PI*((K*(Z(I+1,ND) - Z(I-1,ND))/(H*2.*(1-K)))                         29
                     1 - (K*Z(I,ND)/(H*(I-1)*(1.-K) + K)))*RPS                                              29
 0017                 ZGAM(I,ND) = 2.*PI*RI*(Z(I,ND) - Z(I,NS))/(HT*H)                                     29
 0018          30     GDOT(I,ND) = SQRT(RGAM(I,ND)*RGAM(I,ND) + ZGAM(I,ND)*ZGAM(I,ND))                     29
 0019                 DO 40 J=2,ND                                                                          29
 0020                     RGAM(ND,J) = 2.*PI*((K*(Z(ND,J) - Z(NS,J))/(H*(1.-K)))                            29
                     1 - (K*Z(ND,J)/(H*ND*(1.-K) + K)))*RPS
 0021                 ZGAM(ND,J) = 0.0                                                                      29
 0022          40     GDOT(ND,J) = ABS(RGAM(ND,J))                                                          29
 0023                 DO 50 I=2,NS                                                                          29
 0024                 RGAM(I,1) = 0.0                                                                       29
 0025                 ZGAM(I,1) = 2.*PI*RI*Z(I,2)/(HT*H)                                                    29
 0026          50     GDOT(I,1) = ABS(ZGAM(I,1))                                                            29
 0027                 GDOT(ND,1) = 0.0                                                                      29
 0028                 RETURN                                                                                29
 0029                 END

  *OPTIONS IN EFFECT*  ID,EBCDIC,SOURCE,NOLIST,NODECK,LOAD,NOMAP
  *OPTIONS IN EFFECT*  NAME = SHATE    , LINECNT =       56
  *STATISTICS*    SOURCE STATEMENTS =       29,PROGRAM SIZE =     22786
  *STATISTICS*  NO DIAGNOSTICS GENERATED
```

APPENDIX II

EXPERIMENTS WITH POLYETHYLENE

The initial trials of the concentric cylinder apparatus were made with a linear, high density polyethylene (Sclair 8107, DuPont of Canada, Sarnia). The flow characteristics of the polymer, shown in Figure II-1, were determined by an Instron Capillary Rheometer. A primary reason for choosing this material was that it was available in powder form. This minimized loading problems, particularly air inclusion, that occurred with pelletized polymers.

These preliminary runs showed that shortly after starting, the surface of the polymer melt was no longer planar but had developed a wavelike appearance. It could be seen, at low speeds, that the crest of this "wave" travelled with the same approximate velocity as the inner cylinder.

Following the crest was a trough that was not quite 180° behind the crest. As the run progressed the wave became more pronounced and, after about seven minutes had elapsed, the polymer coinciding with the trough was noticed to have stopped shearing. Thereafter the non-sheared portion grew until finally only an arc of about 20° of the circumference showed evidence of shear. The sequence of events is illustrated in figure II-2. Throughout the run no evidence of the "Weissenberg effect" could be detected visually.

FIGURE II-1: $\log_{10}$ Viscosity Versus $\log_{10}$ Shear Rate for the Polyethylene Used.[10] The Data was Obtained from a Capillary Rheometer

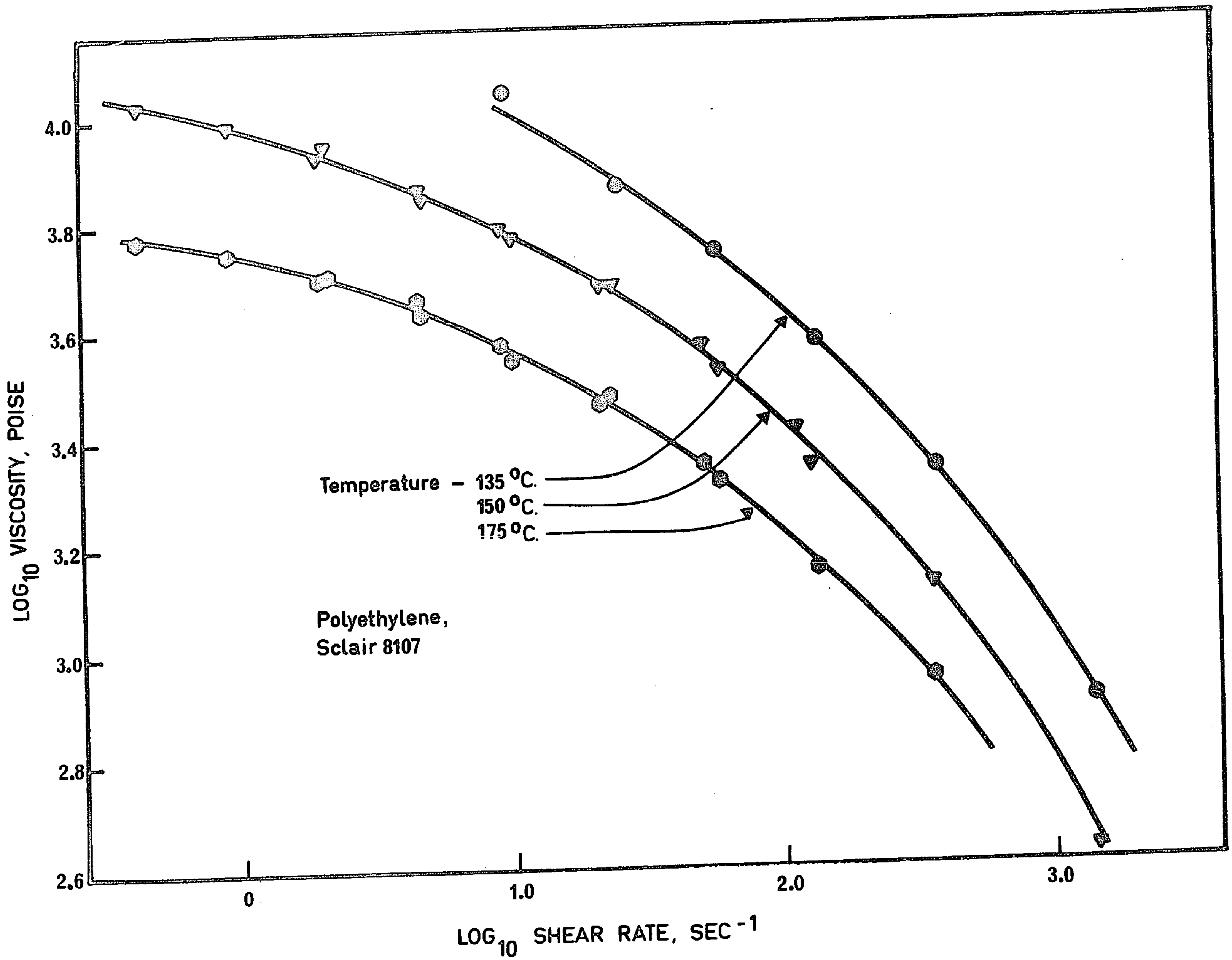
4.0
3.8
3.6
3.4
3.2
3.0
2.8
2.6
LOG10 VISCOSITY, POISE
0
1.0
2.0
3.0
LOG10 SHEAR RATE, SEC -1
Temperature – 135 °C.
150 °C.
175 °C.
Polyethylene,
Sclair 8107

FIGURE II-2: The Progressive Loss of Shearing of the Melt Encountered During the Runs with Polyethylene is Illustrated in This Sequence of Sketches

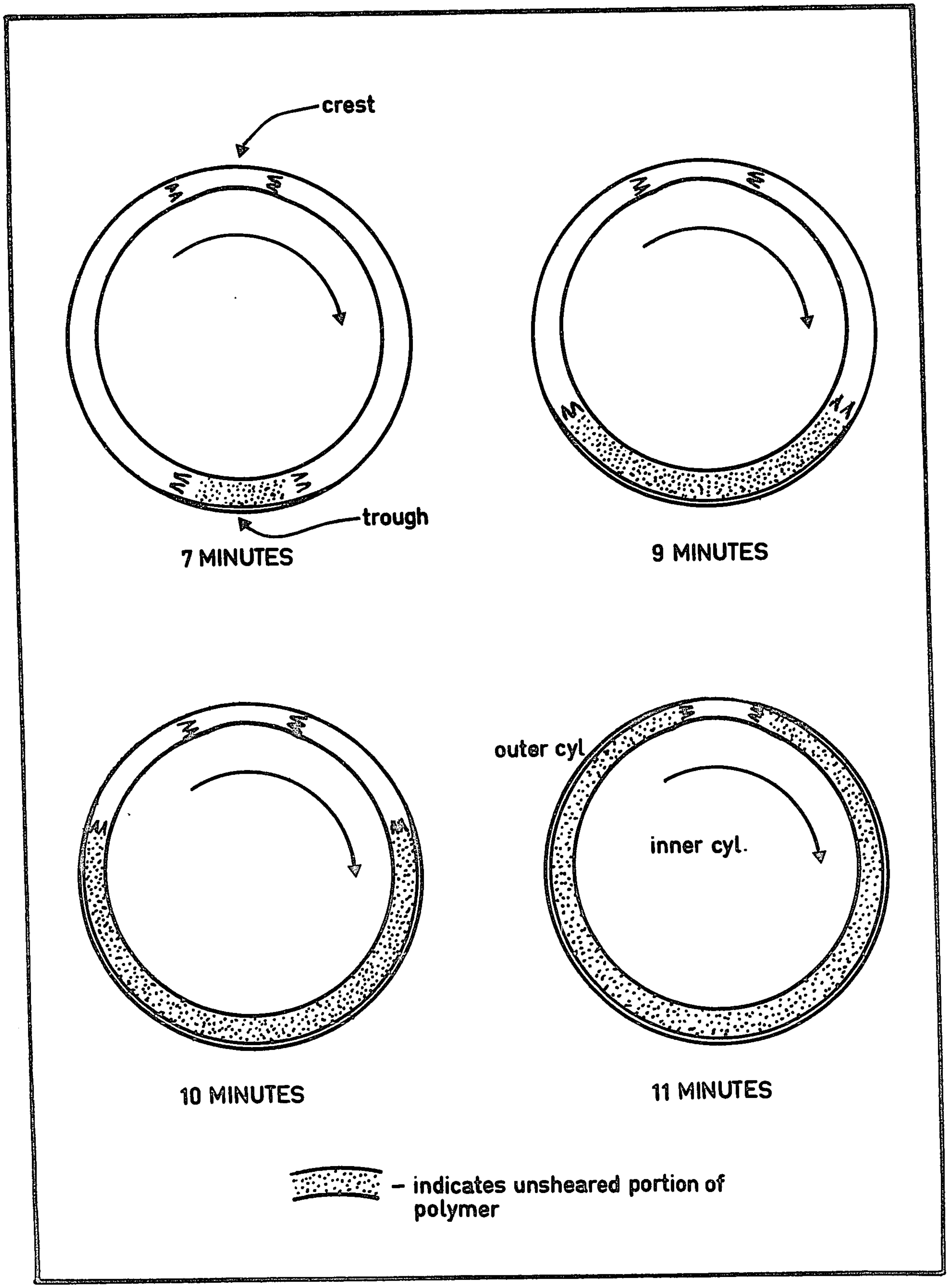
crest
trough
7 MINUTES
9 MINUTES
outer cyl
inner cyl.
10 MINUTES
11 MINUTES
- indicates unsheared portion of polymer

A number of runs were made at different temperatures and inner cylinder speeds. It was found that only at the highest temperatures (about 425°F and above) and the lowest RPMs (less than 15 RPM) could continuous shearing conditions be maintained throughout the gap. Even these runs developed the wavelike appearance, arousing the suspicion that cylindrical Couette flow was not obtained. The effect was dependent on temperature and rotational speed. Low temperatures (ie. high melt viscosities) and high speeds produced the effects in less time after startup.

It was suspected that lack of concentricity of the cylinders might be the cause of the "instability". The two cylinders were carefully adjusted for the best possible concentricity at 400°F. The apparatus was at this temperature for six hours before the adjustment was made to allow temperature equilibrium to be reached. After adjustment the apparatus was not allowed to cool, but was filled with polymer and the run made at the same temperature. Continuous shear operation was possible up to approximately 30 RPM. Beyond that speed, varying amounts of unsheared arc appeared, depending on the speed. As before, the wavelike surface was noticed, but diminished in magnitude.

The apparatus was then, disassembled and cleaned, and the inner cylinder was checked for roundness. It was found that the deviation from roundness was primarily a high spot on the inner cylinder that corresponded roughly with the location of the wave crest. A superficial explanation would be that the high spot on the inner cylinder was acting like a hole on the inner cylinder and because of the free surface the polymer deformed in the vertical direction. When it had been deformed it did not flow back immediately when the lobe had passed because of the very high melt viscosity. Obviously, either efforts could be made to reduce out-of-roundness and eccentricity to a negligible level (such that the problem would not occur) or the free surface could be eliminated. Since the sum of roundness errors and eccentricity was on the order of 10^{-3} inches in an apparatus whose basic dimension (diameter) was approximately 6 inches reducing these further would be costly and difficult.

The alternative of eliminating the free surface was explored. After numerous unsuccessful attempts, the following device was evolved to close the gap and eliminate the free surface. The seal was made from a one-eighth inch thick strip of polytetrafluorethylene (PTFE) of a length equal to the gap circumference. The edge of the strip inserted into the gap had a fishtail slot milled into it. A steel support ring was fitted over the edge strip that extended out of the gap. The supporting ring had three pivoted bars attached to it that were secured to other pivots attached to the outer cylinder. The drag exerted on the seal caused it to rotate a small amount, and this rotation, in turn, forced the seal down further into the gap exerting a moderate pressure on the melt. The pressure caused the milled slot to open, effecting the seal with the cylinder walls. The apparatus was operated for periods of an hour or more without any leakage. Monitoring the driving motor torque by observing the armature current, gave evidence that there was no loss of shearing as was previously observed.

An immediate consequence of the use of the sealing ring was that an additional end effect was introduced. This meant that the region of uniform shear would be smaller than planned. Although the sealing ring solved one flow problem a second difficulty was discovered. This is described in the next section.

II-2 TEMPERATURE PROFILES

The equations of motion and energy were written for the apparatus and solved numerically (see Appendix I). The viscosity was allowed to be a function of: shear rate and temperature, and thermal conductivity was a function of temperature. To test the validity of the solutions it had been planned to determine velocity profiles using tracer particles. With the addition of the upper sealing ring this scheme was no longer feasible. However, because the equations of energy and motion are coupled through the viscosity, it is possible to compare theoretical and experimental temperature profiles and from this, infer the correctness of the velocity profile.

The Tempil Corporation markets a range of temperature sensitive products in the form of pellets and sticks. These materials are crystalline waxes with sharply defined (± 2°F) melting points and are colour coded as to temperature. A number of different melting point waxes in the range of interest were procured and their melting points verified. The pellets were ground to a powder and tumble blended with the polyethylene powder. The concentration used was about 1% by volume.

Attempts to determine the temperature profile by using a number of these waxes simultaneously in the polyethylene were not successful due to diffusion of the dyes in the waxes into the mixture. Accordingly, a blend of a single wax and the polymer was made and used. Conditions for the run were:

RPM = 40

inner wall temperature = 325°F initially

outer wall temperature = 320°F initially

depth of polymer in gap, H = 2.1 inches

wax melting point = 350°F

Five minutes after the run commenced the inner and outer wall temperatures had risen to 335^{o}F and 330^{o}F, respectively. These temperatures did not change appreciably in the next six minutes and at the end of this time the apparatus was stopped and cooled to room temperature. After sectioning, the microscope revealed the pattern reproduced in figure II-3. In the outside cool area, the particles were sharp and angular showing no evidence of melting. In the central portion of the cross-section no particles could be found. At the interface of the particle-containing and particle-free areas the particles appeared rounded and smooth. The demarcation between the two areas was sharp and well-defined. Further, the rounded smooth particles showing evidence of melting were contained in a narrow band of about two particle diameters in width (approx: .004 inches).

Unfortunately, although the method seemed satisfactory, there was indication of "secondary" flows in the apparatus. The existance of a circulatory flow superimposed on the main Couette flow and originating at each end of the gap was indicated by the pattern of unmelted particles.

It is hypothesized that this circulatory flow is caused by the normal stress differences originating in the viscoelasticity of the melt. The shear rate in the two corners where the moving wall meets the seals is high and can conceivably

FIGURE II-3: The Distribution of the Unmelted Wax Particles in a Cross-Section of the Polyethylene.

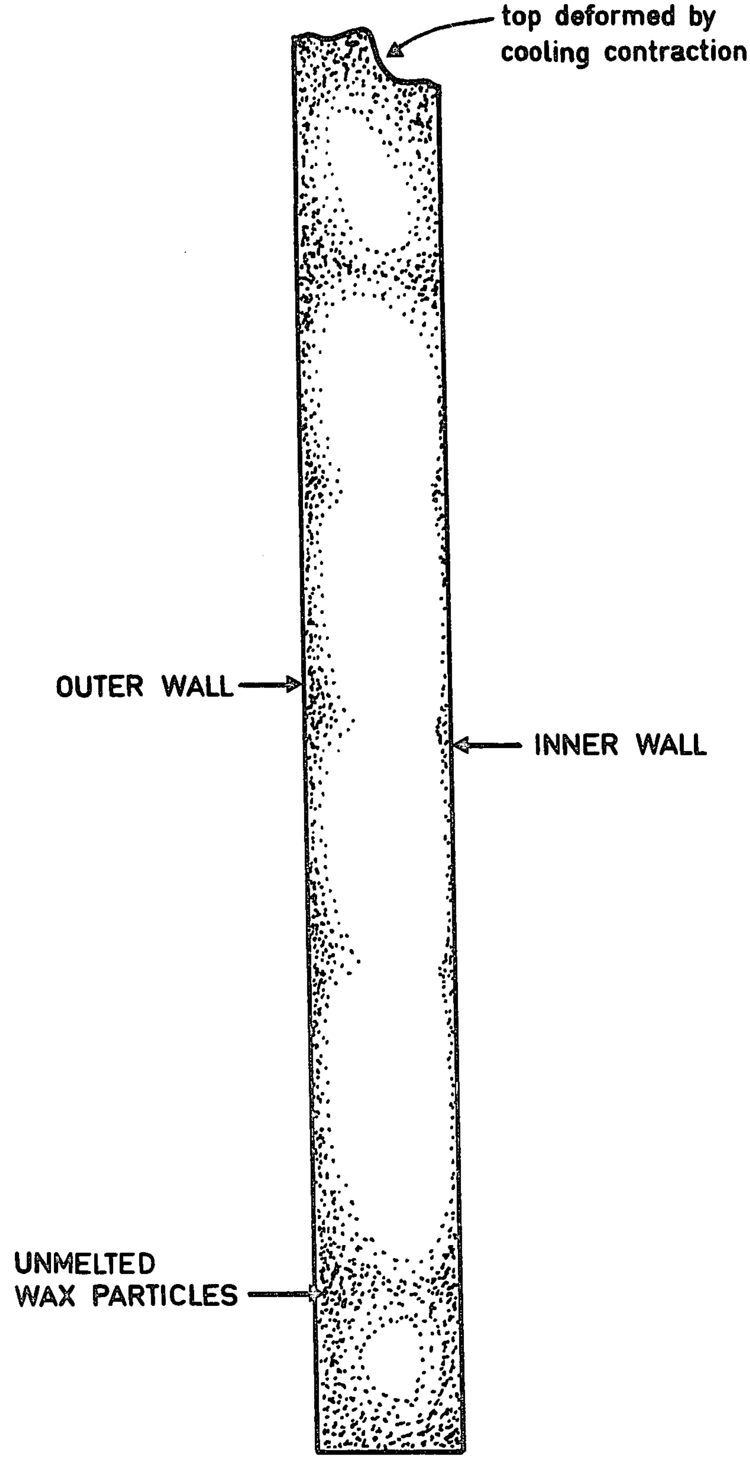

top deformed by
cooling contraction
OUTER WALL
INNER WALL
UNMELTED
WAX PARTICLES

generate appreciable normal stress differences. Further, the shear rate gradient is large in these corners. This flow is not predicted by the numerical solution because the constitutive equation used for the fluid does not allow for the viscoelastic nature of the polyethylene melt. This flow may be of a similar nature to that observed by Ginn and Denn for viscoelastic fluids (83,84).

APPENDIX III

DETERMINATION OF THE PROPERTIES OF POLYETHYLENE GLYCOL

III-1 VISCOSITY

The viscosity of the polyethylene glycol used was determined with three viscometers: a Brookfield Viscometer, model with temperature controlled cup and bob accessory and the Ferranti-Shirley and Rheometics Mechanical Spectrometer cone and plate instruments. The latter two viscometers were used in the steady shear mode of operation. The viscosity was measured from shear rates of 1 sec^{-1} to 270 sec^{-1} and was found to be constant over this range. The viscosity change with temperature was also measured and found to follow an Arrhenius relationship. The results are shown in figure III-1. The Mechanical Spectrometer was also used to estimate the normal stress difference for polyethylene glycol. No normal stress difference was observed within the sensitivity limit of the instrument, which is about 2×10^4 dynes/cm^2.

III-2 THERMAL CONDUCTIVITY

In addition to viscosity, it was necessary to know the thermal conductivity for the purposes of solving the energy equation. There are only limited measurements of the thermal

FIGURE III-1: Viscosity Versus the Reciprocal of Temperature for the Polyethylene Glycol Used in This Work

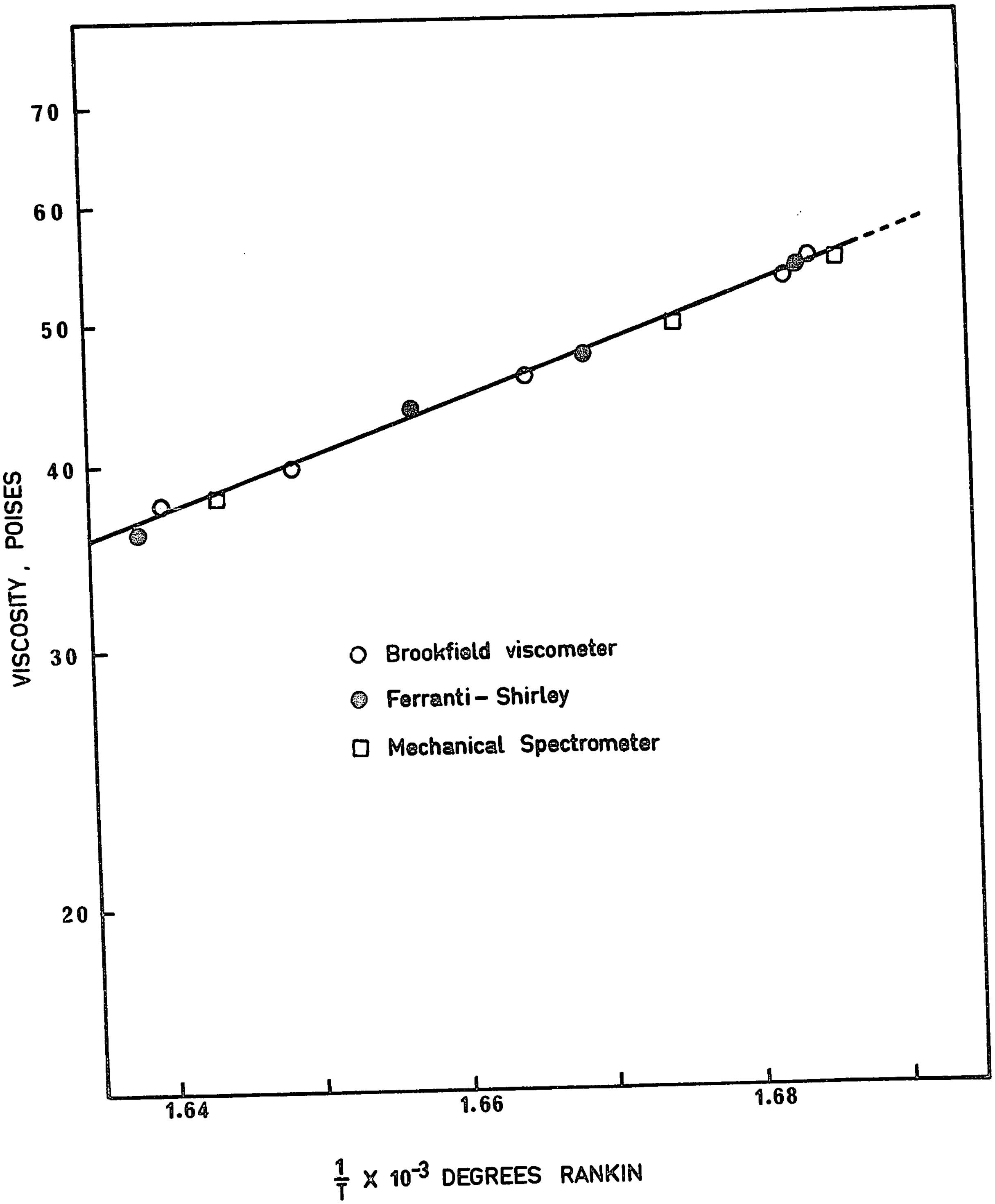
70
60
50
40
30
20
VISCOSITY, POISES
Brookfield viscometer
Ferranti – Shirley
Mechanical Spectrometer
1.64
1.66
1.68
1/T X 10^-3 DEGREES RANKIN

conductivity of polymer melts reported in literature. Lohe (85) has measured the thermal conductivity of polyethylene glycol as a function of temperature and degree of polymerization (molecular weight). Since the molecular weight of the material used in this work was not known accurately, and an apparatus to measure thermal diffusivity was available, it was decided to determine the thermal properties experimentally. The apparatus and method used closely followed that of Shoulberg (86).

The melt density was found by standard pycnometer techniques and the specific heat data were provided by the manufacturer. The thermal conductivity was then calculated from:

$$\kappa = \alpha \rho C_p \qquad \text{III-1}$$

where

κ = thermal conductivity

α = thermal diffusivity

ρ = density

C_p = specific heat at constant pressure

The experimental results are shown in figure III-2.

FIGURE III-2: Thermal Conductivity Versus Temperature for Polyethylene Glycol

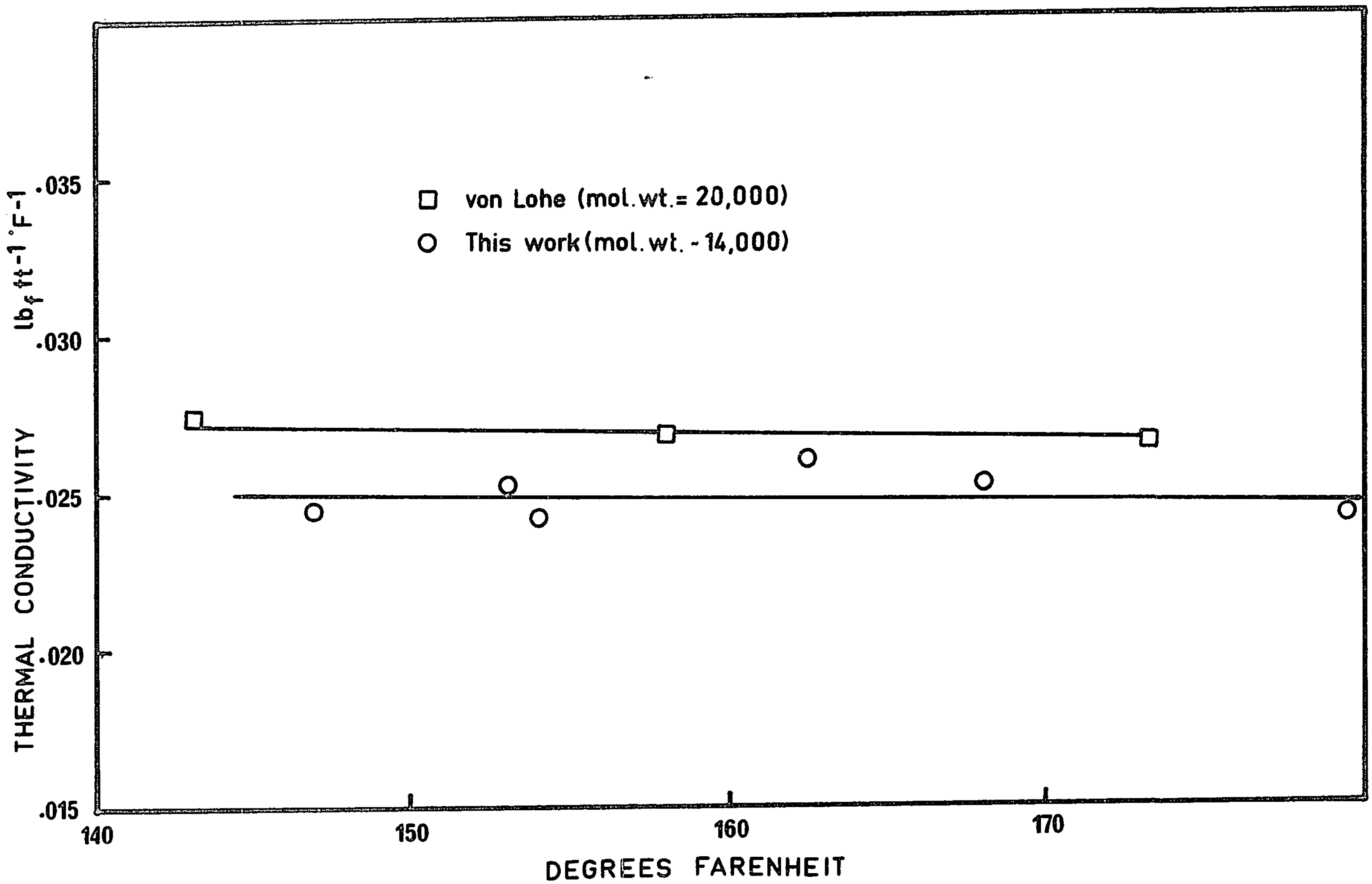
von Lohe (mol.wt.= 20,000)
This work (mol.wt. ~ 14,000)
THERMAL CONDUCTIVITY (lb_f ft-1 °F-1)
.035
.030
.025
.020
.015
140
150
160
170
DEGREES FARENHEIT

APPENDIX IV

DERIVATION OF THE MASS BALANCE EQUATION

IV-1 INTRODUCTION

The final, working form of the mass balance equation is obtained by substituting the relationships resulting from the two-particle split assumption and the distribution of degradation products into the basic mass balance. The appropriate equations are:

basic balance	$D_i = G_i - L_i$	$1 \le i \le N$	IV-1
two-particle split assumption	$g_{j-i,j} = g_{i,j}$	$i < j \le N$	IV-2
distribution relation	$g_{K,i} = c_{Ki} g_{K+1,i}$	$i > K+1$	IV-3

The derivation first substitutes equations IV-2 and IV-3 into the gain term, G_i, in equation IV-1. The substitution into the loss term, L_i, is then done and the simplified expressions combined to get the working form of the mass balance.

IV-2 SUBSTITUTION INTO THE GAIN TERM

The gain term, G_i, in equation IV-1 may be written as:

$$G_i = \sum_{j=i+1}^{N} g_{i,j} \qquad 1 \le i \le N \qquad \text{IV-4}$$

where $g_{i,j}$ can be substituted from equations IV-2 and IV-3. Working first with equation IV-2, this equation states that $g_{i,j}$ may be replaced by $g_{j-i,j}$ if $j > i$. However, allowing i and j to range through all values results in a duplication of relationships as well as trivial ones (e.g. if j = 6 and i = 3, equation IV-2 yields $g_{3,6} = g_{3,6}$). The trivial equations and the duplication can be eliminated by placing restrictions on the range of i such that:

$$g_{j-i,j} = g_{i,j} \qquad i \leq i \leq \frac{j-1}{2} \qquad \text{IV-2}$$

Turning to the distribution relation, equation IV-3, and rewriting it in terms of i and j and rearranging yields:

$$g_{i+1,j} = \frac{1}{c_{ij}} g_{i,j} \qquad j > i+1 \qquad \text{IV-5}$$

For values of $i+1 > 2$ equation IV-5 can be written in terms of $g_{1,j}$ and the appropriate coefficients, c. This is done by repeated substitution to give:

$$g_{i,j} = \frac{1}{c_{1j}c_{2j}c_{3j}\cdots c_{i-1j}} g_{1,j} \qquad 2 \leq i \leq \frac{j}{2} \qquad \text{IV-6}$$

where the limits have been changed for the reasons given above. Equation IV-6 is more compactly written as:

$$g_{i,j} = C_{ij}\, g_{1,j} \qquad 2 \leq i \leq \frac{j}{2} \qquad \text{IV-7a}$$

where

$$C_{ij} = \prod_{K=1}^{i-1} \frac{1}{c_{Kj}} \qquad \text{IV-7b}$$

Now, equation IV-2a states that for the range of $g_{\ell,j}$, $1 \le \ell < j$, $g_{\ell,j}$ may be substituted for $g_{j-\ell,j}$ if $1 \le \ell \le \frac{j-1}{2}$. Thus, for values of $1 \le i \le \frac{j-1}{2}$ equation IV-7a is substituted directly into equation IV-4. Values of i (or ℓ) $> \frac{j-1}{2}$, $g_{j-\ell,j}$ are first substituted into equation IV-7a (and IV-7b) and the result substituted into equation IV-4. The equation for G_i then becomes:

$$G_i = \sum_{j=i+1}^{N} C_{ij}\, g_{1,j} \qquad 1 \le i \le N \qquad \text{IV-8}$$

where

$$C_{ij} = \prod_{K=1}^{j-(i+1)} \frac{1}{c_{Kj}} \qquad i+2 \le j \le 2i \qquad \text{IV-8a}$$

$$C_{ij} = \prod_{K=1}^{i-1} \frac{1}{c_{Kj}} \qquad 2i+1 \le j \le N \qquad \text{IV-8b}$$

The range of coefficients C can be completed from the definition of the coefficients **c** and gives:

$$C_{ij} = 1.0 \qquad 2 \le j \le N \qquad \text{IV-8c}$$

$$C_{i(i+1)} = 1.0 \qquad 2 \le i \le N-1 \qquad \text{IV-8d}$$

IV-3 SUBSTITUTION INTO THE LOSS TERM

The loss term, L_i, is handled in a manner similar to G_i. L_i is first written in the form:

$$L_i = \sum_{j=1}^{i-1} \frac{j}{i} g_{j,i} \qquad 2 \le i \le N \qquad \text{IV-9}$$

Examining equations IV-4 and IV-8 shows that,

$$g_{i,j} = C_{ij}\, g_{1,j} \qquad \text{IV-10}$$

Thus, from equations IV-9 and IV-10

$$L_i = \sum_{j=1}^{i-1} \frac{j}{i} C_{ji}\, g_{1,i} \qquad 2 \le i \le N \qquad \text{IV-11}$$

Because j is a dummy index in equation IV-11 it is convenient to define

$$C_{ii} \equiv \sum_{m=1}^{i-1} \frac{m}{i} C_{mi} \qquad 2 \le i \le N \qquad \text{IV-12}$$

and

$$C_{ii} \equiv 0 \qquad i = 1 \qquad \text{IV-13}$$

Equation IV-11 is now

$$L_i = C_{ii}\, g_{1,i} \qquad 1 \le i \le N \qquad \text{IV-14}$$

where C_{ii} is given by equations IV-12 and IV-13.

IV-4 SUMMARY

The final mass balance equation is obtained by substituting for L_i and G_i in equation IV-1 to yield:

$$\sum_{j=i+1}^{N} C_{ij}\, g_{1,j} - C_{ii}\, g_{1,i} = D_i \qquad 1 \le i \le N \qquad \text{IV-15}$$

where

$$C_{1j} = 1. \qquad 2 \le j \le N \qquad \text{IV-15a}$$

$$C_{j(j+1)} = 1. \qquad 2 \le j \le N-1 \qquad \text{IV-15b}$$

$$C_{ij} = \prod_{K=1}^{j-(i+1)} \frac{1}{c_{Kj}} \qquad i+2 \le j \le 2i \qquad \text{IV-15c}$$

$$C_{ij} = \prod_{K=1}^{i-1} \frac{1}{c_{Kj}} \qquad 2i+1 \le j \le N \qquad \text{IV-15d}$$

$$C_{ii} = 0 \qquad i = 1 \qquad \text{IV-15e}$$

$$C_{ii} = \sum_{K=1}^{i-1} \frac{K}{i}\, C_{Ki} \qquad 2 \le i \le N \qquad \text{IV-15f}$$

Although this form of the mass balance seems cumbersome, it has the advantages that the essential equation IV-15 can be manipulated easily and the definitions of the coefficients, C, are well suited to machine computation. If the coefficients are presumed known, then there are N equations and 2N-1 unknowns ($g_{1,1} = 0$). The equations IV-15 are not all independent since it is possible to write an overall mass balance on the ultimate particles:

$$\sum_{i=1}^{N} i\, D_i = 0 \qquad \text{IV-16}$$

but if IV-16 is included the number of equations and unknowns is unchanged.

APPENDIX V

NUMERICAL SOLUTION OF THE EQUATIONS FOR THE EQUILIBRIUM AND STEP-CHANGE CASES

V-1 EQUILIBRIUM CASE

The set of differential equations to be solved is:

$$\sum_{j=i+1}^{N} \frac{C_{ij}}{C_{jj}} Q_j I_\tau - Q_i I_\tau = \frac{dQ_i}{d\tau} \qquad 1 \le i \le N \qquad \text{4-25}$$

where the coefficients C_{ij} are given by equations 4-10a-f and I_τ is defined by:

$$I_\tau = \frac{\rho_\tau}{\int_\tau^\infty \rho_\tau d\tau} \qquad \text{4-21}$$

For the purposes of this work an exponential relationship was chosen for the strength distribution function, ρ_τ:

$$\rho_\tau = e^{-\beta\tau} \qquad \text{6-6}$$

so that, substituting equation 6-6 into equation 4-21 and integrating yields:

$$I_\tau = \beta \qquad \text{V-1}$$

Equations 4-25, after substituting for I_τ, become:

$$\sum_{j=i+1}^{N} \frac{C_{ij}}{C_{jj}} \beta Q_j - \beta Q_i = \frac{dQ_i}{d\tau} \qquad 1 \leq i \leq N \qquad \text{V-2}$$

The equations, as indicated in Chapter 4, are most easily solved in reverse order by starting with $i = N$. Euler's method of solution (78) was chosen. This simple method sometimes suffers from accumulation of errors as the solution proceeds, but this difficulty is easily overcome if computation time is not important. In the present instance acceptable accuracy was obtained.

The following symbols are used in the computer program.

C	array containing the coefficients c_{ij}
CC	array containing the coefficients C_{ij}
COEFF	a subprogram for computing the coefficients C_{ij}
COEFR	a subprogram for computing the coefficients c_{ij}
D	array containing the rate of change of the number of agglomerates per species per unit change in shear stress
DTAU	incremental change in shear stress
FTERM	variable for intermediate results
ITCT	iteration counter
N	number of beads contained in the largest agglomerate

P, PP, PC	different forms of the rate constant, β
PN1, PN2, SID1, SID2, SID3	variables used for intermediate results
T	array containing the number of beads per species of agglomerate
TA	array containing the number of agglomerates per species
TAU	shear stress
TAUI	initial shear stress
TAUMX	final (maximum) shear stress

```
FORTRAN IV G LEVEL  20                MAIN            DATE = 71287          14/34/20            PAGE 0001

              DIMENSION T(15), C(15,15), CC(15,15), P(15), PP(15), PC(15),
             1 D(15), TA(15)
              READ (5,10) N
           10 FORMAT (I2)
              DO 12 I=1,N
              READ (5,11) T(I)
           11 FORMAT (F10.4)
           12 CONTINUE
              READ (5,15) TAUI, DTAU, TAUMX
           15 FORMAT (3F10.4)
              CALL COEFR(C,N)
              CALL COEFF (C,CC,N)
              TAU = TAUI
              ITCT = 0
           20 CALL SBPP (P,PP,TAU,N)
              IF ( ITCT ) 75, 75, 25
           25 N1 = N-1
              DO 26 I=1,N
           26 TA(I) = T(I)/I
              DO 31 I=2,N1
              PC(I) = 1.0
              DO 30 J=I,N1
           30 PC(I) = PC(I)*PP(J)
           31 CONTINUE
              PC(N) = 1.0
              DO 36 I=2,N1
              FTERM = 0.
              I1 = I + 1
              DO 35 IS=I1,N
           35 FTERM = FTERM + PC(IS)*TA(IS)*CC(I,IS)/CC(IS,IS)
           36 D(I) = FTERM - PC(I)*TA(I)
              FTERM = 0.
              DO 40 IS=2,N
           40 FTERM = FTERM + PC(IS)*TA(IS)*CC(1,IS)/CC(IS,IS)
              D(1) = FTERM
              D(N) = -TA(N)
              PN1 = 0.1
              PN2 = 0.05
           45 SID1 = 0.
              SID2 = 0.
              DO 50 K=1,N
              SID1 = SID1 + K*PN1*D(K)
           50 SID2 = SID2 + K*PN2*D(K)
           51 PN3 = PN2 - SID2*((SID1 - SID2)/(PN1 - PN2))
              SID3 = 0.0
              DO 52 K=1,N
           52 SID3 = SID3 + K*PN3*D(K)
              IF (ABS(SID3).LE.0.000100) GO TO 55
              SID1 = SID2
              SID2 = SID3
              PN1 = PN2
              PN2 = PN3
              GO TO 51
           55 P(N) = PN3
```

FORTRAN IV G LEVEL 20 MAIN DATE = 71287 14/34/20 PAGE 0002

```
              DO 60 K=1,N
              D(K) = PN3*D(K)
           60 T(K) = T(K) + K*D(K)*DTAU
           65 N2 = N - 2
              DO 70 K=1,N2
              KK = N - K
           70 P(KK) = PP(KK)*P(KK+1)
              GO TO 90
           75 WRITE (6,1000)
         1000 FORMAT (1H1)
              DO 80 K=1,N
              D(K) = 0.
           80 P(K) = 0.
           90 WRITE (6,1001)
         1001 FORMAT (1H )
              WRITE (6,1002) ITCT, TAU, DTAU, (T(I), I=1,N)
         1002 FORMAT (1X,I3,15(1X,F7.5))
              WRITE (6,1003) (D(I), I=1,N)
         1003 FORMAT (20X,15(1X,F7.3))
              WRITE (6,1004) (P(I), I=1,N)
         1004 FORMAT (20X,15(1X,F7.5))
              IF(TAU.GE.TAUMX) GO TO 100
              TAU = TAU + DTAU
              ITCT = ITCT + 1
              GO TO 20
          100 STOP
              END
```

FORTRAN IV G LEVEL 20 COEFR DATE = 71287 14/34/20 PAGE 0001

```
              SUBROUTINE COEFR (C,N)
              DIMENSION C(15,15)
              DO 50 I=4,N
              IF (IFIX(I/2.).EQ.(I/2))  GO TO 20
              LIM = (I-3)/2
              GO TO 30
           20 LIM = (I-2)/2
           30 DO 40 K=1,LIM
           40 C(K,I) = SQRT(1.0/FLOAT(K))
           50 CONTINUE
              RETURN
              END
```

```
*OPTIONS IN EFFECT*  ID,EBCDIC,SOURCE,NOLIST,NODECK,LOAD,NOMAP
*OPTIONS IN EFFECT*  NAME = COEFR   , LINECNT =      56
*STATISTICS*    SOURCE STATEMENTS =        12,PROGRAM SIZE =       634
*STATISTICS*  NO DIAGNOSTICS GENERATED
```

```
FORTRAN IV G LEVEL  20            COEFF            DATE = 71287         14/34/20            PAGE 0001

 0001              SUBROUTINE COEFF (A,C,N)
             C     SUBROUTINE CALCULATES THE COEFFICIENTS EXPRESSING THE
             C     RELATIVE FREQUENCY OF THE TYPE OF SPLIT .
 0002              DIMENSION A(15,15), C(15,15)
 0003              DO 20 IR=1,N
 0004              DO 20 IT=1,N
 0005           20 C(IR,IT) = 0.0
 0006              DO 50 IR=1,N
 0007              DO 50 IT=2,N
 0008              IF(IR.GT.IT)GO TO 78
 0009              IF(IR.EQ.1) C(IR,IT) = 1.0
 0010              IF(IR.EQ.IT) C(IR,IT+1) = 1.0
 0011              IF(IT.GT.(IR+1).AND.IT.LE.2*IR) GO TO 200
 0012              IF(IR.LT.2) GO TO 50
 0013              IF(IT.GT.2*IR.AND.IT.LE.N) GO TO 250
 0014              GO TO 50
 0015          200 IX=IT-IR-1
 0016              C(IR,IT)=1.
 0017              DO 100 IV=1,IX
 0018              C(IR,IT)=C(IR,IT)*1/A(IV,IT)
 0019          100 CONTINUE
 0020              GO TO 50
 0021          250 IZ=IR-1
 0022              C(IR,IT)=1.
 0023              DO 300 IV=1,IZ
 0024              C(IR,IT)=C(IR,IT)*1/A(IV,IT)
 0025          300 CONTINUE
 0026              GO TO 50
 0027           78 C(IR,IT)=0.
 0028           50 CONTINUE
 0029              DO 60 IT=1,N
 0030              IF(IT.EQ.1) C(IT,IT)=1.0
 0031              IF(IT.EQ.1) GO TO 60
 0032              IY=IT-1
 0033              SUM=0.
 0034              DO 90 IR=1,IY
 0035              SUM=-ABS(SUM)-(FLOAT(IR)/FLOAT(IT))*C(IR,IT)
 0036              IF(IR.EQ.IY) C(IT,IT)=-SUM
 0037           90 CONTINUE
 0038           60 CONTINUE
 0039              DO 87 IR=1,N
 0040              WRITE (6,1111) IR, IT, (C(IR,IT), IT=1,N)
 0041         1111 FORMAT (5X,2I5,15(F7.4))
 0042           87 CONTINUE
 0043              RETURN
 0044              END
```

```
FORTRAN IV G LEVEL  20            SBPP             DATE = 71287         14/34/20            PAGE 0001

 0001              SUBROUTINE SBPP (P,PP,TAU,N)
 0002              DIMENSION P(15), PP(15)
 0003              N1 = N - 1
 0004              DO 10 I=2,N1
 0005           10 PP(I) = 1.0
 0006              RETURN
 0007              END
```

V-2 STEP-CHANGE CASE

The numerical solution for this case was divided into two parts. The first part computes f_j as a function of the shear deformation (which is proportional to time for a constant shear rate). The second part solves the overall mass balance equations which are identical to those for the equilibrium case except for the inclusion of the variable f_j. The equations to be solved to determine f_j are:

$$\frac{de_{i\sigma}}{dt} = \sum_{j=i+1}^{N} \frac{C_{ij}}{C_{jj}} \rho_\sigma \int_{\sigma_1}^{\sigma} \frac{\frac{de_{j\sigma}}{dt} + \rho_\sigma \frac{dA_{jt}}{dt}}{\int_{\sigma_1}^{\infty} \rho_\sigma \, d\sigma} d\sigma - K\dot{\gamma} e_{i\sigma} \qquad 4\text{-}54$$

$$s_{j\sigma} = \rho_\sigma \int_{\sigma_1}^{\sigma} \frac{e_{j\sigma} + A_{jt}\rho_\sigma}{\int_{\sigma_1}^{\infty} \rho_\sigma \, d\sigma} d\sigma \qquad 4\text{-}53$$

$$f_j = \frac{\int_{\sigma_1}^{\sigma_5} s_{j\sigma} \, d\sigma}{\int_{\sigma_1}^{\infty} s_{j\sigma} \, d\sigma} \qquad 4\text{-}43$$

In this work only the specific case of an exponential strength distribution function was solved, so that the additional relationships required are:

$$\rho_\sigma = e^{-\beta\sigma} \qquad 6\text{-}6$$

$$A_{jt} = - K \dot{\gamma} A_{jo} e^{-K\dot{\gamma}t} \qquad 4\text{-}56$$

$$\rho_\sigma \frac{dA_{jt}}{dt} = - K\dot{\gamma} A_{jt} \rho_\sigma \qquad 4\text{-}55$$

The computational scheme used is given in the flow chart shown in figure V-1. The computations were done by using subprograms available in the IBM Scientific Subroutine Package (87) to solve the differential equations and perform the required integrations. These subprograms are not reproduced here, but a brief description of each is given below to relate it to its position in the flow chart.

Subroutine COEFF - This subroutine computes the coefficients C_{ij} given the values of the coefficients c_{ij}. A listing of this subroutine is given with the equilibrium case program listing. This subprogram is not part of the IBM package.

Subroutine QTFQ - This subroutine integrates a numerically tabulated function using the trapezoidal rule.

Subroutine HPCG - is a subroutine to solve ordinary first-order differential equations. It uses Hamming's modified predictor-corrector method, which is noted for its accuracy and minimal amount of computation.

Subroutine DIST - is a subroutine to calculate to the resulting distribution of agglomerates after f_j has been computed. It is the equilibrium case program modified to a subprogram and with the parameter f_j inserted into the mass-balance equations.

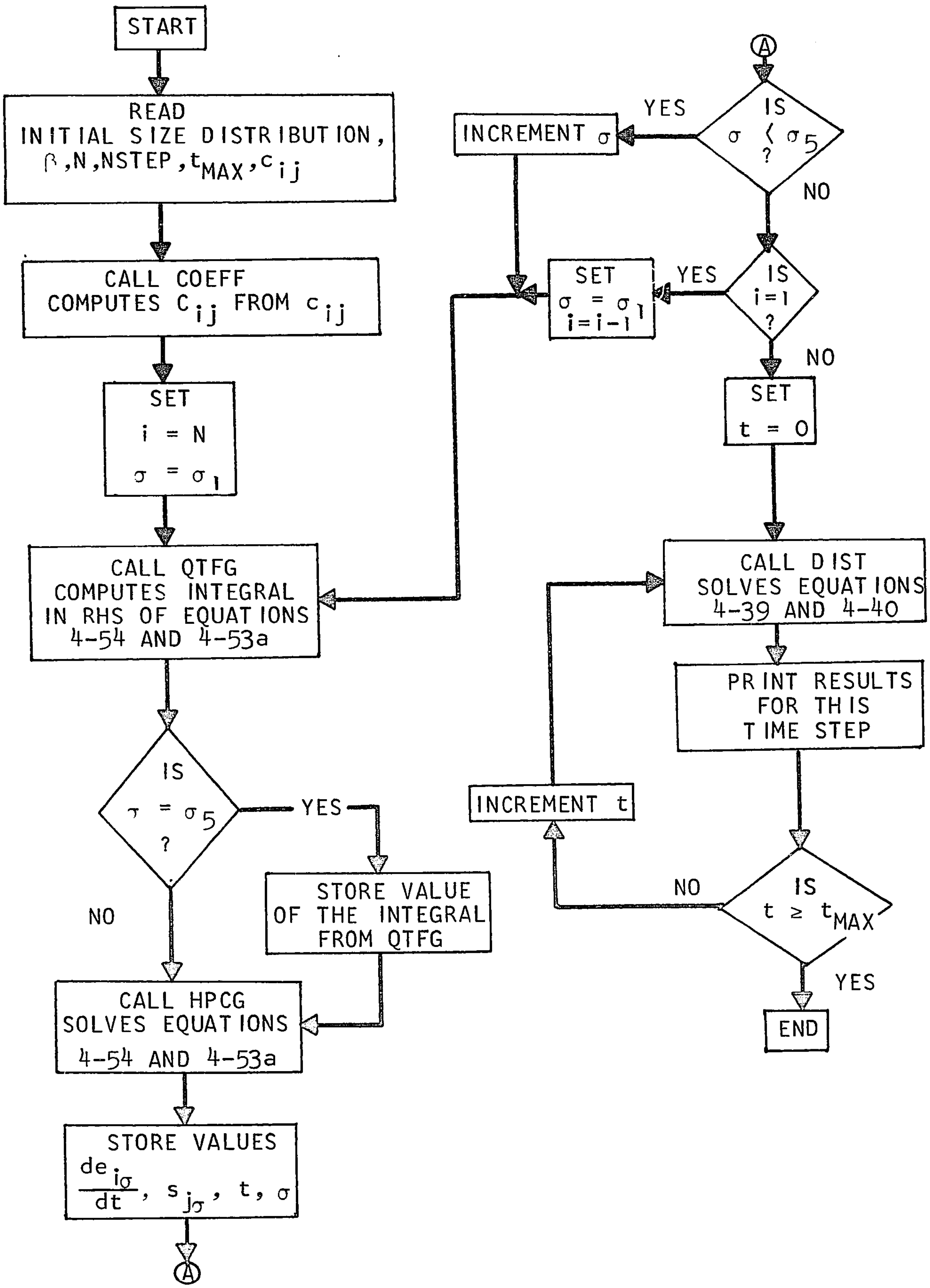

FIGURE V-1 Flow Chart of Numerical Solution for Step-Change in Shear Stress Case

It was found that a worthwhile saving in computation time was obtained by differentiating equation 4-53 to obtain:

$$\frac{ds_{j\sigma}}{dt} = \rho_\sigma \int_{\sigma_1}^{\sigma} \frac{\frac{de_{j\sigma}}{dt} + \rho_\sigma \frac{dA_{jt}}{dt}}{\int_{\sigma_1}^{\infty} \rho_\sigma \, d\sigma} d\sigma \qquad 4\text{-}53a$$

The integral on the right-hand side of equation 4-53a is identical with the integral in equation 4-54 requiring only one integration for both equations. Further, due to the nature of the subprogram HPCG, both equations 4-53a and 4-54 can be solved with one call to this subprogram which then returns the appropriate $e_{i\sigma}$ and $s_{j\sigma}$.

APPENDIX VI

RELATIONSHIP BETWEEN THE DISTRIBUTION OF BREAKING AGGLOMERATES AND THE DISTRIBUTION OF PRODUCTS DURING NON-EQUILIBRIUM DEAGGLOMERATION

VI-1 BREAKAGE OF GAINED AGGLOMERATES Q'_{ig}

The derivation begins by examining the agglomerates, $E_{i\sigma}$, in the strength range from σ to $\sigma + d\sigma$, of the gained i-particle agglomerates, Q'_{ig}, that are breaking (refer to figure 4-4). These agglomerates have an instantaneous distribution function $e_{i\sigma} = e_{i\sigma}(\sigma, t)$ such that

$$E_{i\sigma} = e_{i\sigma}\, d\sigma \qquad \text{VI-1}$$

It follows from the assumption of a random distribution of breaking strengths throughout all positions of all agglomerates that the breakage products entering the species κ, $\kappa < i$, must have the same strength distribution, regardless of the value of κ. Thus, there is only one distribution function for the products which is the same for the sum of all the products, or for an individual species contained in the products.

It also follows from the above stated assumption that when the agglomerates, designated by $E_{i\sigma}$, degrade the products will have a fractional strength distribution which is identical with the fractional strength distribution of the original (initial) agglomerates based on the range from σ to ∞. The process is illustrated in figure VI-1, where the breakdown of agglomerates contained in the range from σ_2 to $\sigma_2 + d\sigma$ is shown. These agglomerates, when broken, generate products that have a distribution function, $B_{i\sigma_2}\rho_\sigma d\sigma$, where the distribution function satisfies:

$$\frac{B_{i\sigma_2}\rho_\sigma d\sigma}{\int_{\sigma_2}^{\infty} B_{i\sigma_2}\rho_\sigma d\sigma} = \frac{A_{io}\rho_\sigma d\sigma}{\int_{\sigma_2}^{\infty} A_{io}\rho_\sigma d\sigma} \qquad \text{VI-2}$$

Because the agglomerates contained in the differential increment from σ_2 to $\sigma_2 + d\sigma$, $E_{i\sigma_2}$, produced the distribution $\int_{\sigma}^{\infty} B_{i\sigma_2}\rho_\sigma d\sigma$, the scaling factor, $B_{i\sigma_2}$, must be differentially small, and

$$E_{i\sigma_2} = \int_{\sigma_2}^{\infty} B_{i\sigma_2}\rho_\sigma d\sigma \qquad \text{VI-3}$$

Since the scaling factor $B_{i\sigma_2}$ is independent of the agglomerate strength, σ, equation VI-3 can be written:

$$E_{i\sigma_2} = B_{i\sigma_2} \int_{\sigma_2}^{\infty} \rho_\sigma d\sigma \qquad \text{VI-4}$$

It is obvious that some of the breakdown products have strengths less than the shear stress in the fluid and that these products contributed to the number of breakable agglomerates in the species to which they belong.

FIGURE VI-1: The Strength Distribution of the Breakdown Products of Agglomerates Having a Strength σ_2 in Species i

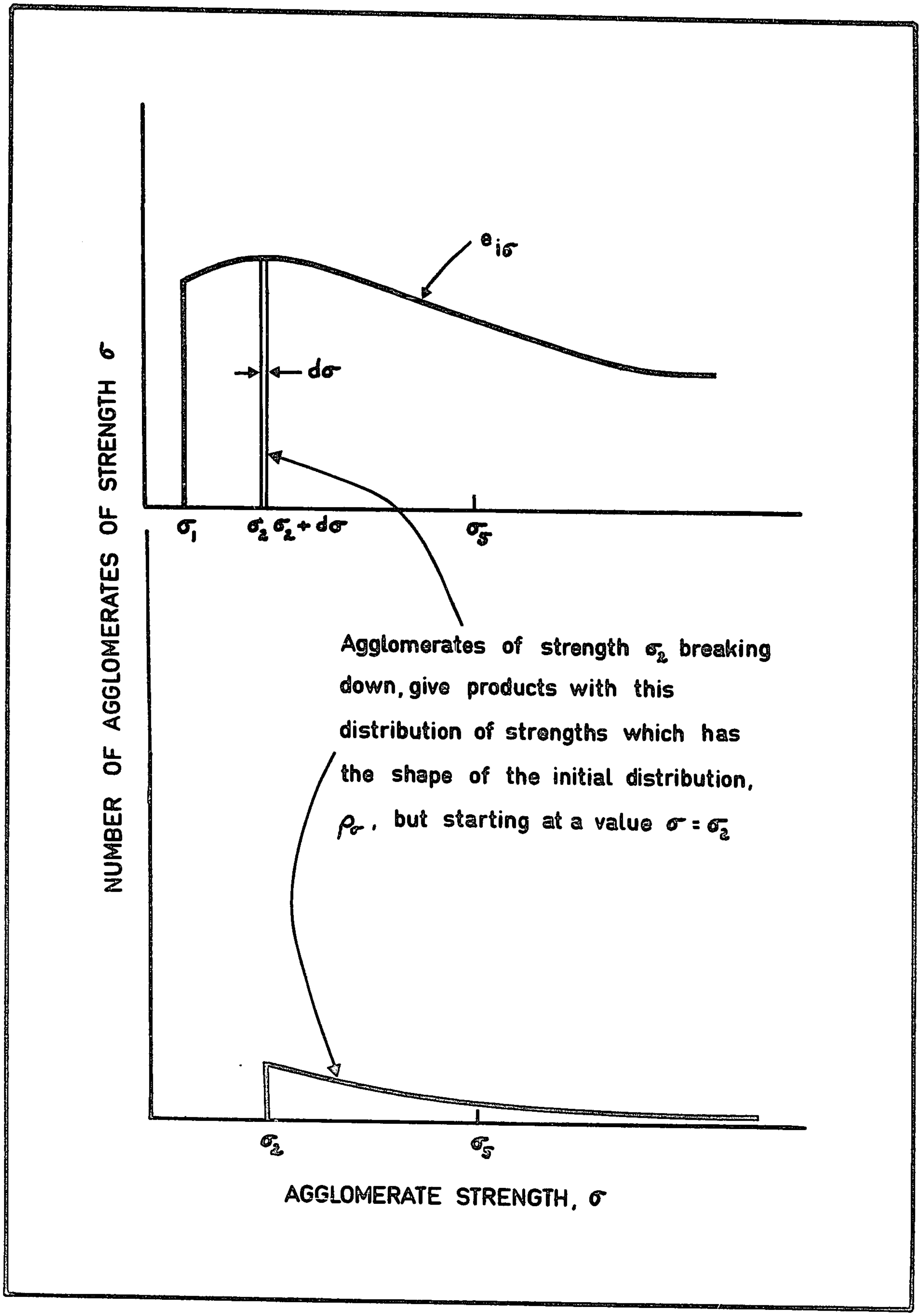

NUMBER OF AGGLOMERATES OF STRENGTH σ
e iσ
dσ
σ1
σ2 σ2 + dσ
σ5
Agglomerates of strength σ2 breaking down, give products with this distribution of strengths which has the shape of the initial distribution, ρσ, but starting at a value σ = σ2
σ2
σ5
AGGLOMERATE STRENGTH, σ

In the preceding discussion only agglomerates of strength, σ_2 were considered, but all agglomerates of strengths from σ_1 to σ_5 degrade to give breakdown products. The resulting strength distribution function of all the products from i-particle breakdown is $h_i = h_i(\sigma, t)$. It is the sum (integration) of the contribution of each strength increment in the breaking (i-particle) agglomerates. The formation of the products' strength distribution from the breaking species is depicted in figure VI-2.

The number of i-particle agglomerates in the strength range between σ and $\sigma + d\sigma$ is E_i and produce a distribution in the products given by:

$$E_{i\sigma} = B_{i\sigma} \int_{\sigma}^{\infty} \rho_{\sigma} \, d\sigma \qquad \text{VI-5}$$

Thus, in figure VI-2, each loss in the ranges σ_2 to $\sigma_2 + d\sigma$, σ_3 to $\sigma_3 + d\sigma$, σ_4 to $\sigma_4 + d\sigma$ .... etc produces a gain which has a distribution of the form $B_{i\sigma_2} \int_{\sigma_2}^{\infty} \rho_{\sigma} \, d\sigma$, $B_{i\sigma_3} \int_{\sigma_3}^{\infty} \rho_{\sigma} \, d\sigma$, $B_{i\sigma_4} \int_{\sigma_4}^{\infty} \rho_{\sigma} \, d\sigma$ ... etc. Each gain makes a contribution of $dh_{i\sigma*}$ to the overall value of the distribution function, $h_{i\sigma*}$, at a breaking strength $\sigma*$, thus

$$dh_{i\sigma*} = B_{i\sigma*} \, \rho_{\sigma*} \qquad \text{VI-6}$$

FIGURE VI-2: The Overall Strength Distribution of the Breakdown Products in the Strength Range from σ_1 to σ_5

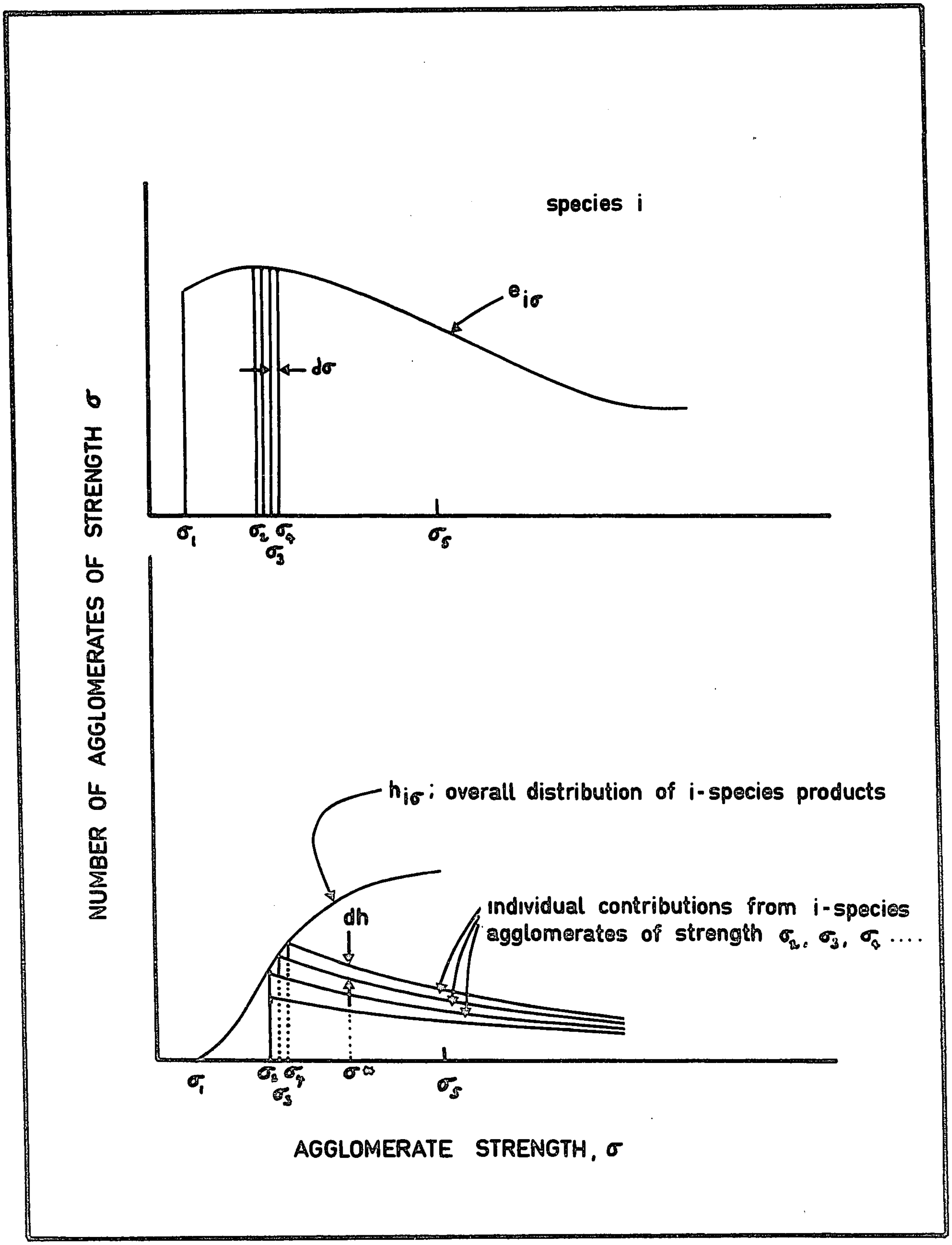

species i
$e_{i\sigma}$
$d\sigma$
σ_1
σ_2 σ_4
σ_3
σ_S
NUMBER OF AGGLOMERATES OF STRENGTH σ
$h_{i\sigma}$: overall distribution of i-species products
individual contributions from i-species agglomerates of strength σ_2, σ_3, σ_4 ....
dh
σ_1
σ_2 σ_4
σ_3
σ^*
σ_S
AGGLOMERATE STRENGTH, σ

From equations VI-1 and VI-5

$$E_{i\sigma} = e_{i\sigma}\, d\sigma = B_{i\sigma} \int_{\sigma}^{\infty} \rho_{\sigma}\, d\sigma \qquad \text{VI-7}$$

Rearranging equation VI-7

$$B_{i\sigma} = \frac{\frac{\partial e_{i\sigma}}{\partial \sigma}\, e_{i\sigma}\, d\sigma}{\int_{\sigma}^{\infty} \rho_{\sigma}\, d\sigma} \qquad \text{VI-8}$$

and substituting for $B_{i\sigma}$ into equation VI-6 and integrating from σ_1 to the breaking strength σ^*, $\sigma^* < \sigma_5$, gives the value of $h_{i\sigma}$ for that breaking strength, $h_{i\sigma^*}$:

$$h_{i\sigma^*} = \rho_{\sigma^*} \int_{\sigma_1}^{\sigma^*} \frac{e_{i\sigma}}{[\int_{\sigma_1}^{\infty} \rho_{\sigma}\, d\sigma]}\, d\sigma \qquad \sigma_1 \leq \sigma^* \leq \sigma_5 \qquad \text{VI-9}$$

It is noted that the upper limit for σ^* in equation VI-9 is σ_5. The integration cannot be carried beyond σ_5 since the i-particle agglomerates do not degrade for strengths greater than σ_5. The deagglomerating particles produce products in the strength range σ, $\sigma_5 < \sigma \leq \infty$, as shown in figure VI-3. The value for $h_{i\sigma^*}$, $\sigma_5 \leq \sigma^* \leq \infty$, can be obtained by carrying the integration in equation VI-9 to σ_5 and inserting the appropriate value of σ^* in the function ρ_{σ^*};

FIGURE VI-3: The Overall Strength Distribution of the Breakdown Products in the Strength Range $\sigma \geq \sigma_5$

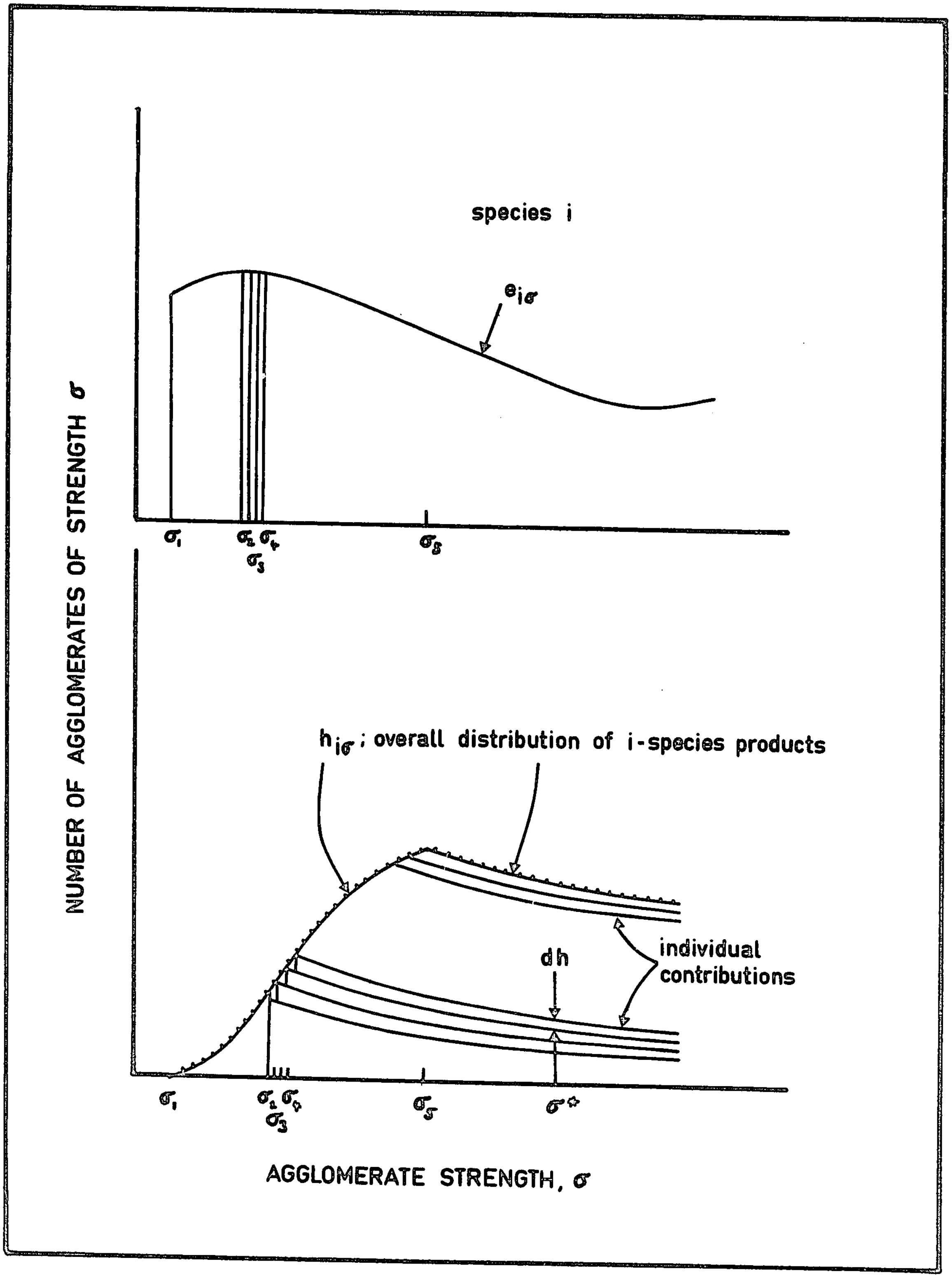
species i
$e_{i\sigma}$
σ_1
σ_2 σ_4
σ_3
σ_5
$h_{i\sigma}$; overall distribution of i-species products
dh
individual contributions
σ_1
σ_2 σ_4
σ_3
σ_5
σ^*
NUMBER OF AGGLOMERATES OF STRENGTH σ
AGGLOMERATE STRENGTH, σ

$$h_{i\sigma^*} = \rho_{\sigma^*} \int_{\sigma_1}^{\sigma_5} \frac{e_{i\sigma}}{[\int_{\sigma_1}^{\infty} \rho_\sigma d\sigma]} d\sigma \qquad \sigma_5 \le \sigma^* \le \infty \qquad \text{VI-10}$$

VI-2 BREAKAGE OF REMAINING ORIGINAL AGGLOMERATES, Q'_{ior}

These agglomerates, which are breaking simultaneously with the gained breakable agglomerates, have an instananeous strength distribution function such that:

$$D_{i\sigma} = A_{it} \rho_\sigma d\sigma \qquad \text{VI-11}$$

where $D_{i\sigma}$ is the amount contained in the strength range between σ and $\sigma + d\sigma$.

Now, comparing equations VI-11 and VI-1 it is obvious that $A_{it}\rho_\sigma$ is equivalent to $e_{i\sigma}$. Thus from equations VI-9 and VI-10 the distribution function, $b_{i\sigma}$, for the breakage products of Q'_{ior} is:

$$b_{i\sigma^*} = \rho_{\sigma^*} \int_{\sigma_1}^{\sigma^*} \frac{A_{it} \rho_\sigma}{[\int_{\sigma_1}^{\infty} \rho_\sigma d\sigma]} d\sigma \qquad \sigma_1 \le \sigma^* \le \sigma_5 \qquad \text{VI-12}$$

and

$$b_{i\sigma^*} = \rho_{\sigma^*} \int_{\sigma_1}^{\sigma_5} \frac{A_{it} \rho_\sigma}{[\int_{\sigma_1}^{\infty} \rho_\sigma d\sigma]} d\sigma \qquad \sigma_5 \le \sigma^* \le \infty \qquad \text{VI-13}$$